DEPARTMENT OF ENGINEERING SCIENCE
UNIVERSITY OF OXFORD

Advanced Finite Element Analysis of Deep Excavation Case Histories

Yuepeng Dong

A thesis submitted for the degree of Doctor of Philosophy at University of Oxford

Christ Church

Hilary Term 2014

Declaration

I declare that, except where specific reference is made to the works of others, the contents of this thesis are original and have never been submitted, in part or as a whole, to any other university for any degree, diploma or other qualifications.

This thesis is the result of my own work and includes nothing which is the outcome of work done in collaboration.

Yuepeng Dong

December 2013

Acknowledgements

There are a number of people I need to acknowledge here during my study at Oxford.

Firstly, I would like to thank my supervisors, Dr Harvey J. Burd and Professor Guy T. Houlsby, for their generous time of regular meetings and valuable advices during discussions. Guy encouraged me to apply for Oxford and provided guidance in the application, while Harvey is the leading supervisor for my research. I am fortunate to have them both as my supervisors, and this experience will stay in my memory forever. The examiners, Prof. David Potts and Prof. Tony Blakeborough, commented on this thesis and gave corrections during and after the viva.

Secondly, it is my alma mater, Shanghai Jiao Tong University, where I started learning Civil Engineering, built up my friendship, developed my leadership, and enhanced my skills in research. My experiences and skills in Shanghai are essential for my research in Oxford, and also critical to help me secure a postdoctoral position working with Prof. Andrew J. Whittle at MIT. My whole study in Oxford is sponsored by a scholarship from China Scholarship Council, and the application was made in Shanghai. The case histories in the thesis are provided by Dr Zhonghua Xu, a PhD graduate from Shanghai Jiao Tong University, who did the field measurement and analysed the field data in his PhD thesis.

Thirdly, many thanks also go to my colleagues and friends in the university and colleges. With them, I never feel lonely in Oxford. The daily communication with my fellow students in the department is entertaining and enlightening. The experience in OUSU is enjoyable, first in the Environment & Ethics Committee, and then serving as the MPLS Divisional Graduate Representative. The social life in my college, Christ Church, is amazing and unforgettable, both involving in the governing committee of Christ Church GCR as OUSU Representative and Bar Representative, and also rowing in the prestigious Christ Church Rowing Club.

Last but not least, I wish to thank my parents and sister who encouraged my study abroad and never made me worry about them in China.

Abstract

Deep excavations have been used worldwide for underground construction, but they also alter the ground conditions and induce ground movements which might cause risks to adjacent infrastructure. Field measurements are normally carried out during excavations to ensure their safety, and also provide valuable data to calibrate the results from the numerical analysis which is an effective way to investigate the performance of deep excavations. This thesis is concerned with evaluating the capability of advanced finite element analysis in reproducing various aspects of observed deep excavation behaviour in the field through back analysis of case histories. The finite element model developed considers both geotechnical and structural aspects such as (i) detailed geometry of the excavation and retaining structures, (ii) realistic material models for the soil, structures and the soil-structure interface, and (iii) correct construction sequences. Parametric studies are conducted first based on a simplified square excavation to understand the effect of several important aspects, e.g. (i) the merit of shell or solid elements to model the retaining wall, (ii) the effect of construction joints in the retaining wall, (iii) the effect of the operational stiffness of concrete structural components due to cracks, (iv) the thermal effect of concrete beams and floor slabs during curing process and due to variation of ambient temperature, (v) the effect of soil-structure interface behaviour, and (vi) the effect of stiffness and strength properties of the soil. Two more complex case histories are then investigated through fully 3D analyses to explore the influence of various factors such as (i) neglecting the small-strain stiffness nonlinearity in the soil model, (ii) the selected K_0 value to represent the initial stress state in the ground, (iii) the appropriate anisotropic wall properties to consider the joints in the diaphragm wall, (iv) the parameters governing the settlements of adjacent buildings and buried pipelines, (v) the effectiveness of ground improvement on reducing the building settlement, (vi) the variation of construction sequences, (vii) the effectiveness of earth berms, and (viii) ignoring the openings in the floor slabs. This research has strong practical implications, but cautions should also be taken in applications, e.g. element types and parameter selection.

Table of Contents

Chapter 1 Introduction

1.1 Background

Deep excavations are widely used in urban areas for the development of underground space, e.g. subway stations, basements for high-rise buildings, underground car parks and shopping centres. However, the excavation process inevitably alters the stress states in the ground and may cause significant wall deformations and ground movements. Especially when the excavation is close to adjacent infrastructure, e.g. buildings, tunnels, buried pipelines, piled foundations, the excavation induced ground movements must be carefully monitored and controlled within an acceptable amount, to avoid any potential damage to these classes of infrastructure. The failure of an excavation may have catastrophic consequences, and special care must be taken to avoid such failure. One disaster of this sort is the collapse of a deep excavation adjacent to Nicoll Highway in Singapore on 20 April 2004 (Fig.1.1), resulting in four casualties and a delay of part of the Circle Line subway project.

Fig.1.1 Singapore Nicoll Highway collapse adjacent to an excavation

The main causes of failure are various, e.g. unexpected soil conditions, rupture of the anchoring or bracing system (e.g. buckling or inadequate connection to the wall), violating the designed construction sequences (e.g. overexcavation). In most cases, however, the pre-failure

performance is more important, and considerable efforts have been made to understand the characteristics of the soil and structural deformations. To reduce the excavation-induced deformations, an appropriate retaining wall and support system should be designed, as well as employing adequate construction methods. As the excavation becomes deeper and larger in scale, and may be constructed in problematic soils, challenges arise for the research, design, and construction of deep excavations. Therefore, the performance of deep excavations should be better understood through more sophisticated approaches, e.g. real-time monitoring systems, and advanced numerical predictions.

Ground movements around deep excavations critically depend on both the ground conditions (e.g. initial stress states, stiffness and strength properties, and groundwater conditions), retaining schemes (e.g. types of the retaining wall and support system, rigidity of retaining structures), and the methods of construction (e.g. top-down, bottom-up, open-cut, and excavation sequences). Excessive lateral wall displacements are largely due to an inadequate support design (e.g. flexible retaining wall, insufficient strut or anchoring system, and inadequate embedment length), and can also result from construction errors (e.g. excessive excavation).

Retaining structures should be designed with respect to their lateral displacements, which can be reduced by adopting a stiffer wall, by reinforcing the anchor or strut system, or by pre-stressing these components. This general stiffening of the retaining system, however, leads to an increase in lateral soil pressure, bending moments in the retaining wall, and forces in the struts or anchors. Braced excavations with a top-down construction method are usually preferred in practice to reduce wall deformations and ground movements.

Numerical analysis can consider both the geotechnical and structural aspects in the deep excavations such as the soil properties, details of structures, and construction sequences, and provide necessary information on the performance of deep excavations for design purpose. It can also be used to predict the behaviour of deep excavation and provide guidance for the construction.

Field monitoring of the performance of deep excavations during the construction process can provide immediate feedback to engineers to ensure the safety of the project. The measured field data is a valuable resource to calibrate and verify numerical analyses and facilitate a better understanding of the general performance of deep excavations. This creates a link between numerical analysis and observational method.

1.2 Limitations in previous and current research

Traditionally, geotechnical design of retaining structures has been carried out using simplified analyses or empirical approaches (e.g. closed form linear elastic based, limit equilibrium and limit analysis, beam-spring approach). However, these approaches do not provide engineers with all the desired information. In particular, often only limited indications of soil movements and no information on the interaction with adjacent structures are available (Potts and Zdravkovic 2001). In addition, when applying such methods of analysis, some limitations and approximations are made. For instance, a closed form solution cannot incorporate a realistic constitutive model of soils which satisfies all the fundamental requirements. Limit equilibrium and limit analysis fail to satisfy at least one of the fundamental theoretical requirements; they only give information on stability, without any information regarding movements or structural forces under working load conditions, as well as movements in adjacent soil, structures and utilities. The beam-spring approach, within the simple numerical methods, is able to provide information about wall movements and structural forces. However, such kinds of methods do not provide information on the overall stability, movements of the surrounding soil and effects on the adjacent structures, services and utilities. Moreover, the complexity and uncertainty involved in design and analysis increase with the degree of soil-structure interaction and depend on type of retaining structure to be employed, which could not be well understood from traditional design methods.

Deep excavations represent a complicated soil-structure interaction problem. It is, therefore, essential to make optimum use of previous experience and case histories in similar conditions,

e.g. the empirical methods proposed by Peck (1969) and Clough and O'Rourke (1990). However, it is not reliable to extrapolate these results to deep excavations with different retaining systems, soil conditions, and construction methods. In addition, obtaining similar relationships using the empirical approach is rather difficult, since capturing the isolated effects of the various factors requires a significant number of well documented and controlled case studies. Assessing and analysing such a large number of case studies are difficult, if not impossible.

In an effort to understand better the behaviour of deep excavations, field measurements are normally conducted during the construction process, and a number of well-documented case histories worldwide have been reported (O'Rourke 1981, Finno, Atmatzidis et al. 1989, Ou, Liao et al. 1998, Ou, Liao et al. 2000, Long 2001, Finno and Bryson 2002, Liu, Ng et al. 2005, Ou, Hsieh et al. 2010, Liu, Jiang et al. 2011, Ng, Hong et al. 2012). However, it is difficult to use these case histories for prediction purposes. Occasionally, case studies include class "C" predictions where the measured excavation performance is matched with back analyses using numerical analyses, but those numerical analyses were largely simplified (e.g. 2D analyses or simple 3D analyses, and with conventional soil models). The field measurement during the excavation can provide timely feedback on the performance of the excavation, but it is unable to predict what is happening in the next stage.

Numerical modelling is an effective way to investigate the performance of deep excavations, but careful calibration is required before it can be appropriately applied for predictions. A significant amount of numerical analyses have been conducted on deep excavations, but these analyses are usually simplified, for example, by adopting 2D analyses. Although simple, the traditional two dimensional analyses (e.g. plane strain and axisymmetric analysis) rely on simplifying assumptions, and therefore the information they can provide is limited and sometimes misleading. In reality all geotechnical problems involving retaining structures are three dimensional, and ideally three dimensional analyses, fully representing the structure's geometry, loading conditions and variations in ground conditions across the site, should be undertaken. Moreover,

comparison with field observations shows that successful prediction requires consideration of the small-strain nonlinearity of the soil. Therefore, advanced constitutive models for soils are desired and the input parameters should be calibrated with high-quality soil testing including the measurement of small-strain stiffness properties. Meeting all these entire requirements poses many challenges to practical engineers and researchers. Consequently, limited data have been reported in the literature presenting a fully three dimensional finite element analysis of the performance of deep excavations.

1.3 Advantages of advanced numerical analysis

The advances of sophisticated computer hardware and software have resulted in the application of advanced numerical analysis to geotechnical problems, like deep excavations. Advanced numerical analysis, largely based on finite element analysis, is able to satisfy all the theoretical requirements (e.g. stability, equilibrium, and constitutive relations), include a realistic soil constitutive model, incorporate proper boundary conditions, consider complex construction sequences, and account for the effects of time on the development of pore water pressures. The analysis allows the complete history of the boundary value problem to be computed and provide information on all design requirements.

The application of inexpensive but sophisticated numerical modelling has resulted in considerable advances in the analysis and design of retaining structures, especially in the prediction of the performance in serviceability conditions and the mechanisms of soil-structure interaction.

However, it should be noted that advanced numerical analysis can be complex when applied to geotechnical problems. It requires a deep understanding of soil mechanics, constitutive modelling and nonlinear numerical methods, as well as familiarity with the algorithms implemented in the software to be employed for the analysis (Potts and Zdravkovic 2001).

1.4 Objectives and practical implications of this research

The objective of this research is to gain insight into the mechanisms of soil-structure interaction in deep excavations through advanced finite element analyses and calibration with field data from well-documented case histories. The finite element model developed is shown to capture the main features of the performance of completed deep excavations with a moderate level of complexity. The influence of several important aspects in deep excavations is investigated through parametric studies on a simplified square excavation and detailed analyses of two complex case histories collected from Shanghai. Although the methods in this thesis can be used for more general purposes, the research is concentrated on deep excavations constructed using the top-down method in Shanghai soft ground.

The research in this thesis is expected to have practical implications on the design, construction, and research in deep excavations. The ultimate purpose is to evaluate the capability of advanced finite element analysis in replicating various aspects of observed performance in the field through calibration with field data, and provide confidence in the use for prediction purposes. Accurate predictions of the performance of deep excavations are important criteria in the design and analysis of the retaining structures. Predictions conducted during the design process can be used to verify the feasibility of a certain construction scheme, and optimise the construction sequence. The findings and lessons learnt from numerical analyses are inspirations and motivations for the research.

1.5 Structure of the thesis

Chapter 1 describes the background of deep excavations, limitations of previous and current research, the advantage of advanced numerical analysis, and objectives of this research and practical implications.

Chapter 2 reviews the previous studies and recent progress in the analysis of deep excavations, including the theoretical and empirical methods, laboratory tests and field observations, and numerical analyses. Special attention is given to the field measurements which reflect the real

excavation behaviour, and numerical analyses which are effective in the investigation of various aspects in deep excavations.

Chapter 3 describes the modelling procedures using advanced finite element analysis of deep excavations based on the commercial software ABAQUS, and addresses various important aspects which should be considered in the analysis. A multiple yield surface soil model and the derivation of input parameters for Shanghai clay are also included in this chapter.

In Chapter 4, a series of parametric studies are conducted on a simplified example of a square deep excavation with a top-down construction method. The influence of a number of important aspects in deep excavations is investigated. The parametric studies also provide useful preparatory information for the more complex case studies described in the subsequent chapters.

Based on the experience and understanding from the parametric studies in Chapter 4, a more complex deep excavation case history in Shanghai, the basement excavation for Shanghai Xingye Bank building, is investigated in Chapter 5. The computed results are calibrated with the field data, and the sensitivity of a number of parameters is investigated through parametric studies. This chapter focuses on the excavation behaviour itself in the absence of adjacent infrastructure.

Chapter 6 further extends the finite element model developed in Chapter 5 and places more focus on the performance of adjacent infrastructure that is influenced by the excavation, i.e. the settlements of adjacent buildings and buried pipelines during the excavation process.

Chapter 7 presents a different case study, based on a deep excavation case history with more complex geometry and construction sequence, the excavation for the North Square of Shanghai South Railway Station. The purpose of this study is to investigate various aspects related to the construction sequence, the earth berms, and opening accesses in the floor slabs.

Chapter 8 summarises the work of previous chapters and gives some general conclusions and recommendations for possible future work.

Appendix A and B include the relevant field data for the two case histories analysed in this thesis. These data are collected from Xu (2007) who did the field measurement and analysed the data in his PhD thesis.

Chapter 2 Literature review on deep excavations

2.1 Introduction

The deep excavation is a complex subject in geotechnical engineering and has been studied using various methods, e.g. theoretical and empirical methods, laboratory tests, field measurements, and more sophisticated numerical analysis. However, all these methods have their limitations, although they have contributed in various degrees to the understanding of the performance of deep excavations. Some of these methods are reviewed and discussed in this Chapter. Emphasis, however, is put on the various aspects of observed performance of deep excavations in the field and the capability of finite element analysis to replicate these observed behaviours.

2.2 Theoretical and empirical methods

Theoretical and empirical methods provide some basic understanding of the performance of deep excavations in a different way, but they also have limitations due to their simplicity and assumptions. Some of these methods are reviewed in this section.

2.2.1 Classical earth pressure theory

The design of retaining walls requires the evaluation of active earth pressure which is largely based on the classic solutions of lateral earth pressure provided by Coulomb (1776) and Rankine (1857). Coulomb (1776) first studied the earth pressure problem using the limit equilibrium method to consider the stability of a wedge of soil between a retaining wall and the failure plane. It is well verified for the frictional soil in active state, but is not the case for either the cohesive soil or for the passive state. The point of application of active thrust is assumed at a distance of one-third of the height of the wall from its base and independent of various parameters such as soil friction angle, angle of wall friction, backfill angle, and wall inclination angle. Rankine (1857) presented a solution for lateral earth pressures in retaining walls based on the plastic equilibrium. He assumed that there is no friction between the retaining wall and the soil, the soil

is isotropic and homogenous, the friction resistance is uniform along the failure surface, and both the failure surface and the backfilled surface are planar. Caquot and Kerisel (1948) presented tables of active earth pressure coefficients derived from a method which directly integrates the equilibrium equations along the combined planer and logarithmic spiral failure surface. They included the friction factor between the retaining wall and the soil, and assumed a curved failure surface which is recognised to be very close to the actual failure surface. The active and passive coefficients were developed for cohesionless soils, but they can be used for evaluating long-term conditions in cohesive soils where complete dissipation of pore water pressure occurs.

These classical earth pressure theories and their further development form the basis of earth pressure calculations used today, but they are only applicable under certain conditions to estimate roughly the earth pressures on the wall. Moreover, they do not consider the construction process and give no indications on the wall deformations and ground movements in the more complex braced deep excavations.

2.2.2 Stability analysis

Stability analysis is important in the design of retaining structures in clay, and is normally conducted using limit equilibrium methods or finite element methods. Limit equilibrium calculations are usually carried out in the design and involve assuming the classical active and passive earth pressure distributions on the back and front of the wall and taking moments about the position of the prop.

Terzaghi (1943) suggested a mechanism consisting of a soil column outside the excavation which creates a bearing capacity failure. The failure is resisted by the weight of a corresponding soil column inside the excavation and also by adhesion acting along the vertical edges of the mechanism. Bjerrum and Eide (1956) assumed that the base of the excavation can be treated as negatively loaded perfectly smooth footing, and collected information on total or partial failure cases to analyse the basal heave failure of deep excavations in soft clays. The calculated factor of safety is shown to be below 1.0 for the cases where failure occurred, and just above 1.0 for the

cases where partial failure occurred or no failure was observed. Clough and Hansen (1981) further considered the strength anisotropy of the clay in the expression of factor of safety proposed by Terzaghi (1943), and suggested that the basal heave factor of safety defined in isotropic soil would overestimate the factor of safety for an anisotropic soil, and this effect becomes more important as the degree of anisotropy increases. O'Rourke (1993) further modified the basal stability calculations to include flexure of the wall below the excavation level, and assumed that the embedded depth of the wall does not change the geometry of the basal failure mechanism. However, an increase in stability was anticipated due to the elastic strain energy stored in flexure. This gave stability numbers that were functions of the yield moment and assumed boundary conditions at the base of the wall.

However, the limit equilibrium approach does not consider the initial stress state in the soil, the type of retaining structures, the construction methods, and soil and wall movements.

2.2.3 Stress path method

The soil behaviour depends not only on the current stress state, but also on the stress history. The removal of soil in deep excavations mainly results in a decrease of the vertical stress in the soil inside the excavation and a loss of lateral constraint for the soil on the retained side. As the excavation behaviour is influenced by the stress state of the soil, understanding the stress paths in the field during the excavation process is necessary to identify critical elements influencing the shear strength and determine appropriate strength and stiffness parameters through laboratory tests for design and analysis. The stress path method (Lambe 1967) provides an rational approach to understand the variations of effective stress in the soil elements at some typical locations caused by both horizontal and vertical stress relief during the excavation.

Ng (1999) interpreted the field stress paths adjacent to a diaphragm wall during a deep excavation and compared with some relevant laboratory triaxial stress path tests. It was found that the field effective stress paths in front of the wall are similar to the laboratory stress paths in undrained extension tests, whereas field stress paths behind the wall do not correspond well with

those from laboratory undrained compression tests. The possible reason is that the soil at the soil-wall interface had already reached, or was close to, the active condition after wall installation, resulting from a substantial horizontal stress relief during the wall construction. This may indicate that the conventional undrained assumption does not hold for the soil located immediately behind the wall during a relatively rapid excavation in stiff clay.

Hashash and Whittle (2002) used nonlinear finite element analysis to interpret the evolution of lateral earth pressures acting on the well-braced diaphragm walls for deep excavations in clay and explain the soil arching mechanism. It was demonstrated that the stress path experienced by a soil in front of the wall at the final excavation level follows a typical path of plane strain passive mode of shearing, whereas the soil elements behind the wall on the retained side follow more complicated stress paths due to rotations of the principal stress directions and reversal in shear direction caused by the soil arching mechanism. Results also showed that lateral earth pressures can exceed the initial stresses at elevations above the excavated grade, producing apparent earth pressures higher than those anticipated from empirical design methods (Peck 1969).

2.2.4 Empirical methods

Empirical methods are used to interpolate the performance of deep excavations from the analysis of previous published field data in different areas of the world and local experiences.

Terzaghi (1943) suggested that the average earth pressure is approximately uniform with depth and has small reductions at the top and bottom of the wall based on field measurements. Terzaghi and Peck (1967) proposed the apparent earth pressure envelopes based on field measurements from various locations for predicting maximum strut loads in a braced excavation. However, these diagrams do not represent the real distribution of earth pressures at any vertical section in an excavation, and this method has been evaluated by many different researchers such as Wong, Poh et al. (1997), Charles (1998), and Hashash and Whittle (2002).

Peck (1969) summarised the ground surface settlements from field measurements of deep

excavations in different areas of the world and classified the settlement curve into three zones depending on the type of soil and workmanship, and this method was expected for rough estimates of ground surface settlements under various conditions. However, the general description of settlement curves neglects important factors such as soil conditions, wall installation methods, types of retaining structures, and the construction sequence. In addition, these case histories are prior to 1969, and the excavations are supported by flexible sheet piles or soldier piles with lagging which result in much larger ground movements than those supported by much stiffer diaphragm walls with top-down construction methods. Consequently, it is difficult to use this empirical method for the prediction of a particular deep excavation project. Clough and O'Rourke (1990) suggested that the settlement profile is triangular for an excavation in sandy soil or stiff clay with the maximum ground settlement occurring at the wall. Non-dimensional profiles show that the corresponding settlement extends to 2 and 3 times the excavation depth for sandy soil and stiff to very hard clays, respectively. For an excavation in soft to medium clay, the maximum settlement usually occurs at some distance from the wall, and a trapezoidal shaped settlement trough was proposed. The influence zone extends up to 2 times the excavation depth. Hsieh and Ou (1998) generalised the ground settlement profiles into two types (i.e. the spandrel type and the concave type) and proposed an empirical method for predicting these two types of settlement profiles based on regression analysis of the field observations. They divided the settlement profiles into the primary influence zone which extends to 2 times of the excavation depth, and the secondary influence zone which extends to 4 times the excavation depth. The maximum ground settlement occurs approximately at half of the excavation depth behind the wall, and the settlement at the wall is about half of the maximum ground settlement. This empirical method may be used for prediction of ground surface settlement profiles, but the accuracy of the prediction depends on a number of factors such as soil profiles, retaining systems, and construction methods. Kung, Juang et al. (2007) developed a semi-empirical model to determine the maximum wall deflection and ground surface settlement

caused by a braced excavation in soft to medium clays, based on database of 33 case histories and results from a large number of finite element analyses. The developed model mainly consists of three components to estimate the maximum wall deflection, the deformation ratio between maximum lateral wall deflection and maximum ground surface settlement, the maximum ground surface settlement, and the ground surface settlement profile. Regression-based equations were used to analyse the relationship of the input variables which may affect the maximum wall deflection and the deformation ratio. Model bias was assessed, and precision of this model was regarded to be high enough for practical application. The proposed model was verified using case histories not used in the development of the model.

Mana and Clough (1981) correlated the normalised maximum observed wall movements over the excavation depth with the factor of safety against basal heave by Terzaghi (1943), based on the analyses of several case histories in soft to medium clays. The constant non-dimensional movement at high safety factor is an indication of a largely elastic response, whereas the rapid increases in movements at lower factor of safety are result of yielding in the subsoil. Upper and lower limits were suggested for estimating the expected wall movement. Wong and Broms (1989) propsosed a simple procedure to estimate the lateral deflection of strutted or anchored sheet-pile walls in clay with average to good workmanship. The procedure was developed based on an assumption that the walls are flexible and the lateral deflections are governed by plastic yielding of the soil below the bottom of excavation. No net volume changes were assumed during the excavation, and the volume corresponding to the ground settlement is equal to the volumes associated with the heave and the lateral wall displacement above the bottom of excavation. The excavation width, excavation depth, and secant or tangent moduli of the soil were included in the analysis. Clough, Smith et al. (1989) proposed a semi-empirical procedure to estimate wall movement induced by excavation in clay. The maximum lateral wall deflection is evaluated relative to factor of safety against basal heave by Terzaghi (1943) and system stiffness. The derived curves are based on average condition, good workmanship, and the assumption that

cantilever deformation of the wall contributes only a small fraction of the total movement.

2.3 Laboratory tests and field measurements

The performance of deep excavations has been studied through both laboratory tests and field measurements by a number of researchers, and the main findings are summarised in this section.

The advantage of laboratory tests is that factors influencing the results may be controlled quantitatively. Small-scale centrifuge model tests have been used in an attempt to gain a coherent view of the soil-structure interaction behaviour of deep excavations (Bolton and Powrie 1987, Bolton and Powrie 1988, Bolton and Stewart 1994, Richards and Powrie 1998, Takemura, Kondoh et al. 1999). Centrifuge modelling provides a correctly scaled physical model to enable the prototype behaviour of excavation so that it can be effectively used to investigate soil deformation mechanisms during the excavation process. The tests can be repeated and continued until failure, which is not possible in the full scale projects. Moreover, the tests are time-efficient and can observe the long-term behaviour of a geotechnical construction in soil of low permeability over a reasonably short period of time. However, it should be noted that centrifuge testing has its limitations and the conditions it can model are relatively simple.

Field measurement is an effective method, but it is also expensive and takes a long time to obtain the data, and this process is not repeatable. A number of case histories of deep excavations have been reported worldwide with well-documented field data, e.g. in the UK (Skempton and Ward 1952, Wood and Perrin 1984, Simpson 1992), in Chicago (Wu and Berman 1953, Finno, Atmatzidis et al. 1989, Finno and Nerby 1989), in Shanghai (Liu, Ng et al. 2005, Xu 2007, Wang, Xu et al. 2010, Liu, Jiang et al. 2011, Ng, Hong et al. 2012), in Singapore (Wong, Poh et al. 1996, Lee, Yong et al. 1998), in Hong Kong (Leung and Ng 2007), and in Taiwan (Ou, Hsieh et al. 1993, Ou, Liao et al. 1998, Ou, Shiau et al. 2000). These case histories vary from one to another in geological conditions, retaining structures, and construction methods, which make the correlation and comparison difficult, but generally they recorded the main excavation behaviour,

e.g. wall deformations, ground movements, earth and pore water pressures, strut loads and wall bending moments, and deformation of adjacent infrastructure. Therefore, they provide valuable resources for understanding the more comprehensive behaviour of deep excavations, and also for calibrating the numerical analyses.

2.3.1 Wall deformation

The wall deformation (i.e. lateral deflection and vertical movement) is the major concern in deep excavations and is monitored in most field measurements. The pattern and magnitude of the wall deformation are influenced by a number of factors, e.g. the soil condition (e.g. stiffness, strength, anisotropy, and creep), the support system (e.g. stiffness, connections, and thermal effects), and construction methods (e.g. top-down, bottom-up, and cut and cover).

The wall deflections are normally measured with inclinometers, but the readings need to be adjusted to be consistent with the surface survey, because inclinometers usually only record the deflection pattern of the wall by assuming no displacement at the toe of the wall. In practice, however, a non-zero displacement at the toe of the wall is confirmed from both field measurements and numerical analyses (Simpson 1992).

There are several general trends from the observed wall deflection:

1) The wall deforms as a cantilever deflecting inwards the excavation prior to the installation of the first level of props.
2) The deflection is bulging after the installation of the first row of props as a result of the rotation of the wall about the prop position and of bending deformation, and the magnitude increases as the excavation proceeds.
3) The largest wall deflection occurs around the excavation level.
4) The wall translates horizontally with displacement at the toe of the wall.
5) The maximum wall deflection depends on various factors such as the soil properties (e.g. stiffness, and strength), the type and stiffness of the retaining system (i.e. the retaining wall, and the bracing structure), and the construction method (e.g. top-down, bottom-up,

and open-cut).

6) The progressive wall deflection observed during the no construction period may be caused by the dissipation of pore water pressure, but the increment is small compared to that induced by the excavation.
7) The wall deflection is smaller close to the wall corner than that close to the wall centre due to the corner effect.

The ratio of H_m/H, where H_m is the depth of the maximum wall deflection and H is the excavation depth, was observed to be approximately 1.0 for excavations in Taipei clay (Ou, Hsieh et al. 1993), and slightly larger than 1.0 in Shanghai clay (Liu, Ng et al. 2005). However, this ratio varies a lot (between 0.5 to 1.4) from one case to another and depends on the soil properties and type of the retaining structures as observed by Wang, Xu et al. (2010). It was also found to be affected by overexcavation (Tan and Wei 2011).

The wall deflections continue after the excavation reached the formation level, but at a reduced rate, probably due to the dissipation of pore water pressure (Liu, Ng et al. 2005). Large incremental wall deflections occur during the inefficient support period. The wall deflections increase during the structure installation process, which may be attributed to the shrinkage of the bracing concrete floor slabs. Sometimes larger than expected wall deflection were observed, which can be caused by many factors, such as overexcavation, long construction duration, or large exposure period without support (Tan and Wei 2011). The wall movement may increase with time while the excavation depth remains unchanged, due to the soil creep and excess pore water pressure dissipation during a long construction period (Ou, Liao et al. 1998), but the creep effect is not evident in Shanghai clay during 60 days of observation (Liu, Ng et al. 2005). Temporary earth berms at the front of a cantilevered wall reduce soil movements effectively but are often uneconomical because of the need to remove the berms successively in short lengths and small volumes (Puller 2003).

The vertical wall movement during construction was observed to involve significant heave (5mm

to 21mm) rather than settlement (Wood and Perrin 1984, Finno, Atmatzidis et al. 1989, Tan and Wei 2011). This may be attributed to two factors: (i) the elastic and plastic rebound of the basal soils inside the excavation due to stress relief, and (ii) movement of the soil close to the retaining wall. However, the heave can be stopped by the installation of floor slabs, and settlement is also observed (Xu 2007), which indicates the complexity of this soil-structure interaction system. The wall deflections are also influenced by the stiffness and strength anisotropy of the natural clays (Clough and Hansen 1981). Long term field measurements have shown that seasonal variation of movements at the top of the wall and wall lateral deflections which increase in winter and reduce in summer (Symons and Tedd 1989).

2.3.2 Ground movement

Ground movement is inevitable in deep excavations, and its magnitude depends on various factors such as soil properties, type of the retaining systems, excavation geometry, construction sequence, and workmanship. Excessive ground movement will cause damage to adjacent infrastructure. Therefore, understanding the characteristics of ground movement is essential in the design of deep excavations, and to take measures to mitigate the adverse impact on adjacent infrastructure.

As discussed earlier in this chapter, the ground surface settlement profile has been studied by several researchers such as Peck (1969), Clough and O'Rourke (1990), and Hsieh and Ou (1998), and various empirical methods have been proposed to generalise the settlement profile and to estimate the excavation-induced ground settlement. Although simple to use, these empirical methods have limited applications because they only represent ground settlements in a direction perpendicular to the retaining wall, and cannot account for the specific ground conditions, excavation geometry, details of the retaining system, and construction sequence in a particular deep excavation project. It is therefore, more important to understand the characteristics of the ground movement from various aspects observed in the field measurements and laboratory tests.

Significant ground movement has been observed during the construction of diaphragm wall

panels and bored piles, as well as during the dewatering process (Farmer and Attewell 1973, Burland and Hancock 1977, Simpson 1992, Charles 1998, Ng, Rigby et al. 1999, Finno and Roboski 2005, Richards, Clark et al. 2006, Finno, Blackburn et al. 2007, Xu 2007). The ground surface settlement in this period can account for up to 40% of the total ground settlement during the whole construction period in deep excavations in Shanghai (Xu 2007) and approximately 30% of the field measurements in London (Tedd, Chard et al. 1984). The horizontal ground surface movements (towards the wall) are generally larger than the vertical surface movements and extended further from the wall (Tedd, Chard et al. 1984). The soil lateral displacement close to the soil-wall interface in the slurry trenching process generally decreases with depth, and slightly recovers during concreting process (Ng, Rigby et al. 1999). Powrie and Kantartzi (1996) observed in centrifuge model tests that both the magnitude and extent of ground movements decrease as the length of the wall panel is reduced during the diaphragm wall installation process. Both settlement and heave were observed in the sublayer of the ground outside the excavation through the measurement from magnetic extensometers (Tedd, Chard et al. 1984, Wood and Perrin 1984).

The ground movements increase in the subsequent excavation process and installation of horizontal support structures. Most field measurements observed settlements at the ground surface in the retained area during the excavation process, and the settlement stabilised quickly following the casting of base slabs. Larger than expected settlements at the ground surface was observed as a result of overexcavation. The largest incremental ground movements occurred when the excavation was approximately half completed. On the contrary, ground heave was observed inside the excavation, caused by stress relief due to the soil removal and swelling as negative excessive pore water pressure dissipated (Tedd, Chard et al. 1984) and the inward movement of the wall. Centrifuge tests showed that the ground movement is restrained by increasing the embedment depth of the retaining wall without increasing the wall stiffness (Richards and Powrie 1998). It is also found in centrifuge tests that it is difficult to recover the

ground settlements and wall deformations once they occur by increasing the strutting force (i.e. preloading), due to the nonlinear behaviour of the soil (Takemura, Kondoh et al. 1999). The ground movements and wall deflection can be reduced by improving the soil in front of the wall inside the excavation, and with earth berms (Lim, 2003).

The distribution of ground movements outside the excavation is actually three dimensional, and is affected by the geometry of the excavation. Finno and Roboski (2005) presented the ground surface movement contour around the excavation observed from a tied-back excavation in clay, and showed that both the vertical and lateral movements tend to follow a bowl shape with the maximum movement near the middle of the excavation and smaller movement near the corner, providing clear evidence of the corner effects.

2.3.3 Earth and pore water pressure

The understanding of the performance of deep excavations can be improved if more knowledge is known of the original in-situ stresses within the soil, and the changes of earth and pore water pressure during the construction.

Tedd, Chard et al. (1984) conducted an extensive instrumentation of a propped embedded retaining wall at Bell Common Tunnel in London, and presented the variation of earth and pore water pressure during the construction period. The total horizontal stress in the ground close to the wall decreased during the wall installation, and the net reduction in total horizontal stress 0.6m behind the wall in London Clay was 3 to 4 times greater than the reductions measured 3m and 6m from the wall. The horizontal total and effective stress slightly recovered after the wall installation but continued to decrease at the back of the wall in the subsequent excavation process, and these reductions were greater near the surface and close to the wall. Excavation also caused significant reductions in total stress in front of the wall which was entirely due to a drop in pore water pressure, and there was a slight increase in effective horizontal stress, which may be expected from the lateral movement of the wall. When the roof structure was being constructed, the total horizontal stresses on both sides of the wall were virtually constant, but

there was a gradual increase in pore water pressure in front of the wall and to a smaller extent at the back of the wall.

The initial in situ pore water pressure is often observed close to the hydrostatic state, and this assumption is normally used in the design. However, the pore water pressure may change during the wall/pile installation and excavation process, as well as the dewatering and drainage. Powrie and Kantartzi (1996) observed in centrifuge model tests that the pore water pressure reduced during slurry trenching and increased during concreting in the diaphragm wall installation process. However, the net change of pore water pressure during these two processes is small, indicating that the initial ground water conditions may reasonably be taken for the subsequent excavation analysis in which the wished-in-place wall installation method is used. Ng, Rigby et al. (1999) observed in the field measurement of a short diaphragm wall panel installation in Hong Kong that the pore water pressures at the soil-wall interface resemble hydrostatic conditions after concreting. Finno, Atmatzidis et al. (1989) reported that the measured pore water pressure outside the excavation rose sharply at the stage of sheet-pile driving, but these excess pore pressures partially dissipated prior to the start of the excavation, and dissipated rapidly during excavation as a result of gradual unloading, and little net change in pore pressures was observed at the end of construction. Richards, Clark et al. (2006) also found that the pore water pressures fell during the bored pile wall excavation and increased during concreting, and the magnitude of the changes decreased with increasing distance from the pile, but overall the pore water pressures rapidly returned to their in situ values on completion of the process. In general, deep excavations result in a decrease of the total mean stress and an increase of the deviator shear stress in the adjacent ground. In saturated normally consolidated or lightly overconsolidated clays, the decrease of the total mean stress induces negative excess pore pressures whereas the increase of shear stress gives rise to positive excess pore pressures. Therefore, the excess pore pressure at the end of construction might be positive or negative. However, long term field measurements showed only very small changes in pore water pressure

after the excavation (Symons and Tedd 1989).

The wall installation process would reduce the horizontal effective stresses in the surrounding ground to below their in situ values (Gunn and Clayton 1992, Symons and Carder 1992), and change the recent stress history of the soil and hence its subsequent stress-strain response in the following excavation (Powrie, Pantelidou et al. 1998). The earth pressures at the soil-wall interface are close to the hydrostatic bentonite pressures during the slurry trenching process for the diaphragm wall panel installation. Lings, Ng et al. (1994) proposed a theoretical bilinear pressure envelope for predicting lateral pressures developed at the soil-wall interface during concreting in a diaphragm wall panel, based on field observations and theoretical considerations. According to Finno and Nerby (1989), installing the sheet-pile wall would cause in situ stresses to be different than K_0 conditions prior to the start of the excavation, and this effect alters subsequent response mainly by reducing available shear resistance for passive loadings and the stiffness on the passive side of the excavation, which contributes to large movements below the base of the excavation.

2.3.4 Prop loads and wall bending moments

The prop loads can be computed from strain gauge measurements prior to installation and changes from the initial values, but corrections are needed to account for the difference of the thermal expansion/contraction of the structural member and gauge wire (Finno, Atmatzidis et al. 1989, Stroud, Hutchinson et al. 1994).

The bending moment (M) of the diaphragm wall can be calculated through the measurements from the reinforcement bar strain gauges, assuming that the variation of stresses over a cross section of the wall is linear and the neutral axis lies along the centre of the wall. Alternatively, the bending moment can be computed from the curvature (κ) of the wall deflection curve using the equation $M = EI \cdot \kappa$, where EI is flexural rigidity. Ou, Liao et al. (1998) found that the bending moment computed from the reinforcement bar strain gauges are generally smaller than that from the wall deflection curve, particularly for the location in the neighbourhood of the

maximum lateral wall deflection, and they explained that the bending moment from the wall deflection curve is computed without considering cracking of concrete, so that the moment of inertia of the wall *I* has not been reduced.

The prop loads and wall bending moments gradually increase as the excavation proceeds, and may slightly decrease after the excavation is completed, due to dissipation of excess pore water pressure. The negative wall bending moment (towards the excavation) is also influenced by the prop loads. Increasing the embedment depth of the retaining wall will lead to an increase in wall bending moment and a reduction in bottom prop load, as shown in centrifuge tests (Richards and Powrie 1998). Results also suggested that the prop loads and bending moments are influenced by the in-situ lateral earth pressure, the soil properties, the geometry and depth of the excavation, construction sequence, and the change of water table level behind the retaining wall (Bjerrum, Clausen et al. 1972).

Temperature effects on the prop loads are important in propped excavations. Perturbations in the axial prop loads were observed which may be attributed to changes in ambient temperature (Wood and Perrin 1984). However, thermal effects are unlikely to have any significant effect on temporary steel props supporting comparatively low flexibility walls. A seasonal variation of bending moment in the retaining wall has been observed in the field measurements, which is probably a result of the thermal expansion and contraction of floor slabs in summer and winter (Symons and Tedd 1989). Boone and Crawford (2000) observed a direct correlation between incremental changes in strut load and temperature during the course of a braced excavation. Blackburn and Finno (2007) found that the internal thermal stresses in the support components composed up to 40% of the total support load.

2.3.5 Deformation and damage of adjacent infrastructure

The excavation induced ground movements may cause deformation and damage in the adjacent infrastructure, e.g. buildings, tunnels, buried pipelines, pile foundations, highways, and bridges. It is important to understand the response of this infrastructure induced by the ground movement,

and to assess properly the damage in the infrastructure caused by excavations. Emphasis here is placed on the response of buildings and pile foundations to excavation-induced ground movement, and the criteria to evaluate the building damage.

Ou, Liao et al. (2000) presented the building responses and ground movements induced by an excavation using the top-down construction method in Taipei. They concluded that the building performance during the excavation may be affected by factors such as the type and size of foundation, the geometry of the excavation, and the shape of the settlement profile. A building near a relatively short excavation side may experience smaller inclination than if it is near a long excavation side. They also suggested that information regarding a building's location relative to the settlement influence zone is helpful in planning building protection measures during excavation. Finno and Bryson (2002) found that the settlement of a building outside the excavation follows the development of lateral movement of the soil and the secant pile wall as a result of undrained deformations in saturated clay, and the reduction of wall stiffness and creep also resulted in larger building settlement. Blackburn and Finno (2007) observed tilts of the adjacent buildings on shallow foundations and found that the buildings tilt towards the excavation as a rigid body due to the rigid connection between the wall and underlying strip footing. Only minor diagonal shear and vertical tensile cracks were detected in the external stone and mortar facades of the external bearing wall, and these cracks occurred at locations where the largest distortions were observed. The vertical cracks in the external wall occurred at the transition point between the flat and sloped settlement distribution which also coincided with a change in footing type and footing elevation. Xu (2007) reported the settlement of adjacent buildings and buried pipelines close to a basement excavation in Shanghai soft clay during the whole construction period. Results indicated that the settlement during the diaphragm wall and pile installation process accounted for up to 40% of the total settlement in the whole period. The buildings settled unevenly, which may be related to the stiffness of the building and the relative location to the excavation. The settlement is larger close to the centre of the diaphragm wall and

smaller around the corner of the excavation. The settlements of buildings also depend on the type of the structures and foundations. For example, reinforced concrete high-rise buildings resting on deep foundations experienced much smaller and more uniform settlements than masonry buildings supported by shallow foundations, as observed by Tan and Wei (2011).

Pile foundations may be adversely affected by nearby deep excavations because the lateral loads imposed by the soil movement induce bending moment and deflection in the piles which may lead to structural distress and failure. Finno, Lawrence et al. (1991) described the performance of groups of step-tapered concrete piles (either unreinforced or lightly reinforced) adjacent to a 15m deep tieback excavation in primarily granular soils. The pile caps are as close as 0.6m to the sheet-pile wall. The observed movements of several of the pile caps were as large as 76mm towards the excavation, which was twice as large as expected for excavations under similar conditions because of the 6m unsupported height of wall before placing the first level of tiebacks. The piles essentially deformed with the soil because they are relatively flexible compared to the soil. Finite element analyses indicated that the actual moments in the piles were not large enough to cause cracking, and the lateral or axial load capacity of the main pile groups was not significantly affected. Poulos and Chen (1997) investigated the response of piles due to lateral soil movements induced by braced excavations in clay layers through numerical parametric analyses and case studies, and concluded that the key factors influencing the response of a single pile include excavation depth, excavation support conditions, and soil and pile properties. Goh, Wong et al. (2003) reported a maximum of 28mm lateral movement of a full-scale instrumented bored pile (1m in diameter and 46m long) which was 3m behind a 0.8m thick diaphragm wall in a 16m deep excavation for a cut-and-cover tunnel in Singapore marine clay. Leung, Chow et al. (2000) found in the centrifuge model tests on a single pile foundation adjacent to a unstrutted deep excavation in dense sand that the induced pile bending moment and deflection decrease exponentially with increasing distance to the wall. Leung, Lim et al. (2003) conducted centrifuge tests on free-head and capped-head pile groups adjacent to an unstrutted deep excavation in sand,

and found that when two piles are arranged in a line perpendicular to the wall, the front pile would reduce the detrimental effect on the rear pile, whereas when they are arranged in a row parallel to the retaining wall, the interaction effect is insignificant. It was also found that the pile cap has a significant influence on the behaviour of the pile group, and the induced bending moment decreases as the number of piles increases. Moreover, the interior piles of the pile group always experience lower bending moments than those of the peripheral piles.

The evaluation of settlement-induced building damage has been discussed by several researchers. Skempton and McDonald (1956) addressed the importance of knowledge on the allowable settlements of buildings for rational foundation design based on observations on actual buildings. They correlated the deflection ration of the structure with angular distortion. Damage was defined as initiation of visible cracking, and was related to angular distortion, maximum and differential settlements. Allowable settlements and distortions were suggested for design based on the results of a survey of existing data on 98 buildings with no damage or damage in varying degree as a consequence of settlements. However, the available data is restricted almost entirely to load-bearing wall structures and to steel or reinforced concrete frame buildings with panel walls of brick or similar construction. Burland and Wroth (1974) modelled a building as a deep isotropic beam to relate strains in the building to the imposed deformations. Tensile strain served as the limiting criterion for visible crack development when used with an elastic analysis of the building. The limiting relative deflections of masonry and brick walls were related to critical tensile strains for varying length to height ratios and building stiffness. They suggested that for sagging type deformations, the neutral axis is located at the middle of the beam, whereas for hogging, the foundation and soil provide significant restraint to deformations, in an effect moving the neutral axis to the bottom of the beam. The limiting deflection ratio was related to maximum bending strain and maximum diagonal tensile strain for a linear elastic beam subjected to a point load with the neutral axis at either the centre or bottom of the beam. The effects of a building that is not adequately represented by an isotropic elastic beam are accounted for by

varying the ratio of Young's modulus to shear modulus for the beam, depending on the type of structure. Boscardin and Cording (1989) extended this deep beam model to include horizontal extension strains caused by lateral ground movements induced by adjacent excavations. A chart relating the deflection ratio and horizontal strains to levels of damage was developed for buildings with brick, load-bearing walls undergoing a hogging deformation with the neutral axis at the bottom. They defined categories of damage based on combinations of angular distortion and horizontal strain and compared recorded cases of damage with damage predicted based on their classification system. They noted that the effect of the horizontal strains depends on the lateral stiffness of a structure. For instance, a framed structure would be affected more by horizontal ground strains than a structure with reinforced concrete walls supported by continuous footings or with stiff floor systems. Direct transfer of horizontal ground strain to the structure is assumed in this approach, with no slip at the interface between the structure and the ground. However, when the ground displaces laterally, relative slip will occur at the foundation level, and the horizontal displacement in the building will be less than that in the ground, as discussed by Geddes (1991). Therefore, this method is likely to be conservative, and may exaggerate the horizontal strain in the structure and lead to unnecessary restriction on the extent of the tolerable vertical differentials.

Boone (1996) proposed a concept for evaluation of building damage resulting from differential ground movement based on consideration of more comprehensive governing factors such as flexural and shear stiffness of building sections, the nature of ground movement profile, location of the building within the settlement profile, degree of slip between the foundation and ground, and building configuration. He used crack width as an indicator of damage severity and defined severity in terms of tensile strains from bending, elongation of the ground, and direct lateral extension. Finno, Voss et al. (2005) presented a laminate beam method of evaluating potential building damage due to excavation-induced ground movements. The method assumes that the floors restrain bending deformations and the walls, whether load bearing or in-fill between

columns, resist shear deformations. Closed form equations are used to relate bending and shear stiffness to normalised deflection ratios. The proposed model was shown to adequately represent the response of a three-story framed structure which was affected by an adjacent deep excavation.

2.4 Numerical modelling

Numerical modelling is an effective way to investigate the soil-structure interaction mechanisms in deep excavations, and has the ability to provide all the required information for design purposes. Some of the numerical modelling processes are described in this section, and the main findings are also summarised.

2.4.1 Model details and simulation process

2D simulations (i.e. plain strain, and axisymmetric analysis) have been widely used to approximate real deep excavations in the design process and for research purposes (Clarke and Wroth 1984, Hubbard, Potts et al. 1984, Potts and Fourie 1984, Finno, Harahap et al. 1991, Powrie and Li 1991, Simpson 1992, Whittle, Hashash et al. 1993, Hashash and Whittle 1996), due to the limitation of software capabilities and computational resources available. However, the limitations of 2D analyses should be recognised, and fully 3D analyses are required if necessary. For instance, 2D analysis is not able to consider the corner effects in deep excavations, which indicate that the wall deformation and ground movement are smaller close to the wall corner than around the wall centre. In addition, 2D plain strain analysis tends to overestimate the wall deflection and ground settlement behind the wall compared to the simplified 3D symmetric square or rectangular analysis (Ou, Chiou et al. 1996, Lee, Yong et al. 1998, Finno, Blackburn et al. 2007), and the difference depends on factors such as geometry of the excavation, the length to depth ratio, the stiffness of the retaining system, the excavation depth, soil properties, and the factor of safety against basal heave.

Zdravkovic, Potts et al. (2005) investigated a number of issues related to the modelling of retaining structures used to support an excavation in 3D finite element analysis and compared

results with equivalent plain strain and axisymmetric modelling. Results showed that the plain strain analysis over predicts the wall deflection and ground movement compared to the 3D analysis, whereas the axisymmetric analysis is closer to the 3D analysis. Both shell elements and solid elements were used to model the retaining wall, and it was found that the wall deflection is larger when the wall is modelled with shell elements, resulting from the lack of beneficial action of shear stresses mobilised on the back of the wall. The anisotropic wall approach was used to consider the discontinuities in the retaining wall, and the wall deflection and bending moment at the wall corner is greatly improved compared to those from the isotropic wall. Analyses of rectangular excavations were conducted and 3D effects were found to be evident. Different wall depths were examined but the effect on the movements and structural forces is negligible.

The advances in hardware and software nowadays have enable the application of fully 3D analysis in deep excavations, which can include more geotechnical and structural details (e.g. ground profile, excavation geometry, retaining system, and construction sequence) and deal with large scale case studies (Hou, Wang et al. 2009, Lee, Hong et al. 2011, Dong, Burd et al. 2012, Dong, Burd et al. 2013, Dong, Burd et al. 2013). Lee, Hong et al. (2011) illustrated the application of large 3D finite element analyses to two case studies, the long trench excavation of Nicoll Highway Station, and the excavation-pile interaction in Common Services Tunnel. The geometry and distribution of retaining structures such as the diaphragm wall, the sheet pile wall, joints between diaphragm wall panels, the soldier piles, and horizontal struts, were represented properly in the analyses. The results were promising in these analyses, and the agreement with field measurement was reasonably good considering the uncertainties and complexities involved in the analysis.

In most analyses, the wall installation process was modelled by the Wished-In-Place (WIP) method which is not able to consider the installation effect on the ground movement and subsequent excavation behaviour. However, the excavation for diaphragm wall panels or bored piles is certain to result in significant in situ total stress relief which will alter the level of

horizontal total stress applied to the retained side of a wall, and can therefore be expected to influence the actual values of prop or anchor forces and of the maximum bending moment in the wall (Gunn and Clayton 1992). Substantial ground movement and reduction of in situ lateral stress have been observed in the field measurements during the construction of embedded retaining walls (Symons and Carder 1992). The installation effects of bored piles and diaphragm walls have been investigated using numerical analyses in 2D (De Moor 1994, Ng, Lings et al. 1995) and 3D (Gourvenec and Powrie 1999, Ng and Yan 1999, Schäfer and Triantafyllidis 2004). Gourvenec and Powrie (1999) found that the magnitude and extent of both lateral stress reduction and soil lateral movement in the vicinity of a diaphragm wall during construction depend on the panel length and are overpredicted in plane strain analyses, which indicates that 3D analyses are required and the panel length should be considered. Ng and Yan (1999) addressed the redistribution of horizontal stress above and below the toe of the wall through the downward load transfer mechanism, and the redistribution of horizontal stress at the edge of diaphragm wall panel via the horizontal arching mechanism, based on a 3D study using FLAC. Nonetheless, these studies did not include subsequent excavation stages and consider the effect of diaphragm wall installation on the subsequent excavation behaviour. Schäfer and Triantafyllidis (2006) compared the results from the Wished-In-Place model and the Wall-Installation-Modelled model based on the simplified 3D finite element analysis of Taipei National Enterprise Centre excavation project in Taipei basin (Ou, Liao et al. 1998), in which both the wall installation and subsequent excavation process were incorporated. They found an increase of up to 20% ground settlements and 15% wall movements generated from the WIM model than the WIP model, which is attributed to an increasing effective stress level in the adjacent ground resulting from the stepwise pouring of the individual panels in normally to lightly over-consolidated clays. Moreover, the modified earth pressure additionally caused higher strut loadings (up to 50%), and the impact was greater in a closer level of the struts to the ground. They also discussed that these results contradicted those from the excavation in highly

over-consolidated soil, because the excavation and the pouring of the wall panels in over-consolidated soil deposits with high earth pressure coefficient at rest result in a decreasing lateral effective stress in the adjacent ground, and thus smaller wall movements and lower strut loadings can be possibly expected. Arai, Kusakabe et al. (2008) performed a 3D analysis including the installation of circular diaphragm walls and subsequent soil excavation, and confirmed that the installation process changes the initial stress state in the ground and affects the wall deformation and ground movement in the subsequent excavation. Finno, Harahap et al. (1991) considered the sheet-pile installation and the subsequent excavation in 2D analysis and found that including the sheet-pile effects would change the wall deflection pattern and result in around 50% larger maximum wall deflection and 70% larger ground surface settlement compared to the analysis without sheet-pile effect. However, the sheet-pile wall installation effect may be different from the diaphragm wall installation effect.

The initial stress state in the ground prior to the construction is related to the vertical effective stress and the coefficient of lateral earth pressure at rest K_0. Potts and Fourie (1984) conducted a series of plain strain analyses of a single propped retaining wall at the top in drained condition using two values of K_0 (0.5 and 2.0), and found that the value of K_0 has a large influence on the excavation behaviour such as the wall displacements and bending moments, the prop force, the ground movements, the stress state and stress path in the soil, and earth pressure on the wall.

Potts and Fourie (1984) assumed two totally different types of construction method, excavated and backfilled, and found that the excavation behaviour was largely different. However, Arai, Kusakabe et al. (2008) reported that the sequence of soil removal inside the excavation has little effect on the performance of the excavation. Due to limited published information regarding the effect of construction sequence, the influence of construction sequence on the excavation behaviour is still unclear.

Potts and Fourie (1985) found that the wall stiffness has a large effect on the wall displacements, earth pressures on the back of the wall, wall bending moments, and prop forces. Bose and Som

(1998) reported that increasing the excavation width generates a large zone of plastic deformation, and eventually the wall deflection and ground settlement increase without altering the lateral force equilibrium on the diaphragm wall. Strut prestressing was found to affect considerably the deflection of the upper portion of the wall while virtually no significant change is evident at the bottom of the wall, and the ground settlement also reduces with the increase in the magnitude of strut prestress. Gourvenec and Powrie (2000) investigated the effect of the removal of sections of an earth berm supporting an embedded retaining wall through a series of 3D finite element analyses. For the particular wall-berm geometry and ground conditions considered in these analyses, relationships between the wall movement, the length of berm section removed, the spacing between successive unsupported sections, and the time elapsed following excavation, were discussed. The results showed that, for a given elapsed time, wall movements are proportional to the length of the excavated berm section provided that the unsupported sections are sufficiently widely spaced. If the spacing between unsupported sections is reduced below some critical value, wall movements then depend on both the length of and distance between the excavated berm sections.

The dewatering and consolidation process are usually neglected in the analyses by assuming undrained conditions, but they can be considered in the analysis straightforwardly. Dewatering of the site can be simulated by controlling the pore pressures at specific locations, and consolidation can be modelled using displacement-pore pressure coupled analysis. In practice, however, the undrained assumption is usually reasonable because the permeability of the soil is small (on the order of 10^{-9}) and the construction period is relatively short (e.g. 1 or 2 years). The excess pore water pressures generated during the construction will dissipate after the completion of the construction, and drained conditions are normally assumed to represent a long-term situation in the design and analysis. Young and Ho (1994) compared the results from undrained, consolidation, and drained analyses (using Mohr-Coulomb soil model) with filed data from a braced excavation, and found that the wall deflection from consolidation analysis has

better agreement with the field measurement than that from undrained and drained analyses which provide the lower and upper limit respectively. However, these three analyses gave similar trends of wall deflections.

Conventional soil models (e.g. Mohr-Coulomb, and Modified Cam Clay) have been used frequently and extensively in the numerical analyses of deep excavations, but they tend to generate unrealistic ground movements, e.g. upward ground movement rather than settlement in the retained area outside the excavation, and larger than expected basal heave inside the excavation, because the small-strain stiffness nonlinearity is not considered in these models (Burland and Hancock 1977, Jardine, Symes et al. 1984, Jardine, Potts et al. 1986). Some successes have been achieved by using more advanced soil models with small-strain stiffness nonlinearity, e.g. the Brick model (Simpson 1992), MIT-E3 soil model (Whittle, Hashash et al. 1993), and the multiple-yield surface model (Houlsby 1999), and consequently the ground movements observed in the field can be accurately reproduced in the analysis.

Most of the retaining structures were represented as linear elastic materials for simplicity, which is generally acceptable. Thermal effects, creep, and openings in the concrete floor slabs were considered in the model by reducing the Young's modulus of the concrete (St. John, Potts et al. 1993), but actually the openings can be modelled explicitly in 3D analysis. Whittle, Hashash et al. (1993) modelled the thermal effects of the concrete floor slabs by applying extra displacement to the retaining wall, but thermal effects can also be modelled in a straightforward way in the analysis. It may not be necessary to consider creep of the concrete floor slabs in the numerical analysis, because Simpson (1992) observed little effect of the creep of the concrete floor slabs in almost five years after construction. The cracks in the concrete retaining wall were also represented by using a reduced stiffness of the material (Ou, Shiau et al. 2000).

Day and Potts (1998) investigated the effects of interface properties on the behaviour of a vertical retaining wall and the deformation of the ground around it through a series of finite element analyses. Zero thickness interface elements were used to model the boundary between

the wall and the soil. Results showed that the limiting active and passive pressure on the wall depend on the maximum wall friction angle, but not on the stiffness and dilation properties of the interface elements, whereas the dilation properties have a significant effect on the ground surface deformation. However, the influence of the interface behaviour on the performance of deep excavations has rarely been reported.

Clough and Hansen (1981) demonstrated that the strength anisotropy of the clay has large influence on the excavation behaviour due to the stress reorientation in the field, whereas the stiffness anisotropy has a relatively smaller influence on the excavation behaviour. Finno, Harahap et al. (1991) used both isotropic and anisotropic bounding surface models in the analysis, and showed that the isotopic soil model produced smaller sheet-pile wall displacement and ground settlement than the anisotropic model and underestimated the observed behaviour. Ng, Leung et al. (2004) investigated the effects of inherent stiffness anisotropy of the soil on the excavation behaviour, using a linear elastic model based on a hypothetical plane strain multi-stage excavation under fully drained conditions, but they found a relatively small difference (1-2mm) of computed ground settlement and wall deflection between the isotropic and anisotropic analyses. However, it may be worth investigating the anisotropic effects by using a more advanced soil model which can consider the stiffness and strength anisotropy of the soil, e.g. the MIT-E3 model.

2.4.2 Constitutive models for the soil, structures, and the soil/structure interface

Except for various details in the modelling process, the key issue to be addressed in capturing the main excavation {Potts, 1984 #392}behaviour is the material constitutive model for the soil, structures, and the soil-structure interface. Some of these models are summarised in this section.

Constitutive models for the soil

In deep excavations, the soil behaviour is usually within a relatively small deformation region (Mair 1993), so the pre-failure performance is more important than failure conditions. The accuracy of numerical solutions largely depends on the ability of the constitutive model to

describe soil behaviour in generalized stress and strain conditions. However, considering the complexity of soil behaviour, it is not realistic to develop a completely generalized effective stress model for all soils. For a given boundary problem, the complexity of the constitutive model should be closely tied to the major aspects of the problem (e.g., stiffness, strength, deformation, dilation, and anisotropy) to be tackled and/or the accuracy of solution which is required (Whittle 1987). Once the soil model is identified, its application in the finite element analysis requires appropriate procedures to derive the model parameters and calibrate the model through laboratory and/or field tests. A number of advanced soil models have been used in the analysis of deep excavations with certain kinds of success, and their characteristics are discussed briefly in this section.

Simpson, O'Riordan et al. (1979) developed a non-linear elastic-plastic model formulated in strain space for London Clay (the 'Brick' soil model) to consider various factors influencing the capability of the numerical analysis to capture the main behaviour of deep excavations, e.g. small-strain stiffness nonlinearity. This model can account for the effects of changes in stress paths, and reproduce the S-shaped curves which represent the small-strain stiffness behaviour of clays. The capability of the model was demonstrated by comparing with the soil behaviour in experiments and back-analysing some excavations in London Clay. Simpson (1992) made a physical analogue in which soil stiffness behaviour is represented as bricks on strings, and the degradation curve was presented in a stepwise manner.

The nonlinear elasto-plastic Mohr-Coulomb model (Potts and Zdravkovic 1999) has been widely used within the Imperial College research group to study excavation and tunnelling problems in London clay (Franzius, Potts et al. 2005, Zdravkovic, Potts et al. 2005). The nonlinear elasticity below yield surface is based on empirical equations derived from experiments on London clay (Jardine, Symes et al. 1984, Jardine, Potts et al. 1986). This is an effective stress soil model and combines the soil parameters from conventional soil tests.

The HS-Small soil model (Benz, Vermeer et al. 2009) is an extension of the Hardening Soil (HS)

model (Schanz, Vermeer et al. 1999) in PLAXIS (Vermeer and Brinkgreve 1998) and uses two additional parameters to describe the stiffness behaviour at small strain, i.e. the initial or very small-strain shear modulus G_0^{ref}, and the shear strain level $\gamma_{0.7}$ at which the secant shear modulus G_s is reduced to 70% of G_0^{ref}. The material parameters of the HS-Small model can be obtained by conducting classical laboratory tests, e.g. triaxial tests and resonant-column tests without special instrumentation. The evaluation of the HS and HS-Small model in the analysis of deep excavations is shown in Lim, Ou et al. (2010).

Houlsby (1999) proposed a simplified soil model within the framework of multi-surface plasticity which takes into account the non-linear behaviour of soil at small strains, and also includes effects such as hysteresis and dependence of stiffness on recent stress history. This model was originally implemented into OXFEM and has been widely used by Oxford researchers in tunnelling installation analyses (Augarde 1997, Liu 1997, Burd, Houlsby et al. 2000, Augarde and Burd 2001, Bloodworth 2002, Wisser 2002, Augarde, Burd et al. 2005, Wisser, Augarde et al. 2005, Pickhaver 2006, Pickhaver, Burd et al. 2010). It has been recently implemented into ABAQUS by the author though the subroutine UMAT (Dong 2011). However, this model is a total stress model and limited to undrained conditions.

The MIT-E3 soil model (Whittle 1993) is an generalised effective stress model, which can describe many aspects of the observed behaviour of K_0-normally and lightly overconsolidated ($OCR \leq 8$) clays including: (a) small strain nonlinearity, (b) anisotropic stress-strain-strength, and (c) hysteretic and inelastic behaviour due to cyclic loading. This soil model has in total 15 parameters, most of which can be obtained from laboratory experiments. The predictive capabilities of the MIT-E3 model and its limitations have been evaluated through detailed comparisons with laboratory test data for Boston blue clay (Whittle 1993, Whittle, Degroot et al. 1994). It has been implemented into ABAQUS and PLAXIS for studies of the performance of braced excavations (Whittle, Hashash et al. 1993, Hashash and Whittle 1996).

Stallebrass (1990) described a 3-surface of kinematic hardening (3-SKH) soil model to consider the effect of recent stress history changes, an extension of the two-surface model (or the 'Bubble' model) from Al-Tabbaa and Wood (1987), while both models in turn are extensions of the Modified Cam clay model. The 3-SKH model has 13 parameters and consists of two kinematic surfaces, namely a history surface and a yield surface, lying within the Modified Cam clay state boundary surface, which is called the bounding surface. All surfaces have the same shape and expand or contract according to a fixed ratio. Grammatikopoulou (2004) addressed the limitations and drawbacks of both models, and made some improvements by modifying the flow rule and yield surface.

Constitutive model for structures

Structural components in deep excavations are mainly reinforced concrete structures and steel struts. The steel struts can be generally modelled as a linear elastic material, but reinforced concrete components are more complicated due to the imperfections in the concrete such as cracks. The concrete behaves as a linear elastic material in compression until it reaches ultimate strength and subsequently fails in a brittle manner. Under tension conditions, since the failure strength is small, linear elastic model is quite accurate and sufficient to predict the behaviour of concrete until failure. However, this simple linear elastic constitutive law is often inappropriate as concrete cracks which is highly nonlinear and inelastic, and in the case of reversal loading.

Several inelastic concrete models are available in ABAQUS to consider the cracks, e.g. the concrete smeared cracking model, and the concrete damaged plasticity model. They provide a general capability for modelling concrete in all types of structures (e.g. solids, beams, shells, and trusses). The smeared cracking concrete model consists of an isotropic hardening yield surface for compressive stress state and an independent crack detection surface to determine the cracking. Oriented damaged elasticity concepts are used to describe the reversible part of the material's response after cracking failure. The model does not track individual macro cracks. Tension stiffening is used to model the post-failure behaviour. The concrete damaged plasticity model is

designed for applications in which concrete is subjected to monotonic, cyclic and dynamic loading under low confining pressures. It consists of the combination of non-associated multi-hardening plasticity and scalar damaged elasticity to describe the irreversible damage that occurs during the fracturing process.

Burd, Houlsby et al. (2000) adopted a relatively straightforward model for masonry structures in which the material has a low tensile strength and infinite compressive strength. If the minor principal strain in the material becomes tensile, tension cracks will form at an angle which is the inclination of the major principal strain direction. The stiffness of the material in the direction perpendicular to the crack is reduced to a small value, and the tensile stress acting across the crack remains at small residual value. This masonry model has been validated against closed form solutions and also field measurements of a large masonry building.

Constitutive model for the soil-structure interface

The soil-structure interface behaviour can be crucial to the overall response of a soil-structure system, and should be taken into account properly in the finite element analyses. One way of considering the interface behaviour is using a rigid perfectly plastic Coulomb friction model. Another approach is to consider the interface as thin continuum interface elements.

Potyondy (1961) found that the skin friction at the soil-structure interface was lower than the shearing strength of the soil, based on a number of experiments on the change of skin friction as a function of several influencing factors, e.g. grain distribution of soil, moisture content, normal load, type of construction material. Boulon (1989) investigated interface behaviour between soil and structures through direct shear tests and proposed a constitutive relation using two different theoretical frameworks (Boulon and Nova 1990).

Powrie and Li (1991) used slip elements to model the interface between the soil and the wall. The slip elements have almost zero stiffness in tension, and a limited elastic shear modulus. The shear resistance is governed by the Coulomb friction criterion. Day and Potts (1994) developed a zero thickness isoparametric 2D interface element for the soil-structure contact analysis of a

retaining wall. The interface stress is characterized by the normal and shear stresses which are related by a constitutive law to the normal and tangential interface element strains. The constitutive law uses a linear elastic perfectly plastic model using a Mohr-Coulomb failure criterion as the yield surface. However, they also experienced numerical problems such as ill-conditioning, poor convergence of solution and unstable integration point stresses. The application of this interface element to the retaining wall analysis is discussed in Day and Potts (1998).

ABAQUS provides the surface-based contact definition approach (e.g. contact pairs). The contact behaviour can be modelled by the extended Coulomb friction model. The extensions include an additional limit on the allowable shear stress, anisotropy and the definition of a secant friction coefficient. The model assumes that no relative motion occurs if the equivalent frictional stress $\tau_{eq} = \sqrt{\tau_1^2 + \tau_2^2}$ is less than the critical shear stress $\tau_{crit} = \min(\mu p, \tau_{max})$, where μ is the friction coefficient, p is the contact pressure, τ_{max} is the user specified shear resistance value. The value of τ_{max} can be related to the undrained shear strength of the soil s_u, after modification of this model through the subroutine FRIC. The modified model is used in this thesis to consider the interface behaviour at the soil/wall and soil/pile interface.

2.4.3 Results obtained and lessons learnt

Numerical analyses have been applied to investigate the performance of deep excavations in a number of aspects such as wall deflections, ground movements, wall bending moment, strut loads, and earth and pore water pressures. Some results obtained and lessons learnt are summarised here.

1) 2D analyses may oversimplify the problem and lead to unreliable or inaccurate results, as discussed in Gourvenec, Powrie et al. (2002), Zdravkovic, Potts et al. (2005) and Lee, Hong et al. (2011), although they have contributed to the understanding of some aspects of deep excavations. 3D effects are obvious and significant in deep excavations, and 3D analyses are entirely feasible in nowadays due to the advances of hardware and software. Therefore, 3D

analyses are encouraged in the analysis, and important aspects such as the ground profile, the geometry of the excavation, the retaining structures, and the construction sequences, should be represented appropriately in the modelling procedure. However, there are very few publications regarding detailed 3D analyses of deep excavations and comparison with field data from case histories.

2) The installation process of diaphragm wall panels and bored piles will result in substantial ground movements, change the ground stress state, as observed in the field (Tedd, Chard et al. 1984, Simpson 1992), and may affect the subsequent excavation behaviour such as the ground movement and structure deformation. Numerical analyses have been conducted on the installation effects of diaphragm wall panels (Ng, Lings et al. 1995, Gourvenec and Powrie 1999, Ng and Yan 1999), and various useful conclusions have been drawn. It is also confirmed that modelling the wall as Wished-In-Place will underestimate the ground settlement, wall deflection, and strut load compared the Wall-Installation-Modelled method in normally to lightly over-consolidated clay, which is attributed to an increasing effective stress level in the adjacent ground resulting from the stepwise pouring of the individual panels (Schäfer and Triantafyllidis 2006). However, in highly over-consolidated soil with high earth pressure coefficient at rest, the excavation and the pouring of the wall panels result in a decreasing lateral effective stress in the adjacent ground, and thus smaller wall movements and lower strut loadings can be possibly expected.

3) Realistic soil constitutive models are crucial to capture the observed performance of deep excavations in the field measurement. Conventional linear elasto-plastic soil models (e.g. Mohr-Coulomb, and Modified Cam Clay) without considering the small-strain stiffness nonlinearity of the soil perform rather poorly in reproducing the observed ground movement in the field (Burland and Hancock 1977, Potts and Zdravkovic 2001), whereas advanced soil models which include more realistic soil behaviours, e.g. the small-strain stiffness nonlinearity, stress history change, anisotropy, can greatly improve the computed results

(Simpson 1992, Whittle, Hashash et al. 1993, Hashash and Whittle 1996, Dong, Burd et al. 2013).

4) The constitutive model for concrete structural components needs to consider the influence of factors such as the construction joints in the retaining wall, cracks in the concrete, and thermal effects of concrete during the curing process and due to the variation of ambient temperature. Modelling the wall with isotropic properties would result in unrealistic wall deformation and bending moment at the corner of the wall, while the anisotropic wall approach proposed by Zdravkovic, Potts et al. (2005) is an adequate method to consider the joints in the retaining wall. The operational stiffness of the reinforced concrete structures is smaller than their nominal value due to the cracks in the concrete, and a reduced Young's modulus from the nominal value of the concrete is suitable in the analysis (Simpson 1992, St. John, Potts et al. 1993). The thermal shrinkage and expansion of horizontal support system will affect the wall deformation and ground movement (Whittle, Hashash et al. 1993), and consideration of thermal effects in the analysis is straightforward (Dong, Burd et al. 2013).
5) Modelling the retaining wall using shell elements will result in larger wall deflection and ground movement compared to modelling the wall using solid elements. This is because shell elements do not have thickness in geometry and thus the shell element wall is in lack of the beneficial bending moment backwards the excavation resulted from the shear stress on the surface of wall around the centreline of the wall (Zdravkovic, Potts et al. 2005).
6) The soil-structure interface properties affect the wall deformation and ground movement, and a realistic contact model is required to consider their effects (Day and Potts 1998). However, detailed investigation of the influence of interface properties on the performance of braced excavations is rarely seen in publications.
7) The in-situ horizontal stress in the ground prior to construction (related to the coefficient of earth pressure at rest K_0) is found to affect significantly the excavation behaviour such as wall deflection and bending moment, ground movement, strut force, stress state and stress

path in the ground, and the earth pressure on the wall (Potts and Fourie 1984), suggesting that such information should be specified close to the in-situ conditions in the numerical analyses.

8) The effect of construction sequence on the performance of braced excavations is still unclear, due to limited information available in literatures. In addition, it is rarely seen in any publications in regard to incorporating adjacent infrastructure in the model and investigating their response to braced excavations.

9) Increasing the wall embedment would not have any influence on the wall deformations and ground movements, but would increase the bending moments in the wall (Simpson 1992, Hashash and Whittle 1996, Bose and Som 1998). The wall stiffness has a large effect on the wall displacements, ground movements, earth pressures on the wall, wall bending moments, and prop forces (Potts and Fourie 1985). Increasing the excavation width will enlarge the wall deflection and ground settlement significantly, but it does not affect too much the strut loads and the lateral forces on the diaphragm wall due to earth pressures (Bose and Som 1998). Strut preloading was found to affect considerably the deflection of the upper portion of the wall while little at the bottom of the wall, and it also reduces the ground settlement with the increase in the magnitude of the preload (Bose and Som 1998). Using a stabilizing platform in front of the embedded retaining wall would reduce both wall movements and the long-term bending moments, resulting from the application of a moment to the wall (Powrie and Chandler 1998). The earth berms were shown to be an effective way to resist the wall deflection, and their effect depends on the geometry of the berm (Gourvenec and Powrie 2000). Cross walls were found to be effective in reducing the wall deflections and ground movements (Hsieh, Ou et al. 2013).

10) It is important to calibrate the numerical results with laboratory tests and field measurements to evaluate the capability of numerical analyses in reproducing the observed behaviour in the tests or the field. Discrepancies between the numerical analysis and laboratory tests or field

measurements might be attributed to a number of reasons, e.g. limitations of the numerical analysis, simplifications and assumptions made in the analysis, the capability of the material models and the reliability of input parameters, and uncertainties in the tests and measurements. Parametric studies are helpful to investigate how significant the influence of a particular factor is and identify which factors are the most important ones.

However, some conclusions should be treated with caution due to the simplifications and assumptions made in the analyses.

2.5 Summary

Deep excavation is a complex soil-structure interaction problem, and its performance is influenced by a number of factors such as soil conditions, the type of retaining structures, construction methods, and the workmanship. Several methods in the analysis of deep excavations are reviewed and discussed in this chapter, e.g. theoretical and empirical methods, laboratory tests and field measurements, and numerical analyses.

Theoretical and empirical methods provide some basic understanding of the behaviour of deep excavations, but they have limited applications due to their simplicity. Laboratory tests, e.g. centrifuge tests, are useful to investigate some aspects of deep excavations through well-controlled procedures, but it should be noted that centrifuge testing has its limitations and the conditions it can model are relatively simple. Field measurements reflect the real performance of deep excavations, and the field data are valuable to calibrate the numerical analyses. However, field measurements are expensive and take a long time to obtain the data, and the process is not repeatable. Moreover, field measurements can only record the data, and are not appropriate for predictions. Numerical modelling is an efficient tool to investigate the behaviour of deep excavations, and can be used for predictions. However, for more reliable prediction purposes, numerical analyses need to consider appropriately both geotechnical and structural aspects such as the irregular geometries, detailed retaining structures, correct construction sequences, realistic

material models, and reliable input parameters. For example, fully 3D analysis is required when necessary, because the 3D effect is significant in deep excavations. In addition, various important aspects need to be addressed adequately in the analysis such as (i) the small-strain stiffness nonlinearity of the soil, (ii) the initial stress state in the ground prior to excavation, (iii) the difference between shell elements and solid elements to model the retaining wall, (iv) the installation effects of the diaphragm wall and bored piles, (v) the soil-structure interface behaviour, (vi) the construction joints in the retaining wall, (vii) cracks in the concrete structure components, (viii) thermal effects of horizontal support system. However, it should be noted that it may not be practical to take into account all these aspects in a single analysis due to the complexity of the problem, and engineers need to focus on the most important ones and make appropriate simplification. It is also valuable to calibrate the numerical analysis with field measurements through detailed case studies. Once satisfactory results are obtained, engineers can apply the numerical analysis with more confidence for the prediction of real projects.

Chapter 3 Advanced finite element analysis of deep excavations

3.1 Introduction

Advanced finite element analysis of deep excavations should adopt accurate modelling procedures for geotechnical and structural behaviour, e.g. (i) the geometry of the excavation, (ii) detailed retaining structures, (iii) correct construction sequence, and (iv) reliable material models and input parameters.

The main issues involved with the numerical analysis of deep excavations include selecting appropriate constitutive models for soils and structures, the simulation of the construction procedure, and the modelling of the soil/structure interface (Potts and Zdravkovic 2001). In this chapter, these issues are addressed in detail based on the use of a commercial finite element software ABAQUS version 6.11. The application of this procedure is demonstrated through parametric studies in Chapter 4, and detailed case studies from Chapter 5 to Chapter 7.

3.2 Components in braced deep excavations

3.2.1 The soil

In finite element analysis, the soil is a critical part to deal with in the modelling procedure. This is particularly related to the partition and mesh of the model according to the excavation geometry, and the selection of element types and constitutive models.

The soil can be modelled with tetrahedral or hexahedral continuum elements in 3D analysis. For each type of elements, there are normally linear or quadratic elements (although higher order elements are also possible) with full or reduced integration. In general, quadratic elements are more accurate than linear elements in theory, but they are also expensive in calculations if the same mesh is used. Hexahedral elements are suitable for excavations with regular geometry, e.g. rectangular ones. Parametric studies are conducted in Chapter 4 to compare the difference

between these element types based on one simplified square excavation. Linear hexahedral elements with reduced integration (C3D8R) in ABAQUS are preferred to model the soil in this thesis, on the balance of accuracy and efficiency. However, higher order elements are recommended for more accurate purposes when computational resource is not a problem.

The performance of deep excavations is strongly influenced by the soil behaviour. In finite element analysis, it is vitally important to use realistic soil models to obtain more reliable results. The selection of constitutive models largely depends on the software that is used. ABAQUS includes several basic models for soils (e.g. Mohr-Coulomb, Drucker-Prager, and Modified Cam clay), and also provides the interface for advanced users to implement their specific constitutive models through the subroutine UMAT or VUMAT. A multiple-yield surface soil model (Houlsby 1999) has been implemented into ABAQUS by the author to consider the small-strain stiffness nonlinearity of the soil, and this model is used extensively in this thesis.

3.2.2 The retaining wall

The retaining wall is generally modelled using either shell elements or solid elements in finite element analysis, if the wall installation process is modelled using the Wished-In-Place (WIP) method. Shell elements have no geometric thickness and are easier to generate in the mesh. In addition, the internal forces and bending moments can be obtained directly. However, it is found that the computed wall deflection and ground movement from shell element wall are larger than those from solid element wall, and this is because the shear stress on the back of soil-wall interface provides beneficial bending moment about the wall centreline when the diaphragm wall is modelled with solid elements, whereas shell element wall does not have this effect (Potts and Zdravkovic 2001, Zdravkovic, Potts et al. 2005). Moreover, when the wall installation process is modelled explicitly in the model, e.g. the Wall-Installation-Modelled method, including the trench excavation, bentonite slurry, and concrete injection, only solid elements are suitable to model the wall because the geometry of the wall needs to be considered. Therefore, solid elements are preferred to model the retaining wall in this thesis. In terms of the output of internal

forces and bending moments, this can be achieved through embedding the shell element wall at the centreline of solid element wall and assigning shell element wall with the same thickness of the retaining wall but a small Young's modulus (e.g. 10^{-6} times the Young's modulus of the retaining wall) if the wall is assumed as a linear elastic material. The low stiffness of the embedded shell element wall will not affect the deformation of soil element wall, but the internal forces and bending moments can be computed from the output of shell element wall.

Another issue related to the retaining wall is modelling the construction joints in the wall, as shown in Fig.3.1. For example, the diaphragm wall is discontinuous in the horizontal direction along the sides of the excavation because it is constructed by sections of wall panels. Consequently, it cannot sustain any significant out-of-plane bending, and the horizontal stiffness of the wall is also much smaller than the stiffness of the solid concrete. The influence of joints can be considered by using the anisotropic wall approach (Zdravkovic, Potts et al. 2005) in which the stiffness in the direction along the joints is reduced. Details are discussed in the later section of this chapter.

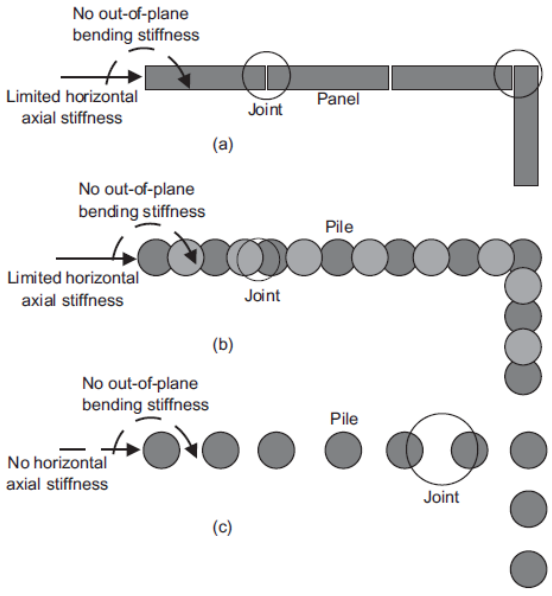

Fig.3.1 Schematic view of different wall types (a) diaphragm wall (b) secant pile wall (c) contiguous pile wall (Zdravkovic, Potts et al. 2005)

The retaining wall is adequate to be represented by a linear elastic material for simplicity. Cracks may exist in the concrete structures and propagate during the excavation, which can be considered by reducing the nominal stiffness of the concrete components or using a more

detailed concrete crack model, such as the concrete damaged plasticity model in ABAQUS. However, using a more sophisticated concrete model will increase the complexity of the analysis. In this thesis, an anisotropic linear elastic model is preferred to represent the retaining wall.

3.2.3 The support system

The support system usually consists of horizontal components (e.g. reinforced concrete beams and floor slabs, and temporary steel pipe props), and vertical components (e.g. piles and columns). In finite element analysis, beam elements can be used to model the beams, piles, columns and steel pipes, whereas shell elements are suitable for floor slabs. Opening accesses are usually designed in the floor slabs during the top-down excavation, and they can be modelled explicitly in the model.

In a similar way to the material model used for the retaining wall, the reinforced concrete components in the support system can also be assumed to behave linear elastically for simplicity or represented by a detailed concrete crack model. The concrete beams and floor slabs will shrink or expand during the curing process and due to the variation of ambient temperature, which may have large influence on the excavation behaviour. The thermal effects can be considered in the analysis in a straightforward way. Moreover, gaps may develop at the connection between the retaining wall and horizontal bracing structures, and concrete floor slabs may creep under service condition, which has the tendency to induce larger wall deformations. These effects can also be approximated by using the thermal shrinkage method.

3.2.4 Adjacent infrastructure

The adjacent infrastructure close to the excavations, e.g. buildings, utility pipelines, tunnels, and pile foundations, may be included in the model if they are major concerns in the project, although this would increase the complexity of the analysis. An example of this approach is given in Chapter 6 in which the deformation of buildings and buried pipelines is investigated.

3.2.5 Constraints and contacts

The connections between different structural components (e.g. retaining walls, concrete beams,

floor slabs, and vertical piles) in deep excavations are usually assumed to be rigid (e.g. cast or welded) in numerical analyses, but they may be more complicated in reality (e.g. pined connections, and gaps) and they may change as the excavation proceeds. For simplicity, tie constraints are applied at the connections of these components in the analyses in this thesis.

The interface behaviour between the soil and structures (mainly the soil/wall interface and the soil/pile interface) can be modelled using contact pairs at the interface associated with a contact model. However, it should be noted that contact is a highly complex mechanism and may cause numerical difficulties. An extended Coulomb frictional contact model is described later in this chapter. The influence of interface properties on the excavation behaviour is investigated in the parametric studies in Chapter 4.

3.2.6 Boundary conditions

The region to be analysed in deep excavations is of relatively small dimensions compared with those of the surrounding medium. In finite element analysis, the normal practice is to extend the mesh to some distance away from the zone of interest, and apply fixed displacement boundary conditions there.

3.3 Material models

3.3.1 Constitutive models for the soil

The built-in soil models in ABAQUS are conventional and do not contain modern concepts of soil modelling, e.g. small-strain stiffness nonlinearity, and recent stress history. Fortunately, ABAQUS provides interfaces for advanced users to implement their own constitutive models through subroutines UMAT and VUMAT. A multiple-yield surface soil model (Houlsby 1999) has been implemented into ABAQUS by the author using UMAT to consider the small-strain stiffness nonlinearity of the soil. This soil model takes into account the non-linear behaviour of soil at small strains, and also includes effects such as hysteresis and dependence of stiffness on recent stress history. It uses multiple yield surfaces within the framework of work-hardening

plasticity theory. Non-linearity of the small-strain response is achieved using a number of nested yield surfaces of the same shape as the outer fixed failure surface. Those inner yield surfaces translate as the stress state changes, while the bounding von Mises failure surface models perfect plastic behaviour with no work hardening. As a stress point moves in the stress space and encounters a yield surface as shown in Fig.3.2, the stiffness reduces as shown in Fig.3.3, and the yield surface moves with the stress point. It thus models the non-linearity of response at small strains, and the effect of recent stress history. Each yield surface is described by two parameters specifying the size of the surface and the magnitude of the stiffness reduction as the yield surface is activated.

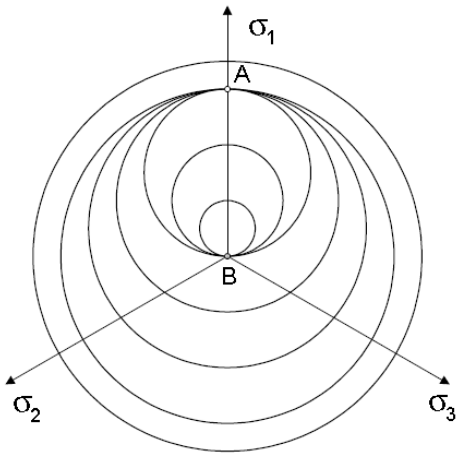

Fig.3.2 Yield surface after stress path from B to A and back to B (Houlsby 1999)

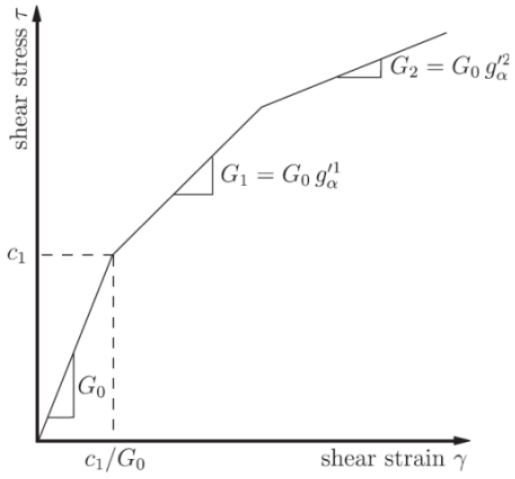

Fig.3.3 Shear stress-strain cure

The derivation of input parameters for this soil model requires the variation of tangent shear modulus G_t with shear strain γ (i.e. the S-shaped curve), the shear modulus at very small strain G_0, and the undrained shear strength s_u. As this thesis focuses on deep excavations in Shanghai

clay, the calibration of this soil model for Shanghai clay is described in this section. The soil properties for Shanghai clay are collected from publications.

Geological and geotechnical condition in Shanghai

The city of Shanghai is situated at approximately 70km from the sea shore, in the large coastal plain limited by the East China Sea and the Yangtze River which is designated as the 'Yangtze River Delta'. The subsoil of Shanghai is composed of Quaternary sediments of the Yangtze River estuary which consist of clay, loam, silt and sand, the different deposits being the final result of the variation from an estuarine to fluviatile sedimentation process (Dassargues, Biver et al. 1991). The top layers of soil with engineering significance were deposited during the Quaternary period. Typical ground strata are thick soft clay comprising quaternary alluvial and marine deposits. From a lithological point of view, the subsoil of these coastal lowlands consists of a thick (about 300m) sequence of low consolidated sediments, sensitive to compaction. High water content, low shear strength, high compressibility, and low ground bearing capacity, are typical characteristics of Shanghai soft clay. The elevation of the ground surface is typically from 2.2m to 4.8m above sea level (Xu, Shen et al. 2009). The main water table is generally 0.5~1.0m below the ground surface. The natural water content of the soft (silty) clay is close to or larger than the corresponding liquid limit, suggesting its soft and compressible features. The permeability of the soft clay is in the order of $10^{-9}\mathrm{m/s}$ (Li, Ng et al. 2012). The soil is normally consolidated or lightly over-consolidated, with an OCR between 1 and 2. The lateral earth pressure coefficient, K_0, is around 0.5. The stiffness of the natural clay is slightly anisotropic due to the deposition process, with the anisotropy ratio of $G_{0(hh)}/G_{0(hv)} \approx 1.2$ (Li, Ng et al. 2012).

Small-strain stiffness nonlinearity

The small-strain stiffness properties of Shanghai clay have not been studied in a systematic way, and only limited data are available in literature. Lu, Li et al. (2005), for example, reported the results of resonant column tests and cyclic triaxial tests on three different types of remoulded soil (sandy silt, silty clay, and medium sand) with shear strain γ in the range 10^{-6} to 10^{-2}. Huang,

Brown et al. (2001) reported experiment data (determined using an unspecified test procedure) for Shanghai soft clay. Wang (2004) presented data, from bender element tests, on the small-strain stiffness of Shanghai clay for shear strains in the range 10^{-4} to 10^{-1}. These data, all in terms of secant shear modulus G_s, are reproduced in Fig.3.4. The data present a consistent pattern, with the exception of the data from Wang (2004) which falls below the trend.

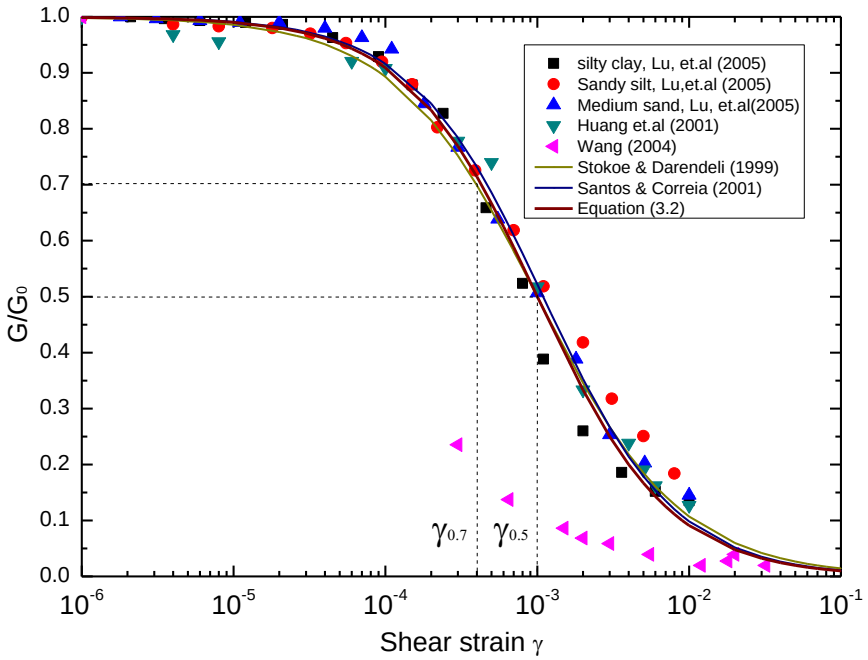

Fig.3.4 Variation of normalised secant shear modulus with shear strain

The modified hyperbolic Equation (3.1) is commonly used to fit the $G_s/G_0 \sim \gamma$ data (Hardin and Drnevich 1972, Stokoe, Darendeli et al. 1999, Darendeli 2001). Such equation is also used by Zhang and Shi (2008) to fit the experimental data (triaxial tests with bender element) of the clay in Nanjing, which is not far from Shanghai.

$$\frac{G_s}{G_0} = \frac{1}{1 + a(\frac{\gamma}{\gamma_{ref}})^b} \qquad (3.1)$$

where γ_{ref} is the reference strain, a, b are curve-fitting variables, b is also called the curvature parameter. Hardin and Drnevich (1972) used $a = b = 1.0$, $\gamma_{ref} = \tau_{max}/G_0$, with τ_{max} being the shear stress at failure. Stokoe, Darendeli et al. (1999) modified the equation and suggested $\gamma_{ref} = \gamma_{0.5}$ at which $G_s/G_0 = 0.5$, and $a = 1.0, b = 0.92$. Santos and Correia (2001) defined $\gamma_{ref} = \gamma_{0.7}$ at which $G_s/G_0 = 0.7$, and $a = 0.385, b = 1.0$ is obtained by best fitting the data by the least squares method.

Note that although the data in Fig.3.4 are taken from a variety of depths, the results (with the exception of Wang (2004), probably due to differences in the sampling and test method) lie close to a unique line. This suggests that the same model can be used to represent the complete set of soil layers that comprise the Shanghai clay. A unified equation is derived, as shown in Equation (3.2), to fit the data in Fig.3.4.

$$\frac{G_s}{G_0} = \frac{1}{1+\frac{\gamma}{\gamma_{0.5}}} = \frac{1}{1+\frac{\gamma}{0.1\%}} \tag{3.2}$$

It is noted that data described above relates to a secant modulus G_s. However, to calibrate the multi-surface plasticity model adopted for the finite element analysis used here, data on the tangent shear modulus G_t , are required. These two parameters are related by Equation (3.3):

$$\begin{cases} \tau = G_s\gamma \\ G_t = \dfrac{d\tau}{d\gamma} = G_s + \gamma\dfrac{dG_s}{d\gamma} \end{cases} \tag{3.3}$$

The model described above (for secant shear modulus G_s) may therefore be shown to give Equation (3.4):

$$\frac{G_t}{G_0} = \frac{1}{\left(1+\frac{\gamma}{0.1\%}\right)^2} \tag{3.4}$$

The $G_s/G_0 \sim\gamma$ and $G_t/G_0 \sim\gamma$ expressions for Shanghai clay are plotted in Fig.3.5. The area below the $G_t/G_0 \sim\gamma$ curve in a linear plot is s_u/G_0, or $1/I_r$.

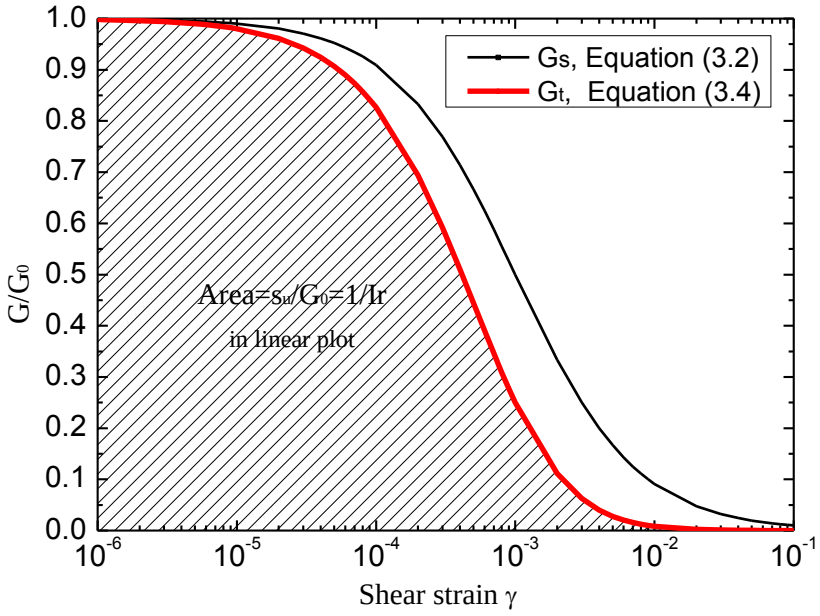

Fig.3.5 Relations for $G_s/G_0 \sim\gamma$ and $G_t/G_0 \sim\gamma$

When the shear strain γ is normalised by the value s_u/G_0, or $1/I_r$, the area below $G_t/G_0 \sim I_r\gamma$ curve is equal to 1, in which case the original γ axis is replaced by $(G_0/s_u)\gamma$, or $I_r\gamma$.

The original half-normalised curve, $G_t/G_0 \sim \gamma$, now becomes a double normalised curve, $G_t/G_0 \sim I_r\gamma$. Equation (3.4) is modified to Equation (3.5) by introducing I_r in the equation.

$$\frac{G_t}{G_0} = \frac{1}{(1 + aI_r\gamma)^2} \qquad (3.5)$$

where $a = 1/(\gamma_{0.5}\, I_r^*)$, I_r^* is the rigidity index from integration of the $G_t/G_0 \sim \gamma$ curve, for Shanghai clay in Fig.3.5, $a = 1.0$.

The new Equation (3.5) is plotted as a double normalised curve in Fig.3.6.

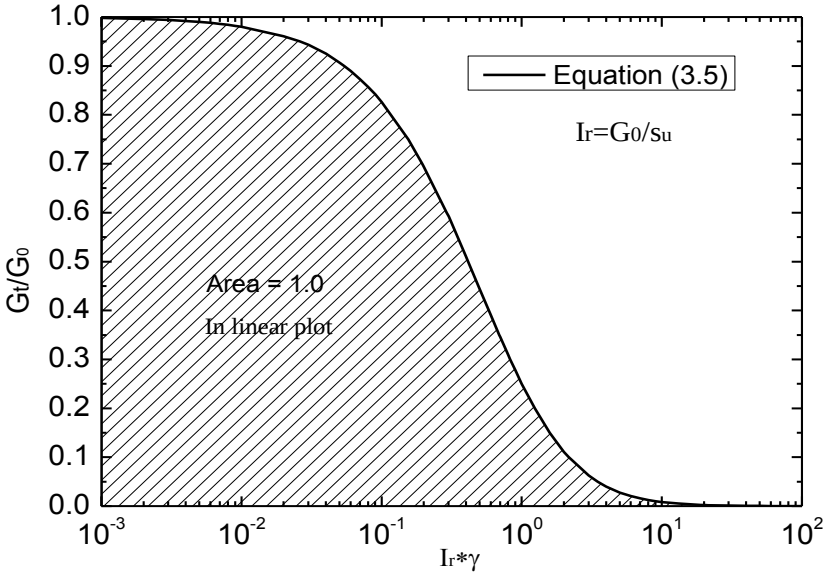

Fig.3.6 Normalized S-shaped curves

This new expression in Equation (3.5) is found to be more useful because it is independent of the specific value of I_r .

Parameter derivation for the multiple-yield surface model

In the multiple-yield surface model, each inter yield surface is associated with one proportional strength parameter $C_n = c_n s_u, 0 < c_n < 1.0$, while the outmost yield surface has the strength at failure s_u. Each yield surface also bounds one region where the stiffness is constant $G_n = g_n G_0, 0 < g_n < 1.0$. The physical meaning of g_n and c_n is illustrated in Fig.3.7, where six yield surfaces are shown and these surfaces are centred in the hydrostatic axis. For example, inside the first yield surface, the region is purely elastic with initial shear stiffness G_0 ($g_0 = 1.0$). Once the

stress state reach the first yield surface, the soil yield and the first yield surface translates with the current stress state with a reduced stiffness $G_1 = g_1 G_0$, until it touches the next yield suface. When the stress state reaches the outmost yield surface, the soil fails, and the stiffness before failure is a tiny cut-off value.

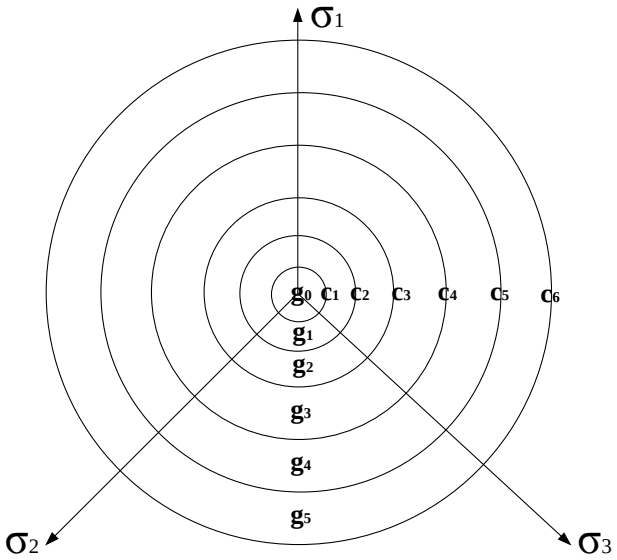

Fig.3.7 Physical meaning of $g_n$andc_n

When n inner yield surfaces are used and there is no loading or unloading, the basic rule is,

$$\begin{aligned} G_0 &= g_0 G_0, 0 < \tau \le c_1 s_u \\ G_i &= g_i G_0, c_i s_u < \tau \le c_{i+1} s_u, 1 \le i \le n \end{aligned} \qquad (3.6)$$

The g_n and c_n parameters for the multiple yield surface model can be derived directly from the normalised S-shaped curve in Fig.3.6, though a procedure explained below. This process is also illustrated in Fig.3.8, where only 5 inter yield surfaces are shown for clarity.

1) Select a suitable set of values of g_i (where $g = G_t/G_0$). For 9 internal yield surfaces as used in this thesis, a total of 9 values of g_i are needed ($g_0 = 1.0$ by default). There is no absolute rule for the distribution of g_n, but g_n should represent the variation of stiffness properly.
2) Determine the values of the normalised shear strain $I_r\gamma_i^g$, as shown Fig.3.8, corresponding to each selected value of g_i. The value of $I_r\gamma_i^g$ is calculated using Equation (3.7) which is derived from Equation (3.5),

$$I_r\gamma_i^g = \frac{1}{\sqrt{g_i}} - 1 \tag{3.7}$$

These data are listed in Table 3.1.

Table 3.1 The values of g_i and the corresponding $I_r\gamma_i^g$

n	1	2	3	4	5	6	7	8	9
g_i	0.9	0.7	0.5	0.3	0.15	0.075	0.03	0.0075	0.00058
$I_r\gamma_i^g$	0.0541	0.1952	0.4142	0.8257	1.5820	2.6515	4.7735	10.5470	40.5227

3) Establish a piece-wise constant approximation for g.

$$\begin{aligned} I_r\gamma \le I_r\gamma_o \quad & g = g_0 \\ I_r\gamma_{i-1} \le I_r\gamma \le I_r\gamma_i \quad & g = g_i, \quad 1 \le i \le n \end{aligned} \tag{3.8}$$

Fig.3.8 illustrates this process and its physical meaning with 5 inner yield surfaces for clarity.

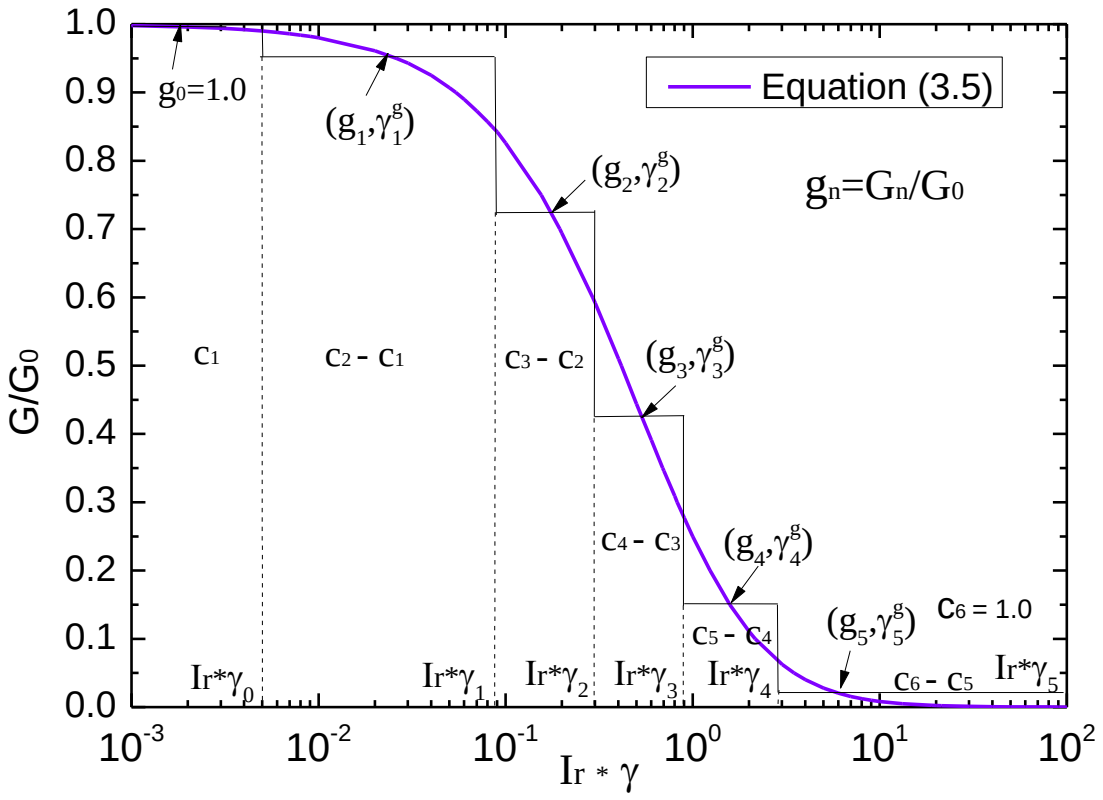

Fig.3.8 Fitting the $G/G_0 \sim I_r * \gamma$ curve

The normalised shear strain $I_r\gamma_0$ is a threshold value within which the soil is linear elastic and has the maximum shear stiffness G_0. The value of $I_r\gamma_0$ can be estimated from the curve where the stiffness starts to degrade quickly, e.g. $I_r\gamma_0 = 5 \times 10^{-3}$. Actually, the selection of $I_r\gamma_0$ does not affect too much the overall c_n values if it is reasonably small. The scientific way of choosing $I_r\gamma_n$ is worth discussion, but the method used here is a feasible way. The basic principle is to make the area below the smooth curve and the stepwise line equal, for each c_i.

The area below the smooth curve $G_t/G_0 \sim I_r\gamma$ is calculated through integration of the Equation (3.5), as shown in Equation (3.9).

$$c_i = \int_0^{I_r\gamma_{i-1}} \left(\frac{G_t}{G_o}\right) d(I_r\gamma) = \frac{I_r\gamma_{i-1}}{1 + I_r\gamma_{i-1}} \tag{3.9}$$

The area below the staircase is calculated from Equation (3.10)

$$\begin{aligned} c_1 &= g_0 \times I_r\gamma_0 \\ c_{i+1} - c_i &= g_i \times (I_r\gamma_i - I_r\gamma_{i-1}) \end{aligned} \tag{3.10}$$

Therefore, the accurate $I_r\gamma_i$ should be calculated from Equation (3.11).

$$\begin{aligned} c_1 &= g_0 \times I_r\gamma_0 \\ c_{i+1} - c_i = g_i \times (I_r\gamma_i - I_r\gamma_{i-1}) &= \int_{I_r\gamma_{i-1}}^{I_r\gamma_i} \left(\frac{G_t}{G_o}\right) d(I_r\gamma) = \frac{I_r\gamma_i}{1+I_r\gamma_i} - \frac{I_r\gamma_{i-1}}{1+I_r\gamma_{i-1}} \end{aligned} \tag{3.11}$$

The corresponding set of data for g_i, $I_r\gamma_i$, and c_i are listed in Table 3.2.

Table 3.2 A suitable set of data for g_i, $I_r\gamma_i$, and c_i

n	0	1	2	3	4	5	6	7	8	9	10
g_i	0.996	0.9	0.7	0.5	0.3	0.15	0.075	0.03	0.0075	0.00058	
$I_r\gamma_i$	0.005	0.1052	0.2926	0.5473	1.1544	2.0945	3.308	6.738	16.23	100	
c_i		0.0050	0.0952	0.2264	0.3537	0.5358	0.6768	0.7679	0.8708	0.9420	0.99

It should be noted there is a cut-off value of the normalised shear strain at 100 where the soil is assumed to reach its ultimate shear strength s_u. The stepwise fitting of the S-shaped curve in Fig.3.6, using the data in Table 3.2, is shown in Fig.3.9.

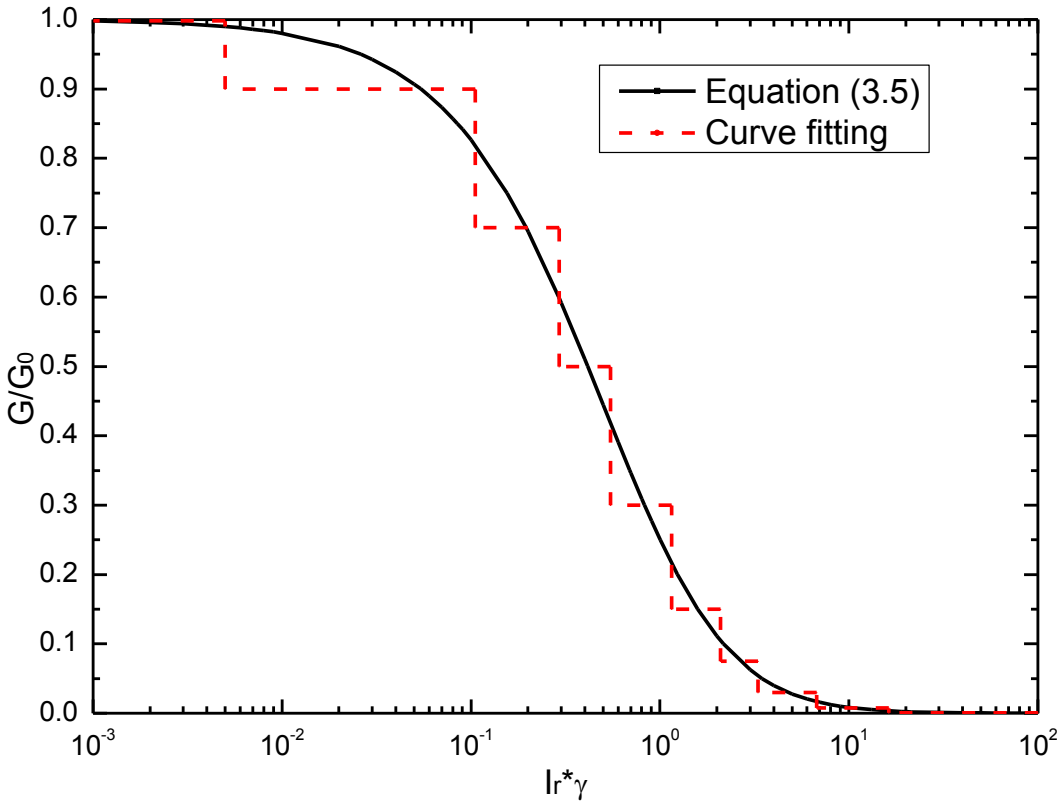

Fig.3.9 Curve fitting for the 9 inner yield surfaces

The normalised $\tau/s_u \sim I_r\gamma$ curves from two different methods, i.e. integration of the $G_t/G_0 \sim I_r\gamma$ equation, and the stepwise linear approximation, are shown in Fig.3.10. The agreement is satisfactory.

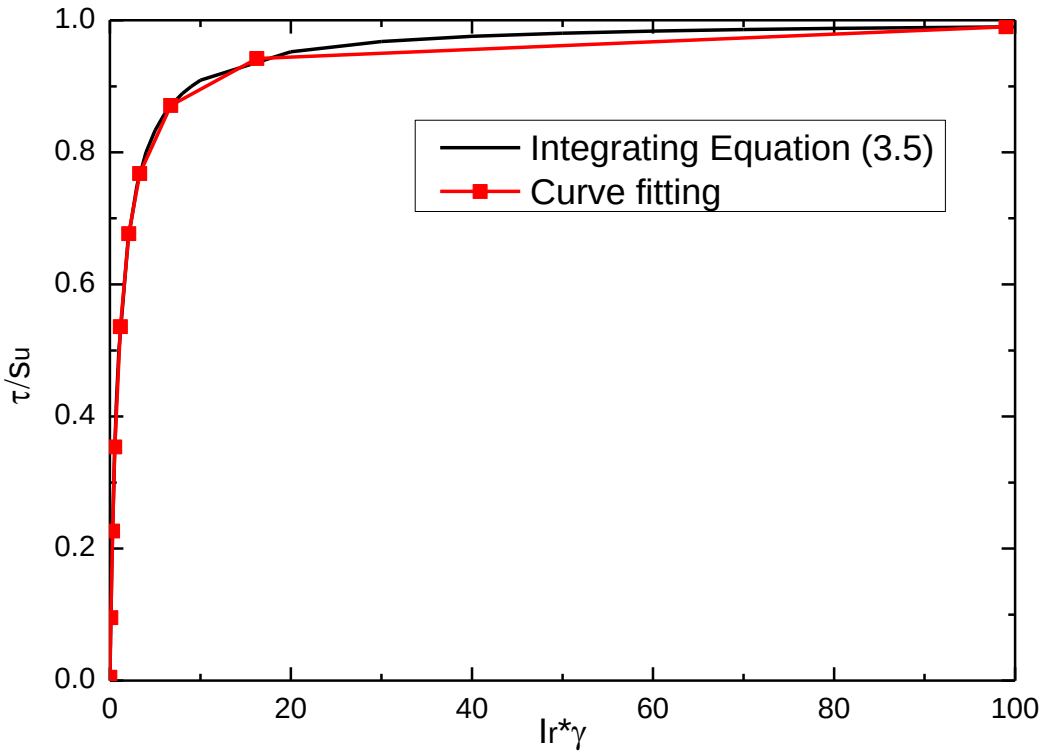

Fig.3.10 The normalised $\tau/s_u \sim I_r\gamma$ curve

The derived parameters for the 9 inner yield surfaces model are listed in Table 3.3. This set of parameters stays the same for one specific $G_t/G_0 \sim I_r\gamma$ relationship, independent on the value of G_0 and I_r selected for the analysis.

Table 3.3 Input parameters for the multi-yield surface soil model

n	1	2	3	4	5	6	7	8	9
g_n	0.9	0.7	0.5	0.3	0.15	0.075	0.03	0.0075	0.00058
c_n	0.005	0.0952	0.2264	0.3537	0.5358	0.6769	0.7678	0.8708	0.942

The undrained shear strength profile

The variation of the undrained shear stress $s_u$with depth is also collected from publications. A set of undrained shear strength data (Dassargues, Biver et al. 1991) measured using shear box tests on soils from the central zone of Shanghai, and additional undrained shear strength data determined using the field vane at two separate sites in Shanghai (Liu, Ng et al. 2005, Ng, Hong et al. 2012), are reproduced in Fig.3.11 which also includes the undrained shear strength data from Xu (2007).

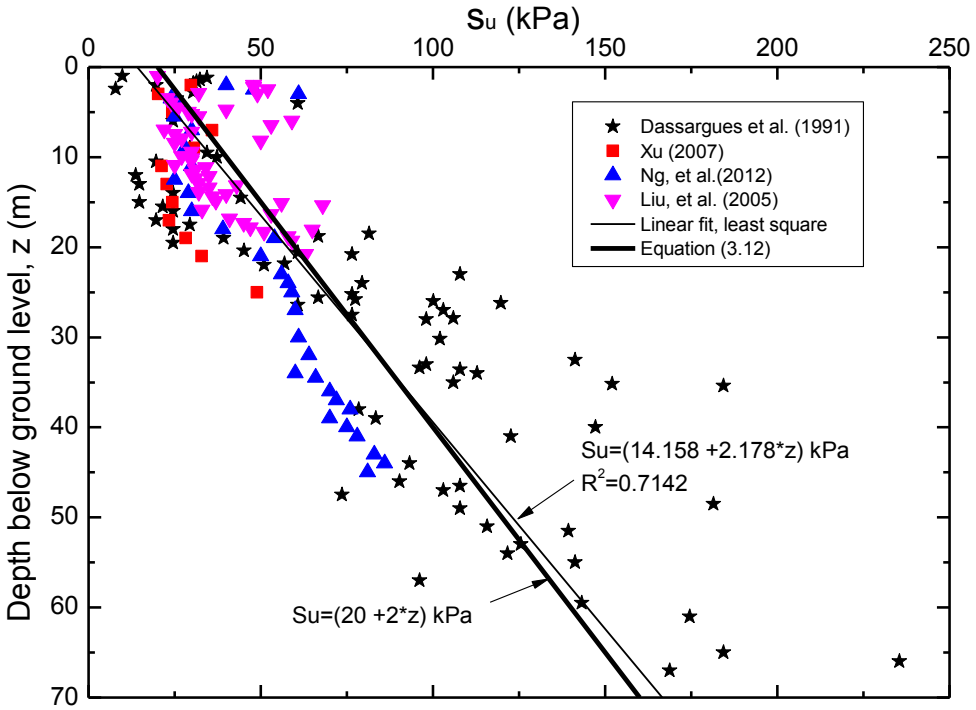

Fig.3.11Undrained shear strength profiles determined from four separate sites in Shanghai

It is reasonable to assume that the undrained strength $s_u$increases linearly with depth. Equation (3.12) is a simplified linear fit, closing approximating the least square best fit.

$$s_u = (20 + 2z\,)kPa \qquad (3.12)$$

Stiffness at very small-strain

The shear modulus at very small strain G_0, can be determined from shear-wave velocity V_s from dynamic geological surveys, expressed in Equation (3.13).

$$G_0 = \rho * V_s^2 = \frac{\gamma}{g} * V_s^2 \qquad (3.13)$$

where ρ is the bulk density, γ is the unit weight, g is the acceleration due to gravity.

Relevant data are given by Cai, Zhou et al. (2000) (from the Quyang district of Shanghai), Chen et al., (2011) (from the site of Shanghai Hongqiao station of the Beijing-Shanghai High-speed Railway), and Lou, Li et al. (2007), Chen, Gao et al. (2011) (from two further sites in Shanghai). In addition, the characteristic value of shear-wave velocity distribution up to 100m depth in Shanghai is reported by Gao and Sun (2005). All these data are reproduced in Fig.3.12.

Like the undrained shear strength s_u, G_0 is also assumed to increase linearly with depth. Moreover, it is convenient to use a constant value of rigidity index $I_r = G_0/s_u$ to link these two variables. Equation (3.14) is derived based on a slight modification to the equation from

linearization using least square method, and a constant value of rigidity index $I_r = 1250$ is assumed.

$$G_0 = 1250 * (20 + 2z)kPa = 1250 * s_u \qquad (3.14)$$

Should more detailed data be available, more sophisticated fits could be used for the strength and stiffness behaviour. The emphasis here, however, is to use simple expressions which capture the main features of the behaviour.

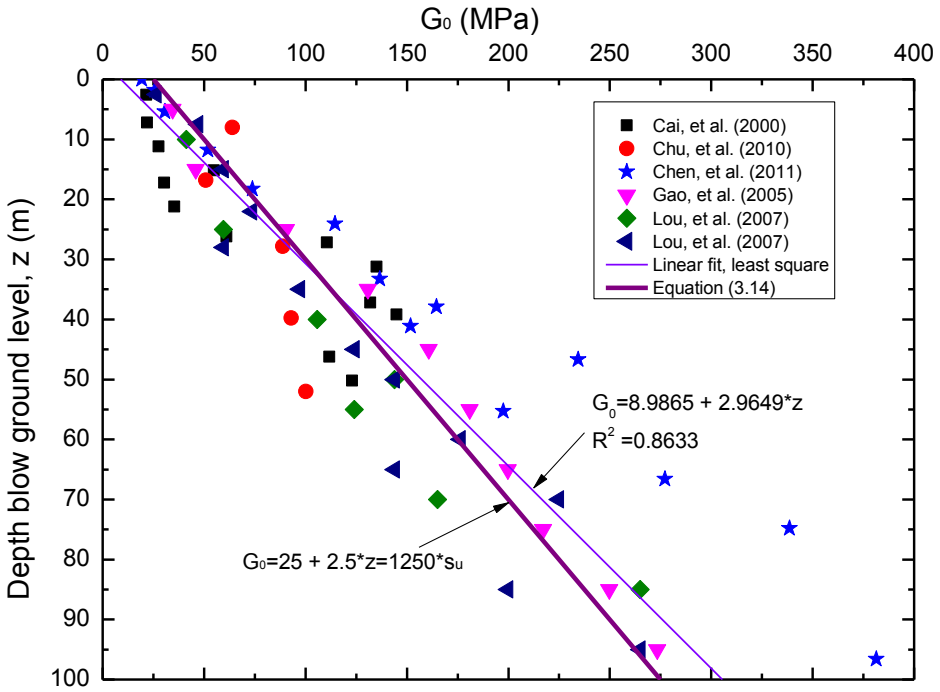

Fig.3.12 Profile of G_0 determined from shear-wave velocity tests in Shanghai

3.3.2 Constitutive models for structural components

The structural components in deep excavations (e.g. the diaphragm wall, horizontal beams and floor slabs, and vertical piles) are mainly reinforced concrete structures, and it is adequate to model them as a linear elastic material for simplicity. The effect of cracks is normally considered by reducing the nominal value of the Young's modulus of the intact concrete.

ABAQUS provides several more realistic models for reinforced concrete structures, e.g. the concrete smeared cracking model, and concrete damaged plasticity model, for advanced analyses. The concrete damaged plasticity model in ABAQUS provides a general capability for modelling reinforced concrete structures. It uses concepts of isotropic damaged elasticity in combination with isotropic tensile and compressive plasticity to represent the inelastic behaviour of concrete.

It consists of the combination of non-associated multi-hardening plasticity and scalar (isotropic) damaged elasticity to describe the irreversible damage that occurs during the fracturing process. However, the disadvantage of using these models is associated with the difficulties in determining the large number of material parameters and the numerical instabilities during the calculation.

As discussed earlier in this chapter, the retaining wall is discontinuous in the horizontal direction and has construction joints in the wall. The anisotropic wall approach (Zdravkovic, Potts et al. 2005) is used in this thesis to consider the effect of construction joints. The retaining wall is modelled as a cross anisotropic linear elastic material to investigate its capability in capturing the observed excavation behaviour. For the local coordinate system in Fig.3.13 (1-direction along the wall thickness, 2-direction along the wall length, 3-direction along the wall depth), the Young's modulus E along 2-direction (the wall length direction) is reduced by a factor of β ($\beta < 1.0$), while the material is isotropic in 1-3 plane.

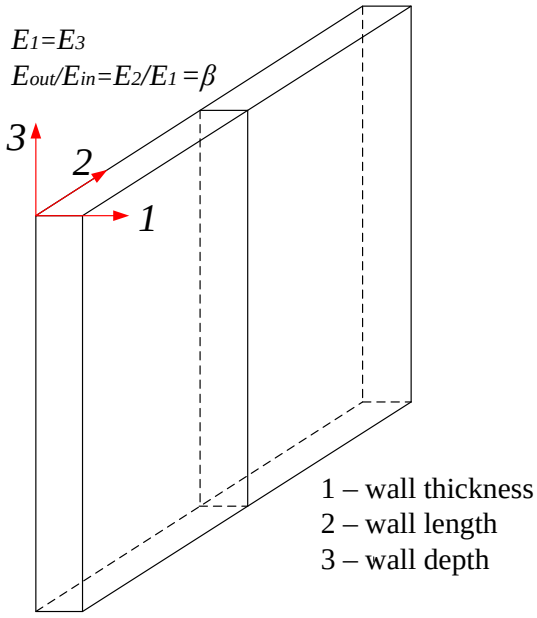

Fig.3.13 Local directions for cross anisotropic wall

In ABAQUS, anisotropic elastic material properties are defined by nine elastic engineering constants, E_1, E_2, E_3, v_{12}, v_{13}, v_{23}, G_{12}, G_{23}, G_{23}, together with the associated material orientations. For cross anisotropic material, only five independent variables are needed. The five independent parameters (E_1, E_2, v_{12}, v_{13} and G_{12}), as well as the other four dependent parameters,

are determined by Equation (3.15).

$$\begin{cases} E_1 = E_3 \\ v_{12} = v_{23} \\ G_{12} = G_{23} \\ G_{13} = \dfrac{E_1}{2(1+v_{13})} \end{cases} \tag{3.15}$$

In addition, material stability requires Equation (3.16),

$$\begin{gathered} E_1, E_2, E_3, G_{12}, G_{23}, G_{23} > 0, \\ |v_{12}| < (E_1/E_2)^{1/2} \\ |v_{13}| < (E_1/E_3)^{1/2} \\ |v_{23}| < (E_2/E_3)^{1/2} \\ 1 - v_{12}v_{21} - v_{23}v_{32} - v_{31}v_{13} - 2v_{21}v_{32}v_{13} > 0. \end{gathered} \tag{3.16}$$

All the parameters are listed in Table 3.4. The values of v_{12} and v_{23} are assumed to be zero because they are not easy to determine. In fact, the strain change in 1- and 3- directions caused by strain increment in 2- direction is relatively small due to the existence of a large number of joints along the length of the diaphragm wall.

Table 3.4 Variables for anisotropic wall properties

$\mathbf{E_1}$	$\mathbf{E_2}$	$\mathbf{E_3}$	$\mathbf{v_{12}}$	$\mathbf{v_{13}}$	$\mathbf{v_{23}}$	$\mathbf{G_{12}}$	$\mathbf{G_{13}}$	$\mathbf{G_{23}}$
30GPa	$\beta \cdot \mathrm{E}_1$	30GPa	0	0.2	0	$\dfrac{\beta \cdot \mathrm{E}_1}{2(1+\mathrm{v}_{12})}$	$\dfrac{\mathrm{E}_1}{2(1+\mathrm{v}_{13})}$	$\dfrac{\beta \cdot \mathrm{E}_1}{2(1+\mathrm{v}_{23})}$

The thermal effects of concrete beams and floor slabs, as discussed earlier in this chapter, may affect the wall deformation and ground movement. In this thesis, the thermal effect is considered in the concrete material properties by specifying a coefficient of thermal expansion α, and a temperature change ΔT. The coefficient of thermal expansion α of concrete does not vary too much, and its average value, $10^{-5}/℃$, is adopted in this thesis. The temperature change ΔT is selected based on experience and back analysis of some case histories.

3.3.3 Constitutive models for the soil-structure interface

An extended version of the classical isotropic Coulomb friction model is available in ABAQUS for use with general contact analysis capabilities. The extensions include an additional limit on the allowable shear stress, anisotropy and the definition of a secant friction coefficient. The standard Coulomb friction model assumes that no relative motion occurs if the equivalent frictional stress τ_{eq} as defined in Equation (3.17)

$$\tau_{eq} = \sqrt{\tau_1^2 + \tau_2^2} \qquad (3.17)$$

where τ_1 and τ_2 are shear stresses on the interface, is less than the critical stress τ_{crit}, which is proportional to the contact pressure p, in the form

$$\tau_{crit} = \mu p, \qquad (3.18)$$

where μ is the friction coefficient. It is possible to put a limit on the critical shear stress,

$$\tau_{crit} = min(\mu p, \tau_{max}), \qquad (3.19)$$

where τ_{max} is a user specified constant. If the equivalent stress reaches the critical stress ($\tau_{eq} = \tau_{crit}$), slip will occur.

In geotechnical engineering, it is reasonable to link τ_{crit} with the undrained shear strength of the soil s_u, e.g., $\tau_{crit} = \alpha \cdot s_u$, where α is an coefficient. In the analyses in this thesis, s_u is a variable and increases linearly with depth. In ABAQUS, however, τ_{max} is a constant in the default setting. Further modification is made through a subroutine FRIC in which τ_{max} is set as a variable, as shown in Equation (3.20),

$$\tau_{crit} = min(\mu p, \tau_{max}), \ \ \tau_{max} = \alpha \cdot s_u \qquad (3.20)$$

This modified version of the extended Coulomb friction model is illustrated in Fig.3.14.

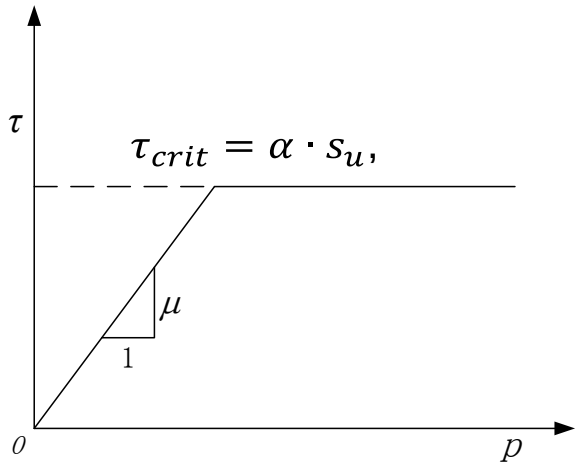

Fig.3.14 Extended Coulomb friction model

In undrained analysis, the critical shear resistance τ_{crit} is limited only by τ_{max}, independent of the coefficient of friction μ, which can be achieved by setting μ as a large value, e.g. $\mu = 1000$. The influence of the value of α on the excavation behaviour is investigated through a number of parametric studies in Chapter 4.

3.4 Modelling procedures

3.4.1 Geostatic analysis

Geostatic stress-displacement analysis is the first step for equilibrium iteration to set up the initial stress state in the ground prior to the construction. The vertical stress is governed by the gravity, while the horizontal stresses are related to the vertical stress through the coefficient of lateral earth pressure at rest K_0. It is noted that K_0 is used for the effective stress expression. When a total stress soil model is used, e.g. the multiple yield surface model used in this thesis, the coefficient for the total stress expression, K_0^t , should be applied. The derivation of K_0^t from K_0 is described in this section.

For the normally consolidated Shanghai clay ($OCR \approx 1$), the value of K_0 can be derived from Jacky's equation, as shown in Equation (3.21),

$$K_0 = \sigma_h'/\sigma_v' \approx 1 - sin\,\varphi' \qquad (3.21)$$

where σ_h' and σ_v' are horizontal and vertical effective stress of the soil in the ground, and φ' is the friction angle of the soil.

The coefficient of lateral earth pressure for the total stress expression K_0^t, can be derived from Equation (3.22),

$$K_0^t = \frac{\sigma_h' + u}{\sigma_v' + u} = \frac{K_0 \cdot \sigma_v' + u}{\sigma_v' + u} \qquad (3.22)$$

where u is the pore water pressure.

The water table in Shanghai clay is normally 0.5m to 1.0m below the ground level. For simplicity, the pore water pressure can be assumed as hydrostatic with depth h below the ground surface, $u = \gamma_w h$, where γ_w is the unit weight of the water. Then the Equation (3.22) becomes Equation (3.23).

$$K_0^t = \frac{\sigma_h' + u}{\sigma_v' + u} = \frac{K_0 \cdot \gamma_s h + \gamma_w h}{\gamma_s h + \gamma_w h} = \frac{K_0 \gamma_s + \gamma_w}{\gamma_s + \gamma_w} \qquad (3.23)$$

where γ_s is the unit weight of the dry soil.

3.4.2 Wall and pile installation

The diaphragm wall is a cast-in-situ reinforced concrete retaining wall constructed using a slurry supported trench method. The installation process includes deep mixing, slurry supported excavation, placing the reinforced cage, concrete casting and curing. The bored pile installation follows the similar process. The installation process modifies the in-situ stress state in the ground close to the trench and influences the starting point for analysis of the post-construction behaviour. In addition, it results in substantial ground movements and settlements of adjacent infrastructure, which may be significant compared to those induced by the excavation itself. The influence depends on the groundwater level, panel width, and changes in pore water pressure during diaphragm wall installation. Therefore, although simple, the widely used Wished-In-Place (WIP) method for the wall and pile installation in the finite element analyses of deep excavations neglects the installation effect on the ground movement and the subsequent excavation behaviour.

The effects of diaphragm wall installation have been investigated through finite element analyses by several researchers, e.g. Ng, Lings et al. (1995), Ng and Yan (1999), Gourvenec and Powrie (1999), and Burlon, Mroueh et al. (2013). The construction of a single panel is modelled by the following procedure:

1) Excavate the trench and apply the hydrostatic bentonite pressure on the trench surfaces simultaneously;
2) Cast the panel with concrete by increasing the lateral pressure inside the trench to a bilinear wet concrete pressure envelope as proposed by Lings, Ng et al. (1994);
3) Cure the concrete panel by replacing the trench with concrete material and remove the applied bilinear concrete pressures simultaneously.

The WIP method is used in this thesis for simplicity.

3.4.3 Soil removal and structure installation

The soil excavation and structure installation can be modelled by deactivating or reactivating the corresponding finite elements in the model.

3.4.4 Dewatering and consolidation

A dewatering process is normally used inside the excavation when the ground water table is high, e.g. in Shanghai. The dewatering and consolidation processes can be conducted using a displacement-pore pressure coupled analysis with an effective stress soil model. The general process in the finite element analysis is described in this section, although they are not modelled in the analyses in this thesis, due to the limitation of the soil model used. The pore water pressure at the ground water table level and the excavated soil surface is set to zero in the analysis. Changes of pore water pressure with time are calculated with the drainage boundary conditions and specification of permeability and consolidation characteristics of the soil.

3.5 Summary

This chapter discussed the procedures of advanced finite element analysis of deep excavations based on a commercial software ABAQUS. The key components in the analysis include the soil, the retaining wall, the support system, adjacent infrastructure, constrains and contacts, and the boundary conditions. The material constitutive models are critical to capture the main excavation behaviour. The models for the soil, structures, and contact which are used in the following chapters are described in this chapter. The input parameters for the multiple-yield surface soil model are derived from published data about Shanghai clay. An anisotropic wall approach is adopted to consider the construction joints in the retaining wall, in which the stiffness along the length of the wall is reduced. The extended Coulomb friction model in ABAQUS is modified through a subroutine FRIC, in which the shear resistance at the soil-structure interface is related to the undrained shear strength of the soil. The main modelling procedures in the analysis are also described in this chapter, including the geostatic analysis, wall and pile installation, soil removal and structure installation, dewatering, and consolidation.

Chapter 4 Parametric studies of an idealised square excavation

4.1 Idealised square excavation

The deep excavation is a very complex soil-structure interaction problem, and its performance is affected by a number of factors such as the ground condition, the excavation geometry, the excavation depth, the type and stiffness of the retaining system, and the construction method. However, considering all of these features in a single analysis is difficult and cumbersome for practical use in the design and analysis of deep excavations. In addition, it is expensive and time-consuming to investigate the influence of these features through complex case history studies. Therefore, it is more reasonable and practical to conduct a series of parametric studies based on one simplified model to understand the influence of several main factors for general purposes. Moreover, the experience and skills obtained in this process are good preparations for the more complex case studies. An idealised square excavation with symmetric geometry is adopted in this chapter to conduct the parametric studies. Some useful findings and conclusions are generated for practical applications in the design and construction of deep excavations.

4.1.1 Geometry of the excavation

The idealised excavation, as shown in Fig.4.1, is the simplification of a typical square 3-level basement excavation (40m×40m in plane, 12m deep) using a top-down construction method. The excavation is retained by a diaphragm wall (1m thick, 30m deep) which is supported by 3 levels of horizontal floor slabs (150mm thick) and beams ($400\text{mm} \times 600\text{mm}$ in section), as shown in Fig.4.1. The floor slabs and beams are supported by vertical piles (800mm in diameter, 30m deep). The vertical distance between slabs is 4m, and the horizontal span of the beams is 8m. Openings are normally designed in the floor slabs for the purpose of lighting, ventilation, and transport of excavated soils, but such details are not included in the model for simplicity.

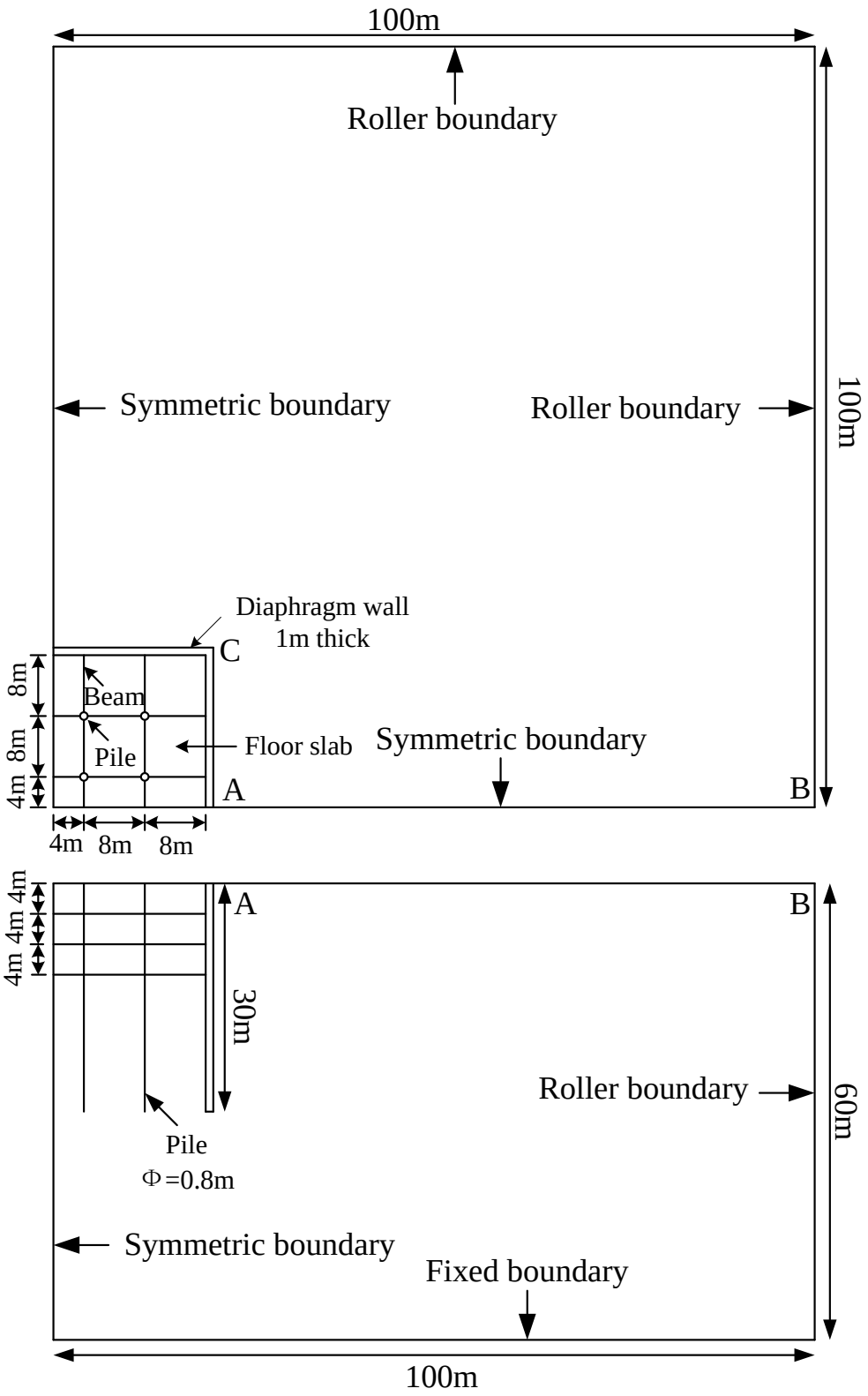

Fig.4.1 Plan and section views of the example excavation

4.1.2 Construction sequence

The construction sequence follows a typical top-down construction method (as shown in Fig.4.2) which is widely adopted all over the world due to the relatively small wall deflection and ground movement induced by the excavation.

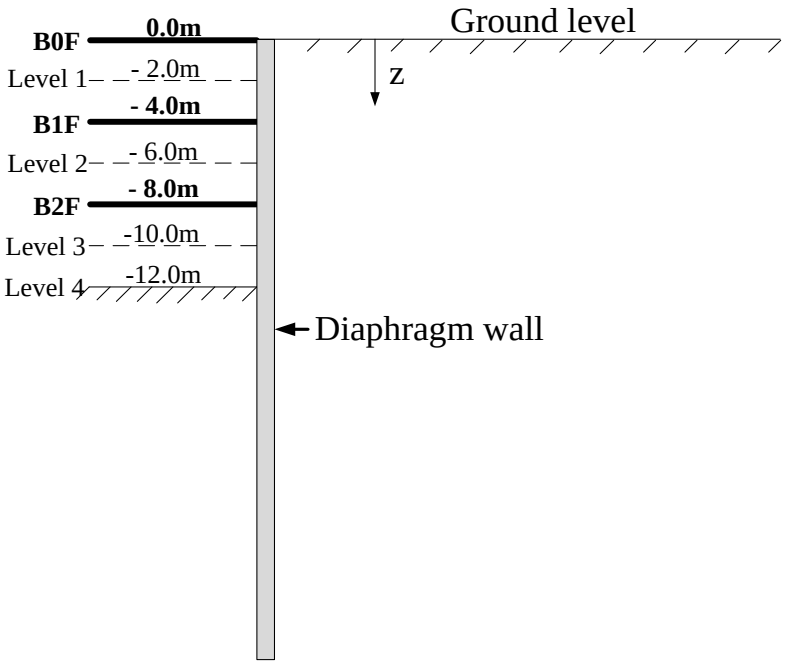

Fig.4.2 Construction sequence

The main activities of the construction are summarised in Table 4.1.

Table 4.1 Construction sequence

Step	Description
1	Install the diaphragm wall and piles.
2	Excavate to level 1 at -2m.
3	Install ground level beams and floor slabs (B0F).
4	Excavate to level 2 at -6m.
5	Install -1 level beams and floor slabs (B1F).
6	Excavate to level 3 at -10m.
7	Install -2 level beams and floor slabs (B2F).
8	Excavate to level 4 at -12m.

4.1.3 Finite element model

The finite element model considers the key structural components in the braced excavation and follows closely the top-down construction sequence. The mesh for the soil and the retaining system is shown in Fig.4.3 and Fig.4.4. The soil and the diaphragm wall are modelled with hexahedral solid elements (shell elements are also used in some analyses to model the diaphragm wall for comparison), while the beams and piles are modelled with beam elements (solid elements are also used in some analyses to model the piles for comparison), and the floor slabs are modelled with quadrilateral shell elements. A large family of element types (e.g. linear and quadratic elements, with full or reduced integration) are available in ABAQUS, but they may have difference in terms of the accuracy and efficiency in the computation. The difference is compared through parametric studies.

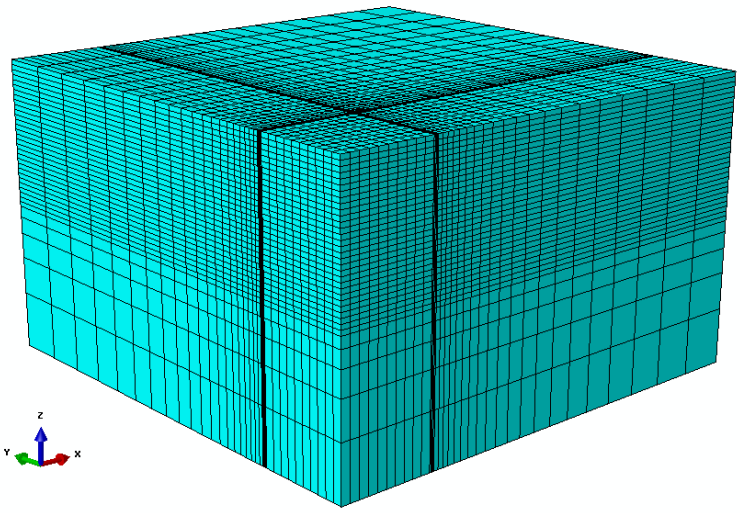

Fig.4.3 Mesh for the soil

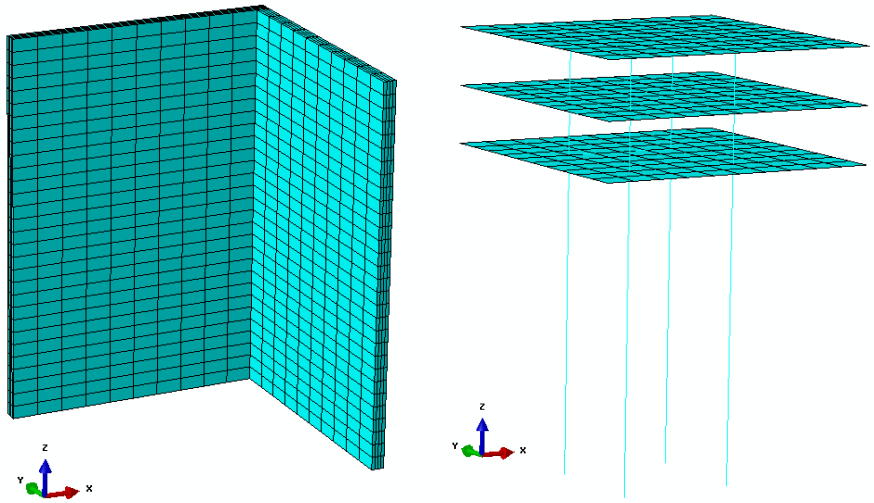

Fig.4.4 Mesh for the diaphragm wall and support structure

As shown in Fig.4.1, two vertical boundaries are symmetric, and the other two are rollers, while the bottom is fixed. Tie constraints are used to connect the beams, piles, floor slabs, and the diaphragm wall, representing rigid connections between cast-in-situ reinforced concrete components, but the real connections may be more complex. The piles are embedded into the soil without any interface properties when the pile is modelled with beam elements, whereas the soil/pile interface behaviour can be considered when the pile is modelled with solid elements. It should be noted that modelling the piles with solid elements is tedious in the mesh generation, especially when the number of piles is large and the retaining system is complex. Both beam elements and solid elements are used to model the piles to compare their difference. Similarly, the diaphragm wall is modelled with both solid elements and shell elements for comparison. The influence of the soil-structure interface properties is also investigated in the parametric analysis.

4.1.4 Material models and input parameters

Throughout the analyses, the soil is represented by the multiple-yield surface model to consider the small-strain stiffness nonlinearity of the soil, associated with the input parameters derived in Chapter 3 for Shanghai clay. The structural components (i.e. the diaphragm wall, the beams, piles, and floor slabs) are assumed to be reinforced concrete materials and behave linear elastically for simplicity. The density of the clay ρ_s is assumed to be $1800kg/m^3$. The water table is assumed to be at the ground surface. The coefficient of earth pressure at rest K_0 is assumed to be 0.5, equivalent to $K_0^t = 0.778$ in total stress expression. All the analyses are conducted in undrained conditions.

4.2 Strategy of the analyses

A strategy of the analyses is made, as shown in Fig.4.5, to organise the analyses and present the results in a systematic way. The basic analysis is conducted first. The results from other analyses with new features are then compared with the basic analysis to investigate their influence.

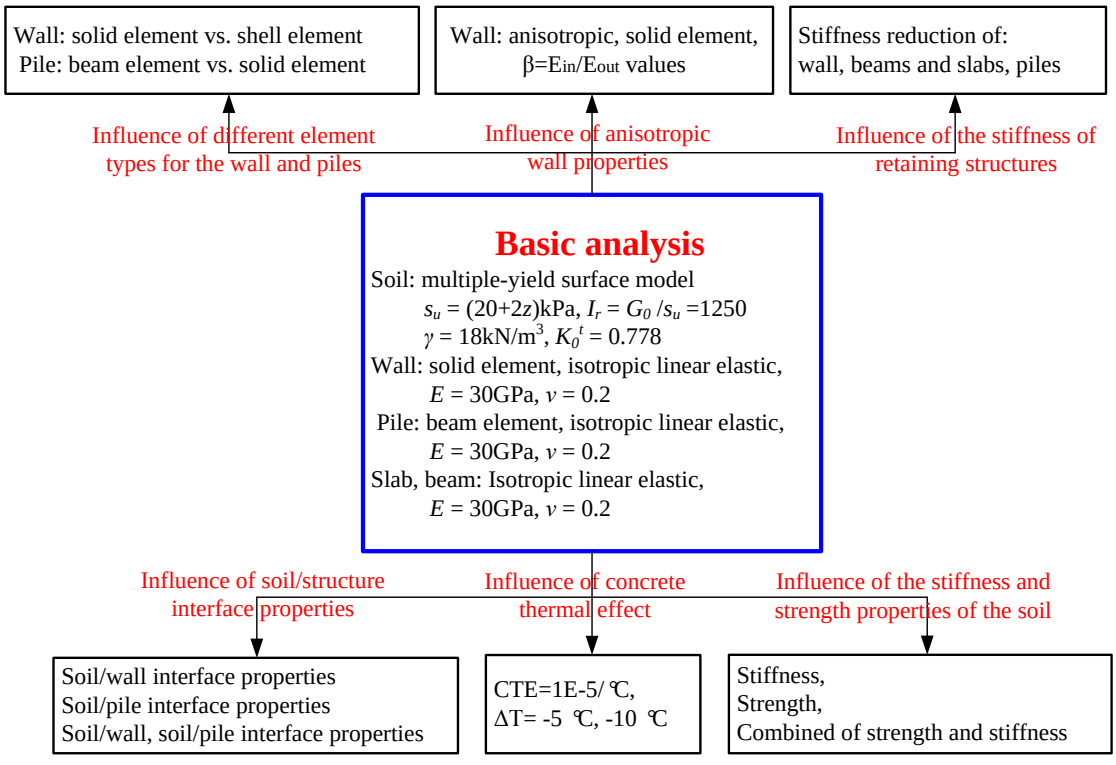

Fig.4.5 Strategy of the analyses

The important features investigated in this chapter include,

1) The influence of element types for the soil and structures, linear and quadratic element, with full and reduced integration;
2) The difference between solid and shell elements to model the wall;
3) The difference between solid and beam elements to model the pile;
4) The influence of soil-structure interface behaviour;
5) The influence of operational stiffness of structural components;
6) The influence of thermal effect of concrete beams and floor slabs;
7) The influence of construction joints in the diaphragm wall;
8) The influence of stiffness and strength properties of the soil;
9) The difference between basic and improved analysis.

The results and discussions are presented in the following sections.

4.3 Influence of element types

4.3.1 Modelling the soil and structures: linear or quadratic elements

The soil and structural components in finite element analysis can be modelled by linear or quadratic elements, with full or reduced integration. For the soil, four elements types are available, linear hexahedral element with full integration (C3D8) and reduced integration (C3D8R), quadratic hexahedral element with full integration (C3D20) and reduced integration (C3D20R). For beams and piles, two element types are available, linear beam element (B1) and quadratic beam element (B32). For floor slabs, there are four element types, linear quadrilateral shell element with full integration (S4) and reduced integration (S4R), quadratic quadrilateral shell element with full integration (S8) and reduced integration (S8R). In general, quadratic elements are theoretically more accurate than corresponding linear elements, but also consume more computing resources and take longer time to run if the same mesh is used. Elements with reduced integration have fewer integration points and are thus cheaper than corresponding elements with full integration. In this section, four analyses with different element types, as

shown in Table 4.2, are conducted to compare their difference based on the same mesh. The soil dominates the analysis as it has the largest number of elements in the model, and the integration points in Table 4.2 refer to the hexahedral solid elements for the soil.

Table 4.2 Comparison between different element types

Case	Element types	Number of Elements	Number of Nodes	Integration points	CPU time(s)
1	Linear, full integration	37700	41740	$2 \times 2 \times 2$	3132
2	Linear, reduced integration	37700	41740	$1 \times 1 \times 1$	2393
3	Quadratic, full integration	37700	159599	$3 \times 3 \times 3$	47103
4	Quadratic, reduced integration	37700	159599	$2 \times 2 \times 2$	43480

Table 4.2 shows that Case 2 (linear element with reduced integration) takes the least time to run, and the difference in CPU time between linear elements (Case 1 and 2) and quadratic elements (Case 3 and 4) is significant. Using reduced integration can slightly reduce the time.

The computed results, including the wall deflection at the wall centre (point A) and ground surface movements behind the wall centre along AB, are shown in Fig.4.6 and Fig.4.7.

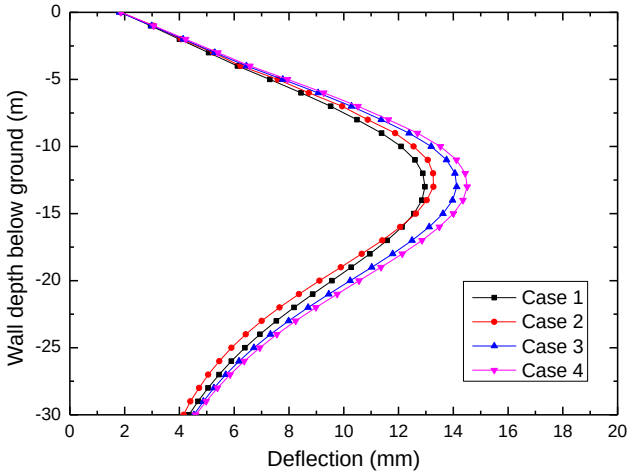

Fig.4.6 Wall deflections at point A

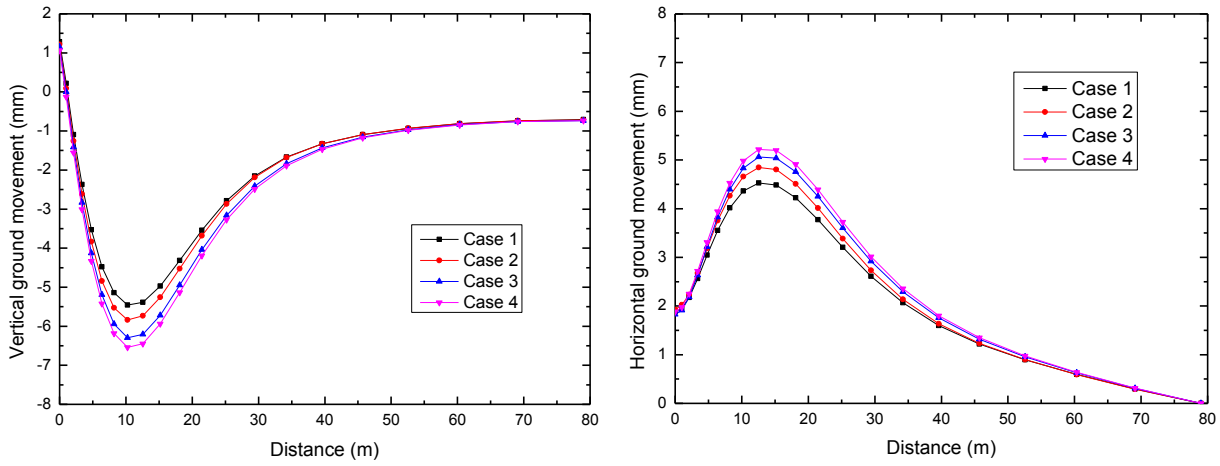

Fig.4.7 Ground movements along AB

In general, the pattern of the computed wall deflection and ground movements is relatively insensitive to the element types, but there is difference in term of the magnitude. Two analyses with linear elements (Case 1 and 2) result in slightly smaller results than the two analyses with quadratic elements (Case 3 and 4) because linear elements are stiffer, whereas the two analyses with reduced integration (Case 2 and 4) produce larger results than the two analyses with full integration (Case 1 and 3) because elements with reduced integration are more flexible. For both linear and quadratic elements, the difference between analyses with full and reduced integration is small. The results from linear elements with reduced integration (Case 2) are close to those from quadratic elements (Case 3 and 4), but Case 2 takes much less time to run. However, it should be noted that linear elements have deficiencies and are particularly susceptible to shear locking when modelling almost incompressible material, like soil in undrained conditions. They will produce too stiff response which results in smaller displacements, and over-predict the strength in some geotechnical problems. Therefore, quadratic elements are recommended for more accurate analysis.

Linear elements are used in the subsequent parametric studies in this chapter mainly for consistency, considering that quadratic elements will cause numerical instabilities in contact analysis in ABAQUS. However, it is noted that this is a serious simplification of the analyses in this chapter and should not be normally taken in the future. In the following case studies from Chapter 5 to Chapter 7, linear elements have to be used so that the complicated geometries could be modelled with the limited computing resources available. Otherwise, the significant increase of nodes by quadratic elements in a reasonable fine mesh will pose considerable challenge to the computating resources. In such cases, the agreement with field data might be fortuitous.

4.3.2 Modelling the retaining wall: solid or shell elements

The retaining wall can be modelled with either solid elements or shell elements in 3D analyses. Shell elements are popular because, (i) details of the wall (e.g. variation of wall thickness) can be neglected in the mesh generation, (ii) they are computationally cheaper due to relatively smaller

number of DOFs, and (iii) they can directly output the internal forces and bending moments. However, Zdravkovic, Potts et al. (2005) pointed out that the computed wall deflections and ground movements are larger from shell element wall than those from solid element wall, which is because shell element wall does not have the beneficial bending moment towards the retained side caused by the shear stress on the wall interface about the centreline of the wall thickness because shell element has no geometric thickness. However, the magnitude of the difference in the computed results may depend on other factors such as the soil condition, the retaining system, and the construction method. Results from two analyses are illustrated in Fig.4.8 and Fig.4.9.

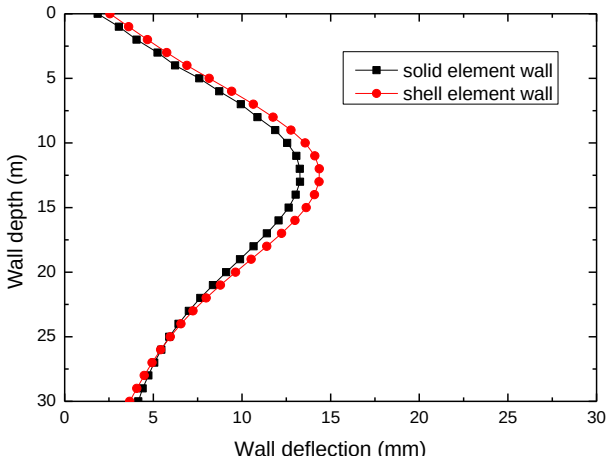

Fig.4.8 Wall deflection at Point A

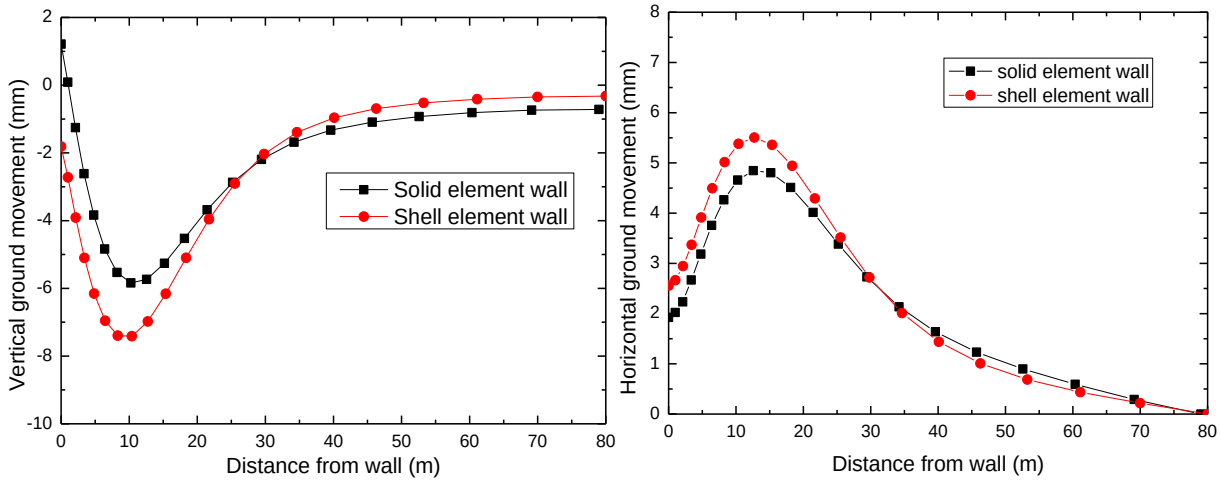

Fig.4.9 Ground movements along AB

The results indicate that both wall deflection and ground movements from the shell element wall are larger than those from the soil element wall. This finding is consistent with that from Zdravkovic, Potts et al. (2005). Considering this difference, solid elements are preferred to model the wall in other analyses in this chapter and case studies in subsequent chapters.

4.3.3 Modelling the piles: solid or beam elements

The piles can be modelled with either beam or solid elements in 3D deep excavations. Beam elements are more suitable for practical use when there are a large number of piles in the analysis, because the detailed geometry can be ignored in the mesh generation. The shortcoming, however, of using beam elements to model the piles in ABAQUS is that the soil/pile interface behaviour cannot be considered, because the contact formulation in ABAQUS is surface-based which is not applicable to beam elements. In contrast, the soil/pile interface behaviour can be considered if the pile is modelled with solid elements, but modelling the geometry of piles would greatly increase the complexity in the mesh generation. This section investigates the difference in using these two element types to model piles when the interface behaviour is not considered. The influence of the interface properties will be discussed later in other sections.

As shown in figures below, although modelling the pile with beam elements results in slightly larger wall deflection and ground movements, the difference is insignificant.

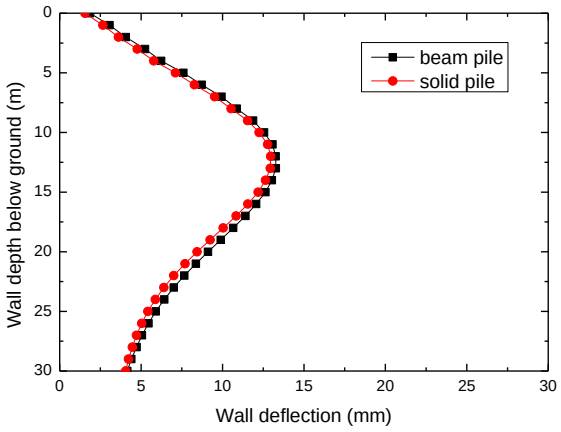

Fig.4.10 Wall deflection at A

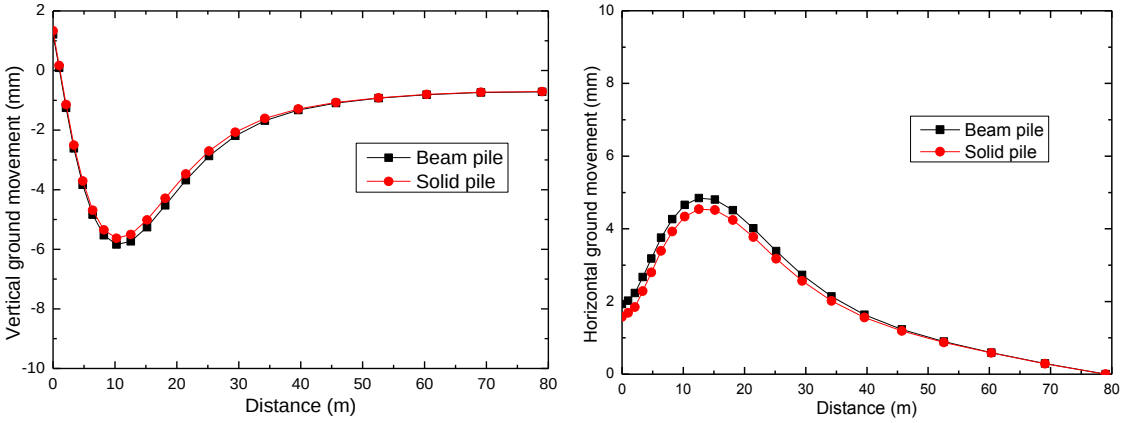

Fig.4.11 Ground movements along AB

The vertical displacement contours of the roof floor slab at the final stage of the excavation, as shown Fig.4.12, also indicates that there is little difference between beam elements and solid elements to model the pile. The comparison suggests that the pile can be modelled by either beam elements or solid elements when the soil/pile contact is not considered. For convenience, beam elements are preferred to model the piles in this situation.

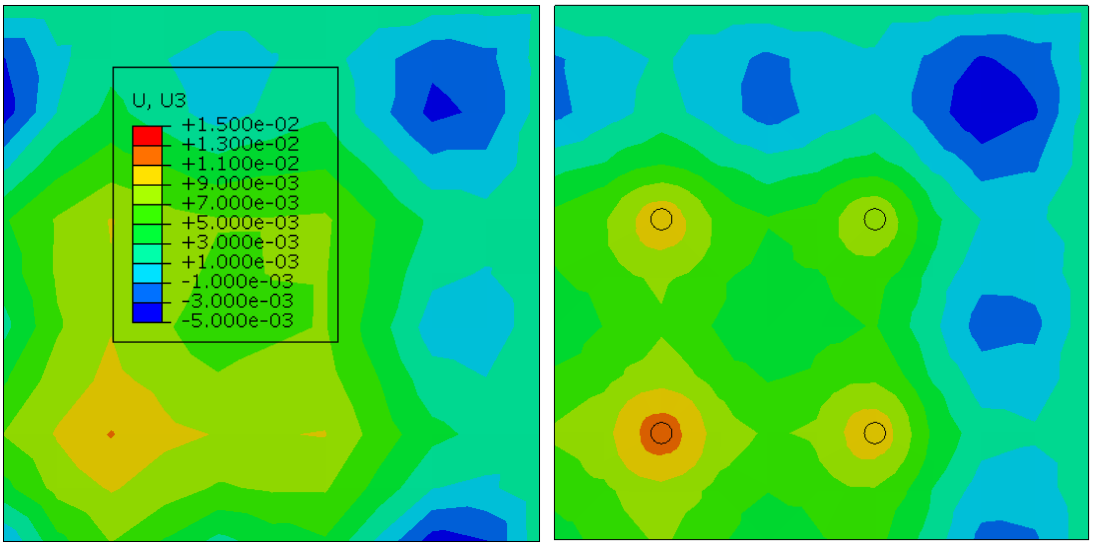

(a) Beam piles (b) Solid piles

Fig.4.12 Vertical displacement contour of roof floor slab (unit:m)

4.4 Influence of the operational stiffness of retaining structures

4.4.1 Influence of the operational stiffness of the diaphragm wall

Potts and Day (1990) showed that the flexibility of retaining walls has a considerable effect on the distribution of earth pressures. As wall flexibility increases, there is increased freedom for stresses imposed by the soil to redistribute and reduce the structural forces in the wall. Unfortunately, this beneficial effect is accompanied by greater wall and soil movements. Therefore, there is a compromise between reduced bending moments and increased movements as the flexibility of the wall is increased.

The reinforced concrete diaphragm wall will inevitably crack as the cement ages, through thermal and drying shrinkage (Puller 2003). The cracks in the diaphragm wall will propagate when excavation proceeds due to the deflection caused by earth pressure and constraints exerted from other structural components (e.g. beams and floor slabs). Ou, Liao et al. (1998) compared

the wall bending moments calculated from the measurement of rebar strain gauge embedded in the diaphragm wall and the curvature of wall deflection from the inclinometer reading, as shown in Fig.4.13, and found that bending moments computed from the strain gauges are generally smaller than those from the wall deflection curve, particularly for the location where the maximum lateral wall deflection occurs and its neighbouring location. This may be because the bending moment from the wall deflection curve is computed without considering cracked concrete so that the moment of inertia *I* is not reduced.

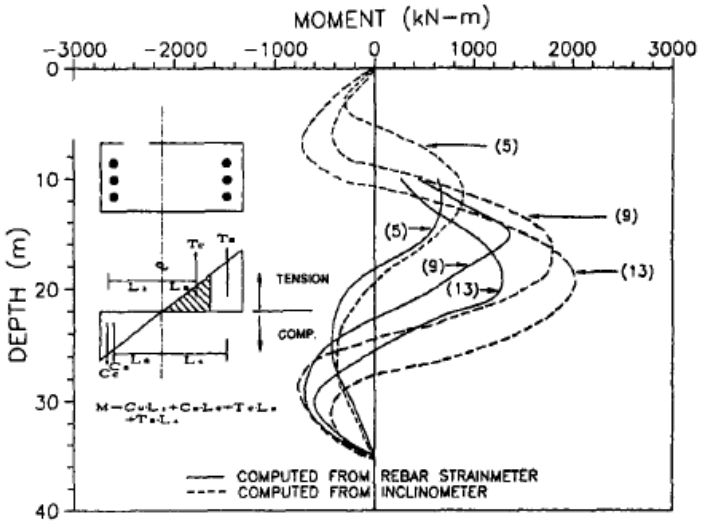

Fig.4.13 Wall bending moments from strain gauge and inclinometer (Ou, Liao et al. 1998)

Ou, Liao et al. (1998) also defined the reduction factor *R* for the moment of inertia *I* as the ratio of the moment obtained from the rebar strain gauge to the moment obtained from the inclinometer measurement. Fig.4.14 shows the variation of *R* with depth in different stages of excavation, and *R* can be as small as 0.5 at some point.

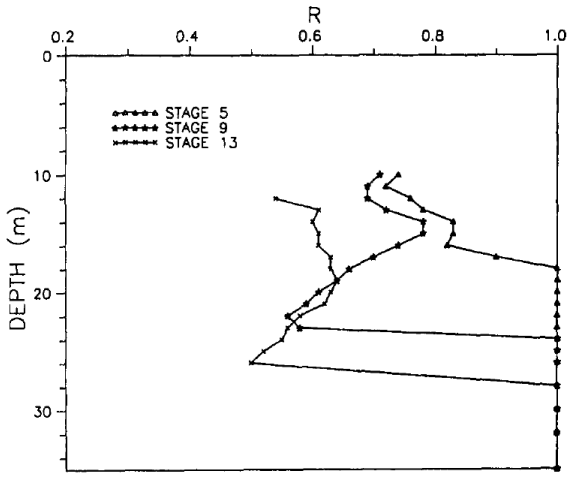

Fig.4.14 Variation of *R* at various stages of excavation (Ou, Liao et al. 1998)

In the numerical analysis, the moment of inertia is a constant once the cross section of the diaphragm wall is decided. However, a smaller Young's modulus E of the concrete can be used instead in an equivalent way to represent the reduced stiffness. In this section, the Young's modulus of the diaphragm wall is computed from $R \cdot E$, where R is a reduction factor and E is the nominal value of intact concrete Young's modulus. Three different values of R (1.0, 0.5, and 0.1) are assumed to investigate its influence on the excavation behaviour. The stiffness of the other concrete structure components is not reduced. The results of these analyses are shown in Fig.4.15 and Fig.4.16.

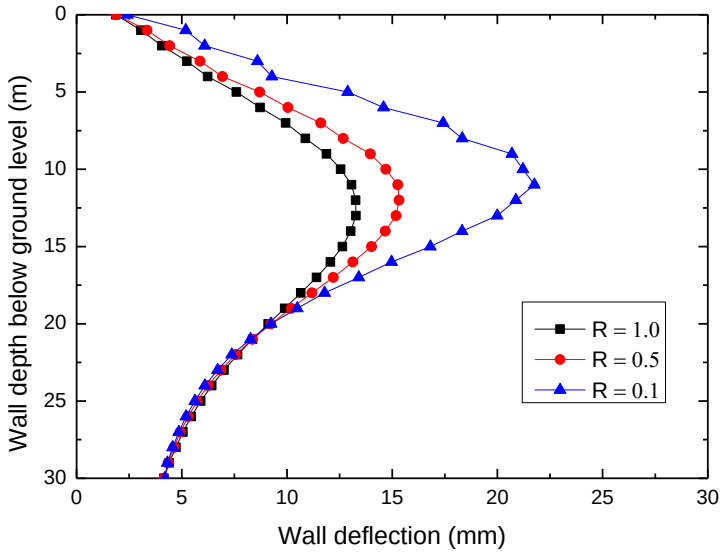

Fig.4.15 Wall deflection at point A

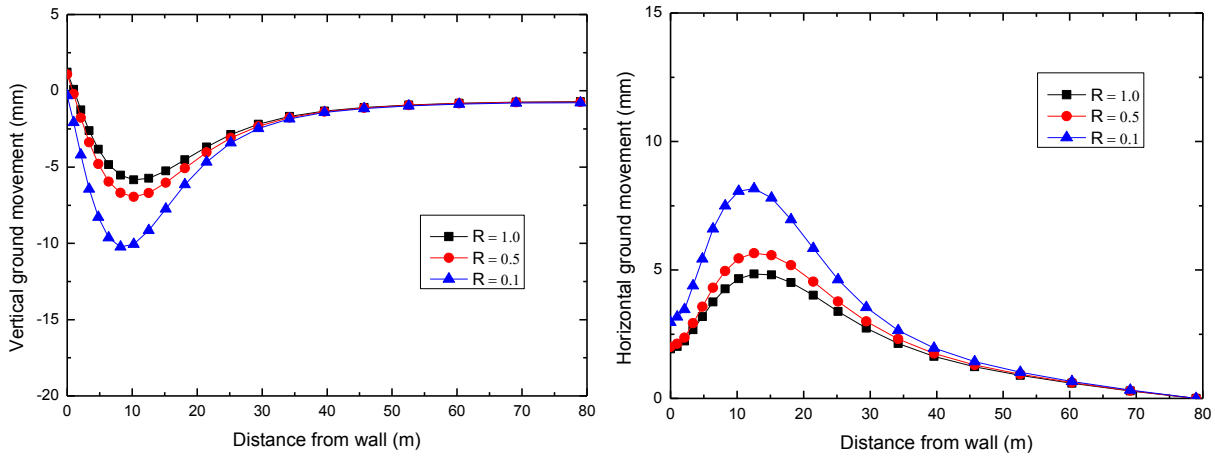

Fig.4.16 Ground movements along AB

The results show that as the wall stiffness decreases, the wall becomes more flexible, resulting in larger wall deflection and ground movements while the deformation pattern is maintained. When the wall stiffness is reduced to half of its nominal value ($R = 0.5$) which is likely to be a realistic

value, the largest wall deflection and ground movements increase approximately 15%. However, for $R = 0.1$, which might be the worst case, there is nearly 70% increase of largest wall deformation and ground movements.

4.4.2 Influence of the stiffness of horizontal beams and floor slabs

The operational stiffness of the horizontal support system (e.g. beams, floor slabs, and struts) may also be different from its nominal value. The stiffness changes as excavation proceeds and may be influenced by a number of factors, e.g. workmanship, thermal effects, cracks and creep of the concrete, misalignment error, and bending phenomena caused by heave of vertical piles (Ou 2006). The stiffness of the horizontal support system was reduced to 80% of its nominal value in some previous numerical analyses (Simpson 1992, St. John, Potts et al. 1993, Ou 2006) to consider these effects. The reduction value, however, may vary from one case to another.

Further calculations have been conducted in which a reduction factor R (1.0, 0.5 and 0.1) is applied to the nominal value of the Young's modulus E of the horizontal beams and floor slabs. The stiffness of other structural components is not reduced. The wall deflection and ground movements are shown in Fig.4.17 and Fig.4.18. It is noted that both the wall deflection and ground movements increase as the stiffness of the horizontal support system is reduced. For $R = 0.5$, the wall deflection and ground movements increase by around 10%. There is, however, significant increase of wall deflection and ground movement if the stiffness is reduced to 10% of its nominal value ($R = 0.1$). In this case, the pattern of the deformation also changes. In reality, the operational stiffness of the horizontal support system is unlikely to be reduced to only 10% of its nominal value ($R = 0.1$), except for extremely poor construction quality. Therefore, the stiffness reduction of the horizontal system may be less important than the stiffness reduction of the retaining wall.

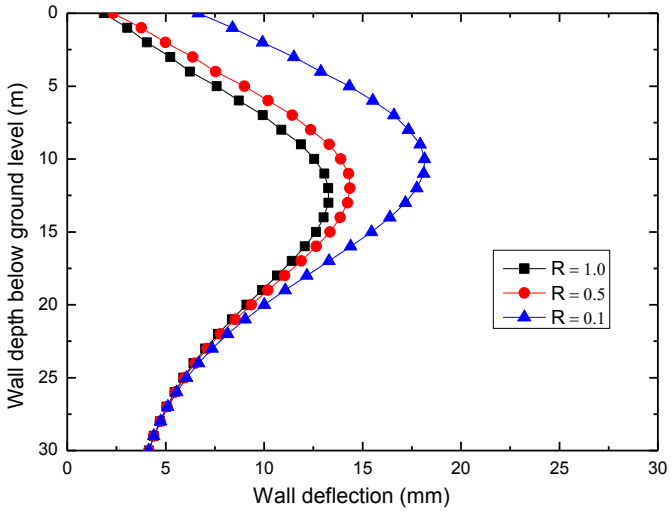

Fig.4.17 Wall deflection at point A

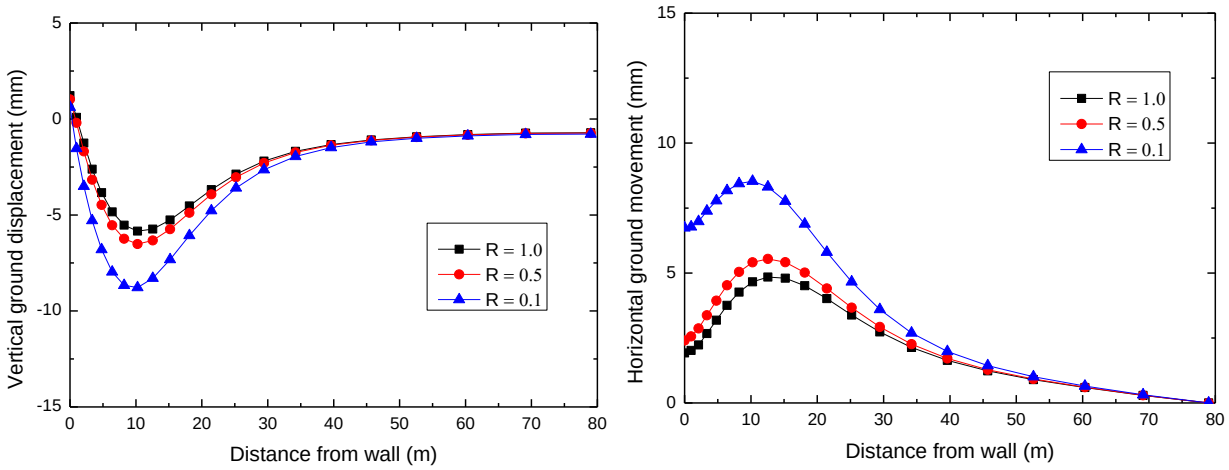

Fig.4.18 Ground movements along AB

4.4.3 Influence of the stiffness of vertical piles

The operational stiffness of the bored piles in the field may also be affected by the construction quality and the imperfections in the concrete. To investigate how the pile stiffness influences the excavation behaviour in the numerical analyses, the reduction factor *R* (1.0, 0.5, and 0.1) is applied to the nominal stiffness of piles. The results are shown in Fig.4.19 and Fig.4.20.

It can be seen that both the wall deflection and ground movements are insensitive to the variation of pile stiffness. Even the stiffness of the pile is reduced to 3GPa (10% of its nominal value), the increase of the wall deflection and ground movements is insignificant. Therefore, the stiffness reduction of vertical piles would not be expected to affect the excavation behaviour. This finding, of course, is not unexpected.

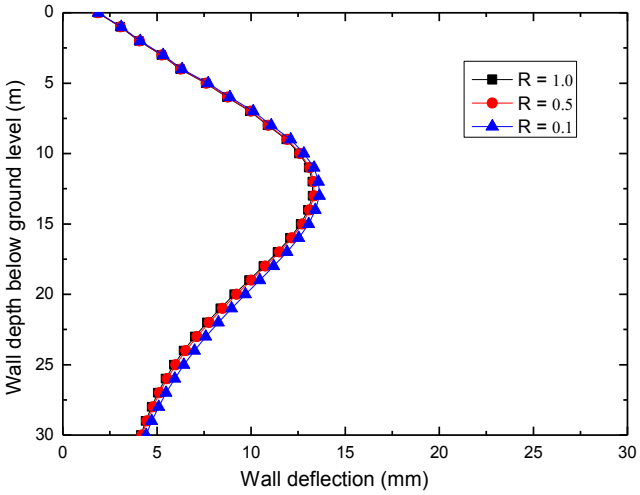

Fig.4.19 Wall deflection at point A

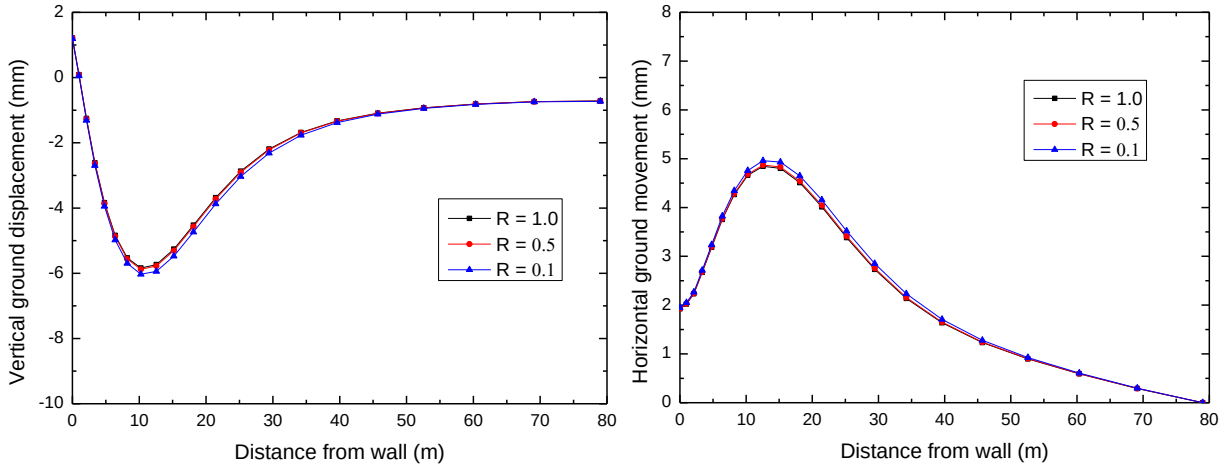

Fig.4.20 Ground movements along AB

4.4.4 Influence of the stiffness of the wall, floor slabs and piles

For a specific deep excavation project, it is reasonable to assume that the stiffness of all reinforced concrete components (e.g. diaphragm wall, horizontal struts, and piles) in deep excavations have similar Young's modulus E. Therefore,the same reduction factor R (1.0, 0.5, and 0.1) is applied to all the reinforced concrete structural components, to investigate its influence on the excavation behaviour. The wall deflection and ground movements are shown below in Fig.4.21 and Fig.4.22. The results indicate that the stiffness reduction of the reinforced concrete structural components has non-trivial influence on the excavation behaviour. However, when the operational stiffness of the concrete structure components is kept within 50% of its nominal value, the increase of wall deflection and ground movements is limited. In extreme conditions ($R = 0.1$), the wall deflection and ground movements increase significantly. Considering the separate analyses in the previous sections, it is concluded that the stiffness of the

diaphragm wall and horizontal support system should be carefully selected in the analysis.

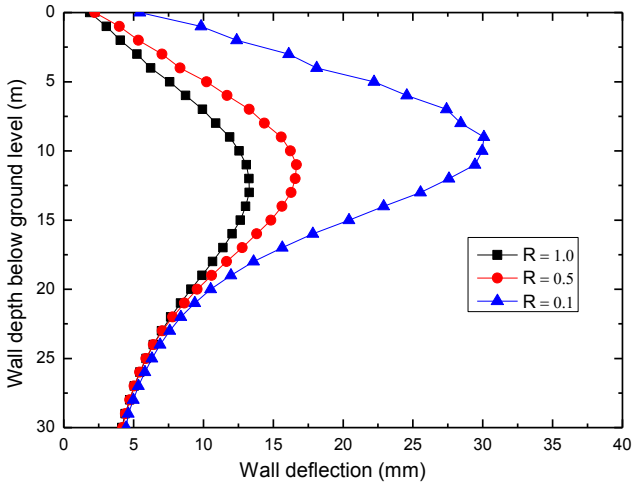

Fig.4.21 Wall deflection at point A

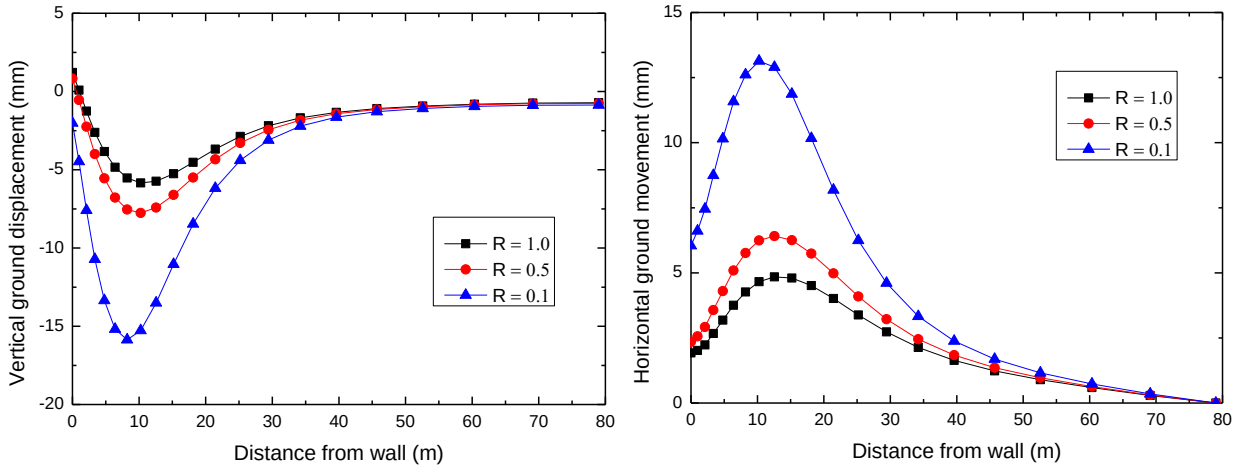

Fig.4.22 Ground movements along AB

4.5 Influence of thermal effects of concrete structures

The concrete structures (e.g. diaphragm walls, beams, floor slabs, and piles) may experience thermal shrinkage and expansion, cracks and creep during the curing process (e.g. hydration and chemical reaction, thermal effect) and as the excavation proceeds due to the variation of ambient temperature. This phenomenon has been addressed by many previous researches, e.g. Whittle, Hashash et al. (1993), Puller (2003), Ou (2006), but it has not been studied in detail yet because the mechanism is rather complicated.

Another issue related to the horizontal support system is the connection with the retaining wall. In finite element analyses, the horizontal support system (e.g. floor slabs, beams) is usually tied to the retaining wall, which constrains all possible degrees of freedom. The real connections,

however, may not be that rigid, and rotations may be allowed, or gaps may develop during the construction. Additional wall displacement may happen to make the horizontal support in compression and interact with the retaining wall. This additional wall displacement can also be considered by the thermal shrinkage of the horizontal support. The amount of shrinkage can be estimated through experience or back analysis of case histories.

The thermal effect of concrete structural components can be included directly in the numerical analysis through the combination of a coefficient of thermal expansion α and a temperature change ΔT. The average value of α for concrete is $10^{-5}/℃$, which does not vary too much. The temperature varies in the concrete during curing process. In the analysis here, a cooling down temperature $\Delta T = -10℃$ is assumed in all the concrete beams and floor slabs during the curing process. Extra temperature change $\Delta T = 20℃$ and $-20℃$ is assumed in the top floor slab due to the seasonal temperature fluctuation.

To investigate the influence of thermal effects of concrete on the excavation behaviour, three cases of analyses, as described in Table 4.3, and conducted and compared with the basic analysis which has no thermal effects.

Table 4.3 Description of the analyses

Case No.	Description
Basic	Basic analysis, no thermal effects
1	Thermal shrinkage during curing process, $\Delta T = -10℃$ to all levels of beams and slabs
2	Thermal contraction due to ambient temperature change, $\Delta T = -20℃$ to top level beams and floor slab only
3	Thermal expansion due to ambient temperature change, $\Delta T = 20℃$ to top level beams and floor slab only

The results from these analyses are shown in figures below. It is found that the thermal effect of concrete beams and floor slabs has a large influence on the computed wall deflection and ground movements. When the concrete cools down $-10℃$ during the curing process, the horizontal concrete beams and floor slabs will shrink and pull the retaining wall, which causes around 15% increase in wall deflection and ground movements. If the temperature change is larger, the thermal shrinkage would be more significant. The seasonal temperature fluctuation is assumed to

affect mainly the roof floor slab. When an additional ±20℃ temperature change is applied to the roof floor slab, the wall deflection varies by around 2mm close to the level of the roof floor slab which contracts or expands. Accordingly, the horizontal ground movement varies a lot, whereas the vertical ground movement is relatively stable. In summary, the thermal effect of the horizontal beams and floor slabs should be considered in the analysis.

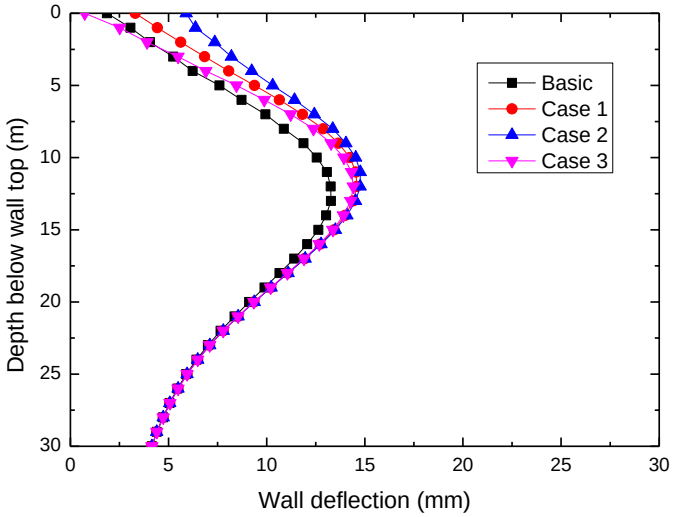

Fig.4.23 Wall deflection at point A

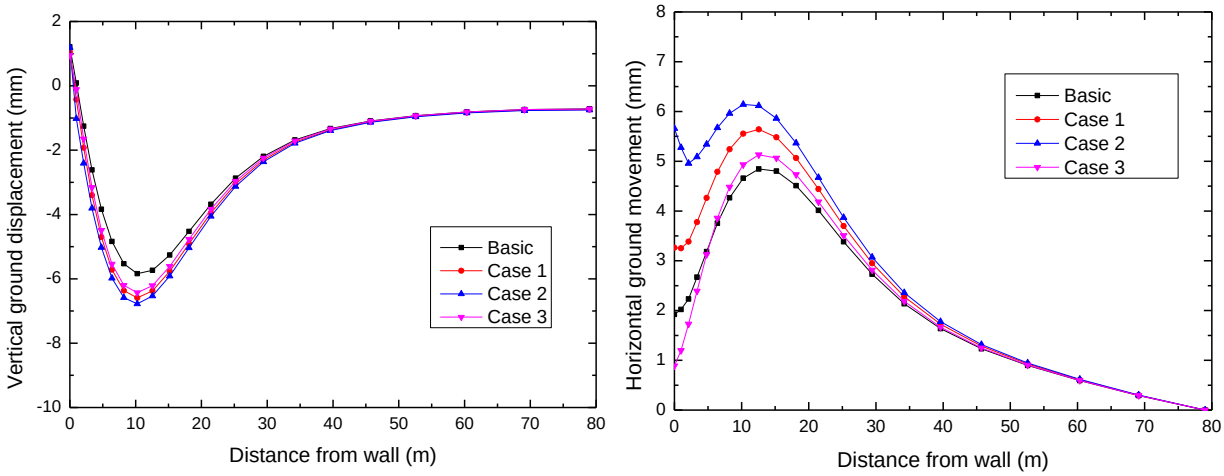

Fig.4.24 Ground movements along AB

4.6 Influence of soil-structure contact and interface properties

The contact between the soil and structures is a critical problem in geotechnical engineering. In deep excavations, there are large areas of interface between the soil and structures (e.g. the soil/wall interface and the soil/pile interface), and the interface properties may affect the excavation behaviour. It is difficult to investigate their influence through in-situ tests or laboratory experiments, but is straightforward through numerical analyses. In previous analyses,

tie constraints are applied at the soil-structure interface, representing rough interface properties, but this assumption does not reflect the real interface conditions. In this section, a frictional contact model is applied at the soil-structure interface associated with different interface properties, to investigate its influence on the excavation behaviour.

4.6.1 Mechanisms of contact between the soil and structures

Frictional behaviour at the soil-structure surface is controlled mainly by the complex phenomena that develop within a very thin layer of soil close to the contact area. This layer of soil can be considered as a zone of intense localisation of shear strains, and the surrounding soil can be thought of as a restraining medium. The interface behaviour may be affected by the surface topography, and the frictional resistance to relative motion at the interface between the two materials is of considerable importance (Butterfield and Andrawes 1972). The soil-structure interface shear resistance is normally slightly less than the strength of the soil, and tends to decrease as the surface roughness reduces. The strength of soil-structure interface drops after the peak strength is reached, because the plane surface facilitates the reorientation of clay particles and the destruction of the bond between particles during shearing. The shear resistance is generally different from the residual strength of the soil which is mobilised after the application of large shear displacement, and depends mainly on the interface material and its roughness, the soil properties, the grain size distribution and shape of the soil particles, the magnitude of the normal stress, and the rate of shear displacement (Lemos and Vaughan 2000).

Understanding the shear strength of soil-structure interface is important in determining the interface properties in deep excavations. During the installation of diaphragm walls and bored piles, the soil close to the surface of these structures may encounter a certain amount of disturbance. The soil on this interface is assumed to have been sheared to critical conditions with operational undrained shear strength $\bar{s}_u$,

$$\bar{s}_u = \alpha \cdot s_u \qquad (4.1)$$

where α is a reduction factor, and s_u is the in-situ undrained shear strength. The reduction factor

is often based on the remoulded strength, and therefore related to the inverse of the sensitivity S_t.

The extended Coulomb friction model described in Chapter 3 is used here to represent the frictional behaviour at the soil/wall and soil/pile interface. The influence of the value of α is investigated through parametric studies.

4.6.2 Influence of the soil/wall interface properties

Five analyses, as described in Table 4.4, were conducted to investigate the influence of soil/wall interface properties on the excavation behaviour, and to understand what is the difference if the contact is not considered and how sensitive is the result to the value of α.

Table 4.4 Description of analyses

Case No.	Description
1	fully rough contact(Basic analysis)
2	$\tau_{crit} = \alpha \cdot s_u$, $\alpha = 1.0$
3	$\tau_{crit} = \alpha \cdot s_u$, $\alpha = 0.5$
4	$\tau_{crit} = \alpha \cdot s_u$, $\alpha = 0.1$
5	Fully smooth contact

The results from these analyses are shown in figures below. It is shown that the computed wall deflection and ground movements are sensitive to the soil/wall interface property. If the interface property is neglected in the analysis, the wall deflection and ground movements would be underestimated. The rough and smooth conditions provide the lower and upper bounds of the possible results, and the real excavation behaviour is expected to situate between these two bounds, depending on the interface properties. The three values of α (1.0, 0.5, and 0.1) may represent three possible contact conditions. When $\alpha = 1.0$, slip happens when all the soil shear strength is mobilised on the interface. In the condition of $\alpha < 1.0$, the shear resistance at the soil/wall interface is smaller the shear strength of the soil due to the disturbance during the wall installation, which means that slip occurs at a smaller shear resistance value than the soil shear strength, thus resulting in larger wall and ground deformation. It is also noticed that the interface property affects the wall horizontal translation and the ground movement close to the wall. In the light that the result is sensitive to the interface properties, a reliable α should be estimated in the analysis.

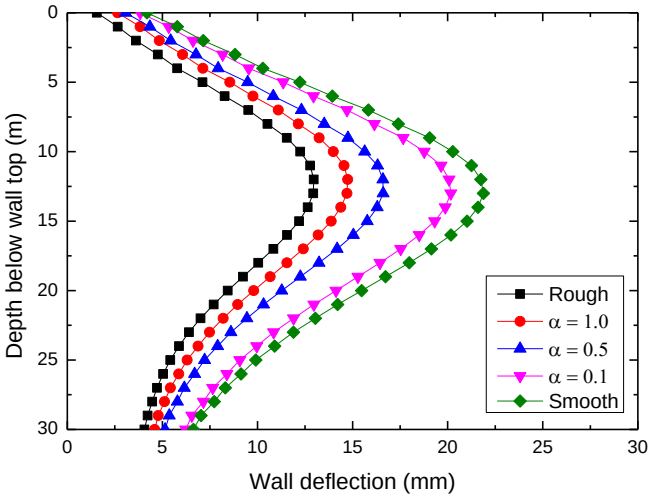

Fig.4.25 Wall deflection at point A

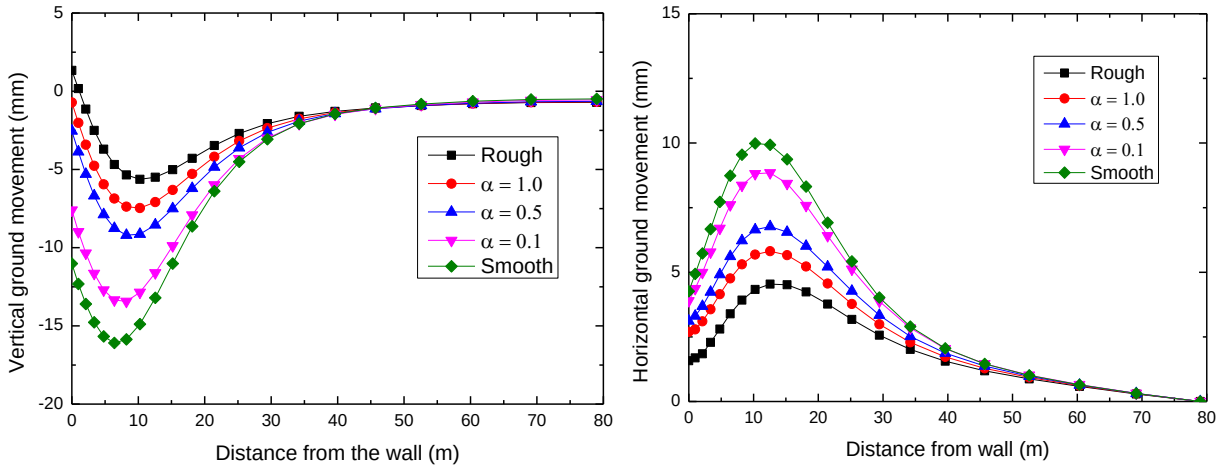

Fig.4.26 Ground movements along AB

4.6.3 Influence of the soil/pile interface properties

Similar analyses have been conducted, as shown in Table 4.5, to investigate the influence of soil/pile interface property on the excavation behaviour. In order to consider the soil/pile contact, the piles are modelled with solid elements. In real cases, however, modelling the piles with solid elements is extremely tedious in more complex case studies which may have irregular geometry and contain thousands of piles. This parametric analysis, therefore, is very useful to understand how large is the influence when the piles are modelled with beam elements and the soil/pile contact is neglected.

Table 4.5 Description of analyses

Case No.	Description
1	fully rough contact (Basic analysis)
2	$\tau_{crit} = \alpha \cdot s_u, \alpha = 1.0$
3	$\tau_{crit} = \alpha \cdot s_u, \alpha = 0.5$
4	$\tau_{crit} = \alpha \cdot s_u, \alpha = 0.1$
5	Fully smooth contact

It is shown in Fig.4.27 and Fig.4.28 that the excavation behaviour is also sensitive to the soil/pile interface properties, and neglecting the contact would underestimate the wall deflection and ground movements, although this influence is relatively smaller than that of the soil/wall contact. It seems that the wall deflection is affected mainly below the final excavation level (12m below the ground surface) with the largest difference around 2mm, which makes sense because the soil/pile contact mainly affects the soil movement inside the excavation. The contact conditions may represent the amount of constraints the piles can provide to the soil movement inside the excavation, and the constraint is reduced when slip is allowed between the soil and piles. The ground movements are also influenced by the soil/pile contact, but mainly in the area around the largest ground movements, which is consistent with the wall deflection. However, the influence of the value of α on excavation behaviour is limited.

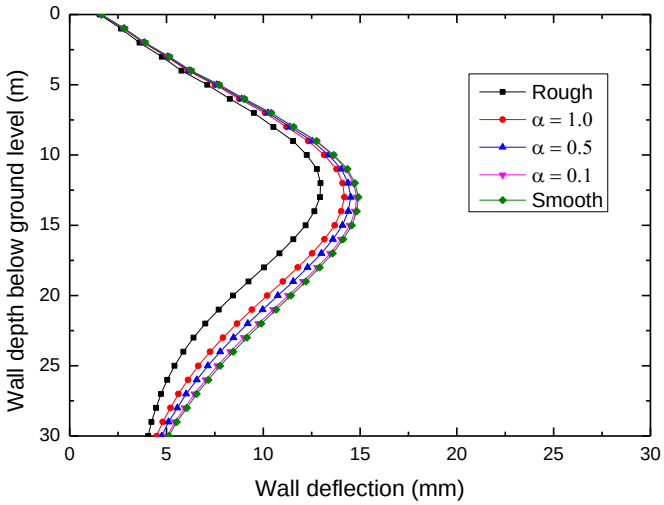

Fig.4.27 Wall deflection at point A

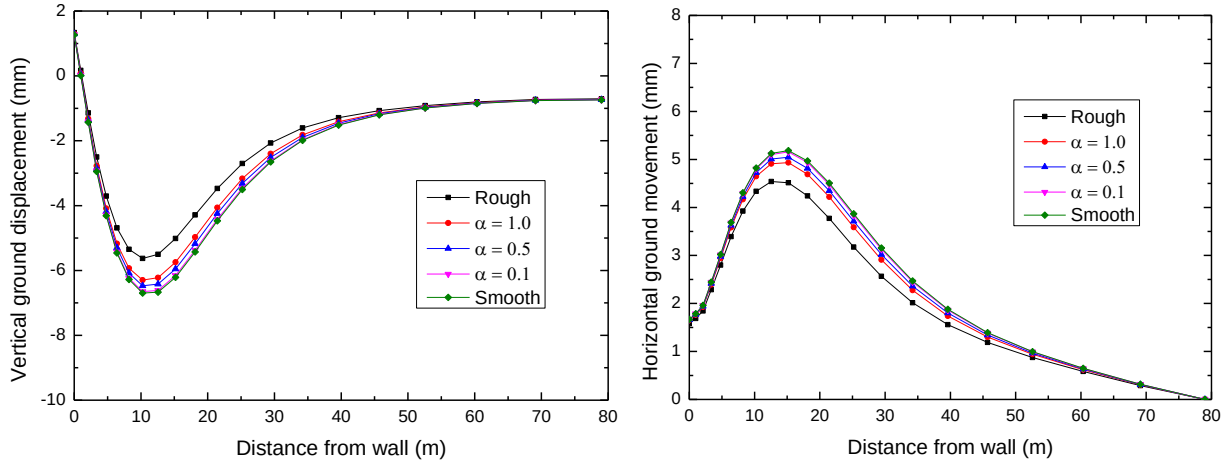

Fig.4.28 Ground movements along AB

The contours of the vertical displacement at the roof floor slab from the rough and smooth contact conditions are shown in Fig.4.29. It is found that all piles go upwards at the top even in the smooth condition, which is consistent with field observations where the piles heave at the top (Xu 2007). The soil/pile contact conditions affect the vertical displacement of the piles and the horizontal support system. When slip is allowed between the soil and piles, the maximum heave at the top of piles is reduced from 13mm in the rough condition to 5mm in the smooth condition. However, Xu (2007) also observed the settlement of piles in the excavation for the North Square of Shanghai South Railway Station which will be discussed in chapter 7. The settlement of piles may happen in the field, but the computed result is heave if the soil/pile contact is not considered in the numerical analysis.

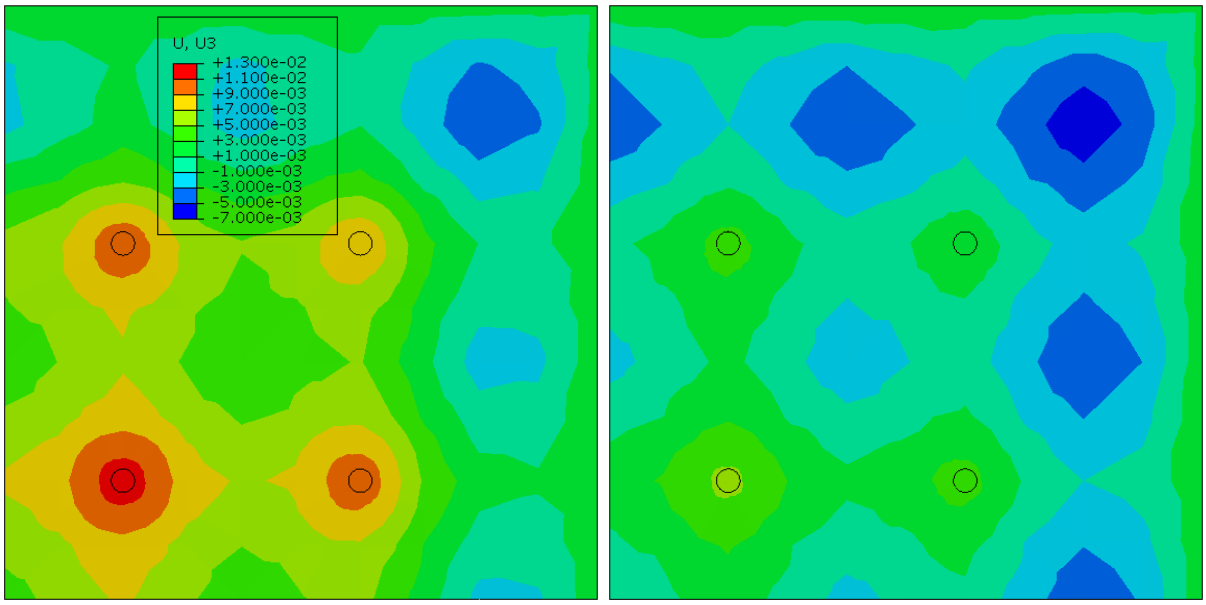

(a) Rough pile (b) Smooth piles

Fig.4.29 Vertical displacement of top floor slab (unit:m)

4.6.4 Influence of the soil/wall and soil/pile interface properties

In this section, both the soil/wall and soil/pile interface behaviours are considered in the analyses. For convenience, the same interface properties (same value of α) are assumed at the interface of soil/wall and soil/pile, as shown in Table 4.6. In practice, the interface properties of soil/wall and soil/pile may be different, but in one particular project the difference is likely to be small due to similar ground conditions and construction quality of the concrete components.

Table 4.6 Description of the analyses

Case No.	Description
1	Fully rough contact
2	$\tau_{crit} = \alpha \cdot s_u, \alpha = 1.0$
3	$\tau_{crit} = \alpha \cdot s_u, \alpha = 0.5$
4	$\tau_{crit} = \alpha \cdot s_u, \alpha = 0.1$
5	Fully smooth contact

As shown in figures below, the combined influence is larger compared to the individual influence of either soil/wall or soil/pile interface behaviour, which is not unexpected.

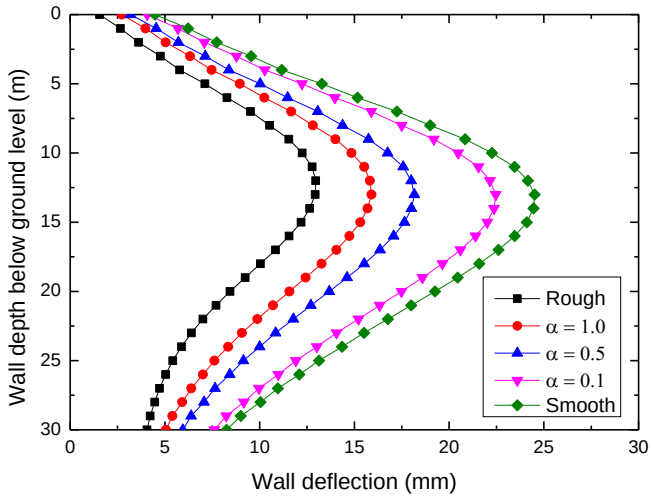

Fig.4.30 Wall deflection at point A

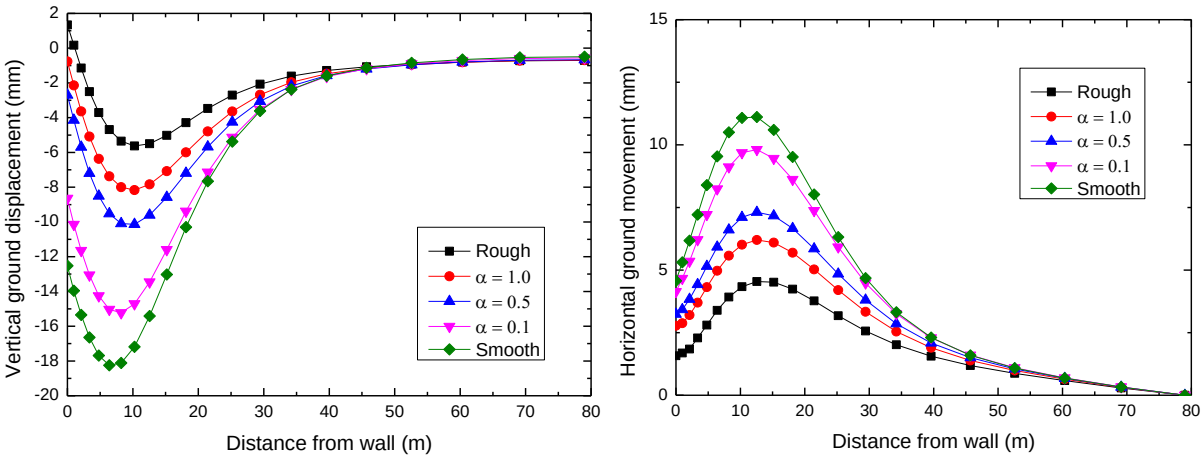

Fig.4.31 Ground movements along AB

The parametric analyses illustrate that the soil-structure interface behaviour has a large influence on the excavation behaviour, and the influence of soil/wall contact is larger than that of the soil/pile contact. When used for prediction of the pre-failure behaviour of deep excavations, neglecting the interface behaviours would underestimate the deformation, which is unconservative. On the other hand, when used in back analysis of case histories, ignoring the interface behaviour may cause relatively large discrepancy with the field measurement.

Therefore, the soil-structure interface behaviour should be considered appropriately in the analyses, and the interface properties should be carefully estimated.

4.7 Influence of the discontinuity in the retaining wall

All previous analyses in this chapter treat the diaphragm wall as an isotopic material which is common in publications (Simpson 1992, Whittle, Hashash et al. 1993, Ou, Shiau et al. 2000). In reality, however, the diaphragm wall is composed of discrete wall panels. The joints between the panels and are typically filled with flexible water proof materials, which suggests that the retaining wall (e.g. diaphragm wall, secant pile wall, contiguous pile wall) is discontinuous in the horizontal direction and consequently cannot sustain any significant out-of-plane bending moment. Moreover, the horizontal axial stiffness of the retaining wall is smaller than the that in the vertical direction (Zdravkovic, Potts et al. 2005). In this section, the retaining wall is modelled as a cross anisotropic linear elastic material to consider the joints and investigate its capability in capturing the excavation behaviour. The Young's modulus E along the wall length direction is multiplied by a reduction factor β ($\beta \leq 1.0$), as discussed in Chapter 3. Five analyses, including the basic analaysis, with different values of β are conducted, as shown in Table 4.7, to investigate its influence on the excavation behaviour. When the wall is modelled as an isotriopic matertial, as in the basic analysis, the value of β equals to 1.0. Zdravkovic, Potts et al. (2005) used the reduction factor of 10^{-5} for the contiguous pile wall which has very loose connections between adjacent piles. The diaphragm wall is stiffer than the contiguous pile wall, and the value of β should be larger than 10^{-5}.

Table 4.7 Description of analyses

Case No.	Description
1	Isotropic wall, $\beta = 1.0$ (Basic analysis)
2	Anisotropic wall, $\beta = 10^{-1}$
3	Anisotropic wall, $\beta = 10^{-2}$
4	Anisotropic wall, $\beta = 10^{-3}$
5	Anisotropic wall, $\beta = 10^{-5}$

As shown in figures below, the anisotropic wall approach can greatly increase the wall deflection at the wall corner which is rather limited in the isotropic wall approach. Field measurements (Xu

2007) observed that the wall deflection at the wall corner remains the similar pattern with that at the wall centre but has a smaller magnitude. This phenomenon can be well captured by the anisotropic wall approach. As the value of β decreases, the wall deflection at the wall corner increases and approaches that at the wall centre. However, the anisotropic wall approach does not affect too much the wall deflection at the wall centre at A and ground movement behind the wall centre along AB.

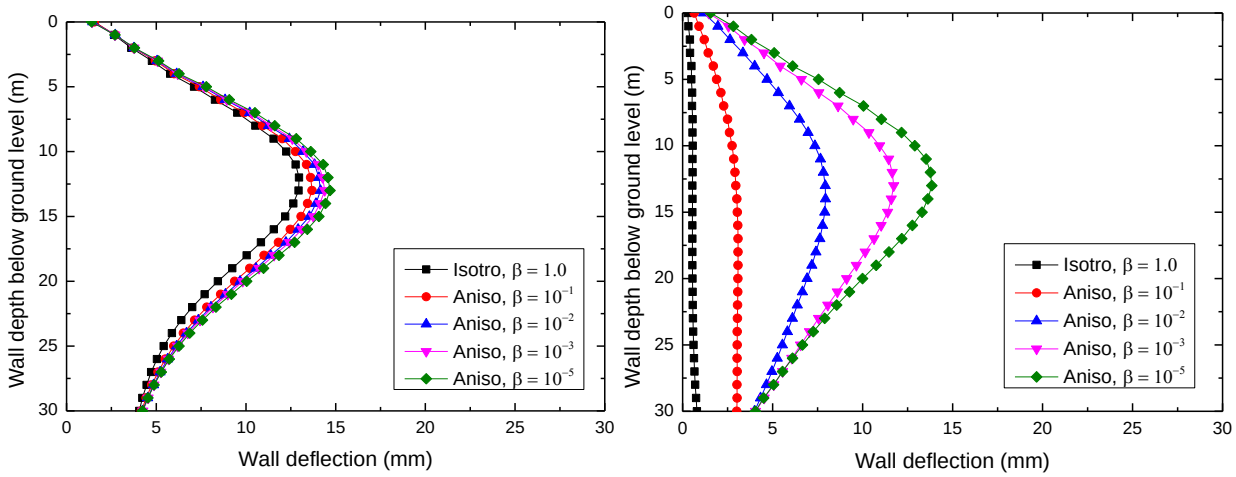

Fig.4.32 Wall deflections at wall centre (A) and corner (C)

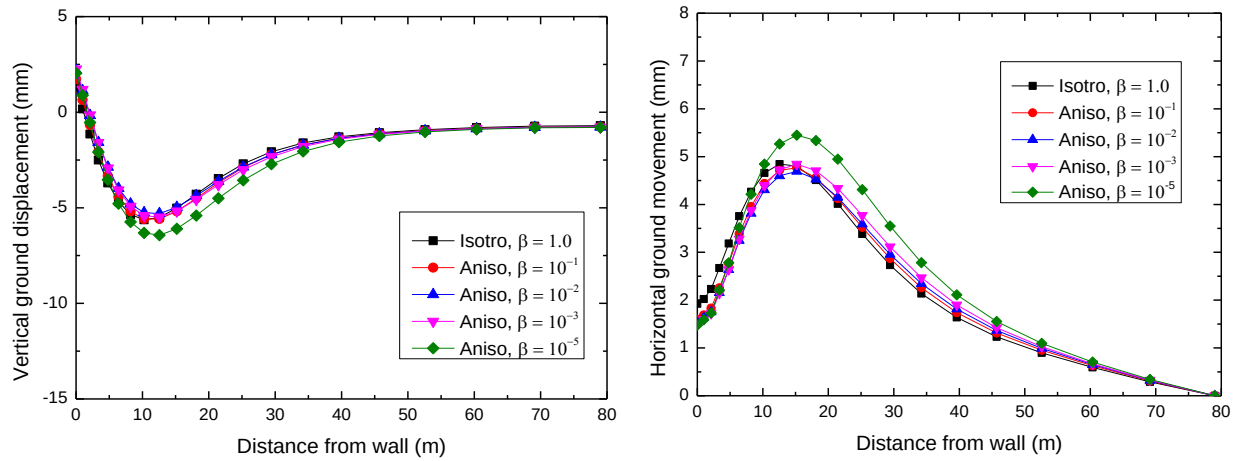

Fig.4.33 Ground movements along AB

As shown in Fig.4.34, the anisotropic wall approach can also modify the vertical ground movement distributions. When $\beta = 10^{-5}$, the corner effect almost disappears.

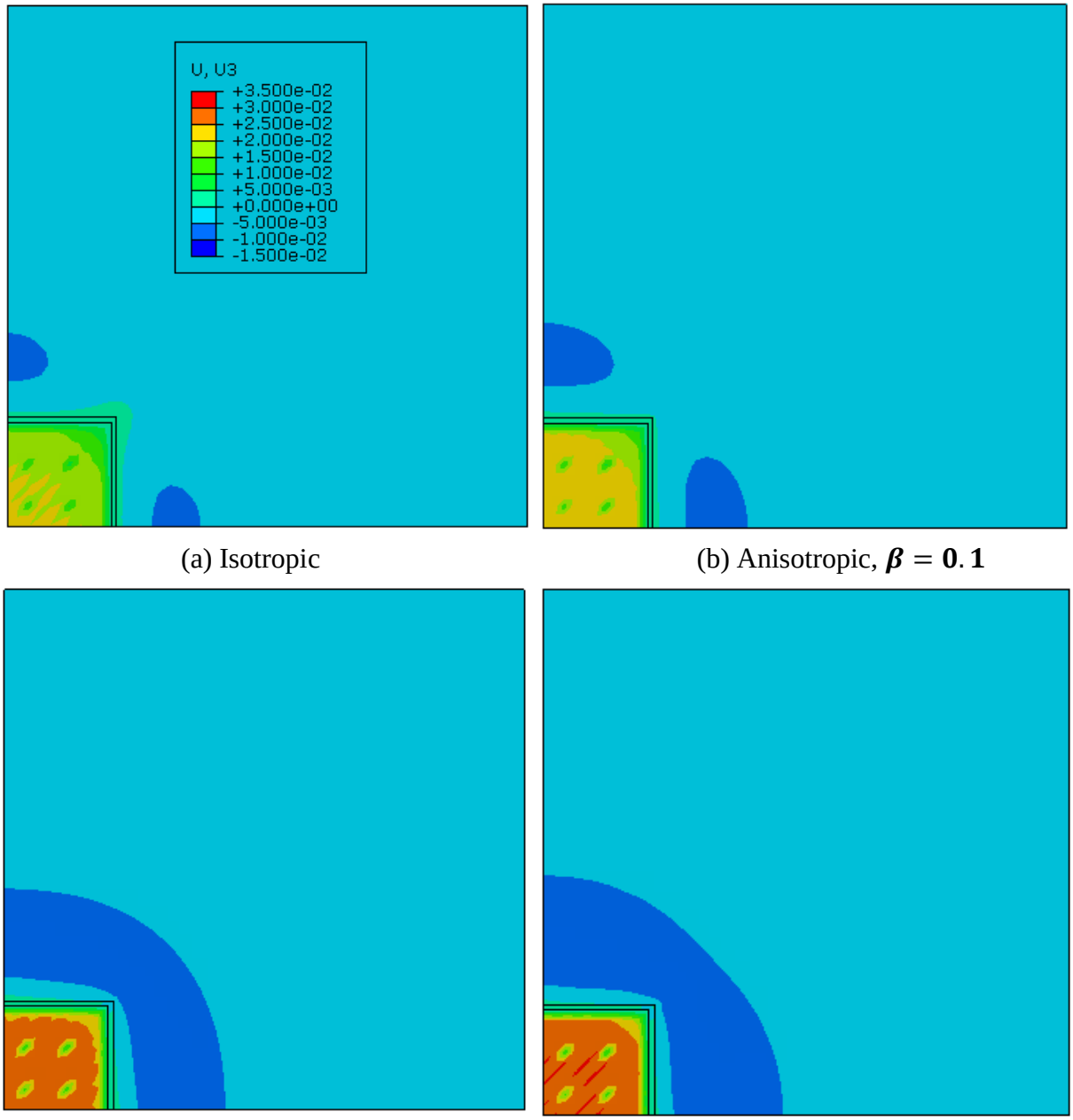

(a) Isotropic

(b) Anisotropic, $\boldsymbol{\beta = 0.1}$

(c) Anisotropic, $\boldsymbol{\beta = 10^{-3}}$

(d) Anisotropic, $\boldsymbol{\beta = 10^{-5}}$

Fig.4.34 Ground vertical displacement (unit:m)

4.8 Influence of stiffness and strength parameters of the soil

The stiffness and strength properties of a certain type of soil can be determined from laboratory experiments or in-situ tests, but the values may vary and depend on the quality of soil samples and test methods. Fig.4.35 illustrates the scattered distribution of the undrained shear strength s_u and the initial small-strain stiffness G_0 profile below the ground surface collected from publications about Shanghai clay. For convenience, equations are derived based on linearization of the data using the least squares method. Moreover, equations are also derived for the upper

and lower bounds for those scattered data. As important input parameters for the soil model, the values of these parameters may affect the computed results.

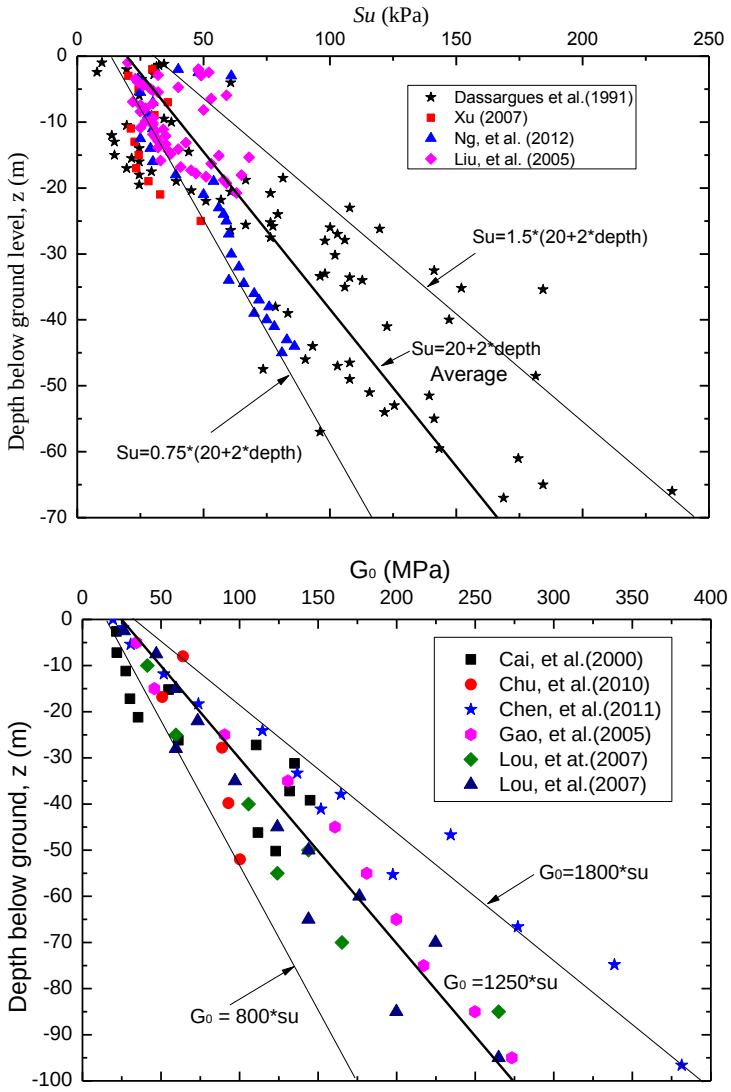

Fig.4.35 Strength s_u and stiffness G_0 profile of Shanghai clay

Four analyses, as described in Table 4.8, are conducted with different expressions of s_u and G_0 to investigate their influence on the excavation behaviour. Smaller values than the basic analysis are selected because they tend to produce larger but conservative results. In case 1, only G_0 is reduced; in case 2, only s_u is reduced; in case 3, both G_0 and s_u are reduced, which may be the worst condition.

Table 4.8 Description of the analyses

Case No.	Description
Basic analysis	$s_u = (20 + 2z)kPa, \quad G_0 = 1250(20 + 2z)kPa;$
1	$s_u = (20 + 2z)kPa, \quad G_0 = 1000;$
2	$s_u = 0.75(20 + 2z)kPa, \quad G_0 = 1250(20 + 2z)kPa;$
3	$s_u = 0.75(20 + 2z)kPa, \quad G_0 = 800(20 + 2z)kPa;$

As shown in the figures below, both the wall deflection and ground movements increase significantly when smaller value of G_0 and s_u is used. Smaller value of G_0 leads to larger displacement due to the soil removal and stress relief, while smaller s_u results in greater deformation because more soil elements yield and experience plastic deformation. This indicates that the input parameters for the soil stiffness and strength properties should be carefully calibrated through reliable site investigations for more accurate prediction purposes.

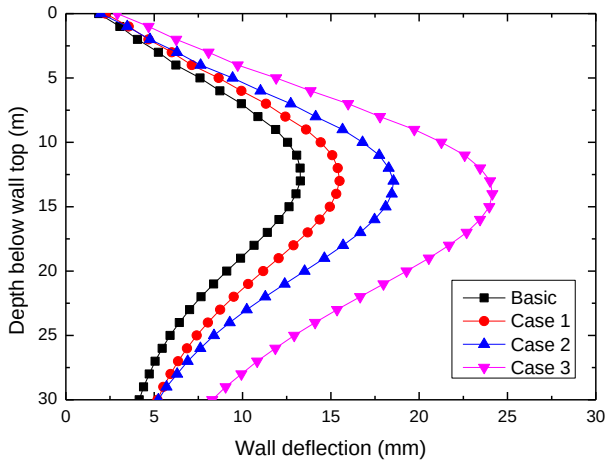

Fig.4.36 Wall deflection at point A

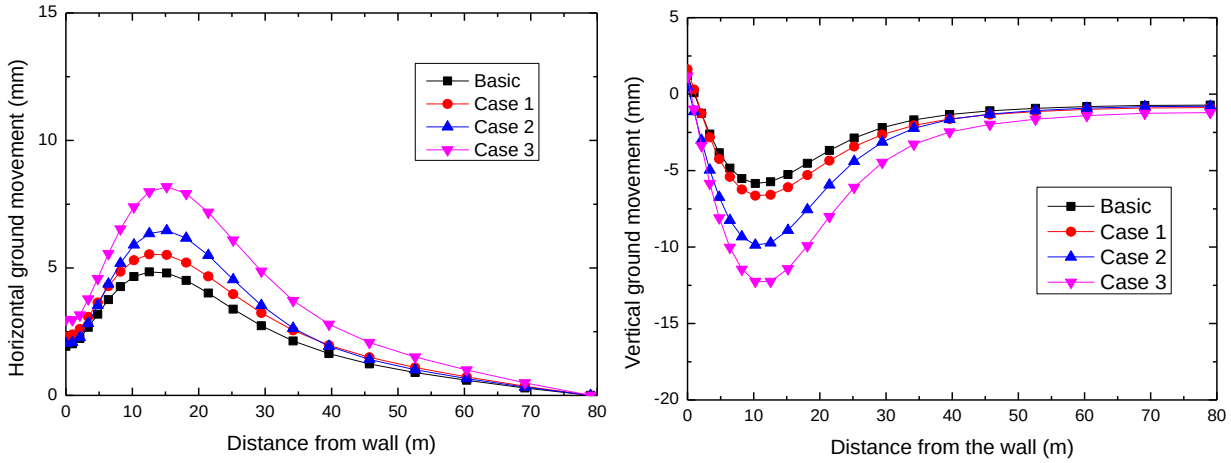

Fig.4.37 Ground movements along AB

4.9 Improved analyses

The influence of a number of important features on the excavation behaviour has been investigated individually in the previous sections, and the results indicate that the basic analysis which does not take into account these features may not be realistic in practical use. Improved analyses which consider part or all of these features are conducted in this section. Ideally, all of

those important features recognised previously should be considered in the numerical analysis to obtain more reliable results, but this may not always be feasible due to a number of limitations, e.g. capability of software, experience of practitioners, and time and computational resources available. In most situations, only part of these features can be included in the numerical analysis. In this section, several possible analyses (listed in Table 4.9) are carried out to understand the difference if some features are ignored in the analysis.

Table 4.9 Description of calculations

Case No.	Description
Basic	Basic analysis,
1	All these aspects are considered in the analysis, stiffness reduction, soil-structure interface behaviour, thermal effect of concrete beams and floor slabs, joints in the diaphragm wall.
2	The soil/pile interface behaviour is removed from case 1
3	Both the soil/wall and soil/pile interface properties are removed from case 1

Case 1 considers all the important features addressed previously and is assumed to be the premium analysis. The diaphragm wall and piles are modelled with solid elements, with soil/wall and soil/pile interface properties ($\tau_{crit} = 0.5s_u$). The stiffness of the reinforced concrete components is reduced to half of the nominal stiffness ($R = 0.5$) to consider the imperfections (e.g. cracks) in the concrete. Concrete thermal shrinkage is considered during curing process ($\Delta T = -10℃$) and the influence of the ambient temperature change ($\Delta T = -20℃$ to the top level beams and floor slabs). The diaphragm wall is modelled as cross anisotropic linear elastic material ($\beta = 10^{-2}$) to consider the discontinuity in the retaining wall.

Case 2 uses beams elements to model the piles and excludes the soil/pile interface behaviour, compared to Case 1. This case is more realistic for practical use because modelling piles with solid elements is extremely tedious in complex case studies which might have thousands of piles, and soil/pile contact cannot be considered when piles are modelled with beam elements in ABAQUS.

Case 3 excludes both the soil/pile and soil/wall contact, compared to Case 1, which is commonly seen in publications. The soil-structure contact is a very complicated nonlinear problem and

frequently causes numerical instabilities and convergence problems during calculations. Therefore, in complex case studies, the contact is often ignored to avoid these numerical problems.

As shown in the figures below, significant difference is seen between improved analyses and the basic analysis, indicating that the computed excavation behaviour would be subject to significant errors if the important aspects recognised previously are neglected in the numerical analysis. If the soil/pile contact is neglected in the analysis, there is not too big difference when comparing case 2 to case 1. However, if the soil/wall contact is further ignored as seen in case 3, the difference is significant when comparing case 3 to case 1. Therefore, results indicate that soil/wall contact has a big influence on the excavation behaviour and should be considered in the numerical analysis when it is possible.

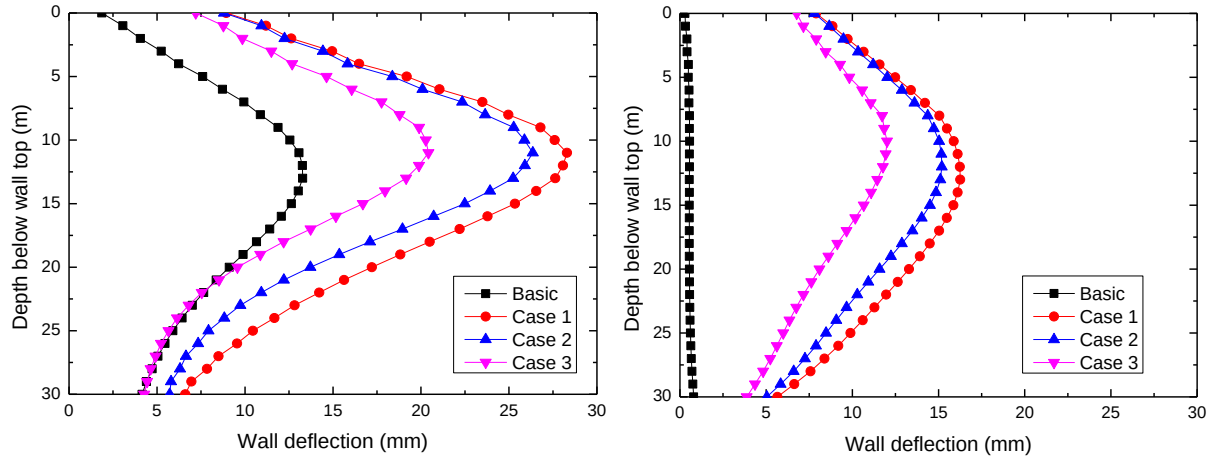

Fig.4.38 Wall deflection at point A and C

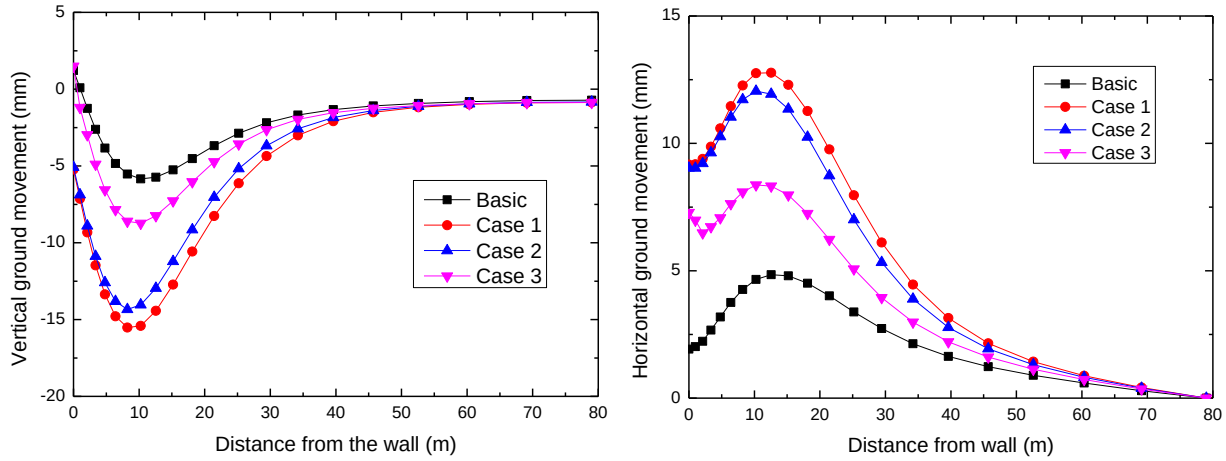

Fig.4.39 Ground movements along AB

Fig.4.40 shows the ground vertical displacement contours at the final stage of excavation from

these analyses. The improved analyses greatly modify the ground movement distribution compared to the basic analysis. The relative small difference between case 1 and case 2 indicates that neglecting the soil/pile contact does not change the ground movement too much. However, case 3 has a large difference with case 1 and case 2, which means that the soil/wall contact affects the ground movement significantly.

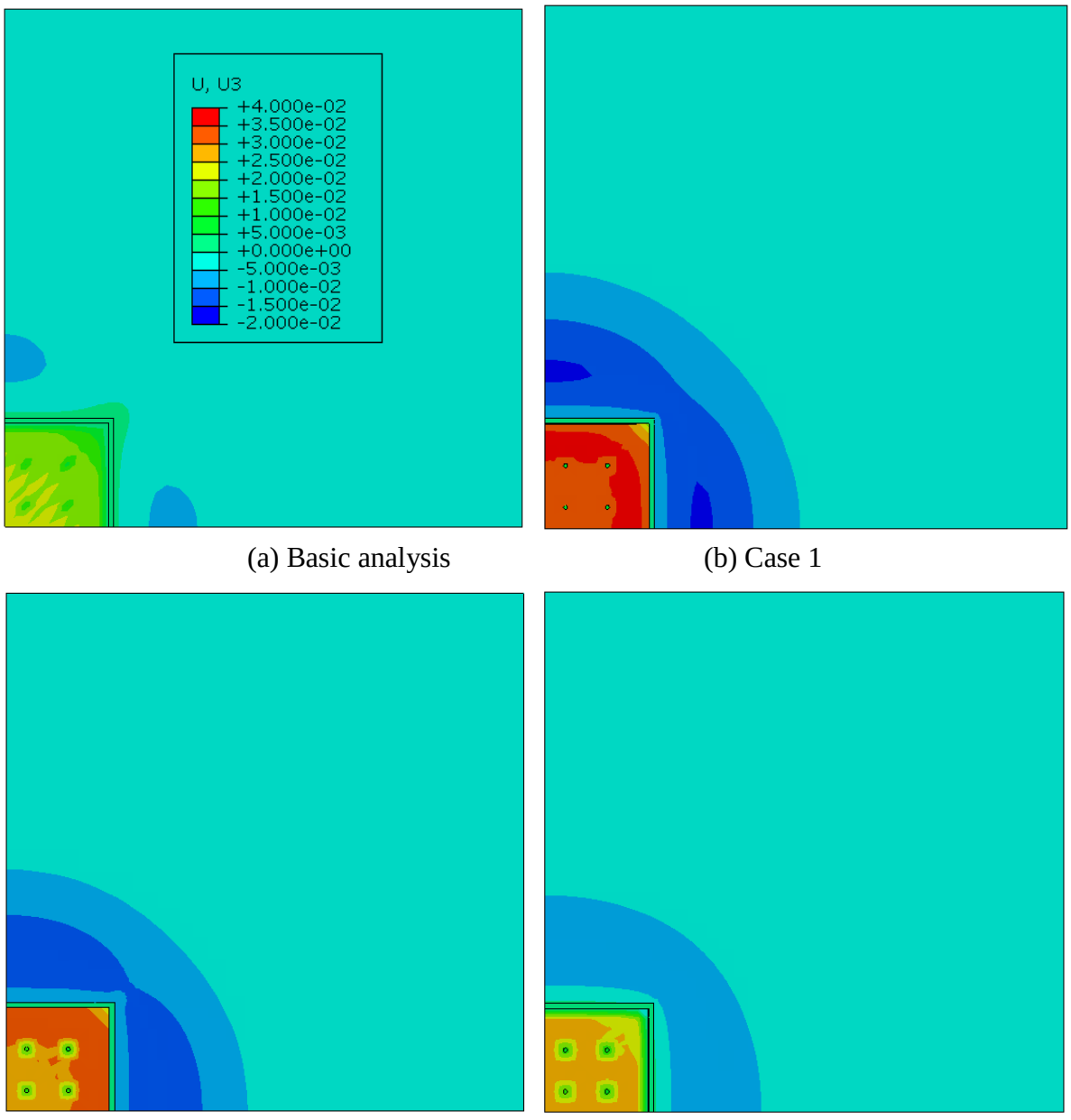

(a) Basic analysis (b) Case 1

(c) Case 2 (d) Case 3

Fig.4.40 Vertical ground movement (unit:m)

4.10 Conclusions

The parametric studies in this chapter are intended to investigate the influence of several

important features in the modelling procedure of deep excavations. There may be a number of ambiguous questions before conducting the analysis, for example,

(a) What kinds of features are needed to take into account in the analysis?

(b) How significant is the influence of a certain kind of features?

(c) What is the difference if a certain feature is neglected?

(d) Is it possible to consider all of the features in one analysis?

(e) Which approach is recommended for practical use?

Following the step-by-step detailed analyses, these questions are addressed appropriately. Some general conclusions are summarised below.

1) Before the analysis, enough information should be collected for the modelling process, e.g. the geometry of the excavation, details of the retaining structures, construction sequences, and reliable material properties for both the soil and structures. Adequate constitutive models for the soil, structural components, and the soil/structure interface are required.

2) Linear elements with reasonably fine mesh in the analysis produce similar patterns in the computed deformations compared with corresponding quadratic elements, and takes much less time to run. However, it should be noted that linear elements have deficiencies and are particularly susceptible to shear locking when modelling almost incompressible material, like soil in undrained conditions. They will produce too stiff response which results in smaller displacements, and over-predict the strength in some geotechnical problems. Therefore, quadratic elements are recommended for more accurate analysis. In more complex case studies, linear elements have to be used so that the complicated geometries could be modelled with the limited computing resources available, but any agreement with field measurements might therefore be fortuitous.

3) Both solid elements and shell elements are suitable to model the retaining wall, but different results from these two element types and the underlying mechanism should be

recognised. Shell elements do not have geometric thickness, and thus the shell element wall does not have the beneficial bending moments resulting from the shear stress on the back of the wall about the wall centre line which constraints the wall deflection towards the excavation. Consequently, the computed wall deflection and ground movement are smaller than those from the solid element wall. Solid elements are preferred to model the wall in this thesis. When the soil/pile interface properties are not included in the analysis, there is only minor difference between beam elements and solid elements to model the piles, but beams elements are much easier to use in the mesh generation. Therefore, beam elements are recommended to model the pile in the large complex case studies which may have hundreds of piles.

4) The computed wall deflection and ground movements are sensitive to the operational stiffness of the concrete structural components (e.g. the retaining wall, beams, and floor slabs). The operational stiffness of the reinforced concrete components may be smaller than their nominal value due to the imperfections (e.g. cracks) in the concrete. Parametric studies have shown that the wall stiffness mainly influences the magnitude of the wall deflection and ground movements, whereas the stiffness of the horizontal beams and slabs influences both the magnitude and pattern of the deformation. However, the stiffness of the piles has little effect on the excavation performance. When a reduced stiffness of both wall and horizontal support system is applied in the analyses, the wall deflection and ground movement increase significantly. Therefore, the operational stiffness of the retaining wall and horizontal system should be selected appropriately in the finite element analysis for design purposes and for prediction of the performance of completed deep excavations.

5) The thermal effects of concrete horizontal support system (i.e. beams, and floor slabs) during the curing process and due to ambient temperature change have significant influence on the magnitude and pattern of the wall deflection and ground movement. The

thermal effects can be included in the analyses in a straightforward way. The thermal shrinkage of concrete beams and floor slabs during curing process will pull the diaphragm wall towards the excavation and increase the wall deflection and ground movement, but the amount of shrinkage needs to be estimated. The ambient temperature change is assumed to affect mainly the roof floor slabs in the top-down excavation. Parametric studies indicate that the thermal shrinkage and expansion of the roof floor slab largely influence the wall deflection close to the top of the wall and the horizontal ground movement, whereas the vertical ground movement is not affected too much. Again, the amount of shrinkage or expansion needs to be estimated.

6) The soil-structure interface behaviour is often neglected in the numerical analyses due to its complexity, but it is shown to have a large influence on the excavation behaviour in the parametric studies. The parametric studies are based on an extended Coulomb friction model in which the shear resistance is related to the undrained shear strength of the soil ($\tau_{crit} = \alpha \cdot s_u$). The computed wall deflection and ground movements are sensitive to the interface properties. However, the influence of soil/wall contact is larger than that of the soil/pile contact. Considering the soil/pile contact also results in smaller vertical heave of piles and floor slabs because slip is allowed at the soil/pile interface. When used for prediction of the pre-failure behaviour of deep excavations, neglecting the interface behaviours would underestimate the deformation, which is unconservative. On the other hand, when used in back analysis of case histories, ignoring the interface behaviour may cause relatively large discrepancy with the filed measurement. Therefore, the soil-structure interface behaviour needs to be considered appropriately in the analyses, and the interface properties needs to be carefully selected.

7) The retaining wall is discontinuous in the horizontal direction along the sides of the excavation because it has construction joints. Consequently, it cannot sustain any significant out-of-plane bending, and the horizontal stiffness of the wall is also much

smaller than the stiffness of the solid concrete. The influence of joints can be considered by using the anisotropic wall approach in which the stiffness in the direction along the joints is reduced by a reduction factor. It is found in the parametric studies that when the wall is represented by an isotropic linear elastic material, the wall deflection at the wall corner is extremely small which is not realistic. The anisotropic wall approach can greatly improve this situation, and the wall deflection at the wall corner depends on the anisotropic ratio β used in the analysis. When $\beta = 10^{-5}$, representing the contiguous pile wall, the wall deflection at the wall corner is very close to that at the wall centre, and the ground movement around the wall corner outside the excavation also increases significantly. However, the wall deflection at the wall centre and the ground movement behind the wall centre are not affected too much by the anisotropic ratio. For practical applications, the value of β should be selected carefully based on experience and back analysis of case histories. For example, the diaphragm wall has better connection conditions than the contiguous pile wall, so the anisotropic ratio is larger than 10^{-5} used for the contiguous pile wall. When field measurement of wall deflections at both wall centre and wall corner is available, the anisotropic ratio can be estimated through back analyses and parametric studies.

8) The numerical results are also sensitive to the input parameters for the stiffness and strength properties of the soil. Both the wall deflection and ground movements increase significantly when smaller value of G_0 and s_u is used. Smaller value of G_0 leads to larger displacement due to the soil removal and stress relief, while smaller s_u results in greater deformation because more soil elements yield and experience plastic deformation. This indicates that the input parameters for the soil stiffness and strength properties should be carefully calibrated through reliable site investigations for more accurate prediction purposes.

9) It has shown in the parametric studies that the excavation behaviour is influenced by a

number of factors, e.g. element types to model the wall, cracks in the concrete structural components, thermal effects of horizontal support system, soil-structure interface properties, joints in the retaining wall, the strength and stiffness properties of the soil. These features need to be considered appropriately in the numerical analysis. However, in some cases, it is difficult to include them all in one analysis due to the complexity. Practitioners need to be aware which the most influential factors are, and how reliable the result is if some factors are ignored in the analysis.

Chapter 5 Basement excavation for Shanghai Xingye Bank building

5.1 Introduction

Deep excavations in urban area of Shanghai are usually close to adjacent infrastructure, e.g. buildings, deep foundations, tunnels, and buried pipelines, which are sensitive to the excavation induced ground movement. In such conditions, the design and construction of deep excavations must consider the possible adverse effect of the excavation and control it within an acceptable level. The design of the excavation, therefore, is completely dominated by the more restricted deformation criteria, rather than the failure. The top-down construction method which results in relatively small ground movement, is consequently widely used in Shanghai.

Deep excavations in Shanghai soil clay are challenging and influenced by a number of factors such as geological conditions, retaining structures, construction methods, and workmanship. Field measurement is, therefore, required during the construction to ensure their safety. Documented field data provide valuable resource to understand the performance of deep excavations, and also to calibrate the results from numerical analyses. Advanced finite element analysis is an effective tool to investigate the excavation behaviour, but its capacity in replicating the observed performance in the field needs to be evaluated through calibration with the field data. In addition, some undetermined parameters can be estimated through parametric studies.

The excavation for the basement of Shanghai Xingye Bank building (Wang and Wang 2007, Xu 2007) is a well-documented deep excavation case history constructed using a top-down method. It is investigated through advanced finite element analysis which considers the irregular geometry of the excavation, detailed retaining structures (e.g. the diaphragm wall, vertical piles, horizontal beams and floor slabs, openings in the floor slabs, and construction joints in the

diaphragm wall), and complex construction sequence (e.g. soil removal and structure installation, earth berms, and casting the base slab). The principal purpose of this study is to investigate the level of detail required in the model to obtain results that provide a realistic representation of data measured during the construction process. Various key aspects in the deep excavations are also investigated through parametric studies, e.g. (i) the appropriate approach to model the construction joints in the diaphragm wall, (ii) procedures to include the effect of imperfections in the concrete floor slabs (e.g. shrinkage, cracks, and creep) on the interaction between the floor slabs and the retaining wall, (iii) the relative merits of using solid and shell elements for the diaphragm wall, (iv) the sensitivity of the analysis to the assumed initial stress in the soil, and (v) the influence of soil constitutive models on the quality of the results.

5.2 Project description

5.2.1 General description

Shanghai Xingye Bank building is a high-rise building (82.5m high) with a three-level basement. The structure is constructed from a reinforced concrete frame and the building is founded on deep piles (Wang and Wang 2007, Xu 2007). Construction of the basement began in February 2002, and finished in December 2003. The excavation is around $80\text{m} \times 90\text{m}$ in plan. The excavation depth, as shown in Fig.5.1, is 14.2m on the west side, and 12.2m on the east side. This building is situated in the central downtown area of Shanghai, and is around 200m to the Bund. The excavation is surrounded by 15 densely packed buildings (eight historic buildings, including some masonry structures) and several old service pipes. These historic buildings have very high standard of protection by the city council, so a comprehensive field measurement was conducted during the excavation process. The measured items include the wall deformation, ground movement, and building settlements.

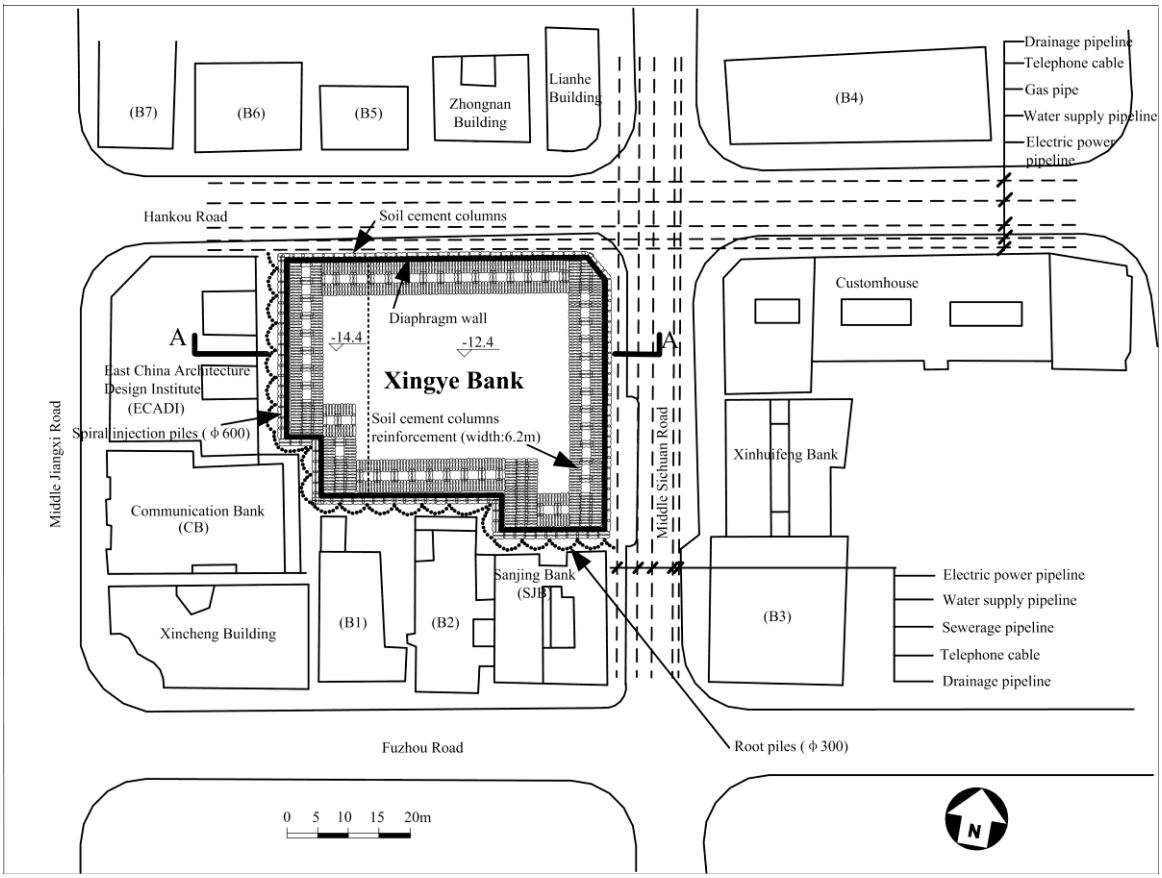

Fig.5.1 Plan view of the deep excavation for Xingye Bank building (Xu 2007)

5.2.2 Geotechnical conditions and soil properties

According to site investigation report (SGIDI 1997), the site is on a flat coastal plain, with ground elevation between 4.80m to 3.87m. The ground water table is 0.5m to 1m below the ground surface. The site is underlain by thick, relatively soft quaternary alluvial and marine deposits. The geological profile and soil properties from site investigation of this project are shown in Fig.5.2. The soil profile is divided into 9 sub layers according to the difference in soil characteristics, physical and mechanical properties. The subsurface consists of a 2.0m thick fill layer and a 0.5m thick clay layer. Underlying is a 5m thick silty clay. Underneath the silty clay is a 9m thick mucky clay with large void ratio, high compressibility, and low shear strength. The fifth layer is a 4m thick silty clay with clay. Then there is a 28m thick silty clay with clayey silt. The subsequent layers are sandy silt (5m), silty clay with sandy silt (6m), and silty clay with silty sand (2m). The natural water content of clay and silty clay layer is close to, or higher than, the liquid limit, suggesting that the soil is either normally consolidated or lightly overconsolidated. The undrained shear strength s_u, determined from field vane shear test, is significantly higher

than the value normally associated with clay at the liquid limit, suggesting that the soft clay is likely to be sensitive. The permeability of the soft layers clay is in the order of $10^{-9}\,\mathrm{m/s}$, indicating that the clay is close to the undrained condition during the excavation.

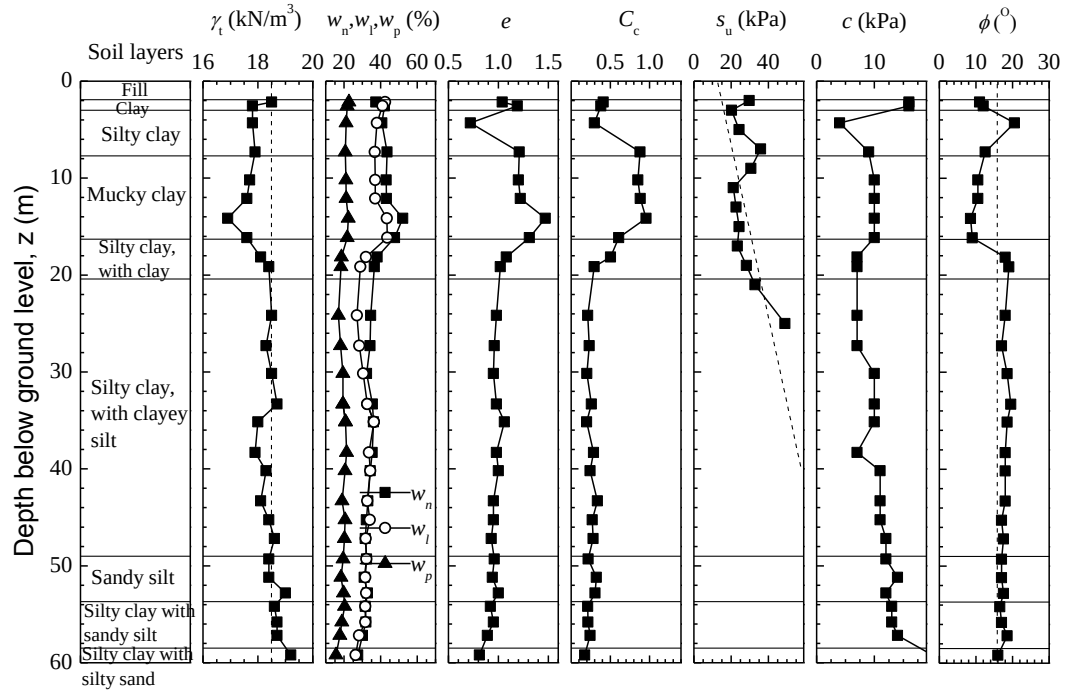

Note: γ_t = unit weight, w_n = water content, w_p = plastic limit, w_l = liquid limit, e = void ratio, C_c = compressive index, s_u = field vane shear strength, c = cohesive strength, ϕ = internal friction angle

Fig.5.2 Geotechnical profile and soil properties of the site (Xu 2007)

The soil properties shown in Fig.5.2 are not sufficient to derive all the input parameters for the advanced soil model in the analysis. For example, there is no information to calibrate the soil model to represent the small-strain stiffness nonlinearity of the soil. In addition, Fig.5.2 only provides the undrained shear strength s_u to a depth of about 24m below the ground level, but the numerical analysis requires data of a much deeper level to the boundary of the model. Due to the limitation of this site investigation, the input parameter derived in chapter 3 based on soil properties collected from published data on Shanghai clay, will be adopted in this case study. The unit weight generally increases with depth, but it is convenient to take its average value, roughly $18.5\mathrm{kN/m^3}$. The friction angle of $15°$ is used to derive the coefficient of lateral earth pressure at rest K_0.

5.2.3 The retaining system

The A-A sectional view (see Fig.5.1) of the excavation in Fig.5.3 shows briefly the structure of

the retaining system which is mainly composed of the diaphragm wall, horizontal beams and floor slabs, and vertical piles and columns. The columns of the main structure (Ø609mm concrete filled steel tabular column) are firmly connected with the underneath bored piles (Ø900mm or Ø800mm, toe at around 60m below the ground level). In the numerical modelling, however, for simplicity the piles and columns are modelled with beam elements using the same properties (Ø900mm, 60m deep below ground level, reinforced concrete material properties).

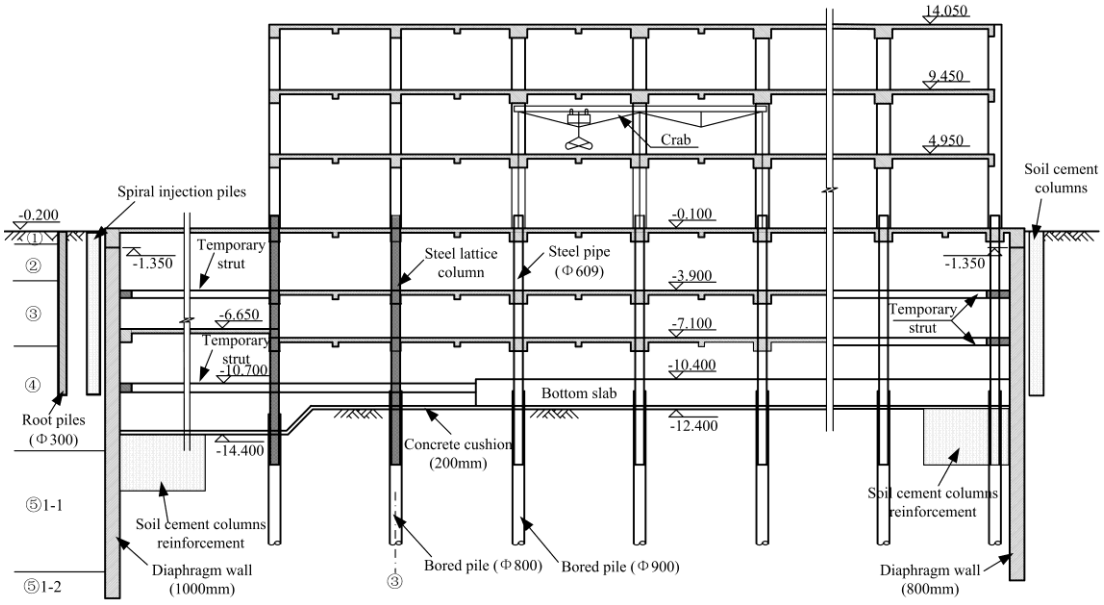

Fig.5.3 Sectional view of Section A-A (unit: m) (Xu 2007)

The diaphragm wall has three types, type A, type B, and type C, as shown in Fig.5.4, considering the environmental protection standard of adjacent buildings and the excavation depth. Type A is 31.2m deep and 1.0m thick, on the west side close to East China Architecture Design Institute (ECADI) building and Communication Bank (CB) building which have the highest protection standard. Type B is 29.2m deep and 1m thick, on the south side close to Sanjing Bank (SJB) building which has a relatively high protection standard. Type C is 25.5m deep, 0.8m thick, on the other two sides due to the relatively lower protection standard of adjacent buildings on these sides. The diaphragm wall was constructed with panels, ranging from approximately 4m to 6m wide. The joints between adjacent panels are filled with flexible waterproof materials, which means that the diaphragm wall is discontinuous in horizontal direction and cannot sustain significant out-of-plane bending moments. A section of root piles and jet grouting piles were

constructed surrounding the diaphragm wall to mitigate the excavation-induced impact on the adjacent historic buildings which are normally 4m to 5m away from the diaphragm wall.

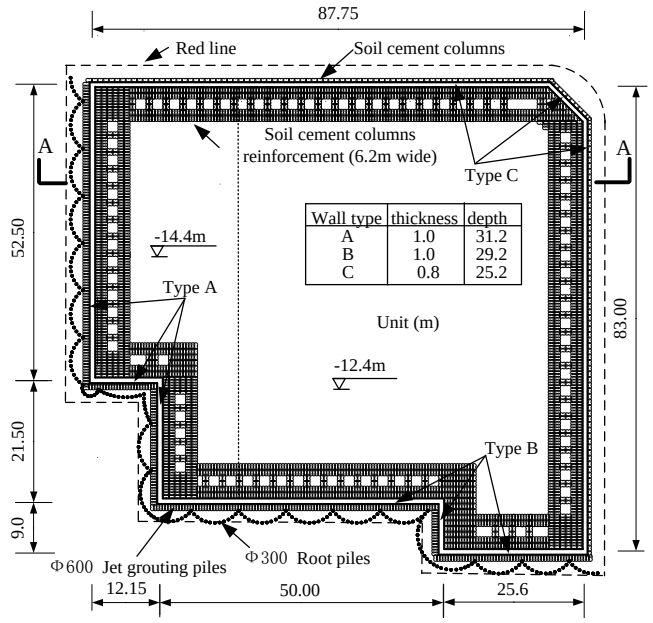

Fig.5.4 Plan view of the diaphragm wall (Xu 2007)

The horizontal support system, as shown in Fig.5.5, is mainly composed of cast-in-situ reinforced concrete beams, floor slabs, and temporary struts. There are also several steel temporary struts, but in the numerical modelling they are treated the same with the reinforced concrete beams for simplicity. Opening accesses are designed in the floor slabs for vertical linkage between different floors (e.g. stair case and elevators) and transport of excavated soils, as well as for lighting and ventilation purposes. These openings are also considered in the numerical model.

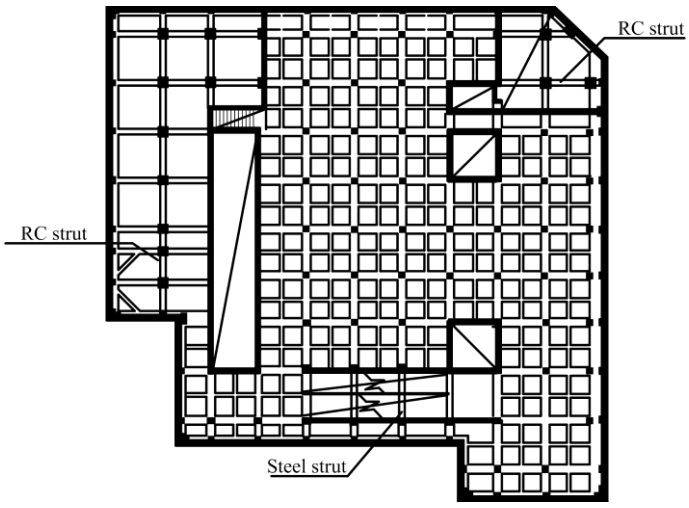

Fig.5.5 First floor beams and floor slabs (Xu 2007)

5.2.4 Construction sequences

The basement of Xingye Bank building was constructed with a typical top-down method. The major construction sequences are summarized in Table 5.1, associated with the corresponding construction period. There are generally 11 stages of construction, and the main construction activities include the installation of the diaphragm wall and bored piles, ground improvement and dewatering, excavation with earth berms, and casting the reinforced concrete components of the basement and superstructure. The numerical analysis follows closely the construction sequences.

Table 5.1 Construction sequences

Stages	Period (day)	Interval (day)	Construction activities
1	02.03.2002~ 06.10.2002	218	Install diaphragm walls and bored piles; conduct ground improvement and dewatering;
2	07.10.2002~ 19.10.2002	13	Excavate to -1.5m, then to -5.3m with earth berms;
3	20.10.2002~ 11.12.2002	53	Cast the roof beams and floor slabs of the basement;
4	12.12.2002~ 30.12.2002	19	Excavate the earth berms to -5.3m;
5	31.12.2002~ 27.02.2003	59	Cast the -1st beams and floor slabs of the basement, and the ground floor of the superstructure;
6	28.02.2003~ 24.03.2003	25	Excavate to -8.55m;
7	25.03.2003~ 11.05.2003	48	Cast beams and slabs for the -2nd floor of the basement, and the first floor of the superstructure;
8	12.05.2003~ 10.07.2003	60	Excavate to -10.7m first, then to -12.4m with earth berms; remove the earth berms to -11.3m;
9	11.07.2003~ 24.09.2003	76	Cast the bottom slab and temporary struts for the -3rd floor of the basement, and the 2nd floor of the superstructure;
10	25.09.2003~ 21.10.2003	27	Excavate the remaining soil to -14.4m (west side) and -12.4m (east side) respectively; cast the concrete cushion;
11	22.10.2003~ 11.12.2003	51	Cast the bottom slab on the west side; remove the temporary struts; construct the remaining structures;

5.2.5 Instrumentations

Due to the high environmental protection standard of adjacent infrastructure, a comprehensive field measurement scheme was carried out during and after the construction process to monitor the performance of the deep excavation and ensure its safety. The detailed layout of instrumentation is shown in Fig.5.6. The main concern is the wall deformation and settlement of adjacent buildings and pipelines.

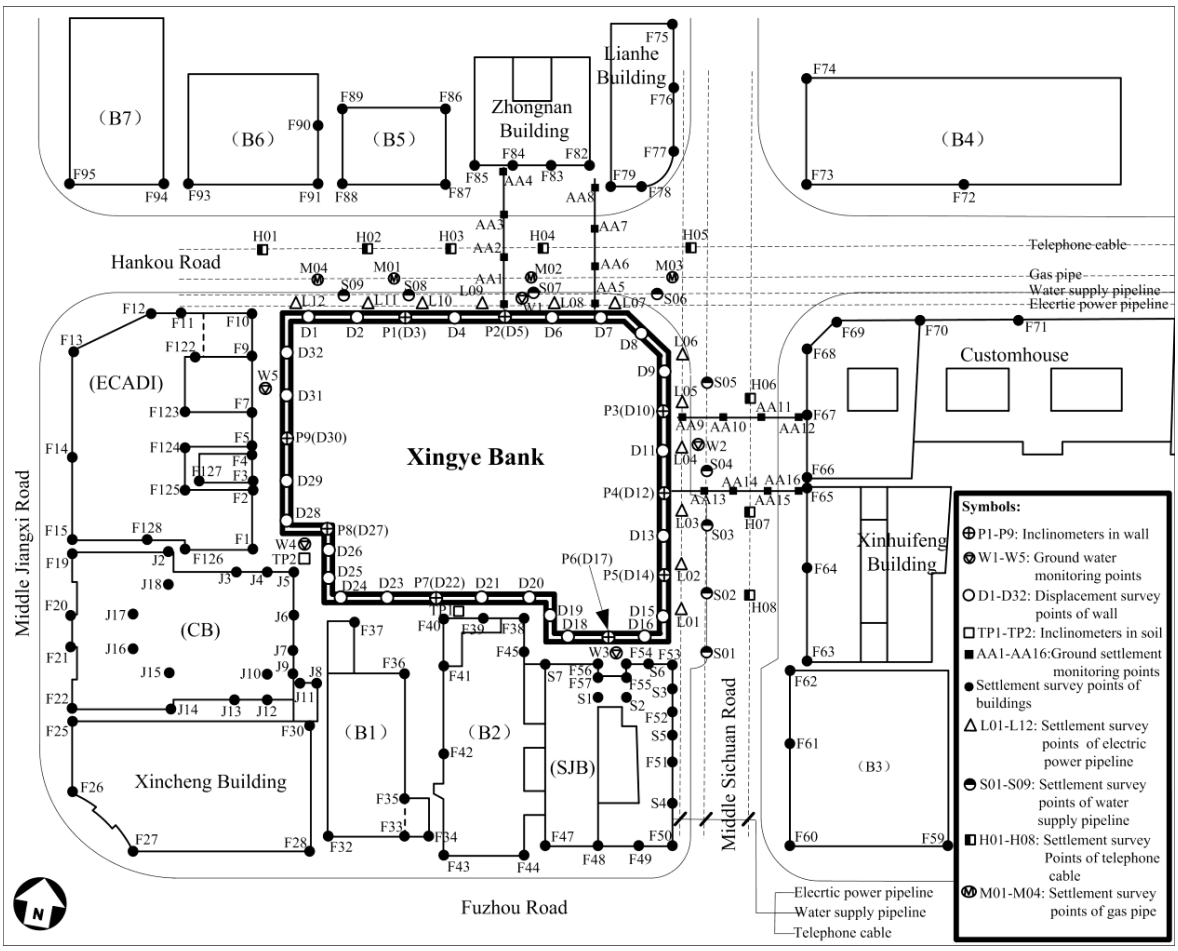

Fig.5.6 Layout of instrumentation at the construction site (Xu 2007)

The main items measured and data recorded are listed below,

1) Wall lateral deflections ($P1\sim P9$), measured by inclinometers;
2) Vertical displacements at the top of the diaphragm wall ($D1\sim D32$), measured by a optical level with an accuracy of 0.1mm;
3) Soil lateral displacement outside the excavation ($TP1\sim TP2$), measured by inclinometers;
4) Ground water level ($W1\sim W5$), measured by standpipe piezometers;
5) Ground surface settlement outside the excavation ($AA1\sim AA4$, $AA5\sim AA8$, $AA91\sim P12$, $P13\sim P16$), measured by a optical level;
6) Pipeline settlements, including electrical power pipelines ($L01\sim L12$), cast-iron water-supply pipelines ($S01\sim S09$) , gas pipelines ($M01\sim M04$) ,and telephone cable pipelines ($H01\sim H08$), measured by a optical level;
7) Building settlements, measured by a optical level; the settlements of ECADI building, CB building, and SJB building were the main focus.

5.3 Finite element model and strategy of the analyses

5.3.1 Finite element model description

Considering the irregular geometry and complex construction activities in this deep excavation, it is complicated and time-consuming to consider every detail in the numerical analysis. It is, therefore, essential and necessary to get grips with the most influential features and ignore the trial ones in the analysis, by making a number of reasonable simplifications and assumptions, as listed in Table 5.2.

Table 5.2Assumptions and simplifications in the numerical analysis

No.	Assumptions and simplifications	Real situation
1	Rough interface between soil and wall	Friction exists at the interface and the interaction mechanism is complicated
2	The wall and piles are modelled as wished-in place.	The installation of diaphragm wall and piles affects the excavation behaviour;
3	The concrete structural components (e.g. the diaphragm wall, piles, beams, and floor slabs) behave elastically.	Nonlinear behaviour might happen, e.g. shrinkage, creep, and cracks.
5	Dewatering and consolidation are not considered.	Dewatering and consolidation exist and might affect the long-term behaviour.
6	Ground improvement around the excavation is not included.	Ground improvements were used both inside and outside the excavation.
7	Surcharge on the ground surface and floor slabs are not considered.	Transport load on the streets and work load on the floor slabs might affect the excavation behaviour.
8	Adjacent buildings and services are not modelled.	There are buildings and utility pipelines outside the excavation.

The mesh and boundary conditions of the whole finite element model are shown in Fig.5.7. This model is intended to represent at an appropriate level of detail of the structure and various construction processes that were involved in the project. The model size is 400m × 400m ×100m, and the boundary is sufficiently remote from excavation edge (around 150m away horizontally, approximately 4 times the excavation radius and 10 times the excavation depth). Four vertical boundaries are rollers, and the bottom is fixed. The model has a total of 102036 elements and 116756 nodes.

The soil is modelled with 8-noded solid hexahedral elements with reduced integration (C3D8R).

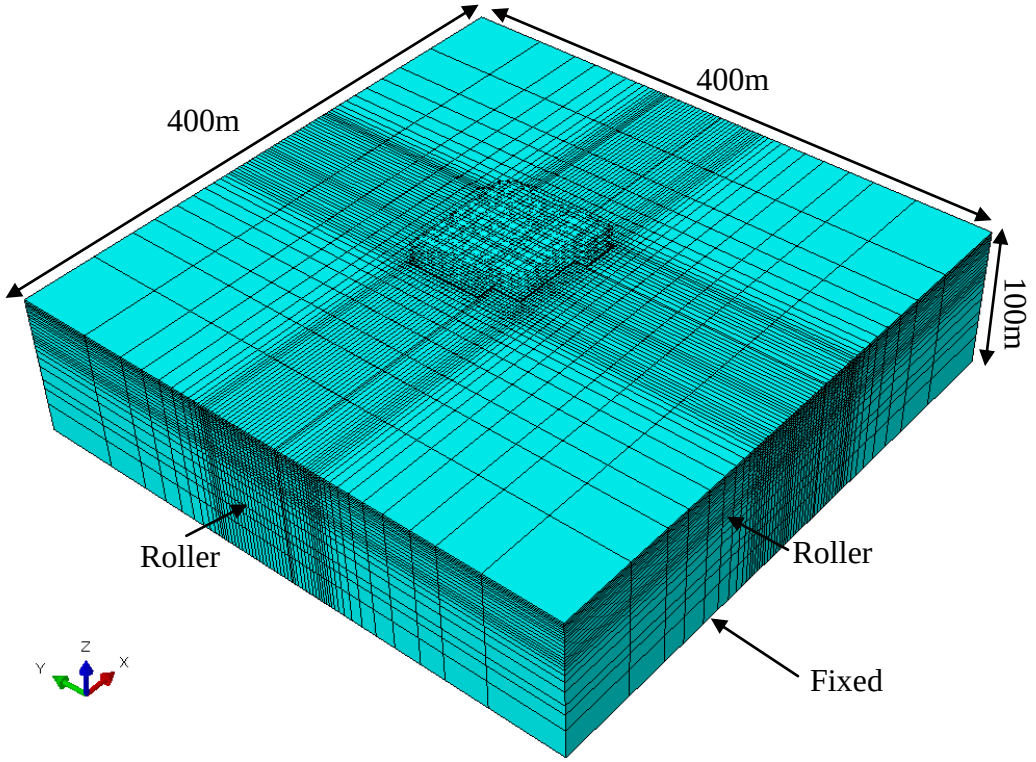

Fig.5.7 Finite element mesh and boundary conditions

The mesh for the diaphragm wall is shown in Fig.5.8. Two types of elements, 4-noded quadrilateral shell elements with reduced integration (S4R) and solid elements (C3D8R) are used to investigate their merit to model the diaphragm wall. The detailed geometry (e.g. the thickness) of the diaphragm wall needs to be modelled when solid elements are used, and there are three elements along the 1m thickness and two elements along the 0.8m thickness.

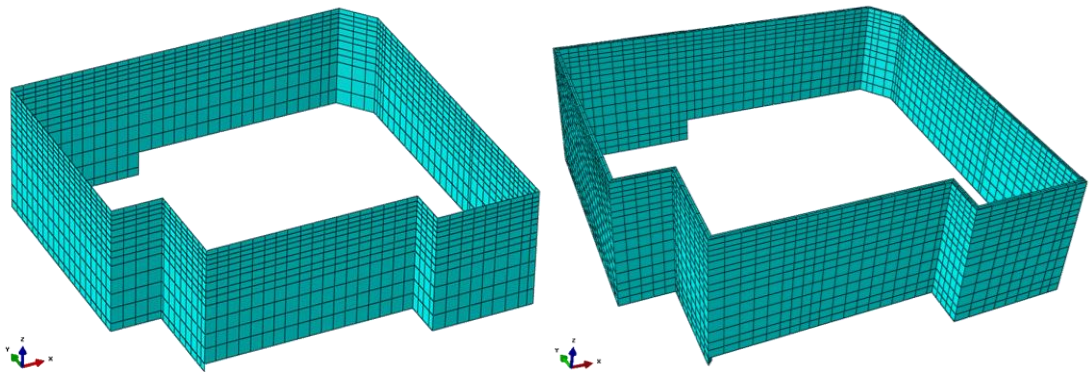

(a) **(b)**

Fig.5.8 Wall geometry and mesh (a) shell element (b) solid element

The support system, as shown in Fig.5.9, includes vertical piles, horizontal beams, and floor slabs. The superstructure constructed during the excavation is also included in the model. The piles and beams are modelled with 3D 2-noded beam elements (B31), while the floor slabs are modelled with 4-noded quadrilateral shell elements with reduced integration (S4R).

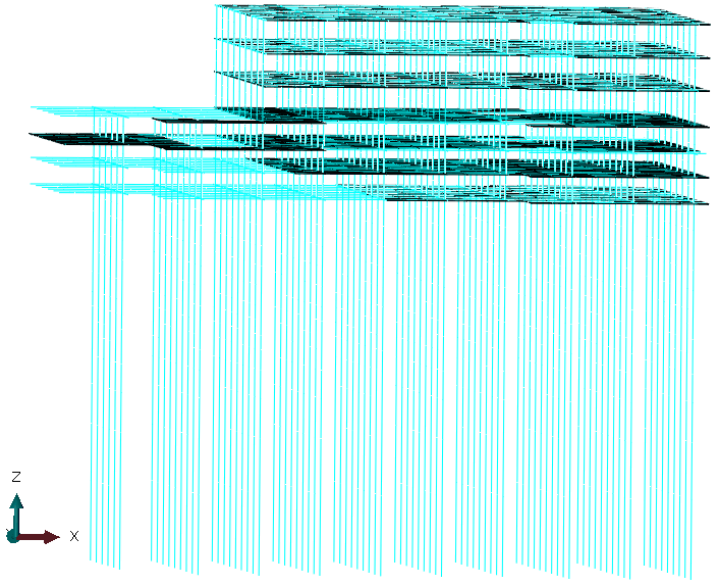

Fig.5.9 The Support system of the basement and the superstructure

The mesh for the beams and floor slabs at three different levels of the basement is shown in Fig.5.10, and compared with the design charts. The open accesses in the floor slabs are considered in the model.

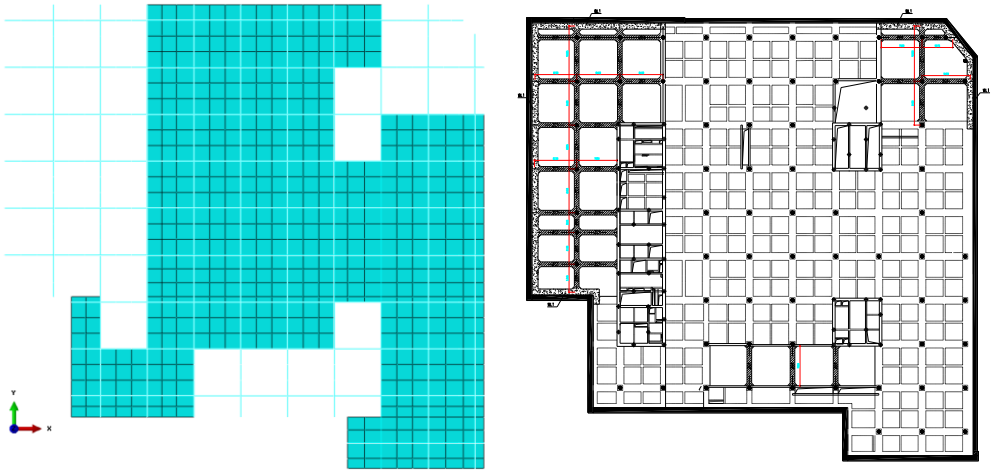

(a) Top level floor slab and beams

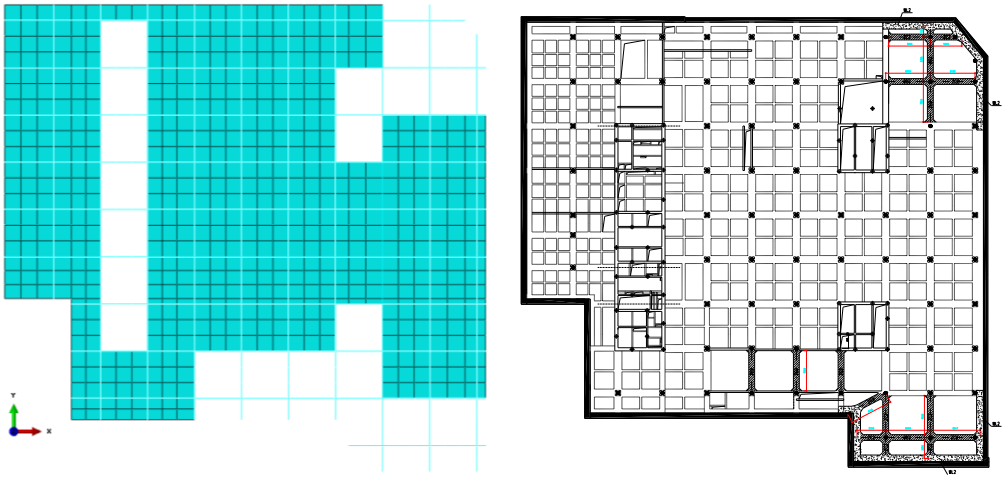

(b) -1st level floor slab and beams

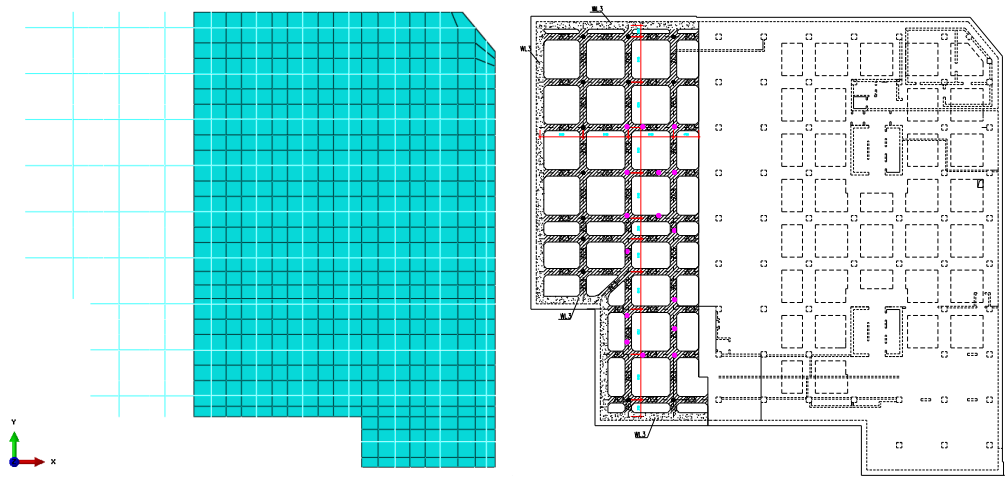

(c) -2nd level floor slabs and beams

Fig.5.10 Beams and floor slabs at each level

The geometry and material properties for the structural components are listed in Table 5.3. St. John, Potts et al. (1993) modelled the reinforced concrete beams and floor slabs as a linear elastic material with a 20% reduction to the nominal Young's modulus of concrete to consider the open access, shrinkage, cracks, and workmanship of the construction. In the analyses here, those effects are represented by the thermal shrinkage, and the Young's modulus is not reduced.

Table 5.3 Geometry and material properties for the structural components

Component		Geometry	Material Properties
Diaphragm Wall	Type A	Depth = 31.2m, Thickness = 1.0m	Both isotropic and anisotropic linear elastic material properties are used to explore their influence on excavation behaviour. $\rho = 2500\,\mathrm{Kg/m^3}, E = 30\mathrm{GPa}, \nu = 0.2, \beta = 0.1$
	Type B	Depth = 29.2m, Thickness = 1.0m	
	Type C	Depth = 25.2m, Thickness = 0.8m	
Piles		Length = 60m, Diameter = 900mm	$\rho = 2500\,\mathrm{Kg/m^3}$, E = 30GPa, $\nu = 0.2$
Beams		Cross section 500mm × 800mm	$\rho = 2500\mathrm{kg/m^3}, E = 30\mathrm{GPa}, \nu = 0.2$ $\alpha = 10^{-5}/℃, \Delta T = -35℃$
Slabs		Thickness = 150mm	

The analyses are conducted assuming in undrained conditions with total stress analysis. This is on the basis that the permeability of clay is low and the construction period is relatively short. The calculations were conducted on the Oxford supercomputer.

5.3.1 Strategy of analyses

A strategy of analyses, as shown in Fig.5.11, has been made to organise the calculations and present the results systematically.

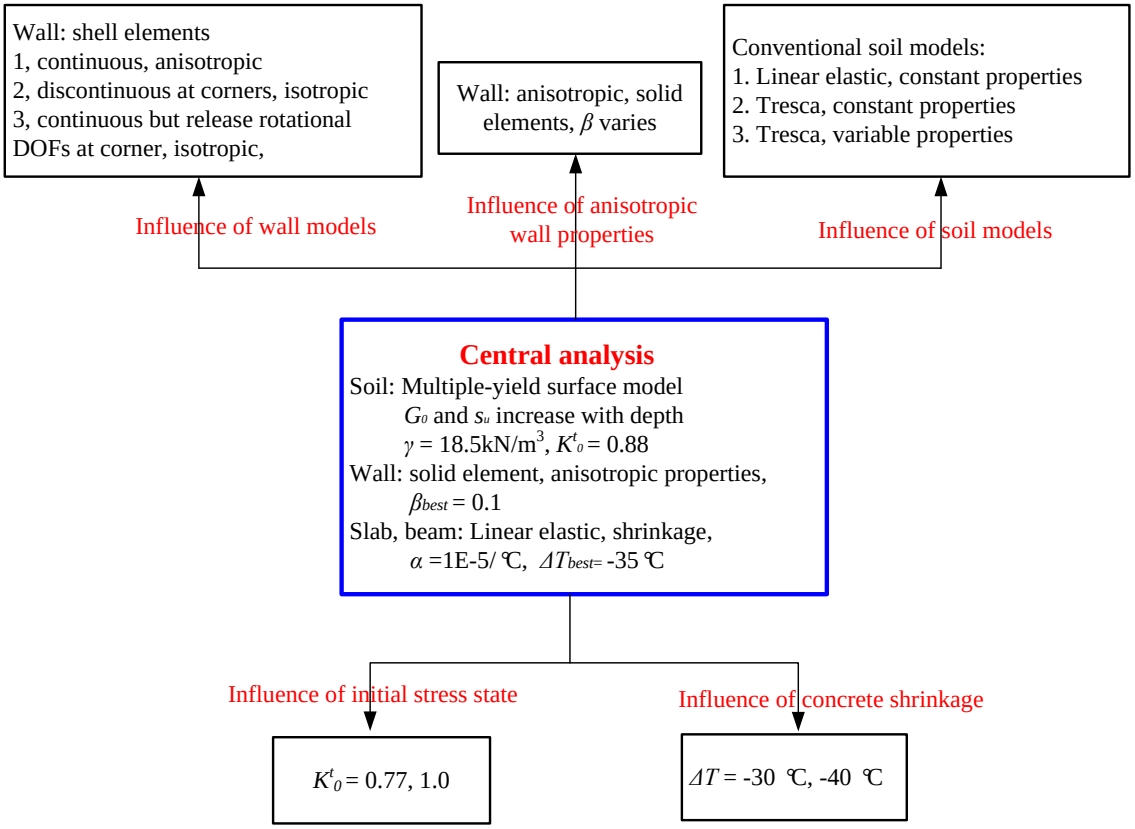

Fig.5.11 Strategy of the analyses

The central analysis is developed first based on an initial assessment of the most appropriate numerical modelling procedures for this particular application. Separate analyses are then conducted to investigate the influence of a certain key aspects of modelling procedure, providing an indication of the sensitivity of the analysis to the model parameters. Two input parameters in the central analysis, β_{best}, and ΔT_{best}, are selected based on back analysis and calibration with the field data. In the other analyses, only one parameter is varied each time.

The parametric study is concerned with the following issues,

1) Influence of concrete thermal effects on excavation behaviour;
2) Sensitivity of the results on the degree of anisotropy adopted to model the diaphragm wall;
3) Effect on the results of using shell elements, rather than solid elements to model the diaphragm wall;
4) Influence of initial stress distribution and different K_0 values on the computed results;
5) Influence of conventional and advanced soil models to represent the soil.

Central analysis

In the central analysis, the various layers that comprise the Shanghai clay are represented by the multi-surface soil model (Houlsby 1999) with the input parameters derived in chapter 3 for Shanghai clay to consider the small-strain stiffness nonlinearity of the soil. The stiffness at very small strain G_0 and the undrained strength s_u are assumed in the model to increase linearly with depth. The undrained shear strengths use the expression $s_u = (20 + 2z)kPa$, and a constant index of rigidity $I_r = G_0/s_u = 1000$ is adopted. It should be noted that these parameters are derived from soil properties in green field condition which is very different from this construction site surrounded by densely packed buildings. For example, the stiffness and strength properties of the soil underneath buildings may be higher due to the building weight. Therefore, this is a limitation of this case study and may cause discrepancy with the field measurement.

The diaphragm wall is modelled with solid elements rather than shell elements in the central analysis. The anisotropic wall approach is used to consider the discontinuities in the diaphragm wall. The anisotropic ratio $\beta_{best} = 0.1$ is selected based on a number of parametric studies using different values of β $(10^{-5}, 10^{-4}, 10^{-3}, 10^{-2}, 10^{-1}, \text{and } 1.0)$ and comparison with the wall deflections at both wall corner and centre.

The concrete beams and floor slabs might contract or expand during the curing process and due to the variation of ambient temperatures (Whittle, Hashash et al. 1993). In addition, the existence of cracks and creep of concrete, and possible loose connections between the diaphragm wall and floor slabs, might cause extra wall deflection inwards the excavation. Considering the complexity of these mechanisms, thermal shrinkage is applied to the horizontal beams and floor slabs to consider these effects for simplicity. This is achieved by setting a realistic coefficient of thermal expansion α associated with a suitable temperature change ΔT after the beams and floor slabs are installed. The average value of α for concrete is approximate $10^{-5}/℃$, and $\Delta T_{best} = -35$ ℃ is selected based on a series of parametric studies ($\Delta T = 0, -5℃, -10℃, -15℃ \cdots$) and comparison with the measured wall deflections and ground movements.

Influence of concrete thermal shrinkage

Shrinkage is basically the reduction of concrete in volume at the absence of applied loads, and the mechanism is complicated and influenced by many factors. There are four main types of shrinkage, (i) plastic, (ii) autogenesis, (iii) carbonation, and (iv) drying shrinkage. Plastic shrinkage is due to moisture loss from the concrete before the concrete sets. Autogenesis shrinkage is associated with the loss of water from the capillary pores due to the hydration of the cement. Carbonation shrinkage is caused by the chemical reaction of various cement hydration products with carbon dioxide present in the air. Drying shrinkage can be defined as the volumetric change due to drying of the concrete, and it can cause cracking in concrete which is due to tensile stresses caused by the restraint conditions. Thus, drying shrinkage is related to not only the amount of shrinkage, but also the modulus of elasticity, creep, and tensile strength of the concrete.

Loose connections might exist between the retaining wall and horizontal supporting system (e.g. struts, floor slabs). For example, Finno, Atmatzidis et al. (1989) observed gaps as large as 12.7mm to 19mm between sheet piles and wales. Struts do not work until enough lateral displacement of the retaining wall occurred to close these gaps. In 3D finite element analysis, this effect can be considered by applying the displacement boundary condition to the wall at the strut level. Alternatively, this effect can be included in the thermal shrinkage of horizontal support system, e.g. beams and floor slabs. Similarly, other factors (e.g. cracks, creeps, and workmanship) which might cause larger wall deflection can also be included in the thermal shrinkage approach.

Whittle, Hashash et al. (1993) addressed the influence of floor slab shrinkage due to the ambient temperature change, but they simulated this effect in a very simple way by assuming a gap of 13mm between the roof/floor slabs and diaphragm wall and applying boundary conditions. However, this method is not practical in the 3D modelling with complex retaining system.

The thermal shrinkage approach is preferred in this case study to consider the thermal effect of

concrete and other factors which may enlarge the wall deflections (e.g. gaps, cracks, creeps, and workmanship). To investigate the influence of concrete shrinkage on the excavation behaviour, two values of temperature change ($\Delta T = -30$ ℃ and -40 ℃) are selected for the parametric study. The results are compared with the central analysis.

Influence of joints in the diaphragm wall

As discussed in chapter 3 and chapter 4, the anisotropic wall approach is an adequate way to consider the joints in the retaining wall, but the value of the anisotropic ratio β needs to be estimated based on parametric studies and comparison with field measurement. Zdravkovic, Potts et al. (2005) used $\beta = 10^{-5}$ for contiguous pile wall. The diaphragm wall is much stiffer than the contiguous pile wall, and a larger value of β is suitable. The value of $\beta = 0.1$ is selected in the central analysis based on parametric studies using different values ($\beta = 10^{-5}, 10^{-4}, 10^{-3}, 10^{-2}, \text{and } 10^{-1}$) and comparison with field data. Results from the analysis with $\beta = 10^{-5}$, and the isotropic wall approach, are presented later and compared with the central analysis to show the influence of the degree of anisotropy for the diaphragm wall.

Influence of shell and solid elements to model the diaphragm wall

As discussed in chapter 3 and chapter 4, modelling the retaining wall with shell elements would result in larger wall deflection and ground movement than using solid elements to model the wall, due to the difference in bending moments caused by the shear stress on the surface of the wall. However, the amount of difference in the results might depend on a number of factors such as the shear stress on the wall surface, the soil properties, and characteristics of the excavation. To investigate the difference between the results from these two wall types, another model is created using shell elements to model the diaphragm wall, with the same material properties as the solid element wall in the central analysis. In addition, to investigate the merit of modelling the discrete wall panels and joints explicitly with shell elements, results from two other models are also presented, (i) a discontinuous wall with no connection at the corner, associated with isotropic wall properties, (ii) continuous wall but releasing the rotational DOFs at the corner, associated

with isotropic wall properties. This parametric study is intended to understand whether the discrete wall approach is superior to the anisotropic wall approach.

Influence of initial stress state in the soil prior to the excavation

As the soil is a nonlinear and stress path dependent material, its behaviour is dependent on both the current stress state and its stress history. The initial stress state in the ground will affect the stress path of the soil in the subsequent excavation process and also the deformation characteristics. The in-situ lateral earth pressure coefficient, K_0 in effective stress expression and K_0^t in total stress expression, reflects the initial stress state in the ground. The relationship between K_0^t and K_0 is discussed in chapter 3. To explore how the initial stress state affects the excavation behaviour, two values of K_0^t (0.77 and 1.0), equivalent to the $K_0 = 0.5$ and 1.0, are used in the parametric study to compare with the central analysis.

Influence of soil models

The quality of the numerical analysis largely depends on the adequate soil models being used. In general, a more realistic prediction of ground movements requires using soil models which account for pre-failure behaviour of the soil, e.g. a nonlinear stress-strain relationship before reaching the ultimate state. Pre-failure stiffness plays a crucial role in modelling typical geotechnical problems such as deep excavations. Research and practice have indicated that for tunnelling and deep excavation problems, numerical modelling without considering the small-strain stiffness of soils will not provide satisfactory agreement with field measurements (Potts and Zdravkovic 2001). Although a number of nonlinear soil models have been proposed to consider the small-strain stiffness of soil, they are normally limited within small research groups of universities and institutes, not available for commercial software, and the input parameters for these models are applicable particularly to a certain type of soil. In addition, they usually comprise a relatively large number of parameters, some of which are not easy to derive from conventional experiments. Therefore, in practice, conventional soil models (e.g. linear elastic, Mohr-Coulomb, Drucker-Prager, Modified Cam-Clay, etc.) are still widely used due to their

simplicity and availability in most finite element softwares for geotechnical analyses.

In order to compare the predictive ability of different soil models in deep excavations, three analyses, as shown in Table 5.4, using the linear elastic model, Tresca model with constant parameters, and Tresca model with variable parameters, are conducted to compare with the central analysis. To make these analyses comparable, some assumptions of the soil parameters are made. For linear elastic analysis and Tresca soil model with constant soil properties, the stiffness G is adopted as G_{50} (stiffness at 50% of the shear strength) from the S-shaped curve in chapter 3, $G_{50} \approx 0.25G_0$, at the depth of 15m (roughly half the wall depth) below the ground surface, $G = 12.5\text{MPa}$. The strength s_u, for the Tresca soil model with constant parameters is also taken at the depth of 15m below the ground surface, $s_u = 50\text{kPa}$. For Tresca model with variable parameters, $G = G_{50} \approx 0.25G_0 = 250s_u$.

Table 5.4 Finite element runs for effects of soil models

Run	Soil models	Stiffness	Strength
1	Linear elastic, constant soil parameters	$G = 12.5\text{MPa}, \nu = 0.49$	Null
2	Tresca model, constant soil parameters	$G = 12.5\text{MPa}, \nu = 0.49$	$s_u = 50\text{kPa}$
3	Tresca model, stiffness and strength increases linearly with depth	$G = 250\text{s}_\text{u}, \nu = 0.49$	$s_u = (20 + 2\text{z})\text{kPa}$

The stress-strain relationship of three types of soil models is illustrated in Fig.5.12.

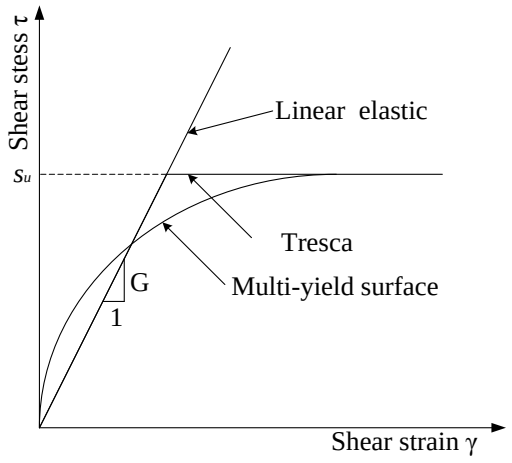

Fig.5.12 Illustration of stress-strain-strength relationship of different soil models

5.4 Interpretation of results

The results from the central analysis are presented first, followed by results from other parametric analyses which explore the influence of several key aspects in deep excavations. The

numerical analyses generated a substantial amount of data, but it is not necessary to show them all in this chapter. Only selected results concerned with locations in Fig.5.13, are presented and compared with the field measurement.

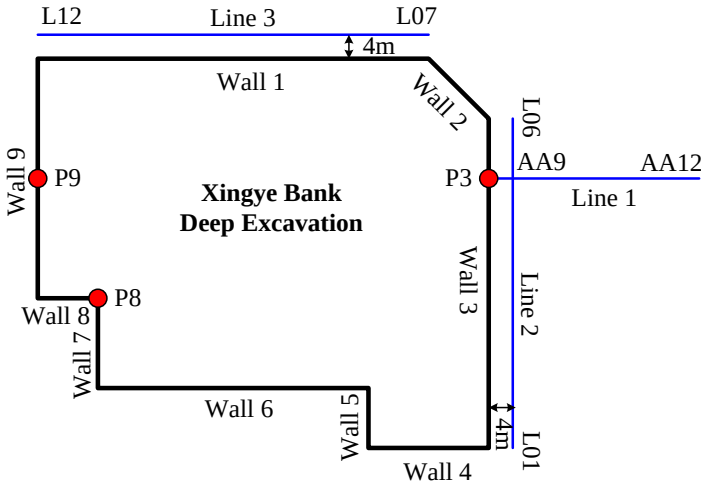

Fig.5.13 Field instrumentation

The wall deflections are measured at totally 9 points (P1~P9), as shown in Fig.5.6. The largest wall deflection was observed at *P*9 because it is located at the wall centre on the side with larger excavation depth and large openings in the floor slabs, whereas the smallest wall deflection was observed at *P*8 at the corner of the wall due to the corner effect. In addition, the wall deflection at corner is useful to calibrate the anisotropic ratio in the anisotropic wall approach. Therefore, wall deflections at *P*9 and *P*8 are focused in this chapter. The wall deflection at P3 is also shown together with the adjacent ground settlement along Line 1.

The vertical movement of the diaphragm wall is also an essential part to understand the wall behaviour. The results are presented following the sequence from wall 1 to wall 9.

The section $AA9 \sim AA12$ (Line 1), as shown in Fig.5.6, is chosen to represent the ground settlement in the direction perpendicular to the diaphragm wall. The section $L01 \sim L06$ (Line 2) and section $L07 \sim L12$ (Line 3) are selected to represent the ground settlements along two directions parallel to the diaphragm wall, although they were monitored to reflect the settlements of buried electrical power pipelines.

The measurement was recorded at every stage of the construction, but the data at the final stage

of excavation are more concerned. Therefore, only these data are interpreted, with others included in Appendix A.

5.4.1 Central analysis

The results from central analysis, as described in Table 5.5, are presented below.

Table 5.5 Finite element runs and description for central analysis

Run ID	Description
Central analysis	Soil Model: Multi- yield surface model, $K_0^t = 0.88,\ s_u = (20 + 2z)kPa,$ $I_r = G_0/s_u = 1000;$ Wall Model: Solid element, $E = 30GPa, \nu = 0.3, \beta = 0.1;$ Beams and Slabs: $E = 30GPa, \nu = 0.3, \alpha = 10^{-5}/℃, \Delta T = -35℃$ Piles: $E = 30GPa, \nu = 0.3;$

Wall deflections

Fig.5.14 shows the wall deflections at *P*9 and *P*8 at the final stage of excavation from the central analysis and field measurement. It should be noted that the field measurement only represents the pattern of the wall displacement, because field data from inclinometer reading assume that the wall does not move at the toe. However, this assumption is usually not correct because the wall is neither deep enough nor embedded in the stiff clay to restrain its toe movement. This error could be corrected by measuring the horizontal movement at the top of the wall at the same time with the inclinometer reading, or extending the inclinometer casing to the deep subsoil. In the case that the total wall deflections are not known from the field measurement, the computed wall deflections are modified by deducting the wall toe deflection to compare with the field data. Both the total wall deflection and the modified one are shown in the figure.

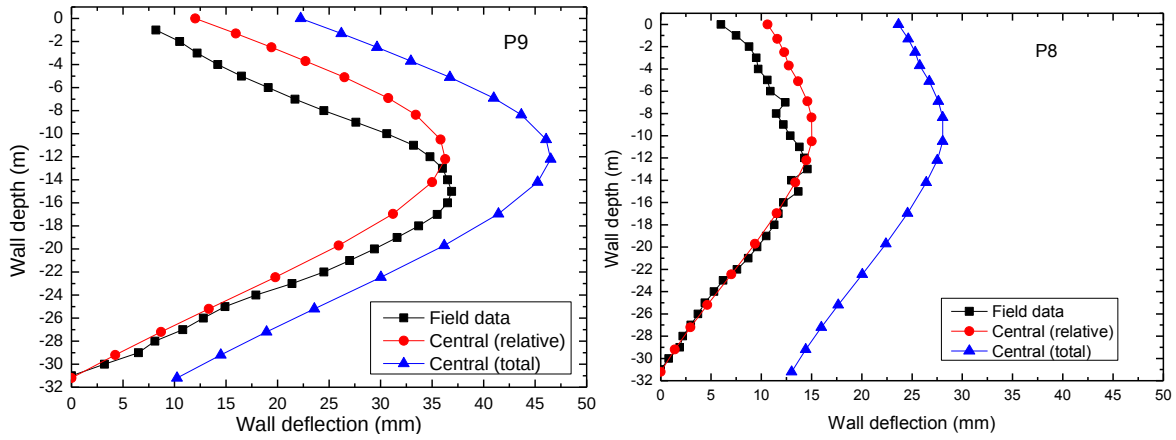

Fig.5.14 Wall deflections at P9 and P8

As shown in Fig.5.14, the pattern of wall deflections at *P*9 and *P*8 agrees well with the field

measurement, although the calculated largest wall deflection is higher than the field data and there is a slight discrepancy in the magnitude of the deflection. This kind of discrepancy is acceptable, and such discrepancy might be attributed to a number of reasons such as the assumptions and approximations made in the analyses, and the material models and input parameters.

Wall vertical movement

The vertical displacement of the wall from numerical analysis is compared with the field data in Fig.5.15. The vertical movement of the diaphragm wall is influenced by the soil movement due to stress relief, its self-weight, and the load from the horizontal beams and floor slabs. The magnitude and direction of the movement might depend on a number of factors such as the excavation depth, soil properties, the retaining structures, soil-wall friction, and construction activities. In this case study, the movement from numerical analysis is upward, which is close to the field data, but the wall heaves more at the corner than at the centre, which is opposite to the field data. It is also noticed that the field measurement also observed wall settlement at some point which is not captured by the numerical analysis.

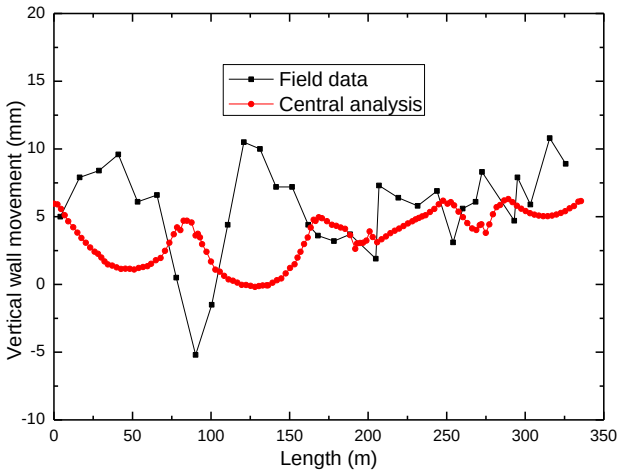

Fig.5.15 Vertical wall displacement

Ground settlement

The ground settlement behind the wall along $AA9{\sim}AA12$ (Line 1) is plotted in Fig.5.16, associated with the wall deflection at $P3$. The calculated ground settlement agrees well with the field measurement, and the largest settlement is almost the same with the field data, but it seems

that the settlement trough is slightly wider than the field data. The calculated wall deflection pattern at *P*3 is very close to the field data.

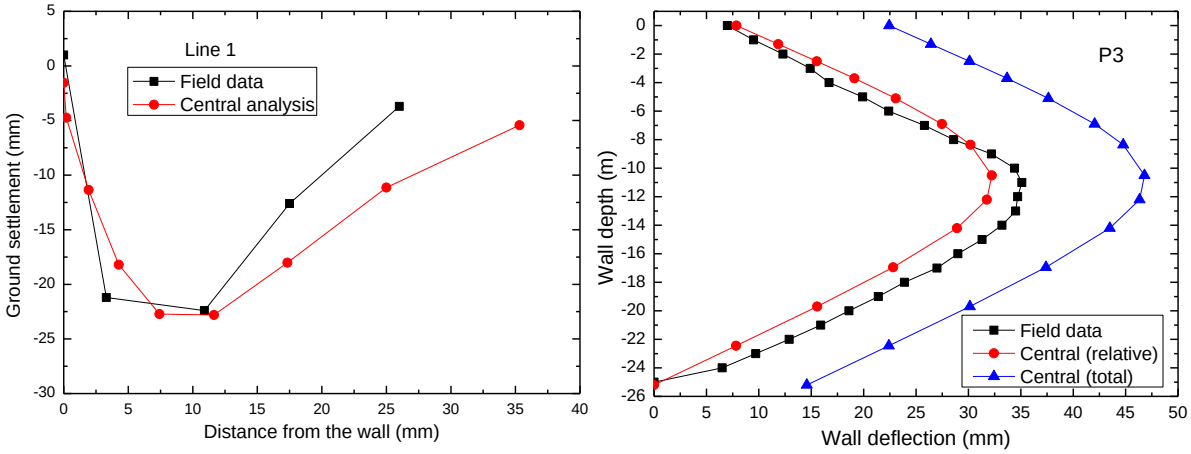

Fig.5.16 Ground settlements along Line 1 and adjacent wall deflection at P3

The ground settlement along Line 2 and Line 3 is shown in Fig.5.17. Please note that the settlement caused by the installation of diaphragm wall installation and bored piles, and the dewatering process, has been subtracted from the total settlement in the field data, because the numerical analysis does not consider these aspects. The agreement of calculated results with field data is satisfactory. The numerical results capture the settlement pattern in the field measurement in which the settlement behind the wall centre is larger than that behind the corner, indicating the corner effect.

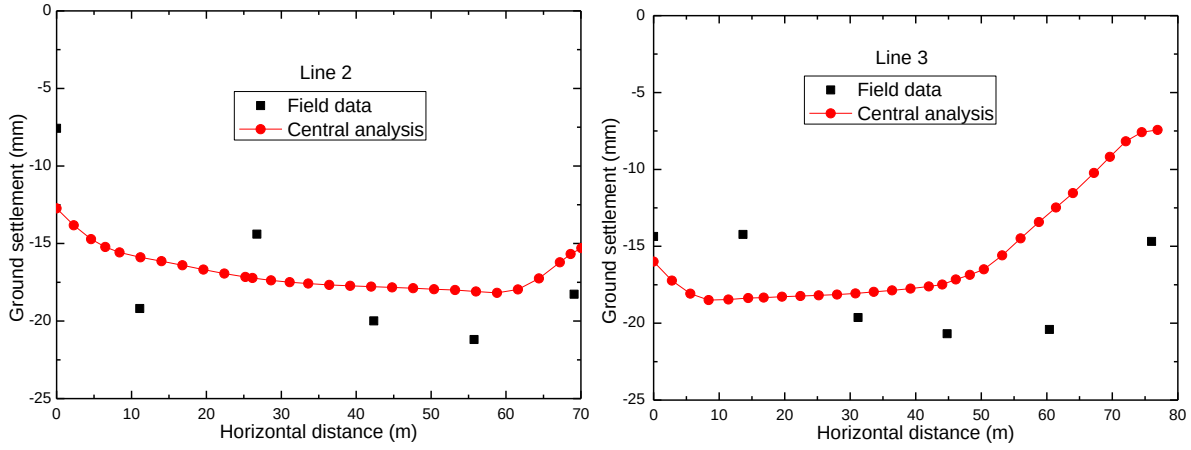

Fig.5.17 Ground settlement along Line2 and Line 3

Contour display

The ground vertical displacement contour is displayed in Fig.5.18. It is clearly seen that the largest ground settlement is concentrated behind the wall centre outside the excavation, while the settlement is smaller around the corner due to the corner effect. The longer the wall, the larger is

the ground settlement area. The basal heave is also evident inside the excavation due to stress relief.

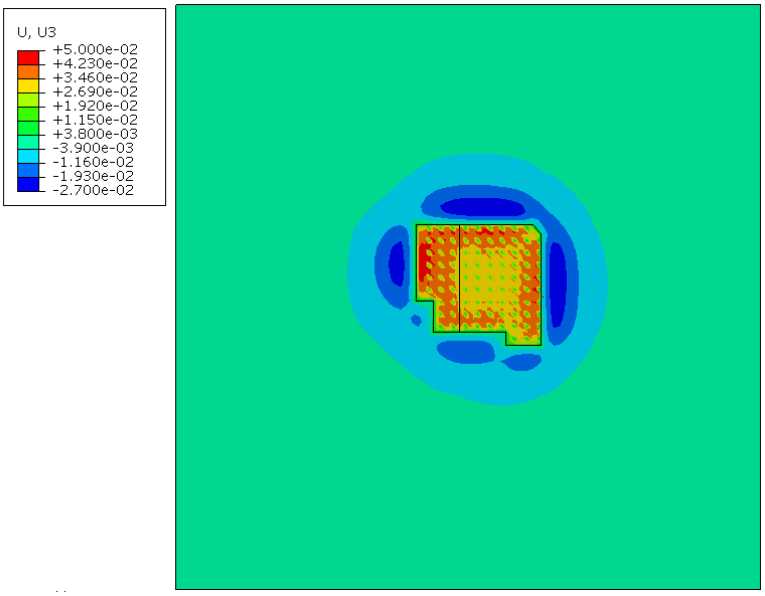

Fig.5.18 Ground vertical displacement (unit:m)

As shown in Fig.5.19, the largest wall deflection is concentrated at the wall centre area close to the excavation formation level, while the deflection at the corner is smaller due to the corner effect. The shape of the diaphragm wall also affects the wall deflection. For example, the wall deflection is larger in the longer piece of wall, while smaller in the shorter piece of wall.

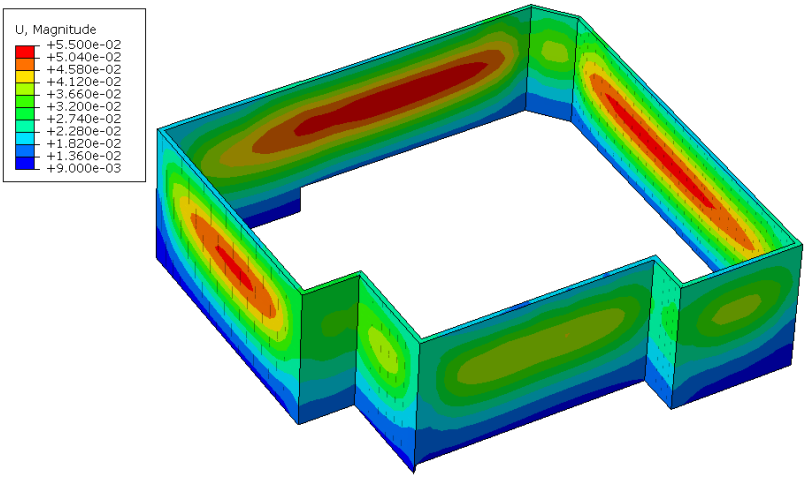

Fig.5.19 Wall deflection (unit:m)

The displacement contour of the support system is shown in Fig.5.20 and Fig.5.21. The piles move upwards due to basal heave. The displacement of beams and slabs are constrained by diaphragm wall and piles, and the differential settlement is clearly seen which may cause cracks inside the concrete.

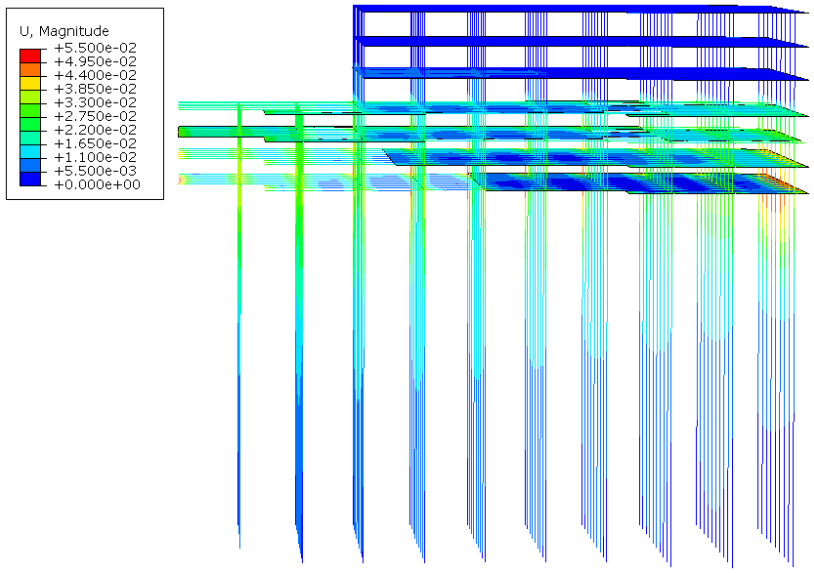

Fig.5.20 Displacement distribution of the supporting system

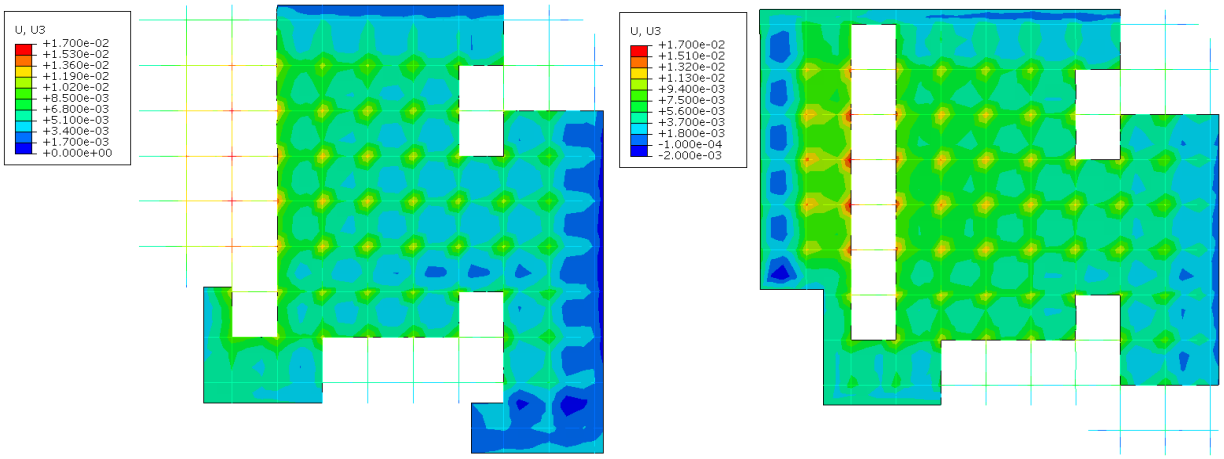

(a)Top floor (b) -1st floor

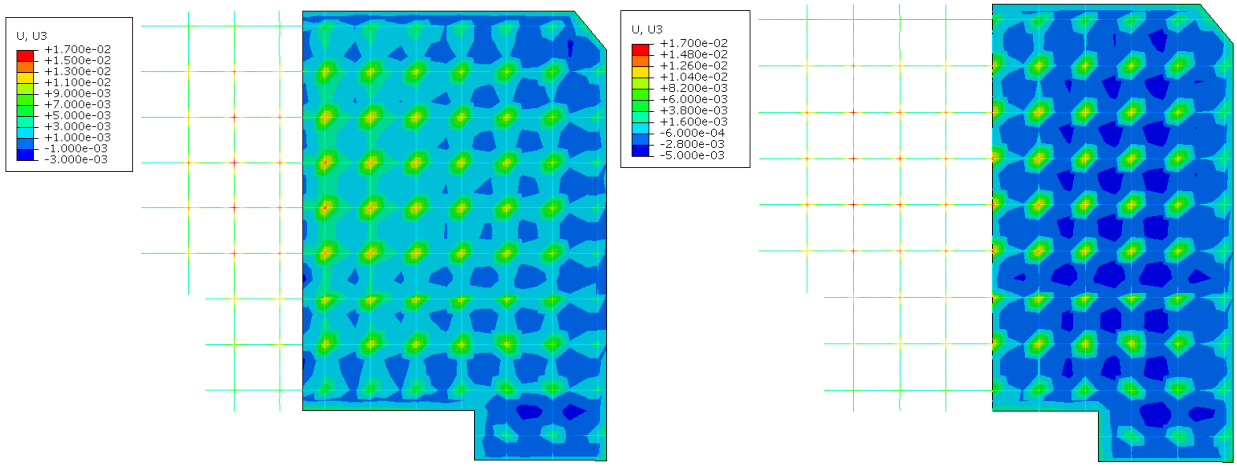

(c) -2nd floor (d) -3rd floor

Fig.5.21 Displacement contours of horizontal beams and slabs in different floors (unit:m)

Summary

As discussed above, the central analysis captures reasonably well the excavation behaviour including both wall deformations and ground movements, which is promising and shows the

capability of advanced finite element analysis. The success can be attributed to the proper modelling of, (i) irregular geometry, detailed retaining structures, and construction sequence, (ii) advanced soil model and reliable soil properties, (iii) anisotropic wall properties to model the joints in the diaphragm wall, (iv) thermal effects of concrete beams and slabs, and other effects that might cause extra wall deflections (e.g. gaps between wall and floor slabs, cracks and creep of concrete structures, workmanship, and overexcavation)

5.4.2 Influence of thermal effects of concrete

Results from another two analyses, as described in Table 5.6, are compared with the central analysis and the filed data, to investigate the influence of thermal effects of concrete on the excavation behaviour due to temperature changes.

Table 5.6 Finite element runs and description

Run Name	Description
Central analysis	$\Delta T = -35℃$
T30	$\Delta T = -30℃$
T40	$\Delta T = -40℃$

Wall deflection

The computed wall deflections at *P*9 and *P*8 are shown in Fig.5.22 and compared with the field data. The results indicate that the wall deflection is sensitive to thermal effects in the concrete. When the temperature varies by 5℃, the beams and floor slabs shrink or expand and the maximum wall deflections change approximate 3mm. The wall deflection change at *P*8 is slightly smaller than that at *P*9 due to the corner effect. Therefore, the thermal effects should not be neglected in the analyses.

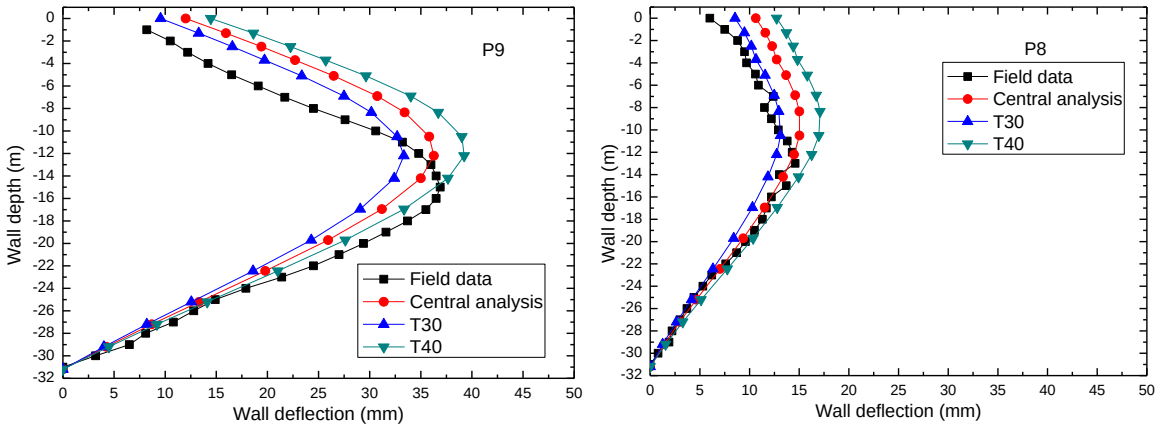

Fig.5.22 Wall deflections at P9 and P8

Wall vertical movement

The wall top movement is shown in Fig.5.23 and compared with the field data. It can be seen that the concrete thermal effects also affect the wall vertical movement, but this influence is relatively small compared to that of the wall deflections. The movement at the wall corner is less sensitive to temperature change than that at the centre due to the corner effect.

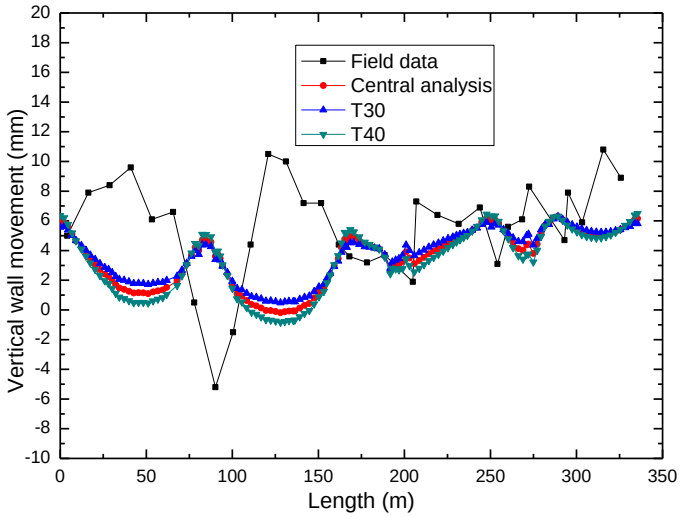

Fig.5.23 Wall top movement

Ground settlement

The ground settlements behind the wall along Line 1 are shown in Fig.5.24, associated with the wall deflection at *P*3. The results show that the ground settlement varies by around 3mm when the temperature of concrete changes 5℃, and similar trend is found in the wall deflection at *P*3.

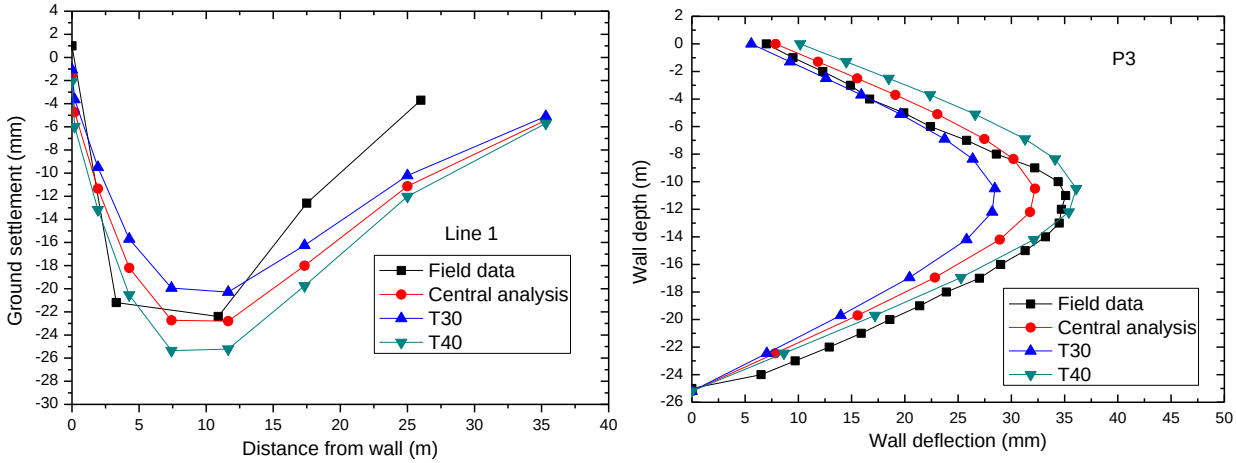

Fig.5.24 Ground settlements along Line 1 and adjacent wall deflection at P3

The ground settlements behind the wall along Line 2 and Line 3 are shown in Fig.5.25. The results are consistent with those along Line 1, which indicates that ground settlement behind the wall is sensitive to the thermal effects of concrete, although the settlement change behind the

wall corner is smaller than that behind the wall centre due to the corner effect.

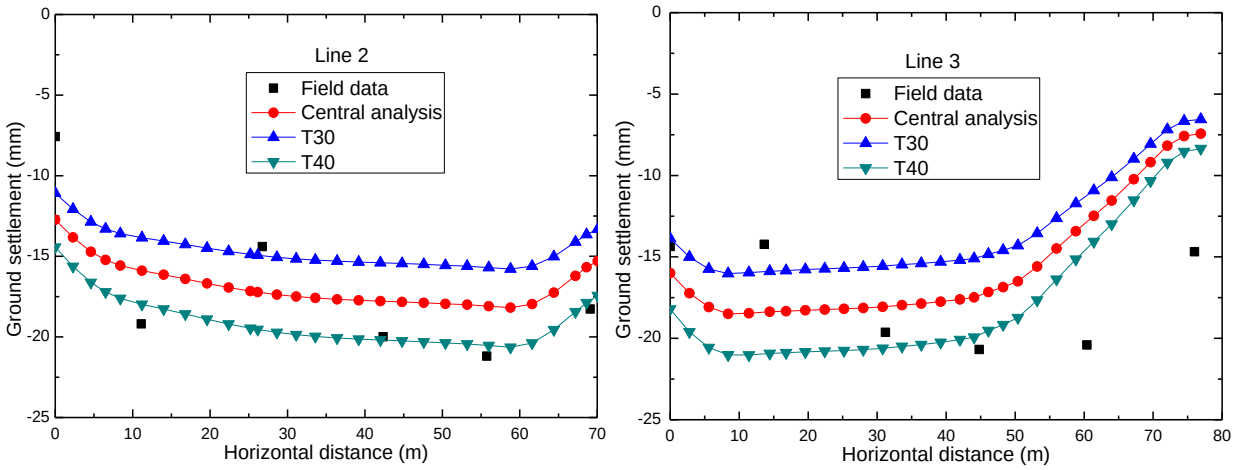

Fig.5.25 Ground settlements along Line 2 and Line 3

Summary

Both the wall deformation and ground settlements are sensitive to the temperature changes of concrete beams and floor slabs. When temperature changes by 5℃, the magnitude of largest wall deflection and ground settlement varies about 3mm. This result confirms that the thermal effects of concrete should not be neglected in deep excavations.

5.4.3 Influence of joints in the diaphragm wall

In order to show the importance of considering joints in the diaphragm wall and investigate the effectiveness of the anisotropic wall approach, results from two more runs (described in Table 5.7) are presented in this section.

Table 5.7 Finite element runs and description

Run Name	Description of analysis
Central analysis	$\beta = 10^{-1} = 0.1$
E5	$\beta = 10^{-5}$
E0 (isotropic)	$\beta = 10^{0} = 1$

Wall deflection

The wall deflections at *P*9 and *P*8 are shown in Fig.5.26. When the wall is modelled with isotropic properties, the wall deflection at the corner has large discrepancy with the field data. The anisotropic wall approach could greatly improve this, but the value of the anisotropic ratio β has a significant influence on the wall deflection at the corner. The wall deflections at both centre and corner increase as the value of βdecreases, but it seems that the wall deflection at the corner is more sensitive to the value of β. Zdravkovic, Potts et al. (2005) used the value $\beta =$

10^{-5} for contiguous pile wall, but this value is too small for the diaphragm wall which is much stiffer. It is found that $\beta = 0.1$ is a good value for the diaphragm wall in this case study.

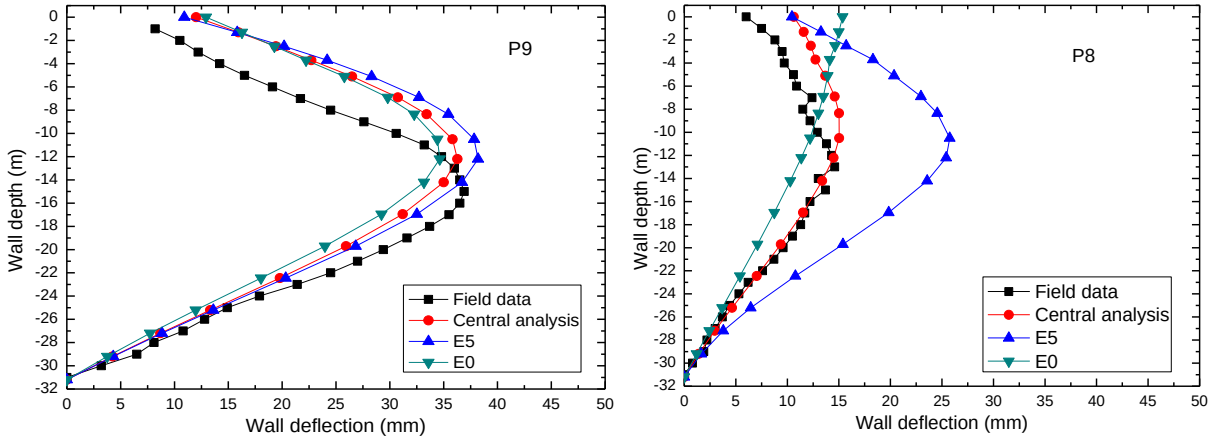

Fig.5.26 Wall deflections at P9 and P8

Wall vertical movement

The vertical wall movements are shown in Fig.5.27. The results from the central analysis and the isotropic wall are similar, but when $\beta = 10^{-5}$ the wall movement becomes irregular probably because this value is too small.

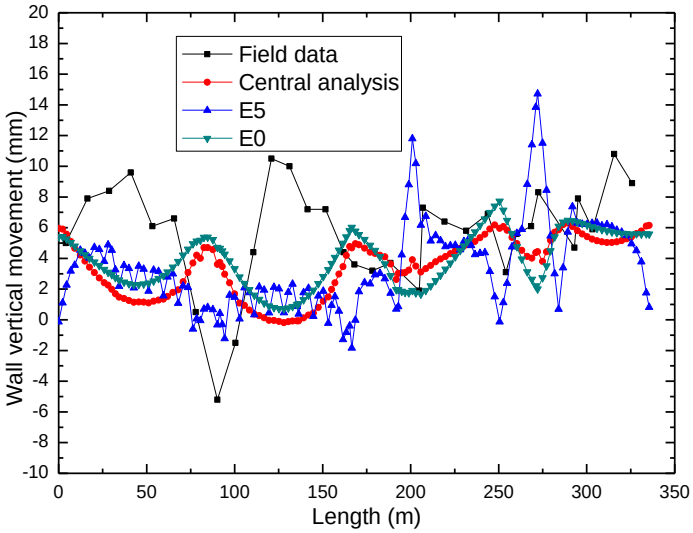

Fig.5.27 Wall vertical movement

Ground settlement

The ground settlement behind the wall along Line 1 is shown in Fig.5.28, associated with the wall deflection at $P3$. When the wall is modelled with isotropic properties, $\beta = 1$, the ground settlement along Line 1 is less than half of that from the anisotropic wall approach, and the wall deflection at $P3$ is also much smaller. However, when the wall is modelled with anisotropic

properties, both the ground settlement and the adjacent wall deflection greatly increase, and the corner effect is reduced. It seems that the ground settlement and wall deflection do not change to much when the value of β varies from 0.1 to 10^{-5}.

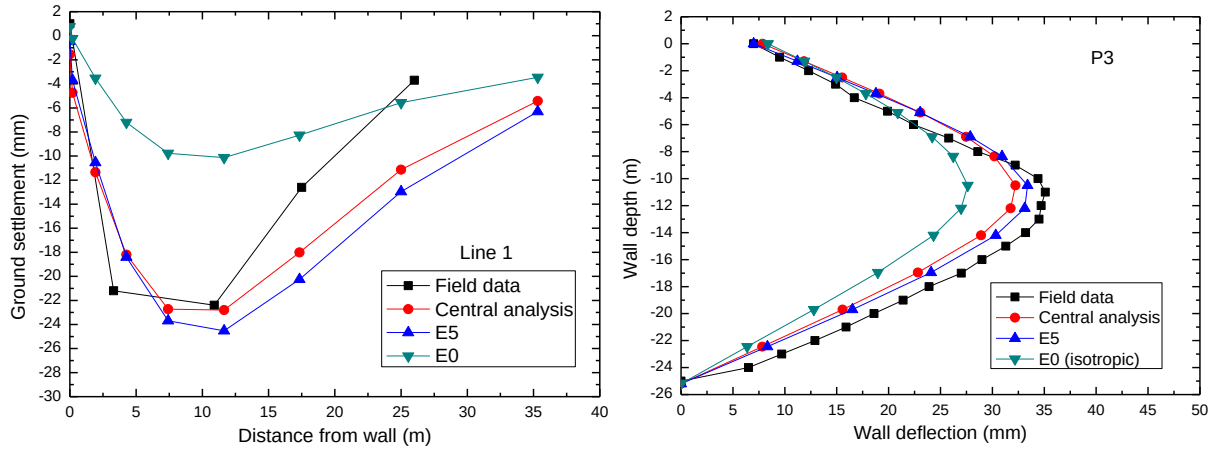

Fig.5.28 Ground settlements along Line 1 and adjacent wall deflection at P3

As shown in Fig.5.29, the ground settlements are influenced by the way that the wall is modelled. The ground settlement at the wall corner is more sensitive to the value of β than that at the wall centre. The value of $\beta = 10^{-5}$ is too small for the diaphragm wall in this case study.

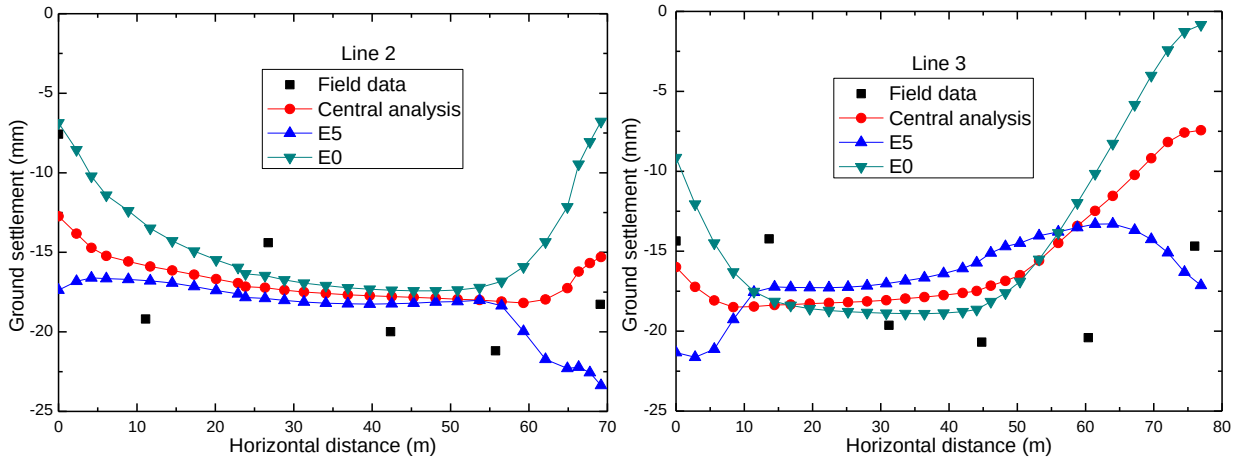

Fig.5.29 Ground settlement along Line 2 and Line 3

Summary

The joints in the diaphragm wall should not be neglected in the numerical analysis and the anisotropic wall approach seems to be an effective way to solve this problem. Simply modelling the wall with isotropic properties cannot capture the wall deflection at the corner and would underestimate the ground settlements close to the wall corner. The results could be greatly improved if the wall is modelled with anisotropic properties, but the value of the anisotropic

ratio β should be carefully selected depending on the type of the retaining wall.

5.4.4 Effect of shell and solid element for the wall

As discussed before, the shell element wall tends to overestimate the wall deflections and ground settlements compared with the solid element wall. In this section, the diaphragm wall is modelled with shell elements, as described in Table 5.8, to show the difference with that using solid element to model the diaphragm wall. One run with continuous anisotropic wall and two runs with discontinuous wall, are compared with the central analysis.

Table 5.8 Finite element runs and description

FEM Run Name	Description of analysis
Central analysis	Soil element wall, anisotropic, $\beta = 0.1$
Shell anisotropic	Shell element wall, continuous, anisotropic, $\beta = 0.1$
Shell isotropic 1	Shell element wall, discontinuous at corner, isotropic
Shell isotropic 2	Shell element wall, continuous at corner but releasing the rotational DOFs, isotropic,

Wall deflection

As shown in Fig.5.30, when the diaphragm wall is modelled with continuous shell elements with anisotropic properties, the wall deflection pattern at both wall centre and corner is similar to that from soil element wall, but the magnitude is around 30% larger, which is consistent with the results in Chapter 4 and those from Zdravkovic, Potts et al. (2005). When the shell element wall is cut at the corner and represented by an isotropic material (Shell isotropic 1), the wall deflection at the centre is not affected too much, whereas the wall deflection at the corner is almost 2 times larger than the field data. It can be expected that when the diaphragm wall is modelled with discrete wall panels using shell elements, the discrepancy of the wall deflection at corner with the field data will be even larger. To improve the wall deflection at corner, the wall are connected at corners with only translational DOFs (no rotational DOFs) as in the case of shell anisotropic 2, but the result shows that wall deflection at corner is similar to that from the isotropic wall approach. This suggests that the discontinuous wall approach with isotropic properties method is not superior to the continuous wall with anisotropic properties.

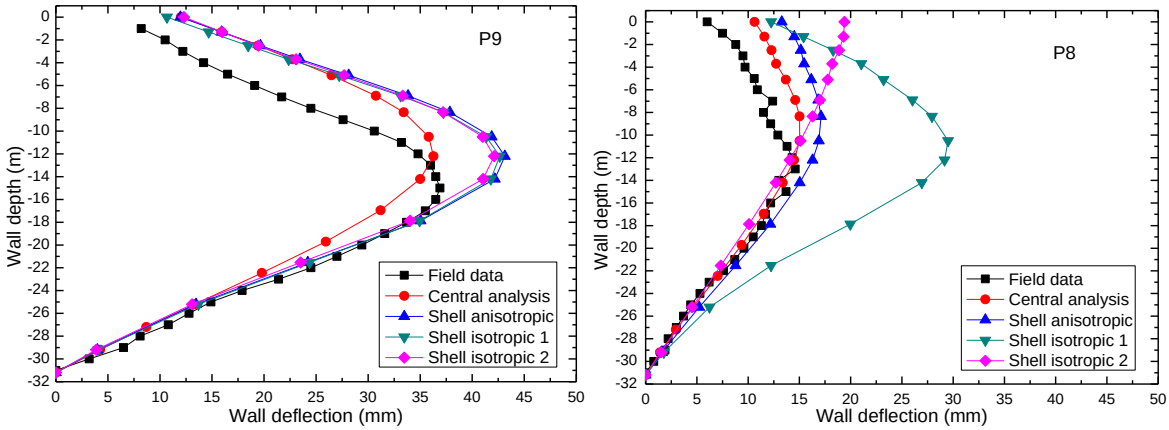

Fig.5.30 Wall deflection at *P*9 and *P*8

Wall vertical movement

As shown in Fig.5.31, the wall vertical movement from shell element wall is generally similar to the result from solid element wall in pattern, but much smaller in magnitude and is far from the field measurement. There are two possible reasons: (i) the shell element wall has no thickness and results in concentrated force at the wall bottom and larger downward movement, which is different from the distributed stress at the wall bottom from solid element wall, (ii) the shell element wall is embedded into the soil and brings additional gravity proportional to its concrete density ρ_c, whereas the solid element wall is installed by replacing the material property of the wall elements from soil to concrete and this introduces less gravity which is proportional to the difference of densities between concrete ρ_c and soil ρ_s. In general, the solid wall installation process is closer to the reality where the diaphragm wall is installed after the trench excavation. There is no significant difference of wall movement between three shell wall approaches.

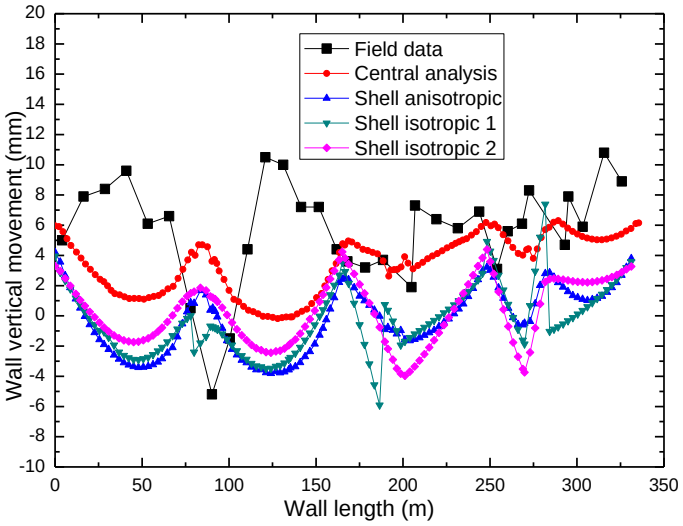

Fig.5.31 Wall top settlement

Ground settlement

As shown in Fig.5.32, when the shell element wall with anisotropic properties results in approximately 30% larger ground settlement along Line 1 and wall deflection at *P*3 compared to the solid element wall in the central analysis. When the wall is modelled by shell elements discontinuous at corners with isotropic properties, the results are very close to the anisotropic shell element wall analysis. However, when the translational DOFs are connected, the ground settlement and wall deflection are reduced.

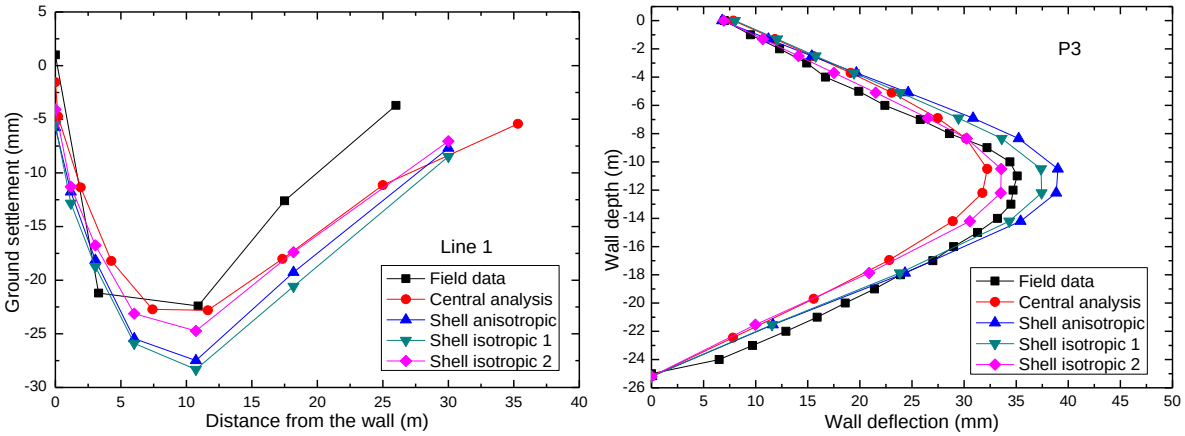

Fig.5.32 Ground settlement along Line 1 and adjacent wall deflection at P3

The ground settlements along Line 2 and Line 3 are shown in Fig.5.33. The result is consistent with the analysis above that the ground settlement behind the wall from shell element wall is larger than that from solid element wall. There is no significant difference between the analyses from anisotropic shell element wall and the isotropic shell element wall discontinuous at the corners, but the one from isotropic shell element wall connecting the translational DOFs shows strong corner effect.

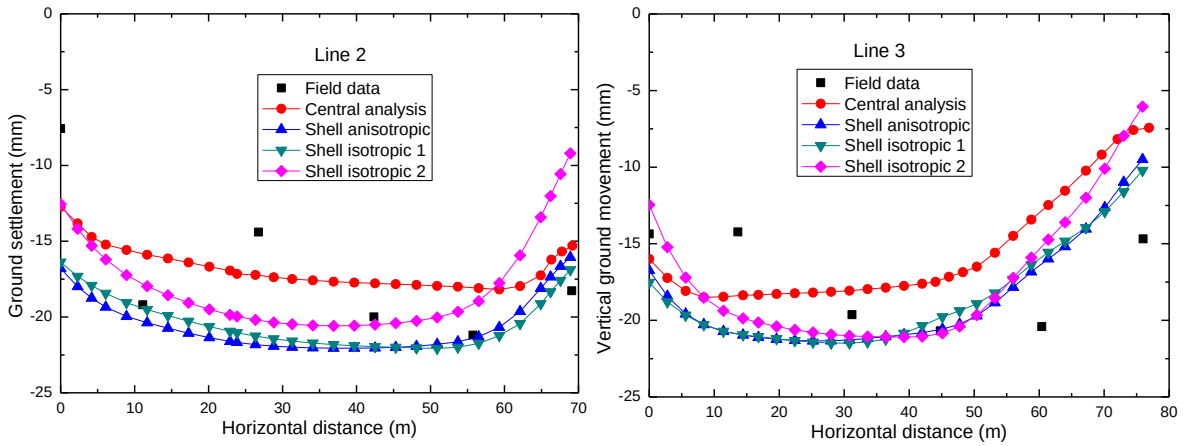

Fig.5.33 Ground settlements along Line2 and Line 3

Summary

In finite element analysis of deep excavations, the retaining wall could be modelled with either shell elements or solid elements, but the difference should not be neglected. The shell element wall tends to overestimate the wall deflections and ground settlements (by around 30% in this case study) because it does not have the beneficial bending moment caused by shear stress on the interface of the wall about the wall centre line as discussed in Chapter 3. Therefore, when the displacement is concerned, solid elements are suggested to model the retaining wall.

Compared to solid elements, shell elements have the potential to model the details of the discrete wall panels and joints explicitly, but it is shown that this approach would result in much larger wall deflection at the wall corner than the field data. On the contrary, the wall deflection at the corner can be captured by the anisotropic wall approach straightforwardly by selecting a suitable anisotropic ratio.

5.4.5 Influence of the initial stress state in the ground

The initial stress state in the ground might affect the performance of deep excavations, and its influence is investigated though analyses with different values of the coefficient of earth pressure at rest. Two calculations, as shown in Table 5.9, are conducted with $K_0^t = 0.77, and\ 1.0$, equivalent to the $K_0 = 0.5, and\ 1.0$ in the effective stress expression, as discussed in chapter 3.

Table 5.9Finite element runs and description

Run Name	Description of analysis
Central analysis	$K_0^t = 0.88$
K077	$K_0^t = 0.77$
K100	$K_0^t = 1.0$

Wall deflection

The wall deflections at $P9$ and $P8$ are shown below, including both total and relative displacements as discussed before. Larger K_0^t value means larger lateral earth pressure on the back of the retaining wall and thus larger lateral stress relief caused by the excavation, so the wall deflections from $K_0^t = 1.0$ are larger than those from the other two analyses. Similar results were also found in Potts and Fourie (1984) and Potts and Fourie (1985), in which they used two values of K_0 (2.0 and 0.5). However, the results from $K_0^t = 0.77$ and $K_0^t = 0.88$ are almost

identical. It is also found thatthe value of K_0^t does not change the wall deflection pattern.

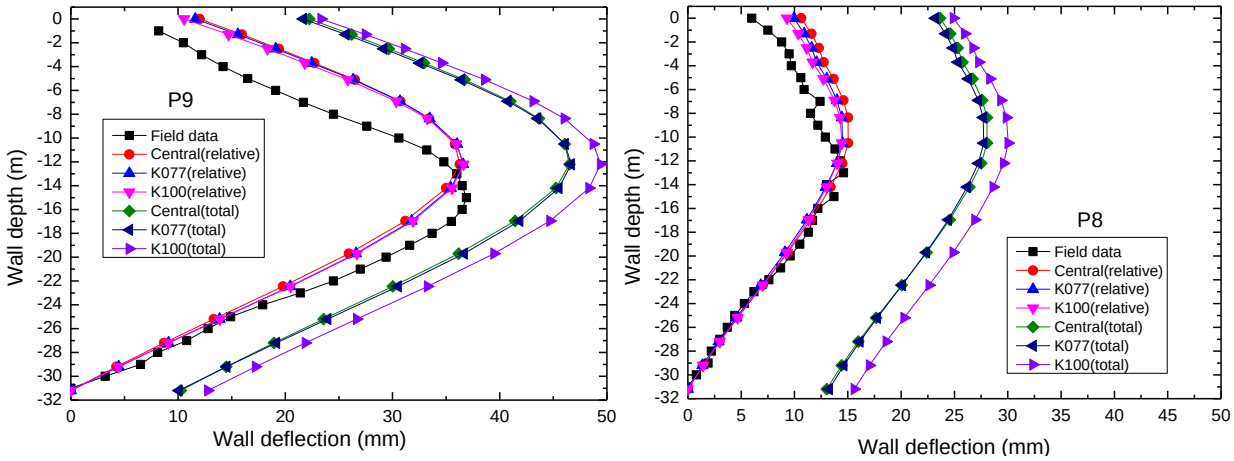

Fig.5.34 Wall deflections at P9 and P8

Wall vertical movement

As shown in Fig.5.35, the larger value of K_0^t results in larger wall vertical movement, which is probably due to the stress relief and wall deflections.

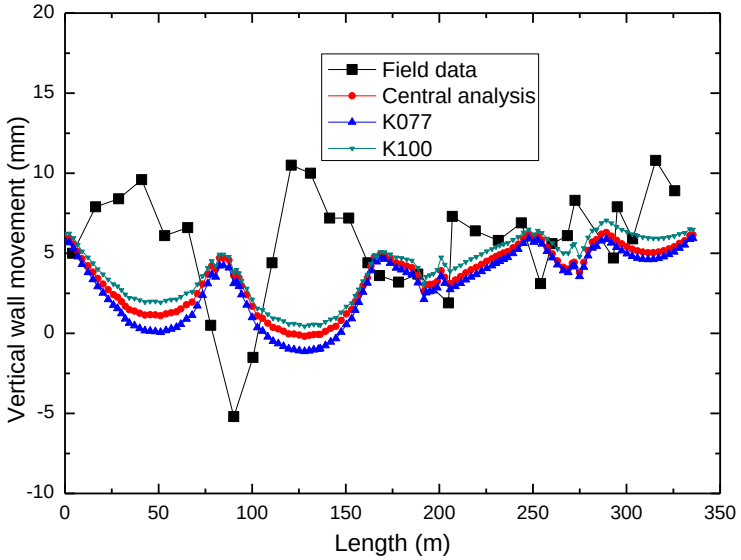

Fig.5.35 Wall vertical movement

Ground settlement

As shown in Fig.5.36, the analysis from $K_0^t = 1.0$ results in the smallest ground settlement but the largest wall deflection among the three analyses, while the analysis from $K_0^t = 0.77$ leads to the largest ground settlement and the smallest wall deflection. This is because the stress state is hydrostatic when $K_0^t = 1.0$, and the soil is stiff and far from failure in this stress state, so the soil deformation in the retained side is expected to be smaller. On the other hand, the deviator stress is larger when $K_0^t = 0.77$ and the stress state is closer to failure, so the soil outside the

excavation is expected to experience larger vertical movement due to lateral stress relief.

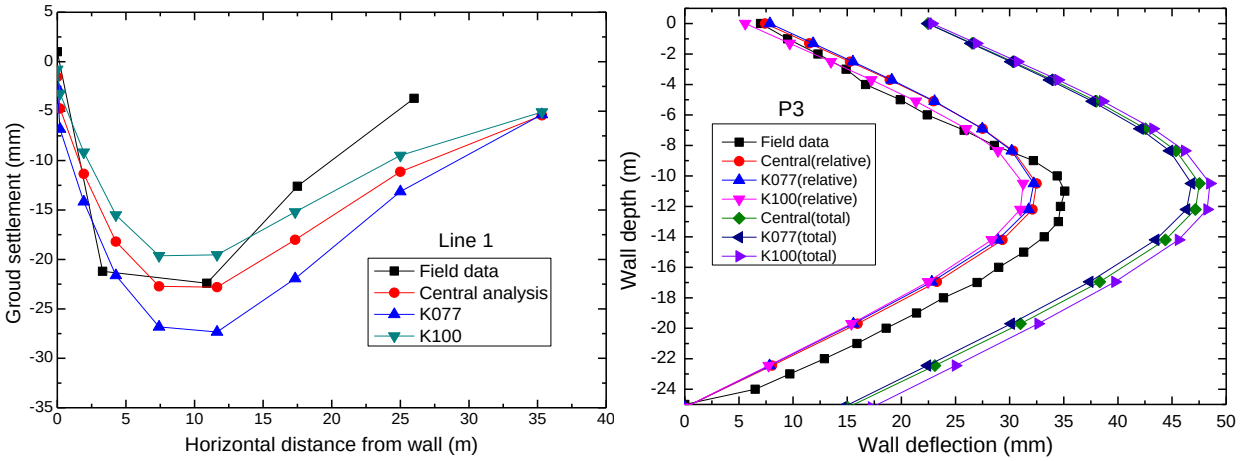

Fig.5.36 Ground settlement along Line 1 and adjacent wall deflection at P3

The ground settlement along Line 2 and Line 3 is shown in Fig.5.37. The result is consistent with the analysis above that larger K_0^t value results in smaller ground settlement outside the excavation. The difference in the settlement is larger close to the wall centre than that close to the wall corner due to the corner effect. The largest difference in the ground settlement between the analyses from $K_0^t = 1.0$ and $K_0^t = 0.77$ is approximate 7mm which is significant.

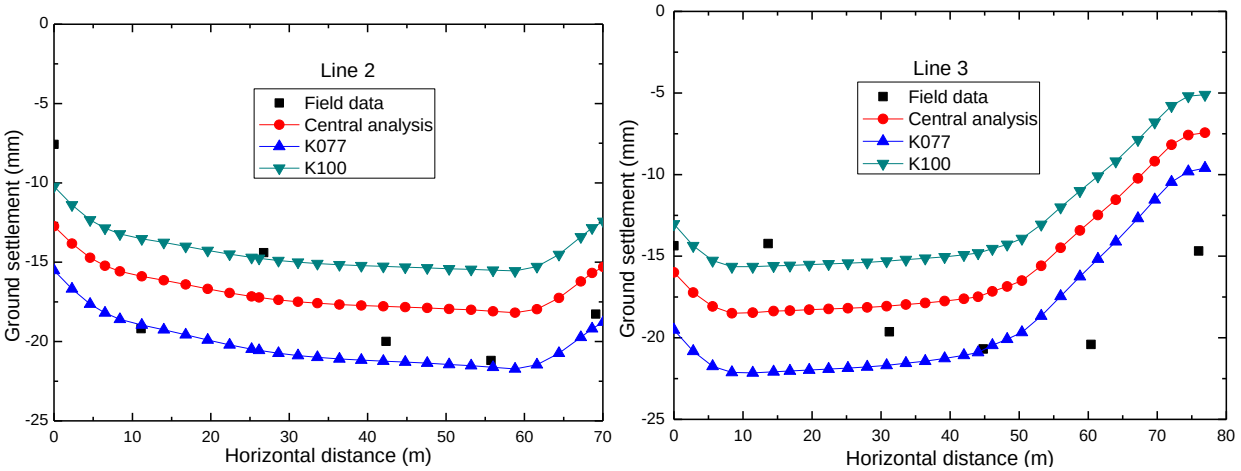

Fig.5.37 Stress path of soil element

Summary

As the soil is a nonlinear history dependent material, its behaviour is dependent on both the current stress state and its stress history. The performance of deep excavations is influenced by not only the stress relief caused by soil removal, but also by the initial stress states in the ground. Results from the above analyses indicate that lager K_0^t value results in larger wall deformation while smaller ground settlement. The pattern of the wall deflection is not sensitive to K_0^t value.

It seems that the value of K_0^t has a larger influence on the magnitude of ground settlement than that of the wall deflection. Therefore, the initial stress state in the ground should be carefully determined in the site investigation, and a reliable value of K_0^t is needed as the input parameter for the numerical analysis. In this analysis, a constant value of K_0^t is used to represent the whole soil profile for simplicity, but actually the value of K_0^t might vary with depth. This issue might be considered in the future analysis.

5.4.6 Influence of soil models

Three more analyses, as shown in Table 5.10, are conducted with different soil models to investigate their influence on the excavation behaviour.

Table 5.10 Finite element runs and description

Run Name	Description
Central analysis	Multiple yield surface model
Elastic	Linear elastic soil model, constant soil parameters
Tresca 1	Tresca soil model, constant soil parameters
Tresca 2	Tresca soil model, stiffness and strength increases with depth

Wall deflection

The wall deflections at *P*9 and *P*8 at the final stage of excavation are shown below, including both the total and relative wall deflections. It is found that both the magnitude and pattern of the wall deflection are significantly influenced by the soil model used in the analysis. The analysis with a Tresca soil model and variable soil properties could capture the pattern of wall deflections quite well both at the centre and corner, but the magnitude of wall deflections is much larger than the central analysis which might be caused by the relatively smaller soil stiffness profile in the analysis. The analyses with a linear elastic model and a Tresca soil model with constant soil properties provide a poor comparison with the field data, and therefore these two models are not recommended for use in the analysis of deep excavations. The central analysis agrees with the field data because it uses the advanced soil model to consider the small-strain stiffness nonlinearity of the soil.

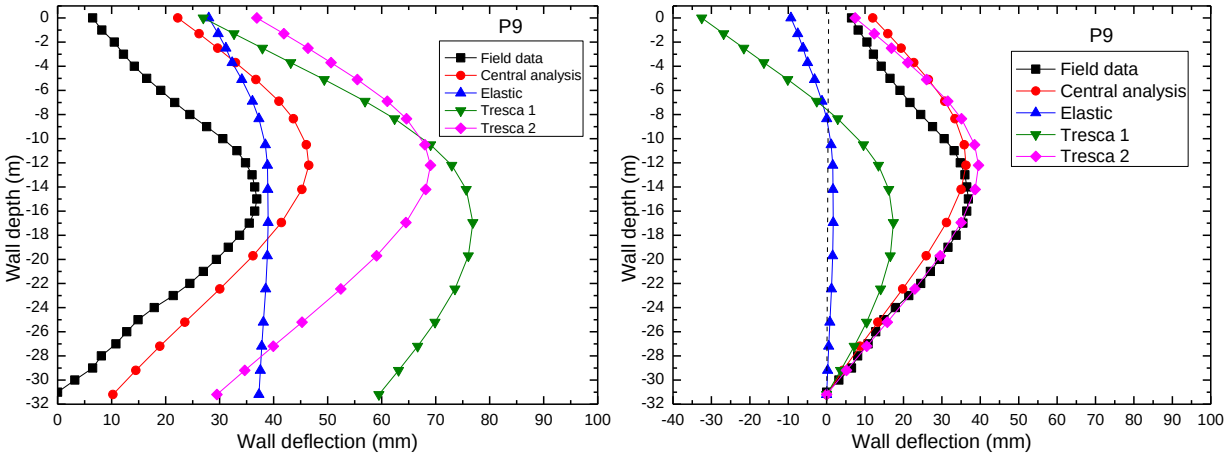

Fig.5.38 Wall deflection at P9 (a) total deflection (b) relative deflection

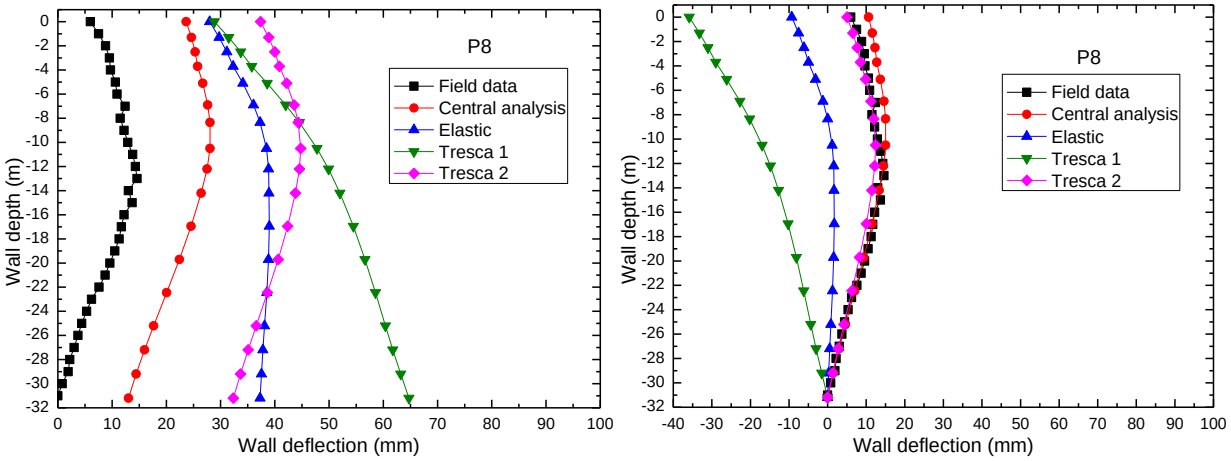

Fig.5.39 Wall deflection at P8 (a) total deflection (b) relative deflection

Wall top settlement

The wall vertical movements are shown in Fig.5.40. The central analysis agrees well with the field data. However, the other analyses with linear elastic model and two Tresca soil models provide much larger upward movement than the field data, although the analysis with Tresca soil model and variable properties performs slightly better.

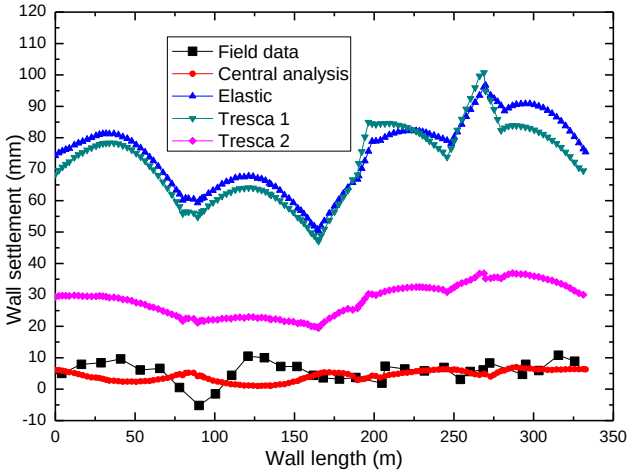

Fig.5.40 Wall vertical movement

Ground settlement

The ground settlement behind the wall along Line 1, Line 2 and Line 3 is shown in Fig.5.41. Again, the results indicate that the central analysis captures the ground movement very well. The Tresca soil model with variable properties, however, fails to reproduce the pattern and magnitude of the ground movement, in spite the fact that it provides a good representation of the pattern of the wall lateral deformation. Analyses with linear elastic model and Tresca soil model with constant properties provide very large upwards ground movement which is unrealistic compared to the settlement observed in the field measurement. Potts and Zdravkovic (2001) also showed that the nonlinear small-strain stiffness-plastic model performs much better than the linear elastic-plastic model in terms of the ground settlement behind the wall. This confirms again the importance to consider the small-strain stiffness nonlinearity of the soil in deep excavations.

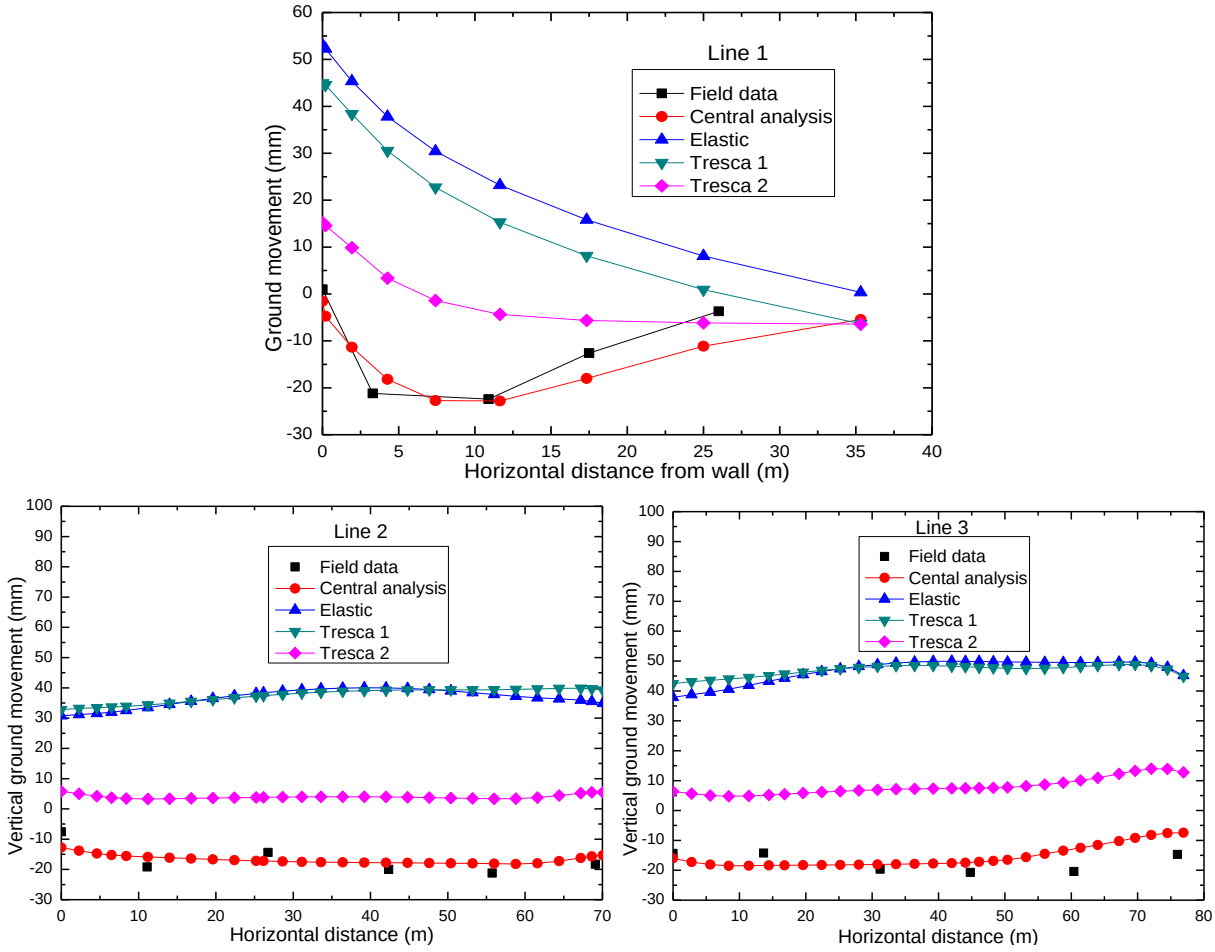

Fig.5.41 Ground movements along Line 1, Line 2 and Line 3

Basal heave

Basal heave is also a major concern in deep excavations because it reflects the stability of the

excavation. Theoretically, the soil inside the excavation will continue heaving as the excavation goes deeper due to stress relief. Xu (2007) analysed the relationship between bottom heave with excavation depth based on records of excavations in Shanghai, as shown in Fig.5.42, and correlated them using linear expressions. The minimum and mean ratio is 0.3% and 0.67% respectively. For a 12m to 14m deep top-down excavation in Shanghai, the recorded basal heave is between 50mm to 80m. When comparing the numerical results with the field record, it is found that only the central analysis produces a realistic value (around 50mm), while the analyses with the other three soil models all largely overestimate the basal heave values. This is probably because the small-strain stiffness nonlinearity of the soil plays the important part.

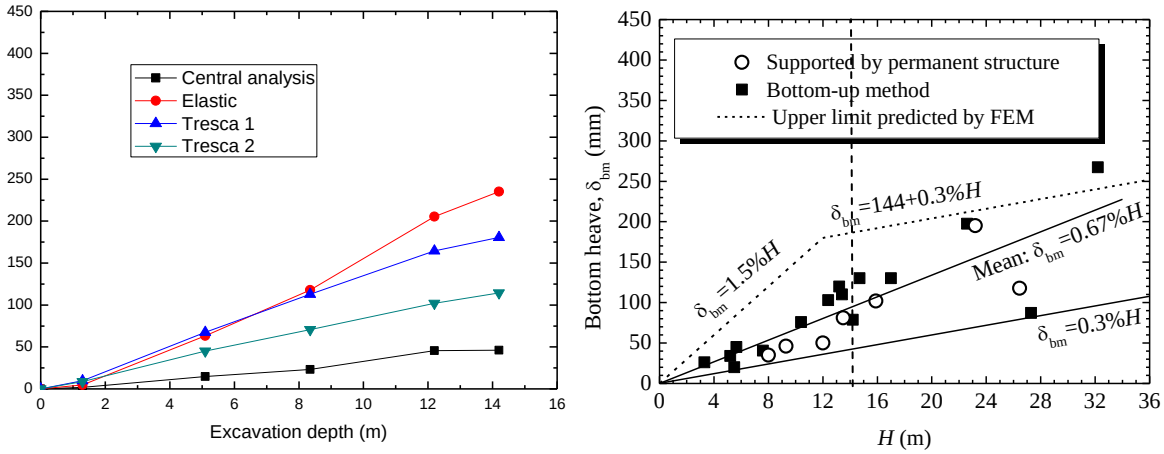

(a) Numeral results (b) Field record (Xu 2007)

Fig.5.42 Relationship between basal heave and excavation depth

Summary

The results from four different soil models clearly show that considering the small-strain stiffness nonlinearity of the soil is crucial to capture the main behaviour of deep excavations. Although the Tresca soil model with variable soil properties could reproduce the pattern of wall deflections, it fails to capture the ground movement. Linear elastic model and Tresca model with constant soil properties are not suggested to use in deep excavations.

5.5 Conclusions

This case study shows how a well-documented case history can be investigated through advanced finite element analysis. The influence of several important aspects has been

investigated through parametric studies. Some useful conclusions are generated.

1) The advanced finite element analysis captures the main behaviour of this deep excavation case history, because it considers detailed geotechnical and structural behaviours such as the irregular geometry, staged construction sequences, and realistic material models and input parameters. The numerical analysis also provides detailed information on the spatial distribution of wall deformation and ground movement. However, discrepancies also exit between numerical results and the field measurement, which may be attributed to the assumptions and simplifications made in the analyses. For example, the influence of adjacent buildings is not considered in the model, and the input parameters for the soil are derived from soil properties from greenfield condition.
2) Reliable material models and input parameters are crucial to reproduce the observed performance in the field. The soil is a nonlinear and history dependent material, and has a sophisticated stress-strain-strength relationship. For practical applications, a realistic soil constitutive model needs to consider the most important features such as small-stain stiffness nonlinearity of the soil, and have moderate level of complexity. Similarly, the model for structural components also needs to address adequately the important features of the concrete such as thermal effects and cracks. When the particular material models are chosen for the soil and structures, the input parameters need to be carefully calibrated to represent the real material behaviour. There is a deficiency in selection of soil parameters in this case study, because parameters derived from soil properties in green field condition are used to represent the site with densely distributed buildings. This may cause discrepancy between the numerical results and field measurement.
3) The small-strain stiffness nonlinearity of the soil is important to produce realistic wall deflection and ground movements in deep excavations. Although the conventional Tresca soil model with variable stiffness and strength properties can capture the pattern of wall deflection, it fails to reproduce the ground movement. Linear elastic model and Tresca

soil model with constant soil properties, although simple, are not suggested for use in deep excavation analysis.

4) Modelling the wall with shell elements tends to produce larger wall deflection and ground movement, approximately 30% in this case study, than using solid elements to model the wall. This is because the shell element wall does not have the beneficial bending moment resulting from the shear stress on the wall surface about the wall centreline, due to its zero thickness in geometry.

5) The diaphragm wall is discontinuous in the horizontal direction because it is constructed by discrete wall panels and has joints between adjacent panels, which means that the diaphragm wall cannot sustain any significant out-of-plane bending. Therefore, modelling the wall as an isotropic material is not appropriate in the analysis, and it will result in unrealistic wall deflection and bending moment at the wall corner. In the anisotropic wall approach, both the axial and bending stiffness along the length of the wall are reduced by using a smaller Young's modulus in this direction. Comparing with the isotropic wall approach, the anisotropic wall approach can greatly improve the wall deflection at the corner and replicate the observed data in the field. However, the anisotropic stiffness ratio β needs to be estimated based on experience and parametric studies, and it is found that $\beta = 0.1$ is a good value for the diaphragm wall in this case study. Attempts have also been made to model the discrete wall panels explicitly with shell elements, but results showed that the wall deflection at the wall corner is much larger than the field measurement. Then connecting the translational DOFs at the wall corner has also been tried, but this time the wall deflection at the corner is similar to the isotropic wall approach. Therefore, after comparison, it seems that the anisotropic wall approach is a suitable way to consider the construction joints in the diaphragm wall. However, an appropriate anisotropic ratio β needs to be carefully determined for different types of retaining walls.

6) The thermal effects of concrete beams and floor slabs due to curing of concrete and variation of ambient temperature have a large influence on the performance of deep excavations, and these effects can be considered in the numerical analysis straightforwardly. Thermal shrinkage of the beams and slabs will pull the diaphragm wall towards the excavation and increase the wall deformation and ground movement, 3mm by 5℃ in this case study. In addition, various other effects which may cause larger wall deflections (e.g. gaps between diaphragm wall and floor slabs, cracks and creep of concrete, workmanship), can also be included in the thermal shrinkage approach. The amount of the thermal shrinkage is controlled by the temperature change which can be selected based on the parametric studies and comparison with the field data.

7) As the soil is a nonlinear and stress history dependent material, its behaviour is dependent both on the current stress states and the stress history. The performance of deep excavations is influenced by not only the stress relief caused by soil removal, but also by the initial stress states in the ground. Three values of K_0^t (0.77, 0.88, and 1.0) are used in the parametric study, and the results indicate that lager K_0^t value results in larger wall deformation while smaller ground settlement. However, the pattern of the wall deflection is not sensitive to K_0^t value. It also shows that the value of K_0^t has a larger influence on the magnitude of ground settlement than that of wall deflection. Therefore, the initial stress state in the ground should be carefully determined in the site investigation, and a reliable value of K_0^t is needed as the input parameter for the numerical analysis.

8) Assuming zero displacement at the wall toe in the field measurement is not correct, and it causes problems to the back analysis of these case histories through numerical analysis because the exact wall deflections are not known. It is advised in the future field measurement to correct this error by measuring the horizontal movement at the wall top at the same time of the inclinometer reading.

Chapter 6 Deformation of adjacent infrastructure induced by deep excavations

6.1 Introduction

Chapter 5 investigated the excavation behaviour in the absence of adjacent infrastructure, e.g. buildings and buried service pipelines. This chapter will focus on the settlement of adjacent buildings and buried pipelines, induced by deep excavations, based on the additional case study of the basement excavation for the Shanghai Xingye Bank building.

As discussed in Chapter 2, the interaction between buildings and deep excavations is particularly complicated, and depends on a number of factors, e.g. the soil and structure properties, building type and configuration, the foundation of buildings, the distance and relative position of buildings to the excavation, and the excavation activities. Adjacent buildings might undergo additional settlement, which might exceed the greenfield settlement due to self-weight and decreased stiffness of the structure and foundation (Jeong Woo, Oon Young et al. 2001). The buried pipelines close to the excavation would deform with the ground movement, and the deformation may be affected by factors such as the amount of ground movement, the soil properties, the geometry and material properties of the pipeline, the distance of the pipeline to the excavation, and the buried depth of the pipeline.

Ground improvement might be used during the basement excavation to treat the soft clay and improve its stiffness and strength characteristics, in order to protect structures from potential damage (Wong and Poh 2000), but it also increases the cost of the project. Therefore, analyses have been made exploring the effectiveness of ground improvement (e.g. root piles and jet grouting piles) around the excavation to mitigate the damage to adjacent buildings.

The finite element model in this chapter is modified based on the central analysis in Chapter 5, and further includes adjacent buildings, buried pipelines, and the ground improvement. The

purpose of the work in this chapter is to (i) demonstrate the appropriate way to incorporate adjacent infrastructure into the previous 3D finite element model in greenfield conditions, (ii) understand the influence of several factors on this complex soil-structure interaction problem, and (iii) find out what are the governing parameters on the settlement of buildings and pipelines.

6.2 Information on adjacent infrastructure

There are 15 main buildings, as shown in Fig.6.1, adjacent to the basement excavation of Shanghai Xingye Bank building, 8 of which are historic buildings under the protection of Shanghai Municipal Council. The ECADI (East China Architecture Design Institute) building, CB (Communication Bank) building, and SJB (San Jing Bank) building were major concerns to engineers, and they were carefully monitored during the construction. To mitigate the damage to adjacent buildings caused by the excessive excavation-induced ground movement, ground improvement (e.g. root piles and jet grouting piles) were undertaken along the West and South sides of the excavation. In addition, there are several buried pipelines distributed on the West and North sides of the excavation.

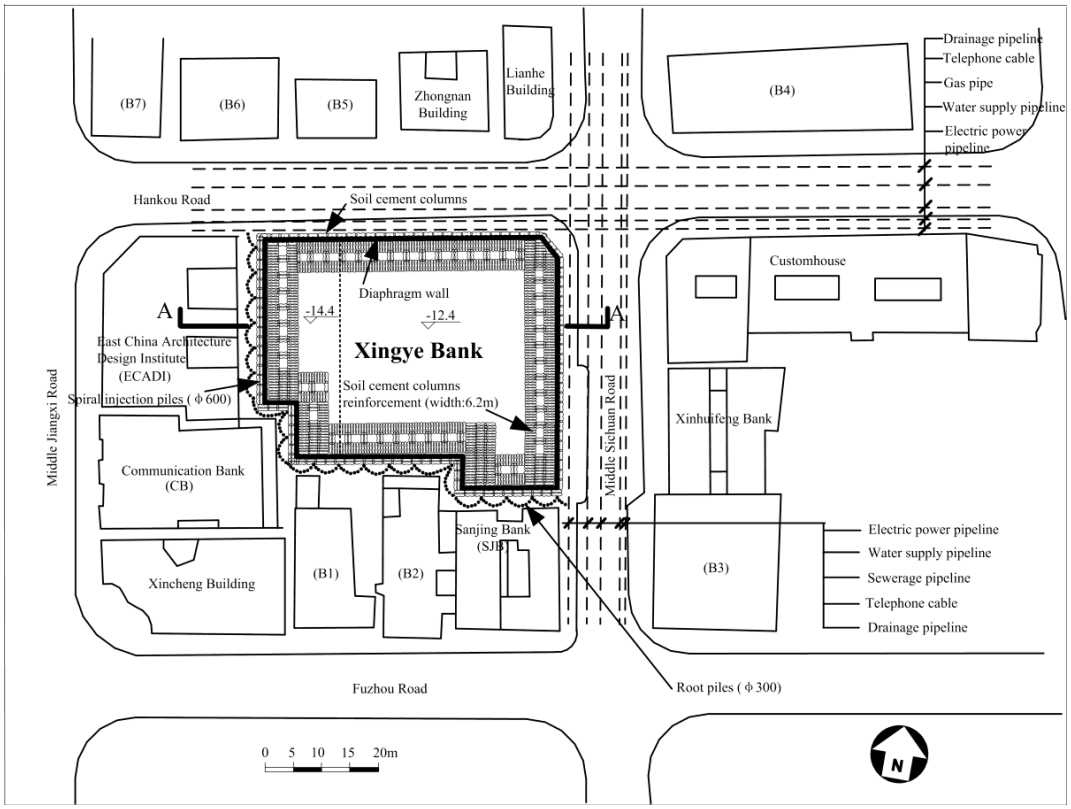

Fig.6.1 Plane view of adjacent infrastructure (Xu 2007)

The settlement of the buildings was measured along the outline of external facades, whereas the settlement of the buried pipelines was represented by measuring the ground surface settlement above the pipelines. The layout of the instrumentation is illustrated in Fig.6.2. The data were initially collected and analysed by Xu (2007), and more complete data is shown in Appendix B.

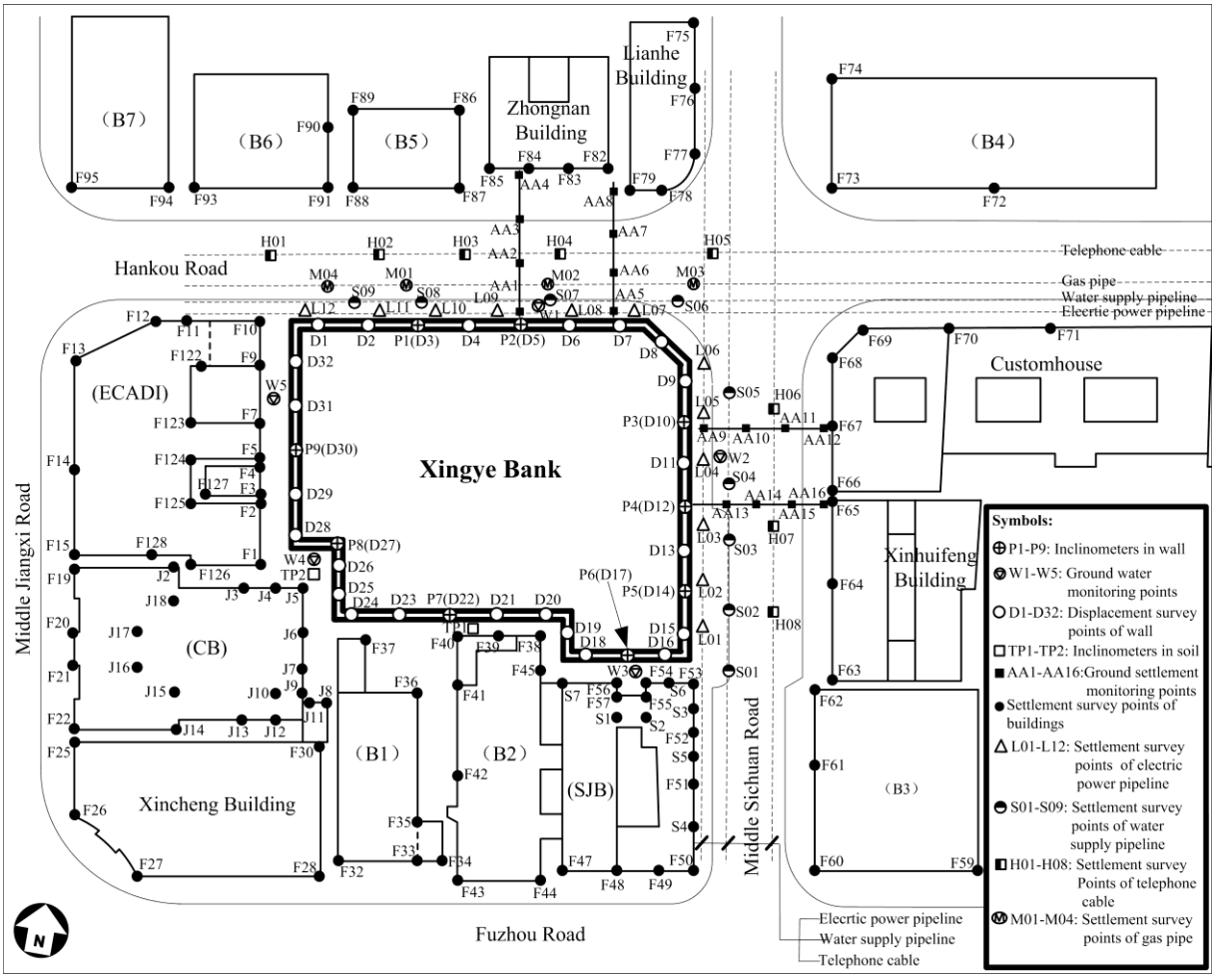

Fig.6.2 Layout of the field instrumentation (Xu 2007)

6.2.1 Information on buildings

ECADI building

The ECADI (East China Architecture and Design Institute) building is situated on the west side of the excavation, about 4.8m from the diaphragm wall. It was originally built in 1949, refurbished twice afterwards, and was completely redecorated in 2000. The visible cracks in the building were repaired, and structural components with reduced bearing capacities were reinforced. The main building has an 8-story reinforced concrete frame structure which is 37.2m high, supported on a reinforced concrete box foundation with timber piles. The facades and internal walls are filled with red bricks. Detailed information about the foundation such as the

structure, the geometry, and the depth, are not known. The stiffness and strength of the timber piles might be reduced due to the deterioration of wood with time. No obvious cracks or damage were observed in the building during and after the excavation.

Fig.6.3 East China Architecture Design Institute (ECADI)

According to the field measurements in Fig.6.4, substantial building settlement occurred during the construction of the diaphragm wall and piles, as well as during the dewatering process prior to the excavation. This pre-excavation settlement (around 10mm) accounts for around 1/3 of the total settlement accumulated in the whole construction period (around 30mm). The building settlement was slightly recovered during the soil removal stage, probably due to the soil swelling caused by the stress relief. On the other hand, the settlement increased during the casting of concrete beams and floor slabs, probably due to the consolidation of soil, and shrinkage and creep of concrete structures. The settlement was slightly stabilised when the basement excavation was completed, with the largest settlement of 27.2mm at point F5.

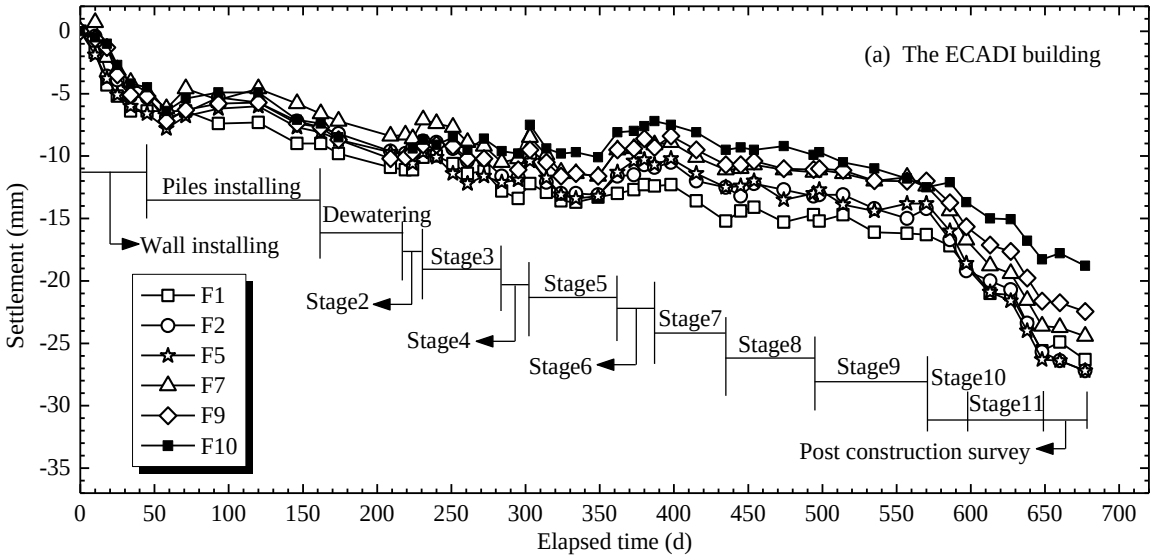

Fig.6.4 Settlement of the ECADI building during excavation (Xu 2007)

CB building

The CB (Communication Bank) building is situated on the South West side of the excavation, with the shortest distance 4.8m to the diaphragm wall. It was built in 1927, and was refurbished afterwards. It has 4 stories as originally designed, and another 3 stories were added on the top in 1940s and 1950s. The current height of the building is 25.9m. The building has a reinforced concrete frame structure which is founded on a slab-and-beam type raft foundation with timber piles (approximately 3.66m to 7.32m deep). The building settled slightly unevenly but is generally stable. Some cracks were observed in the main structure and floor slabs, but overall the building was operating in good conditions before the excavation.

Fig.6.5 Communication Bank Building (CB building)

The settlement at several points on the façades of the building is shown in Fig.6.6. Unfortunately, the building settlement was only recorded from stage 5, and the data before stage 5 was missing.

The pattern of settlement is similar to that of ECADI building. The settlement was slightly recovered during the soil removal, and increased during the installation of structural beams and floor slabs. The largest amount of settlement at the end of excavation is 29.4mm at J5.

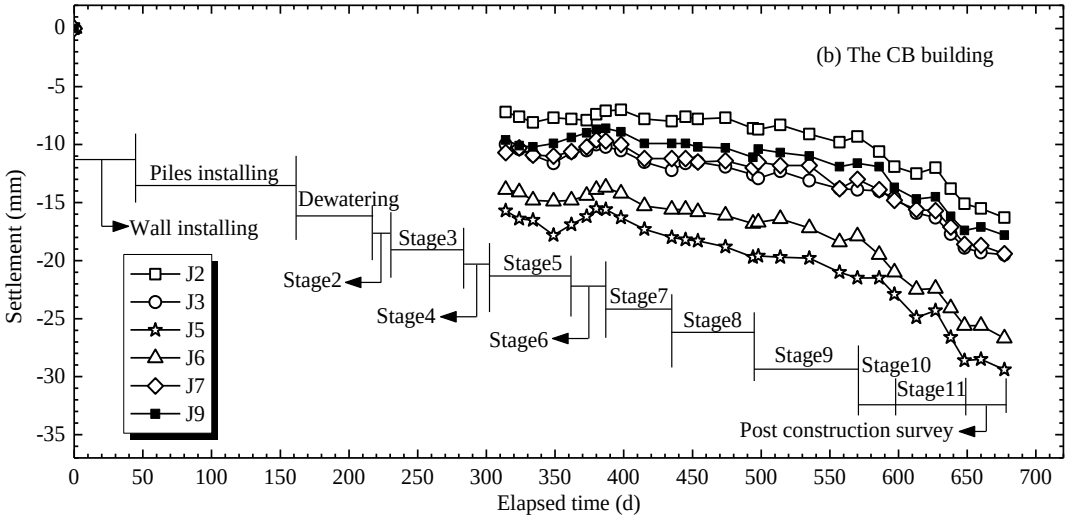

Fig.6.6 Settlement CB building during excavation (Xu 2007)

SJB building

The SJB (Sanjing Bank, now used as China Construction Bank) building is situated on the South side of the excavation, with the shortest distance of 4.0m to the diaphragm wall. It was built in 1934, designed by a British company. It has a 5-storey brick and wood structure (around 20m high), founded on a strip footing. Little information is available about the foundation. The building inclined slightly towards East and North, but the settlement was stable before the excavation. No obvious cracks were observed in the main structure, and the building was generally in good condition before the excavation.

Fig.6.7 Sanjing Bank building (SJB building)

The building was monitored continuously throughout the excavation, with the data shown in Fig.6.8. The pattern of settlement is similar to that of the ECADI building, with the largest settlement 33.4mm at point F56. The total settlement of SJB building is slightly larger than the ECADI building, but it seems that more settlement occurred during the wall and pile installation, as well as during the dewatering process. The differential settlement of SJB building is larger than that of the ECADI building, because the brick-wood structure of SJB building is more flexible than the reinforced concrete structure of ECADI building.

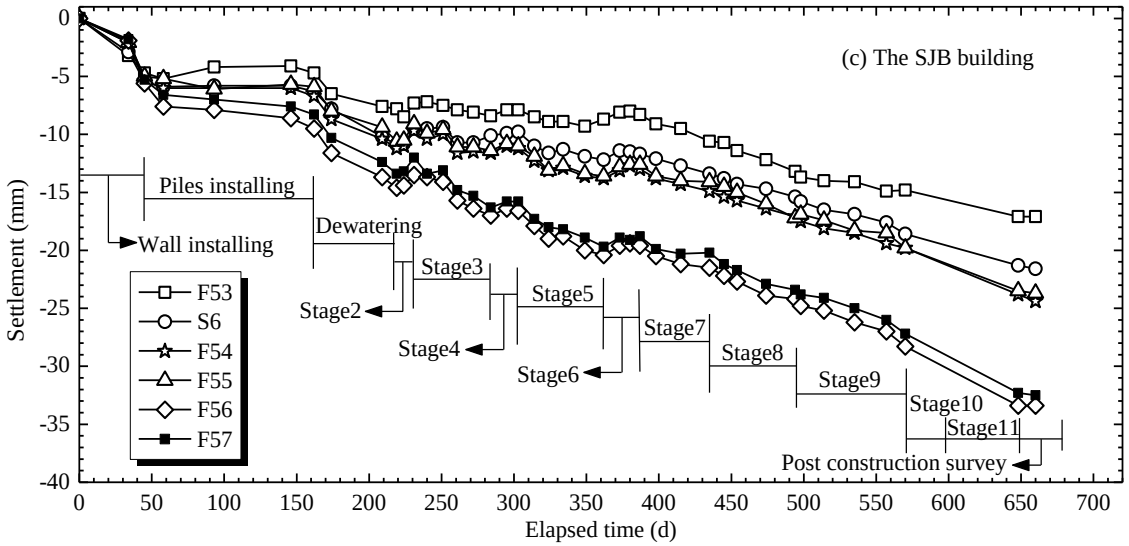

Fig.6.8 Settlement of SJB building during excavation (Xu 2007)

6.2.2 Ground improvement

In order to mitigate the influence of excavation to the adjacent buildings, a line of jet grouting piles and root piles were constructed on the west and south sides outside the excavation. The root piles are 300mm in diameter and 18m deep, with an interval of 1400mm. The jet grouting piles are 600mm in diameter and 18m deep, with an overlap of 100mm. The uniaxial compressive strength of single pile is over 3MPa. Deep mixing piles were also conducted inside the excavation beside the diaphragm wall, intended to constrain the inward wall movement. The treated area is around 6m wide from the edge of the diaphragm wall, and about 5m deep below the final formation level.

6.2.3 Buried Pipelines

There are several buried pipelines (e.g. water supply pipelines, sewage pipelines, drainage

pipelines, gas pipelines, and electrical power pipelines) outside the excavation on the East and North side close to the diaphragm wall (with distance varying from 2.6m to 15m). The buried pipelines might get damaged by excessive ground movements induced by the excavation, which would cause trouble to the municipal services. Therefore, these pipelines were monitored during the excavation process by measuring the ground surface settlement above the pipelines to reflect their movements. The detailed structural behaviour of the pipelines, e.g. the internal stress and strain, structural failure, and buckling, is not the focus of this study. Two electrical power pipelines, L01-L06 and L07-L12, on the two sides of the excavation, are included in the model and analysed in this chapter, because they are the only two pipelines with field data presented in Xu (2007).

Pipeline L01~L06 and L07 ~ L12

Pipeline L01-L06 has a diameter of around 500mm, wall thickness of 20mm, buried depth of 1.3m, and horizontal distance of 4m to the diaphragm wall. Pipeline L07-L12 has similar properties with pipeline L01~L06. The material of these pipelines is concrete. The wall thickness of the pipeline might be thinner because of corrosion. The settlement of these two pipelines during the construction stages is shown in Fig. 6.9. Similar to the settlement of adjacent buildings, significant settlement was observed during the installation of wall and piles, as well as the dewatering process. The settlement increases as the excavation proceeds, and the corner effect is obvious. The largest settlement is approximately 30mm, close to the centre of the wall.

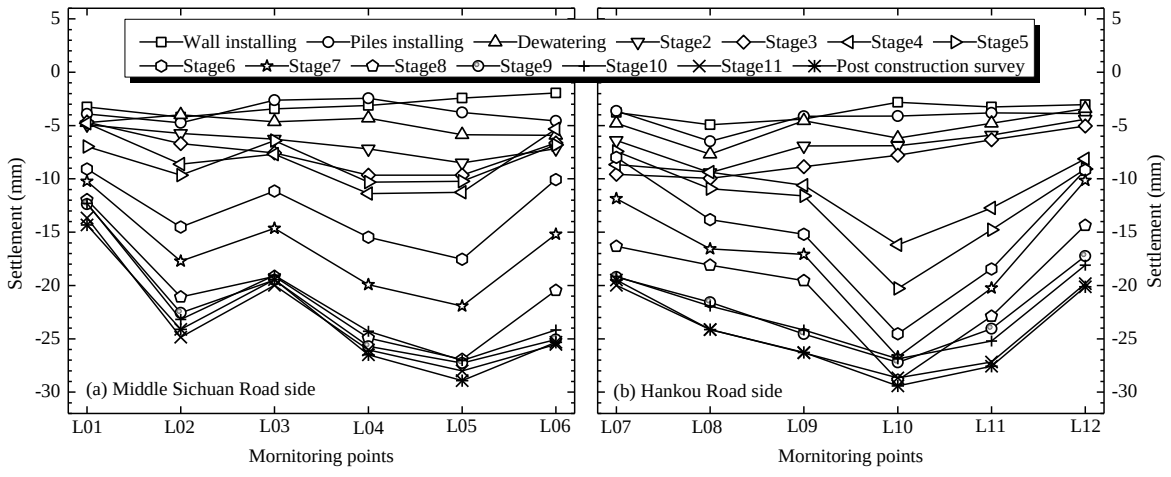

Fig. 6.9 Settlement of electrical power pipelines at different stages (Xu 2007)

6.3 Description of the finite element model

The mesh of the whole finite element model is shown in Fig.6.10. This model is based on the model in the central analysis of Chapter 5, but new features are included, e.g. buildings with foundations, the ground improvement between the diaphragm wall and buildings, and buried pipelines. Some necessary simplifications and assumptions are made in the model. For instance, the detailed geometry of the buried pipelines in the ground such as the shape is not modeled, and they are represented by beam elements; the internal structures and foundations of buildings are assumed according to the documented description, and openings in the walls and floor slabs are not included; the ground improvement is simplified as a layer of continuous shell elements. These simplifications and assumptions might affect the accuracy of the analysis, but they will not affect the genenal conclusions. This case study is intended to show an example of such kind of complex soil-structure interaction problem, understand the response of adjacent buildings and buried pipelines induced by deep excavations, and investigate the influence of several key factors.

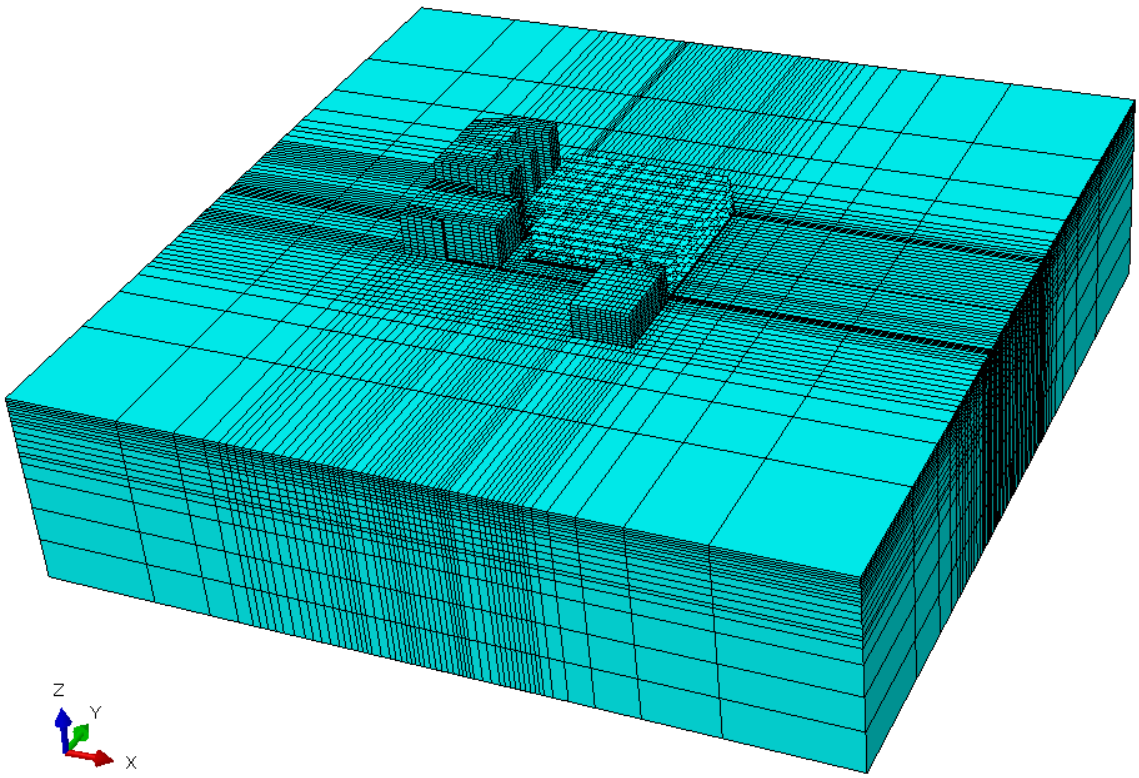

Fig.6.10 Mesh of the whole finite element model

6.3.1 Mesh of the buildings

As shown in Fig.6.11, only the ECADI building, CB building, and SJB building are included in the model. The external and internal walls, as well as the floor slabs, are modelled with linear quadrilateral shell elements with reduced integration (S4R). The bottom of the building is embedded into the foundation. The thickness of external wall, internal wall, and roof is assumed to be 0.3m, 0.2m, 0.15m respectively for simplicity. The beams, columns, and openings in the wall are not modelled. The buildings are assumed to behave linear elastically because no obvious cracks or damage were observed in the buildings during and after the excavation. The material of the buildings is assumed as concrete, but unit weight and stiffness properties are reduced considering the openings and cracks in the concrete structures. Parametric studies are conducted to investigate the influence of building weight and stiffness on the building deformation.

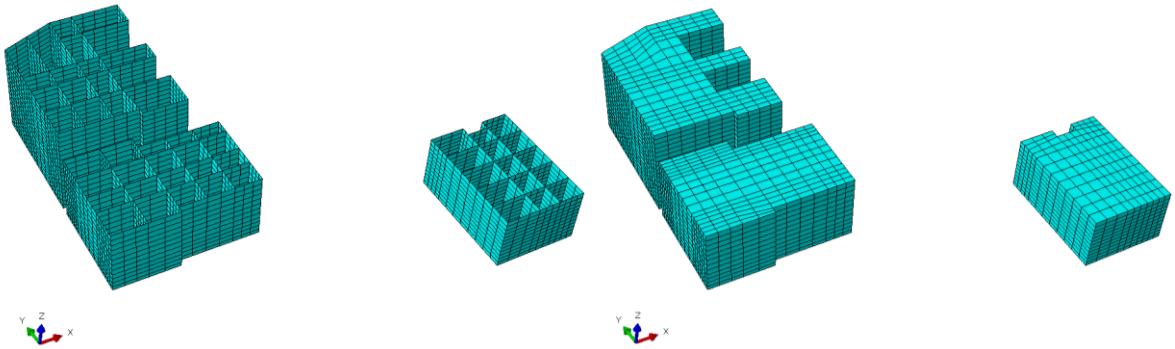

(a) External and internal structures (b) Buildings with floor slabs and roofs

Fig.6.11 Mesh of the buildings

6.3.2 Foundations of the buildings

The foundations of buildings are simplified in the model due to the limited known information about the foundation of these historical buildings. In this case study, piled raft foundations are assumed for ECADI building and CB building, while the SJB building is assumed to have the raft foundation, as shown in Fig.6.12. The raft is 1.3m thick and is extended to 0.5m beyond the external walls in plane. The piles are 0.3m in diameter, and 6.9m deep below the ground surface. The layout of the piles is also assumed. The raft and piles are modelled with solid elements (C3D8R) and 3D linear beam elements (B31) respectively. The external and internal walls are embedded into the raft foundation, and the piles are tied with the raft and embedded into the soil.

The raft and piles are represented by concrete and wood materials respectively. Parametric studies are conducted to investigate the influence of stiffness properties of raft foundations and the effectiveness of piles on the building settlement.

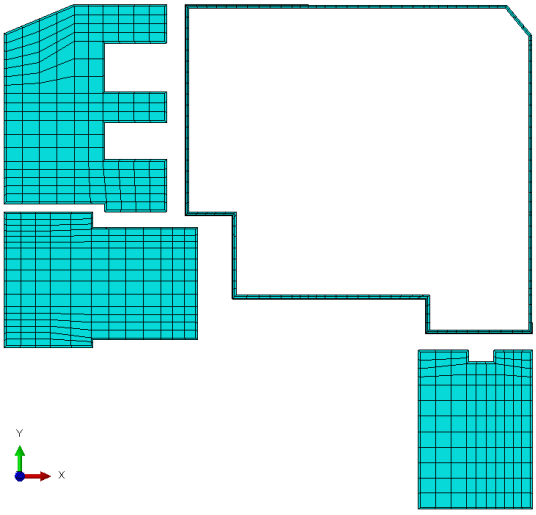

(a) Plan view

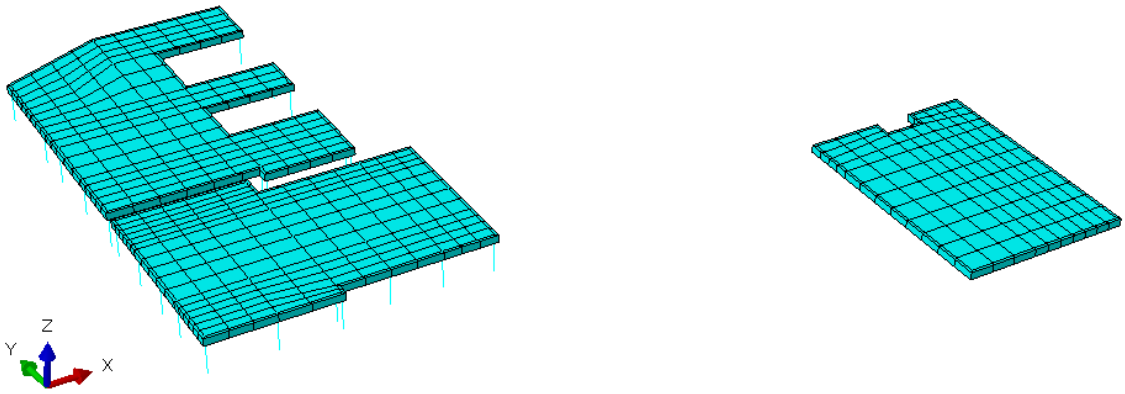

(b) Oblique view

Fig.6.12 Mesh and position of the foundations

6.3.3 Ground improvement

The root piles and jet grouting piles outside the excavation, as shown in Fig.6.13, are approximated using a layer of continuous shell elements (S4R) which are 0.3mm thick and 18m deep. The distance to the diaphragm wall is 2m. In a similar way to the diaphragm wall, the ground improvement is represented by an anisotropic linear elastic material, to account for the discontinuities between adjacent piles. As the properties of the soil-cement mixture are not easy to determine, parametric studies are conducted to investigate the influence of the thickness, stiffness, and anisotropic properties of the ground improvement on the building settlement. The deep mixing piles inside the excavation were neglected in the modelling process due to the

complexity, but it might be worth considering them in the future analysis.

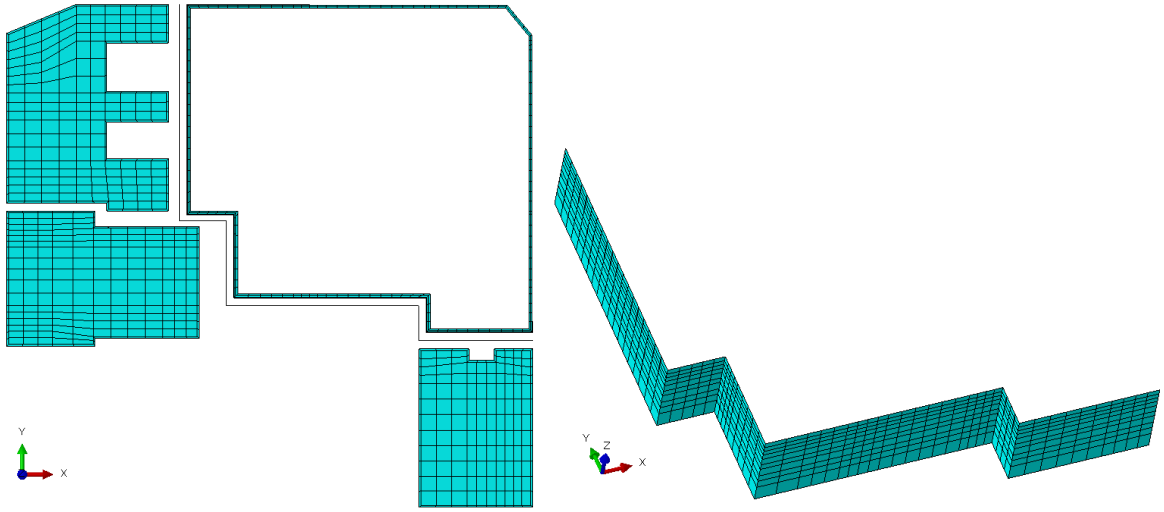

Fig.6.13 Position and mesh of the ground improvement

6.3.4 The buried pipelines

The buried pipelines, as shown in Fig.6.14, are modelled with 3D linear beam elements (B31), so the detailed geometry in the ground is not accounted for. They are embedded 1.3m below the ground surface and 4m to the diaphragm wall. The length extends to the boundaries of the model. The diameter is 500mm, with the wall thickness 20mm. The pipelines are assumed to behave linear elastically for simplicity, due to the relatively small displacement. Parametric studies are conducted to investigate the influence of the diameter, wall thickness, and stiffness parameters on the settlement of pipelines

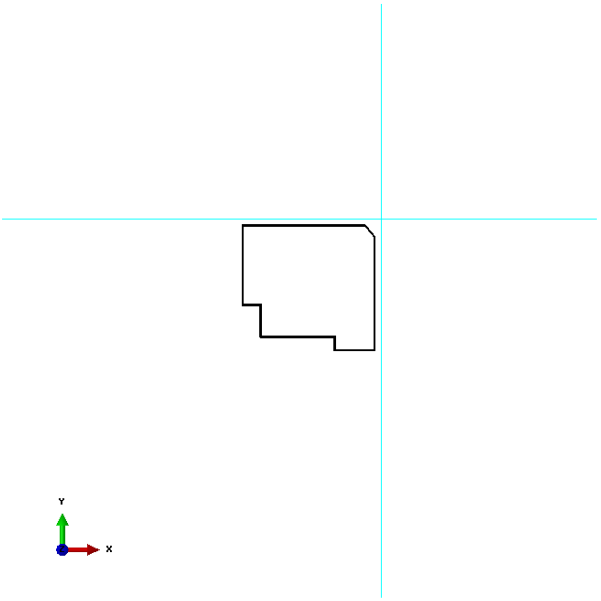

Fig.6.14 Mesh of the pipelines

6.4 Strategies of the analyses

A strategy is made to organise the analyses and to present the results in a systematic way. The analyses focus on the settlement of buildings and buried pipelines induced by the excavation. The central analysis inherits all the parameters from the central analysis in Chapter 5, and adopts new input parameters for the buildings, foundations, ground improvement, and pipelines based on empirical estimations. The value of each of these estimated parameters is then varied individually to investigate its influence on the computed results.

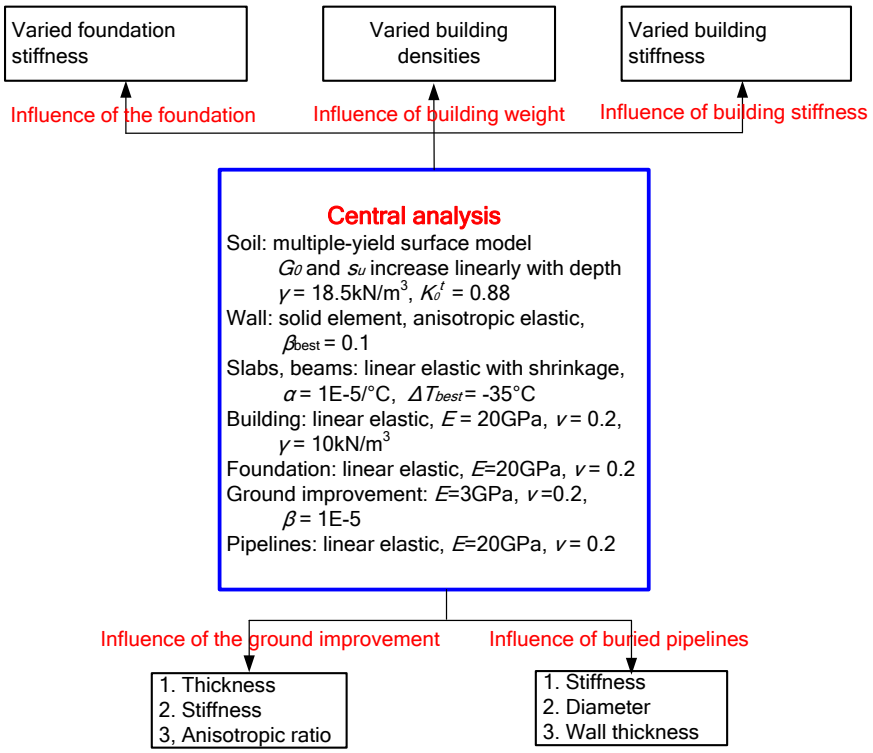

Fig.6.15 Strategy of the analyses

Based on previous experience, the aspects investigated in this chapter include

i) The influence of building stiffness on the building settlement;

ii) The influence of building weight on the building settlement;

iii) The influence of foundation stiffness on the building settlement;

iv) The influence of the properties of the ground improvement (e.g. thickness, stiffness, and anisotropic ratio) on the building settlement;

v) The influence of the properties of pipeline (e.g. diameter, stiffness, wall thickness, element type) on the settlement of buried pipelines.

6.5 Interpretation of the results

6.5.1 Central analysis

Building settlement

The computed building settlements along the building outlines at the final stage of the excavation are compared with the field measurement in the figures below. Please note that the building settlement caused by the installation of the diaphragm wall and bored piles, and the dewatering process, is subtracted from the total settlement, to account for the effect of excavation only.

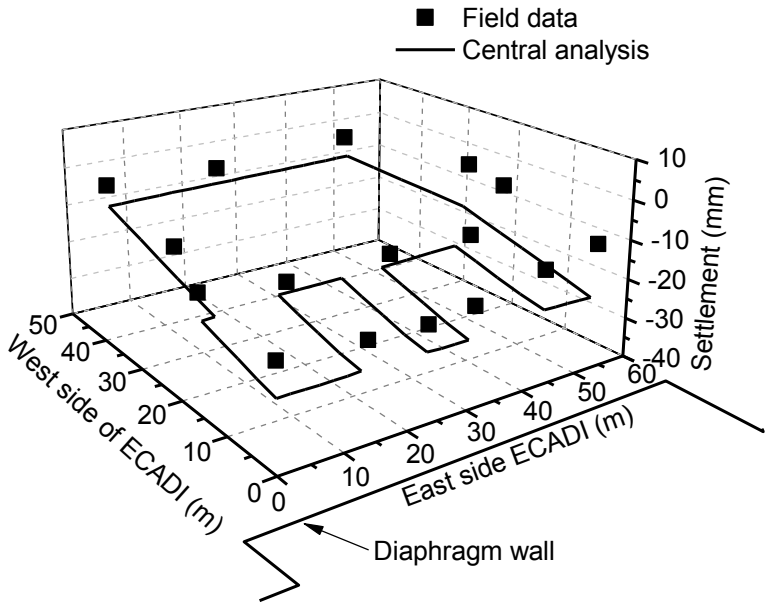

Fig.6.16 Building settlement (ECADI building)

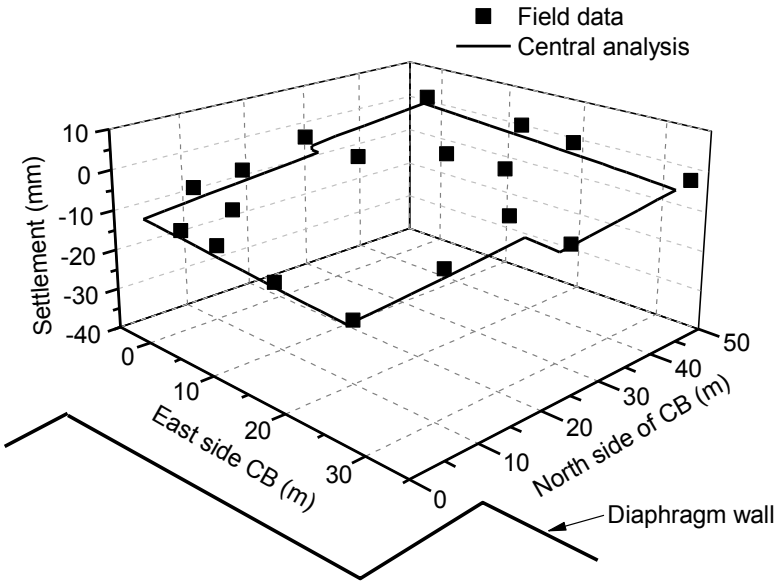

Fig.6.17 Building settlement (CB building)

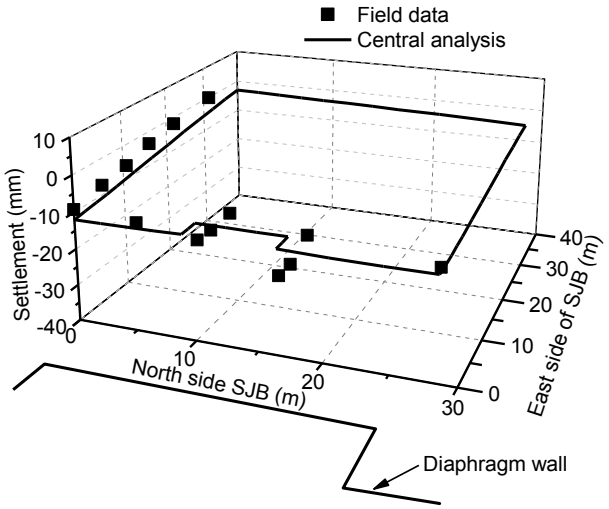

Fig.6.18 Building settlement (SJB building)

The results indicate that all three buildings deform in a rigid manner and tilt towards the excavation, probably due to the high stiffness of the buildings and foundations used in the analysis. The computed settlements generally agree well with, but are slightly larger than, the field measurement, especially the ECADI building. The discrepancy might be attributed to a number of factors, e.g. the soil properties, the structural details and properties, the type of the foundations, and the construction activities. For example, the internal structures and foundations of these buildings are assumed, and the stiffness and weight of the buildings are estimated. In addition, as mentioned in Chapter 5, the soil parameters used in this case study are derived from soil properties in greenfield conditions, but actually the stiffness and strength of soil underneath buildings might be higher than those in the greenfield site. This is one deficiency of the analysis and also one important reason why the computed building settlements are larger than the field measurements. It is difficult to consider all these aspects appropriately in the numerical modelling due to limitations of computational capabilities and uncertainties in determining material properties. This case study does not aim to match precisely the numerical results with the field data, but to understand the influence of these factors through parametric studies.

Pipeline settlement

The computed settlements of buried pipelines from the final stage of the excavation, are compared with the field measurement in Fig.6.19. Similarly, the settlement during the installation of diaphragm wall and bored piles, and the dewatering process, is subtracted from the

total settlement, to account for the effect of excavation only. The ground surface settlements above the buried pipelines are also shown in the figure, because they are commonly used to represent the settlements of the buried pipelines in the field measurement.

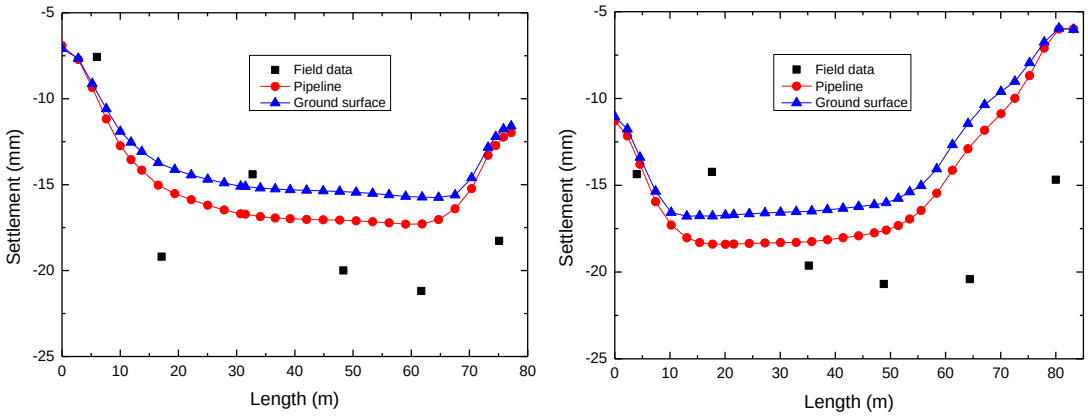

Fig.6.19 Settlement of (a) pipeline 1 (L01 – L06) and (b) pipeline 2 (L07 – L12)

It can be seen that the calculated settlements of two pipelines agree well with the field measurement in pattern, but are slightly smaller in magnitude. It is also found that the ground surface settlements over the pipelines are slightly smaller than the pipeline settlements, but with a similar pattern. This small difference in settlement is probably caused by the swelling of the soil in the retained area of the excavation. If the small difference is neglected, the results suggest that it is reasonable in the practice to use the ground surface settlement to represent the settlement of buried pipelines, and in the numerical analysis the pipelines might not be necessary to include in the model. The influence of several key parameters on the settlement of pipelines will be presented later in this chapter.

Contour display

The displacement contours at the final stage of the excavation are shown in the following figures, in which the distribution of the displacement of buildings and the soil is clearly illustrated.

The vertical displacement of the whole model is shown in Fig.6.20. As can be seen, the soil inside the excavation moves upwards due to the stress relief caused by the soil removal, while the soil outside the excavation settles down, and the settlement is larger behind the wall centre but smaller around the wall corner, indicating the 3D effect or corner effect. The adjacent buildings settle with the ground, and the settlement is larger close to the diaphragm wall and

becomes smaller far away from the excavation, which means the building inclines towards the excavation. It also shows that the ECADI building settles more than the other two buildings.

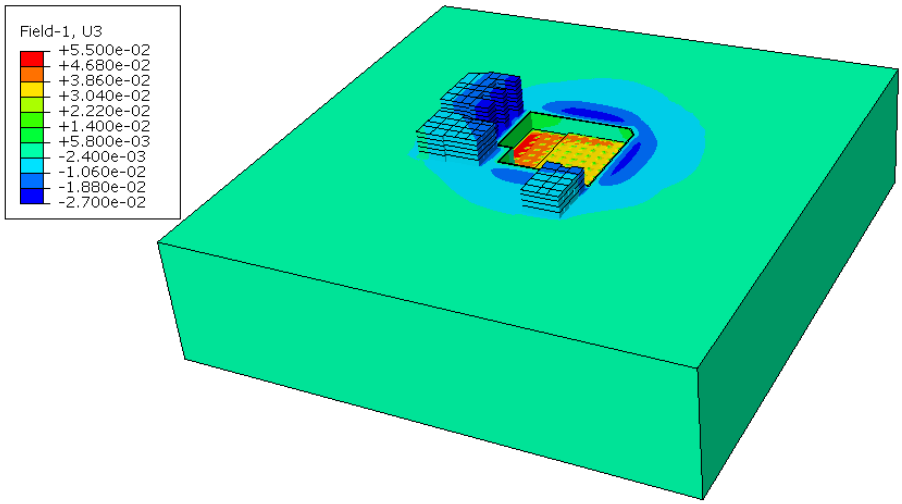

Fig.6.20 Vertical displacement of whole model (unit:m)

It is seen from the plan view of the vertical ground movement in Fig.6.21 that the ground settlements outside the excavation are concentrated in the small areas behind the diaphragm wall and vanish far away from the edge of the excavation. The settlement is smaller around the wall corner due to the corner effect. When comparing the ground settlement patterns in the areas with and without buildings, it is found that the ground movement is modified due to the existence of buildings. The basal heave of the soil inside the exaction is larger at the left side because the excavation is deeper in this side, and is larger close to the diaphragm wall probably due to the inward movement of the wall.

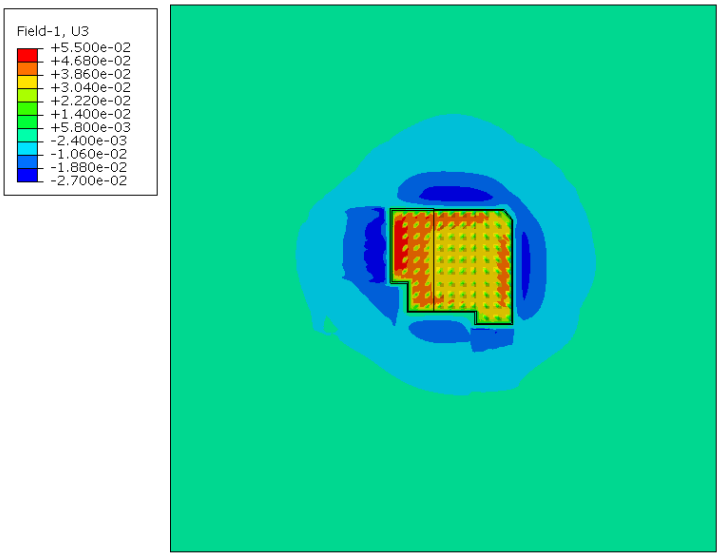

Fig.6.21 Vertical ground movements (unit:m)

The settlement of building and foundation is shown in Fig.6.22 in more detail. It is seen that all buildings settle, and the closer to the excavation the larger is the settlement. The ECADI building settles more than the other two buildings because it is larger in volume and weight, also because it is situated in the area where the largest ground movement might happen.

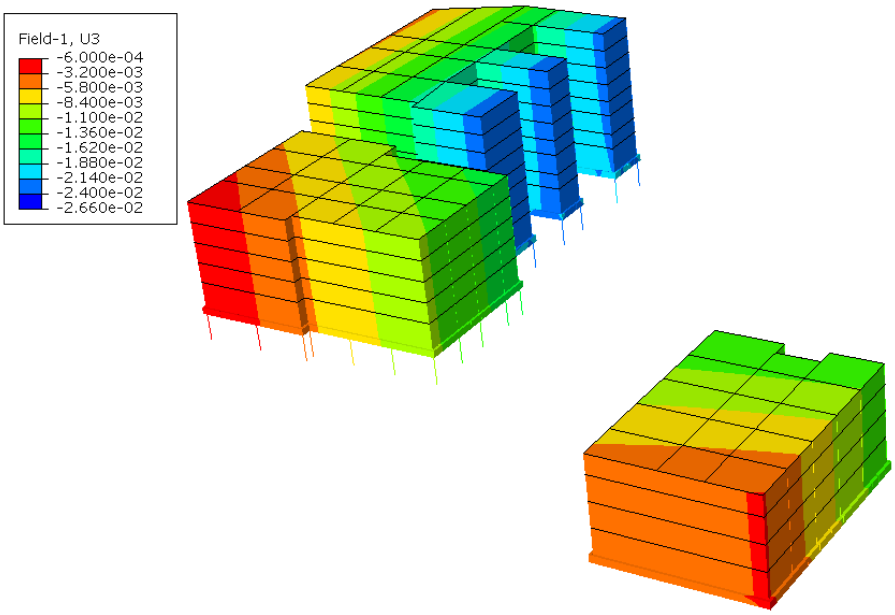

(a) Building settlement

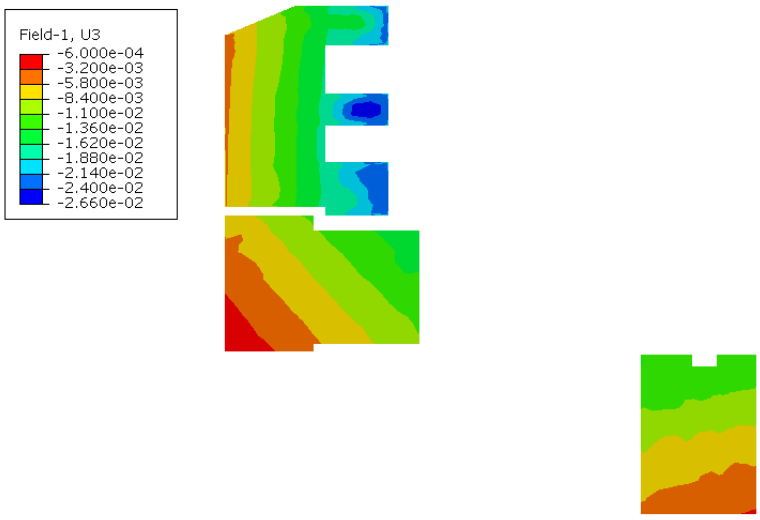

(b) Foundation settlement

Fig.6.22 Building and foundation settlement (unit:m)

The deformation of the ground improvement is shown in Fig.6.23. The ground improvement deforms with the ground and the pattern is similar to the diaphragm wall deformation shown in Chapter 5. The deformation is larger behind the centre of the diaphragm wall at the final excavation formation level, and smaller at the corner.

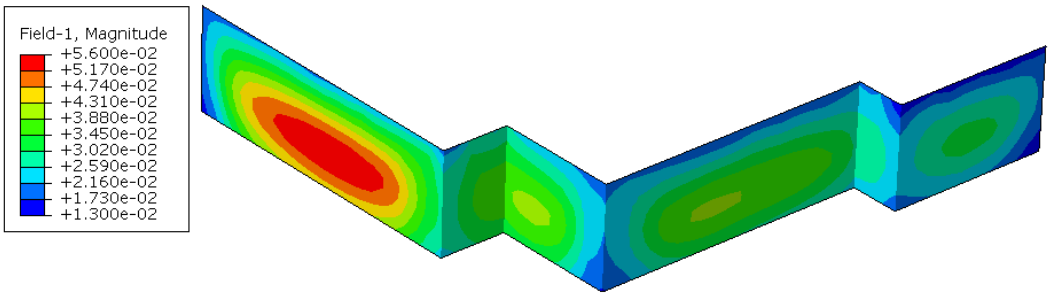

Fig.6.23 Deformation of the ground improvement (unit:m)

The vertical displacement of the buried pipelines is shown in Fig.6.24. It can be seen that the settlement is mainly concentrated in the region behind the excavation, which confirms that the excavation has a large impact on the adjacent buried pipelines.

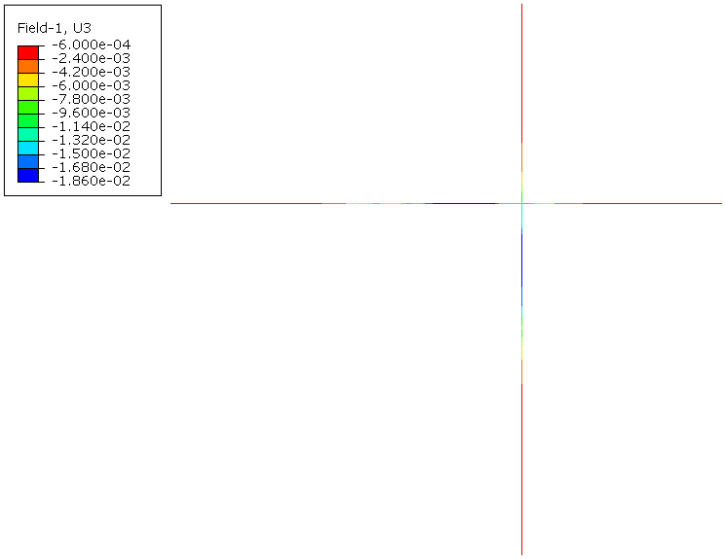

Fig.6.24 Settlement of the buried pipeline (unit:m)

6.5.2 Influence of the building stiffness

The operational stiffness of the building is uncertain and depends on the type and material properties of the structure. In the numerical modelling, details of the structure, e.g. internal walls, beams and columns, window and door openings, need to be simplified and this might affect the overall stiffness of the building. For instance, the walls and roofs are modelled with shell elements, while beams, columns, and openings are not included in the finite element model. It is important, therefore, to estimate the building stiffness and investigate its influence on the computed results through a series of parametric studies. For simplicity, the building is represented by a linear elastic material model. A realistic nonlinear material model seems more reasonable for the building, e.g. the concrete damaged plasticity model in ABAQUS, and the

nonlinear masonry model used in Burd, Houlsby et al. (2000), but this will significantly complicate the analyses due to the introduction of more undetermined variables. Results from analyses with three possible stiffness values, as shown in Table 6.1, are presented in this section. In case 1 (central analysis), E=20GPa is used to represent the reduced stiffness of the structure due to imperfections in the concrete and openings in the wall. The value of E=30GPa used in case 2 represents the intact concrete structures, and might be the largest stiffness of the structure. However, E=1GPa in case 3 is an incredibly small value for reinforced concrete structures, and might be the worst case.

Table 6.1 Influence of the building stiffness

Case No.	Building Stiffness
1 (central analysis)	E=20GPa
2	E=30GPa
3	E=1GPa

As shown in Fig.6.25, the building settlements are almost identical for a Young's modulus of 30Gpa and 20GPa, while the building deforms more flexibly when the Young's modulus is reduced to 1GPa. As the operational stiffness of the building is likely to lie between 30Gpa and 1GPa, the settlement pattern may vary from stiff to flexible, but it seems that the variation in magnitude is not too significant.

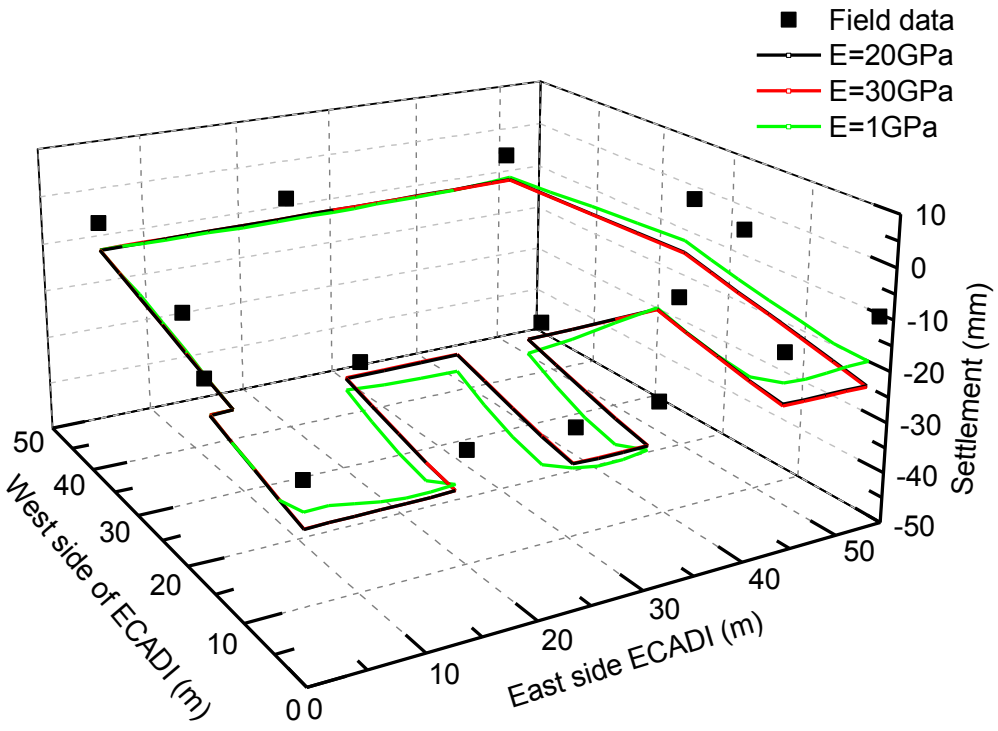

Fig.6.25 Building settlement (ECADI building)

6.5.3 Influence of the building weight

The building weight also needs to be estimated due to a number of uncertainties and simplifications in the numerical model. In addition, the load distribution and transmission mechanism is unclear due to the complex structure of the building. The building weight is largely dominated by the self-weight which is controlled by the density and volume of the material, but in the analysis only the density is varied for simplicity. Results from analyses with three different building densities, as shown in Table 6.2, are presented in this section to investigate the influence of building weight on the computed building settlement.

Table 6.2 Influence of the building weight

Case No.	Self-weight
1 (central analysis)	$\gamma = 1000\text{kg/m}^3$
2	$\gamma = 2500\text{kg/m}^3$
3	$\gamma = 0\text{kg/m}^3$

The results in Fig.6.27 indicate that the building settlement is sensitive to the weight of the building, and larger building weight results in larger building settlement. This suggests that the building weight needs to be estimated more accurately for the analysis. However, even the weightless building leads to slightly larger computed settlement than the field measurement, which indicates that other factors might cause this discrepancy, e.g. the foundation.

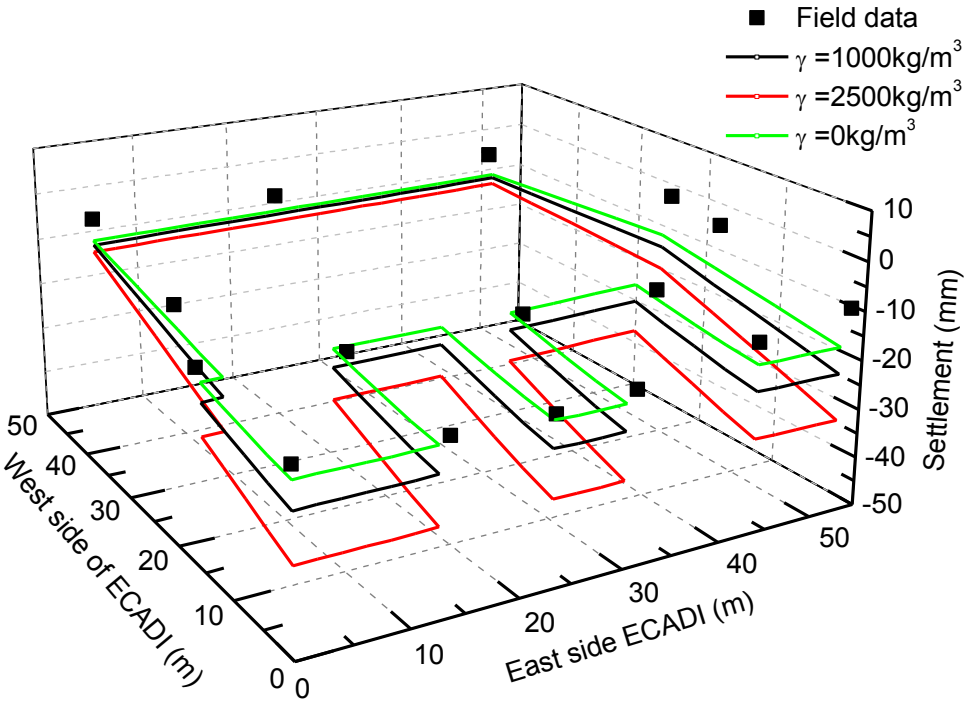

Fig.6.26 Building settlement (ECADI building)

6.5.4 Influence of the stiffness of the foundation

The foundation of buildings plays an important part in soil-structure interaction problems. It will modify the ground movement more or less depending on its structure type and stiffness properties, and therefore influence the building deformation. The details of the foundation for historical buildings are usually not clear because such information might be lost. Therefore, the foundation in the numerical model needs to be simplified. Moreover, the stiffness of the foundation needs to be estimated. In this section, the stiffness of the foundation, as shown in Table 6.3, is varied to investigate its influence on the numerical results.

Table 6.3 Influence of the foundation stiffness

Case No.	Stiffness
1	E=30GPa
2 (central analysis)	E=3GPa
3	E=0.3GPa
4	E= 3GPa (No piles)

Fig.6.27 shows that the stiffness of the foundation has little influence on the building settlement. The piles have minor influence on the building settlement. If the piles are not modelled, the settlement is slightly larger. However, the actual pile layout is unknown, and if it is denser than has been modelled, that could account for the smaller observed settlements.

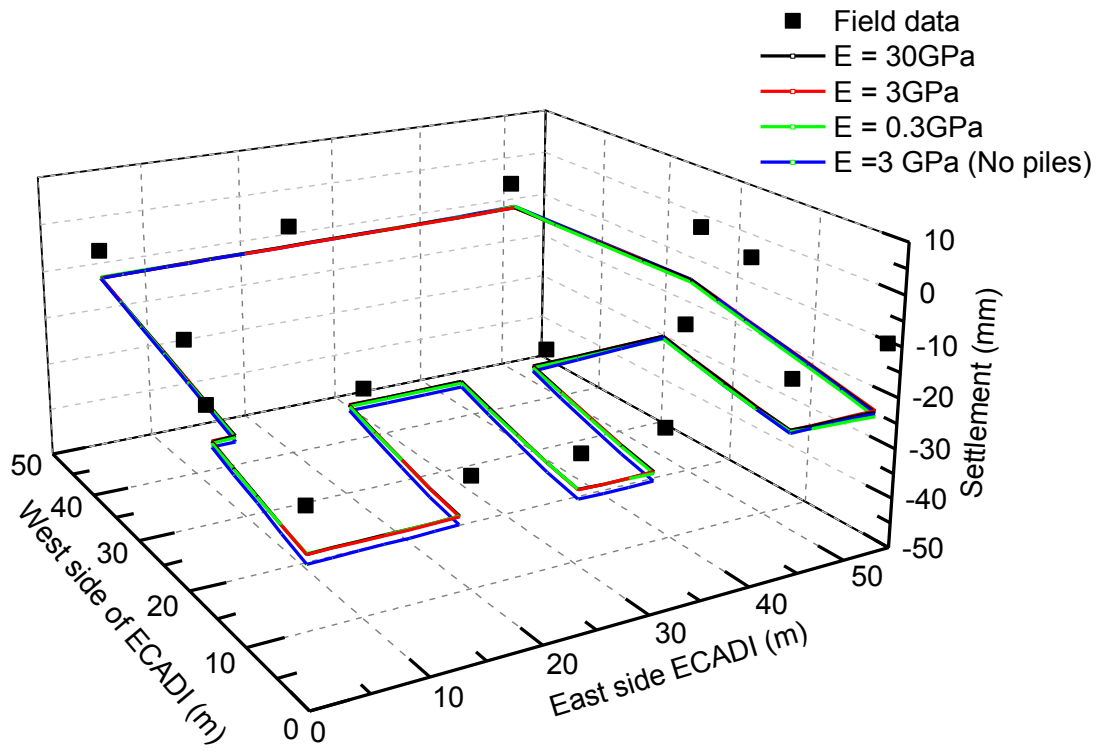

Fig.6.27 Building settlement (ECADI building)

6.5.5 Influence of ground improvement

One method for reducing the excavation-induced ground movement is to strengthen the soil around the diaphragm wall by jet grouting or mechanical deep mixing (Ou, Teng et al. 2008). However, it is difficult to determine the composite strength and stiffness of the treated area. In addition, ground improvement increases the cost of the project. It is therefore, proposed that ground improvement should be conducted only in a region where the building deformation induced by ground movement can be mitigated. In this section, the effectiveness of the ground improvement (e.g. jet grouting piles) conducted around the excavation is investigated, including the thickness, the stiffness, and the connection of the ground improvement.

Influence of the stiffness properties

The stiffness of the ground improvement depends on a number of factors, e.g. cement ratio, construction quality. Estimated stiffness values, as shown in Table 6.4, are used to investigate its influence on the building settlement.

Table 6.4 Influence of the stiffness of the ground improvement

Case No.	Stiffness
1 (central analysis)	E=3GPa
2	E=30GPa
3	E=0GPa (no ground improvement)

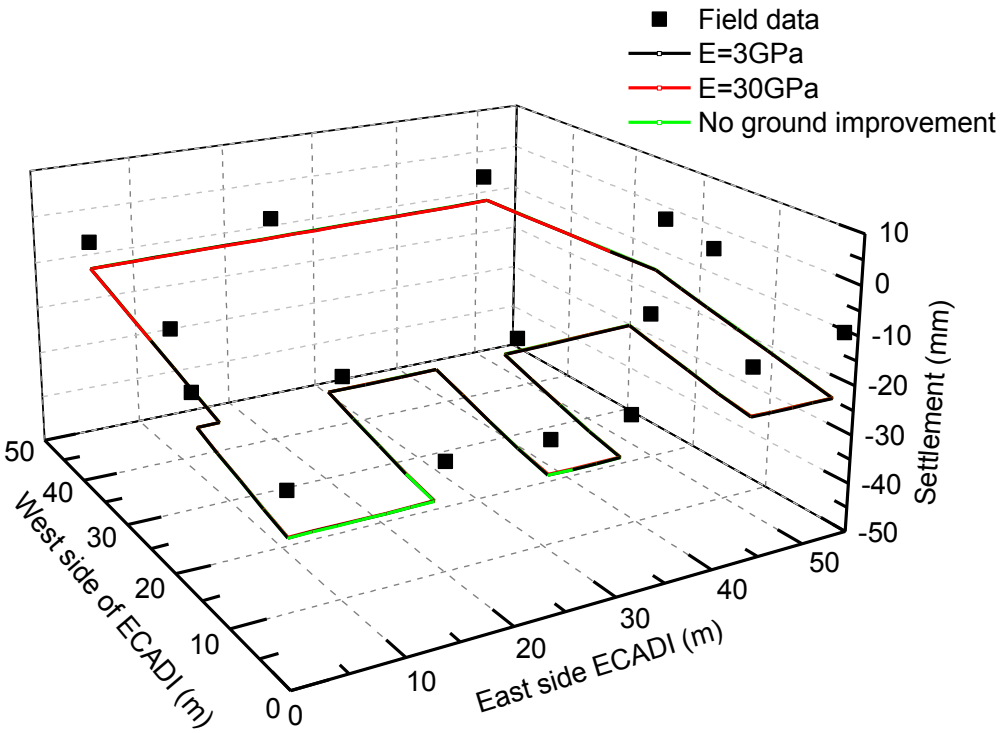

Fig.6.28 Building settlement (ECADI building)

As shown in Fig.6.28, the building settlement is insensitive to the stiffness of the ground improvement, and there is no significant difference whether the ground improvement is modelled or not.

Influence of the equivalent thickness of the ground improvement

The equivalent thickness of the ground improvement depends on the diameter of the jet grouting pipes and also the connection between adjacent piles. Three values of thickness, as shown in Table 6.5, are used to investigate its influence on the building settlement.

Table 6.5 Influence of the thickness of the ground improvement

Case No.	Thickness
1 (central analysis)	H=0.3m
2	H=0m
3	H=1.0m

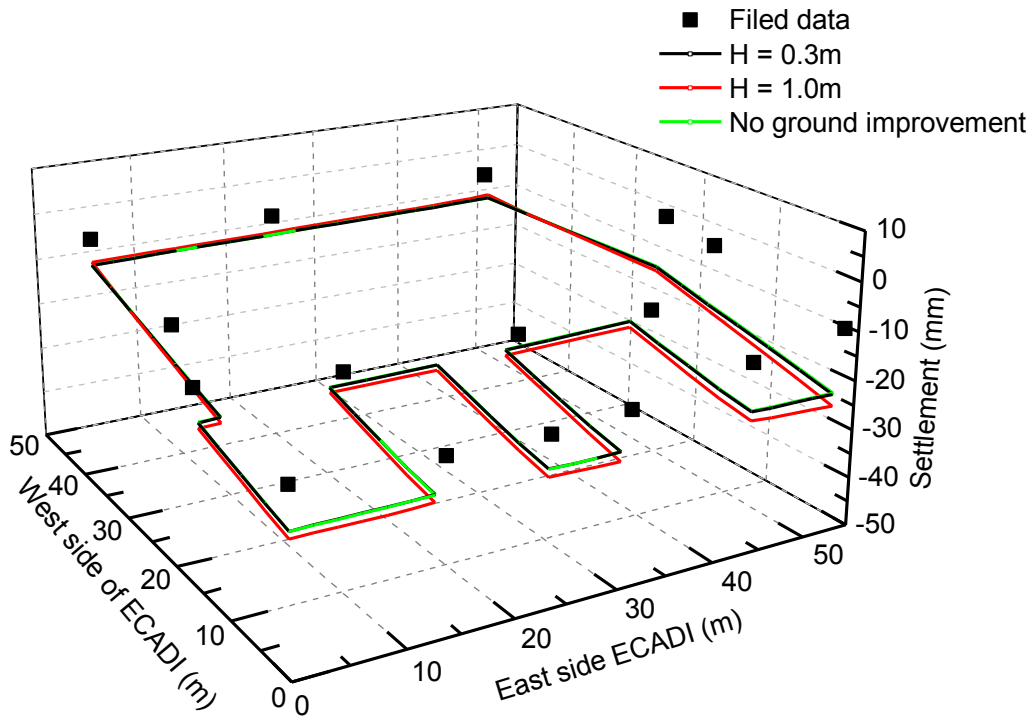

Fig.6.29 Building settlement (ECADI building)

It is surprising to find in Fig.6.29 that the building settlement is slightly increased when the equivalent thickness of the ground improvement increases from 0.3m to 1.0m. This small difference might be caused by the increased stiffness and weight of ground improvement due to the increase of thickness. Again it confirms that the ground improvement has little influence on the building settlement.

Influence of the anisotropic ratios

Similar to the diaphragm wall construction, the ground improvement is not cast as a whole piece, and the connectivity between adjacent piles might influence its overall stiffness. In finite element model, it is tedious to consider such details, and continuous shell elements with anisotropic properties are used to model the whole ground improvement. The anisotropic ratio β is varied, as shown in Table 6.6, to investigate its influence on the building settlement. The value of 10^{-5} used in the central analysis is selected based on the value in Zdravkovic, Potts et al. (2005) for the contiguous pile wall, because the root piles and jet grouting piles in this case history have similar discontinuity with the contiguous pile wall. The isotropic one is another extreme case and is used for comparison.

Table 6.6 Influence of the anisotropic ratio

Case No.	Thickness
1 (central analysis)	$\beta = 10^{-5}$
2	$\beta = 1.0$

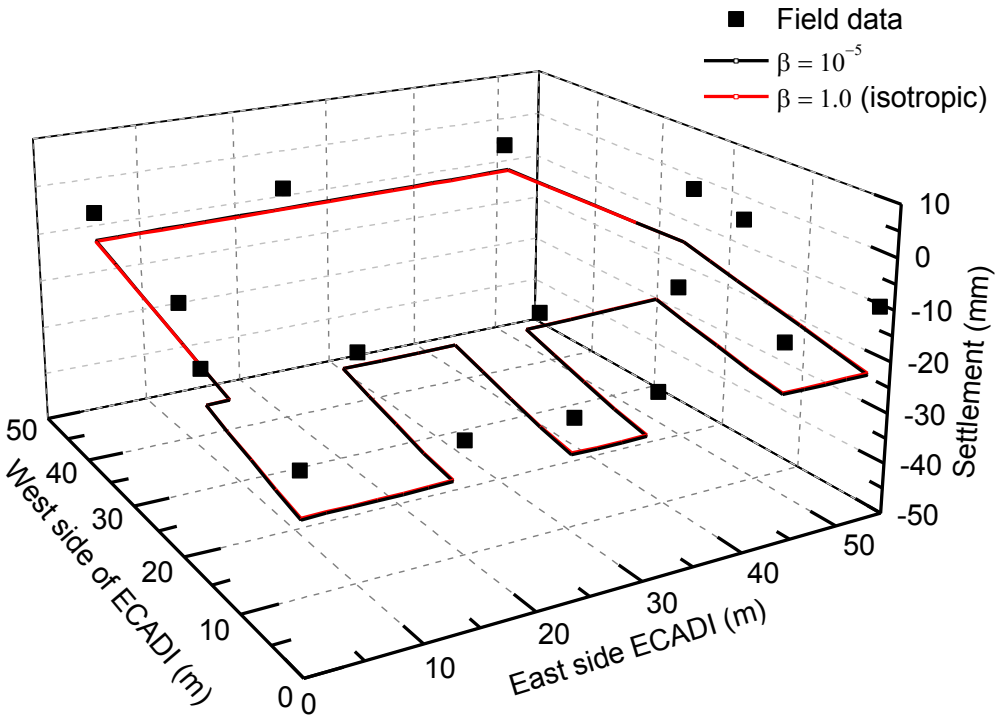

Fig.6.30 Building settlement (ECADI building)

The results in Fig.6.30 indicate that the building settlement is insensitive to the anisotropic ratio used for of the ground improvement. Even though the isotropic property is used, representing that the piles are tightly connected, the building settlement does not change. It seems that the ground improvement has little effect on the building deformation.

6.5.6 The settlement of the pipelines

The geometry and material properties of buried pipelines are not known in some situations. In order to better understand the response of different types of pipeline during the excavation, parametric studies are conducted in this section to investigate the sensitivity of the pipeline settlement to some key factors such as the diameter, wall thickness, and stiffness of the pipeline.

Influence of diameter of the pipeline

Three values of the diameter of pipelines, as shown in Table 6.7, are selected to investigate their influence on the settlement of pipelines. The other parameters such as the wall thickness, and stiffness, are kept the same with the central analysis.

Table 6.7 Influence of the diameter of the pipeline

Case No.	Stiffness	Wall thickness	Diameter
1	E = 20GPa	t = 20mm	D = 300mm
2 (central analysis)	E = 20GPa	t = 20mm	D = 500mm
3	E = 20GPa	t = 20mm	D = 1000mm

The settlements of two pipelines from these three analyses are shown in Fig.6.31. It is found that the results are almost identical, indicating that the diameter of the pipeline has little influence on the settlement of the pipeline.

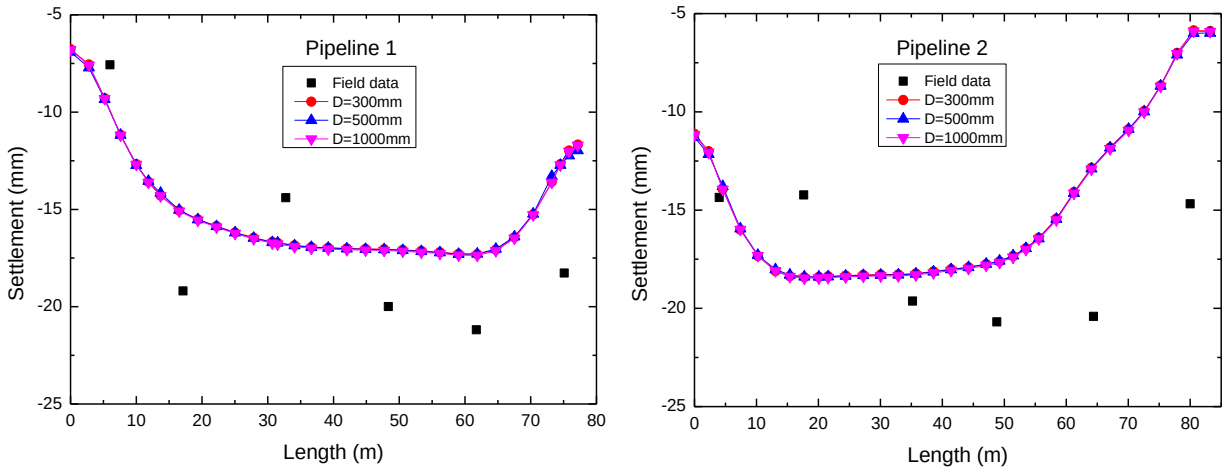

Fig.6.31 Settlement of Pipeline 1 (L01-L06) and Pipeline 2 (L07-L12)

Influence of the wall thickness of the pipelines

The wall thickness of pipelines is varied using three values, as shown in Table 6.8, to investigate its influence on the settlements of buried pipelines. The other parameters, e.g. the diameter, and stiffness, are the same with the central analysis.

Table 6.8 Influence of the wall thickness of the pipeline

Case No.	Stiffness	Wall thickness	Diameter
1	E = 20GPa	t = 10mm	D = 500mm
2 (central analysis)	E = 20GPa	t = 20mm	D = 500mm
3	E = 20GPa	t = 30mm	D = 500mm

The settlements of two pipelines from these three analyses are shown in Fig.6.32. The results indicate that the wall thickness of the pipelines has insignificant influence on the settlement of buried pipelines.

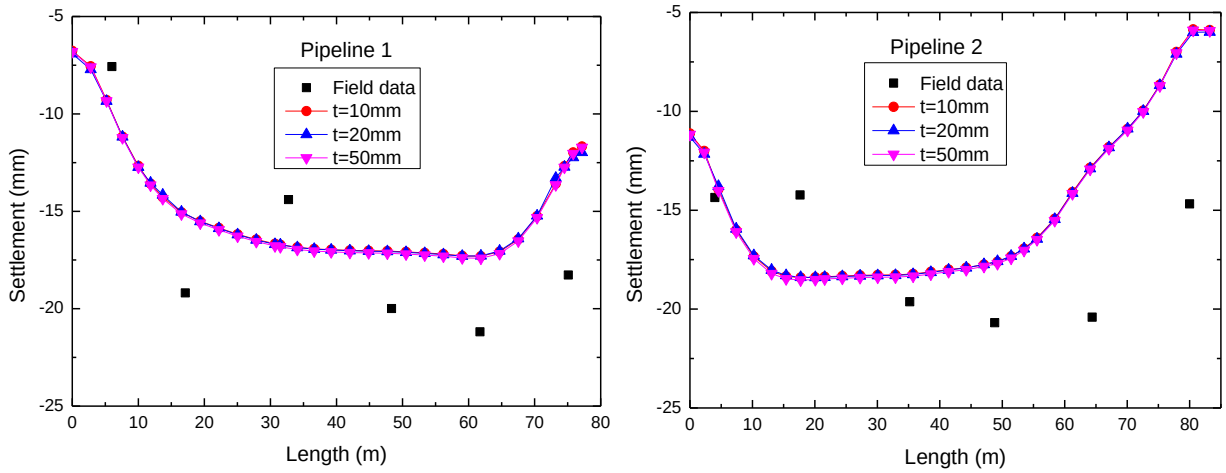

Fig.6.32 Settlement of Pipeline 1 (L01-L06) and Pipeline 2 (L07-L12)

Influence of the stiffness properties

Three values of Young's modulus, as shown in Table 6.9, are used to investigate its influence on the settlements of buried pipelines. Those values might represent different materials of pipelines, e.g. PVC, concrete and steel pipelines, which are commonly used in practice. The other parameters, e.g. the diameter, and stiffness, are the same with the central analysis.

Table 6.9 Influence of the stiffness of the pipeline

Case No.	Stiffness	Wall thickness	Diameter
1	E = 0.2GPa	t = 20mm	D = 500mm
2 (central analysis)	E = 20GPa	t = 20mm	D = 500mm
3	E = 200GPa	t = 20mm	D = 500mm

The settlements of two pipelines from these three analyses are shown in Fig.6.33. There is little difference between the results from the two analyses with stiffness of 0.2GPa and 20GPa. However, when the Young's modulus of the pipelines is increased to 200GPa, both pipelines experience slightly larger but more flat settlement than the other two analyses. Generally, the stiffness of the pipelines has little effect on the settlement of pipelines.

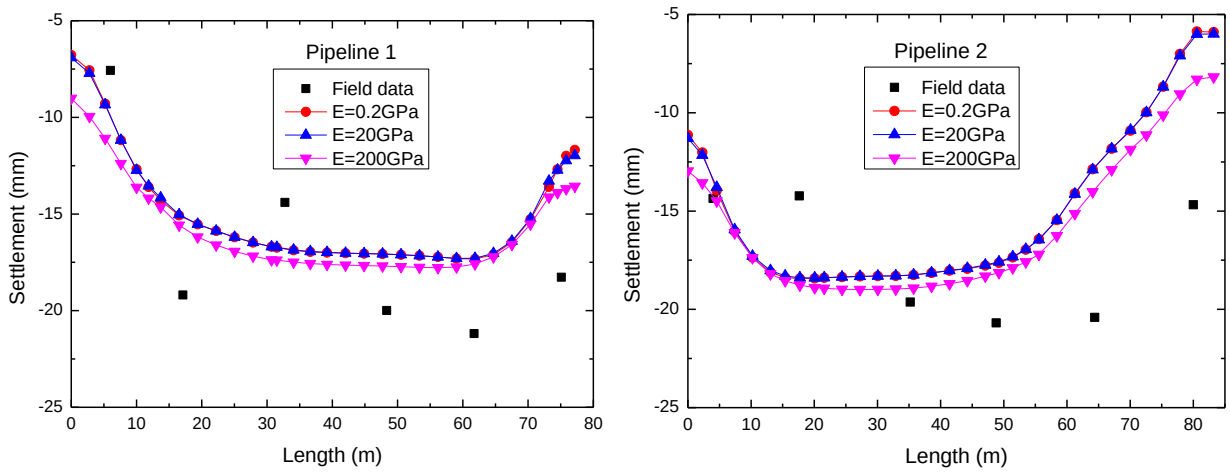

Fig.6.33 Settlement of Pipeline 1(L01-L06) and Pipeline 2(L07-L12)

Influence of beam elements and pipe elements

The pipe elements (PIPE31) are available in ABAQUS. In order to understand whether there is any difference between beam elements and pipe elements to model the pipeline, analyses with these two elements are conducted, and the results are shown in Fig.6.34. It seems that the computed settlement from these two analyses are almost identical, suggesting both beam elements and pipe elements can be used to model the pipeline.

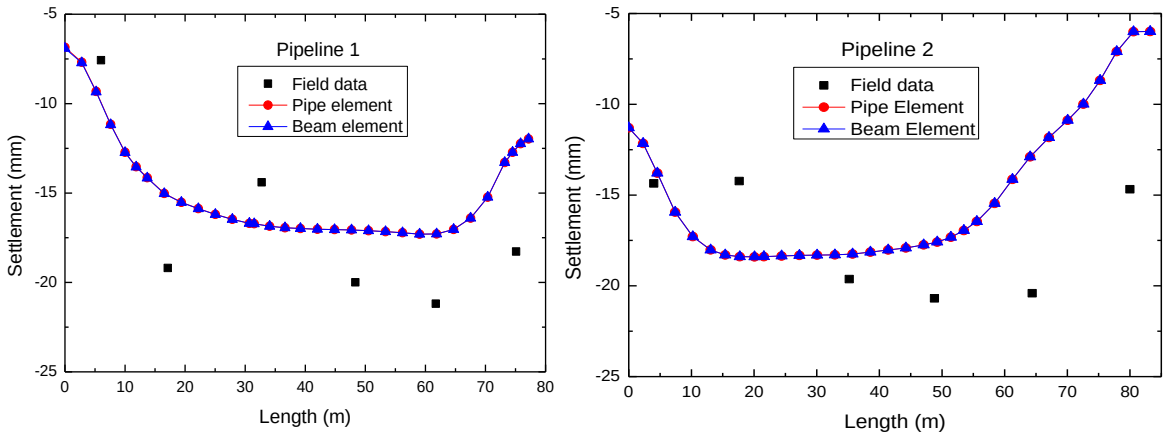

Fig.6.34 Settlement of Pipeline 1(L01-L06) and Pipeline 2(L07-L12)

6.6 Conclusions

This chapter extends the case study of the basement excavation for the Shanghai Xingye Bank building in Chapter 5, and focuses on the settlement of adjacent buildings and pipelines induced by the deep excavation. The finite element model in this chapter inherits all the characteristics of the central analysis in chapter 5, and further includes three adjacent buildings, two buried pipelines, and the ground improvement outside the excavation. The influence of several

important aspects on the settlement of buildings (e.g. stiffness, weight, foundation, and ground improvement) and pipelines (e.g. diameter, wall thickness, stiffness, and element types), are investigated through parametric studies. Some general conclusions are drawn here.

1) In the central analysis, all of the buildings settle a fairly large amount and slightly tilt towards the excavation, which agrees reasonably well with field measurements. However, the computed building settlements are slightly larger than the field data, and the discrepancy might be attributed to a number of reasons, e.g. the simplifications and assumptions made in the analysis, estimated parameters of the buildings, foundations and soils, and the excavation behaviour itself. For example, one important reason may be the selection of soil parameters derived from green field site condition to represent the soil underneath buildings, and the total stress soil model cannot account for the change of soil properties by the overlying buildings. An attempt has not been made to match the numerical results with the field measurement due to the large number of the undetermined parameters, also because this is not the aim of this case study. When comparing the ground settlement contours with and without buildings, it is found that the ground movement is modified due to the existence of buildings.
2) The settlement of the pipelines also agrees well with the field measurement. The buried pipelines settle in a similar pattern with, but in a slightly larger magnitude than, the ground surface settlements above the pipelines, which is probably due to the swelling of the soil in the retained area. This suggests that the buried pipelines follow the ground movement, and it is suitable in practice to use the ground surface settlement above the pipelines to represent the settlement of buried pipelines. It is also shown that the settlement is larger behind the wall centre and smaller at the wall corner due to the corner effect.
3) Parametric studies have been conducted to investigate the influence of several important aspects on the building settlement, and the results indicate that (i) the building weight has

a significant influence on the magnitude of the settlement, (ii) while the building stiffness mainly influences the pattern of the settlement, (iii) the stiffness of the foundation has little influence of the settlement, and piles have minor effect on the settlement, and (iv) the ground improvement has little influence on the settlement. In order to improve the accuracy of the numerical analysis, it is suggested that (i) the internal and external structures of the building need to be modelled in more detail to approximate the actual stiffness and weight of the building, (ii) more information is needed about the foundation of the building, (iii) the building weight needs to be estimated more accurately in the model, (iv) a more realistic material model for the building might improve the results, and (v) the ground improvement might be ignored in the numerical modelling, and its effectiveness needs to be revaluated in the practice.

4) Parametric studies have been carried out to investigate the sensitivity of the settlement of pipelines to several key parameters, e.g. stiffness, diameter, and wall thickness of the pipelines, but the results show that these parameters have insignificant influence on the settlement of pipelines. Both beam elements and pipe elements are used to model the pipelines, but the computed settlement of pipelines is almost identical. This indicates that in the numerical modelling the buried pipelines might be neglected, and the ground settlement at the buried position of the pipelines can be used to represent the settlement of the pipelines. However, these conclusions should be used in caution because some simplifications are made in the analysis. For example, the detailed geometry of the pipelines is not considered, and the pipelines are assumed to behaviour linear elastically. The study in this chapter is an initial attempt to investigate such kind of soil-pipeline interaction problem in deep excavations.

Chapter 7 Deep excavation for the North Square of Shanghai South Railway Station

7.1 Introduction

In large scale top-down deep excavations, opening accesses are usually designed in the horizontal support system to transport the excavated soils and improve the ventilation and lighting conditions. The large openings, however, also reduce the overall stiffness of the horizontal support system, and consequently result in larger wall deflection and ground movement. Therefore, the size of the openings should be considered carefully in the design process. In the finite element analysis, the openings are usually not considered explicitly in the model but in a simplified way by reducing the stiffness of the support system, so their influence on the excavation behaviour is still unclear.

Another issue associated with large scale deep excavations is the variety of construction schemes for a particular project. For example, the construction is usually divided into several zones and then carried out in different sequences, due to the limitation of labour and machinery available. As the soil is a nonlinear material and the stress-strain relationship depends on the loading-unloading stress history, the excavation behaviour may be affected by different construction sequences.

The excavation for North Square underground shopping centre of Shanghai South Railway Station is a typical large scale deep excavation project with a top-down construction method. The construction is divided into several zones for each layer of excavation, and has large opening accesses in the horizontal support system. Moreover, the main excavation is next to a neighbouring excavation using a bottom-up construction method, and is close to several current and new Metro lines. Therefore, it is an ideal case history to investigate the issues mentioned above. This excavation was carefully measured during the construction process, with well

documented field data (Xu 2007). Advanced finite element analysis has been conducted using ABAQUS to simulate the whole construction process and calibrate with the field measurement. Based on the experience of the case study in Chapter 5, construction joints in the diaphragm wall and thermal effects of concrete beams and floors slabs are considered and treated in a similar way in this chapter. The influence of several new aspects, e.g. the construction sequences, the earth berms, and openings in floor slabs, is investigated through parametric studies. A number of general conclusions are drawn for future use.

7.2 Project description

7.2.1 General description

The Shanghai South Railway Station is designed to increase the transportation capacity of the existing passenger terminals, and is a remarkable underground development project in Shanghai. It integrates the subways, the light rail transit system, the ground public transport, the elevated freeway, and the passenger station systematically, and makes the transport interchange more convenient. The whole project includes the Main Station, North Square and South Square, covering an area of over 200,000 m^2. The construction was finished in 2006. The North Square, as show in Fig.7.1, is located to the north side of the Main station.

Fig.7.1 Shanghai South Railway Station

The excavation for the North Square underground shopping centre, as shown in Fig.7.2, is a large and complex deep excavation using a top-down construction method. The excavation is 12.5m deep, and covers an area of around 40000 m^2. The main underground structure has two

basement levels, with a pile-raft foundation. The geometry of the excavation is irregular, roughly 400m in the long direction and 100m in width. The excavation was started in 2003, and completed in 2005.

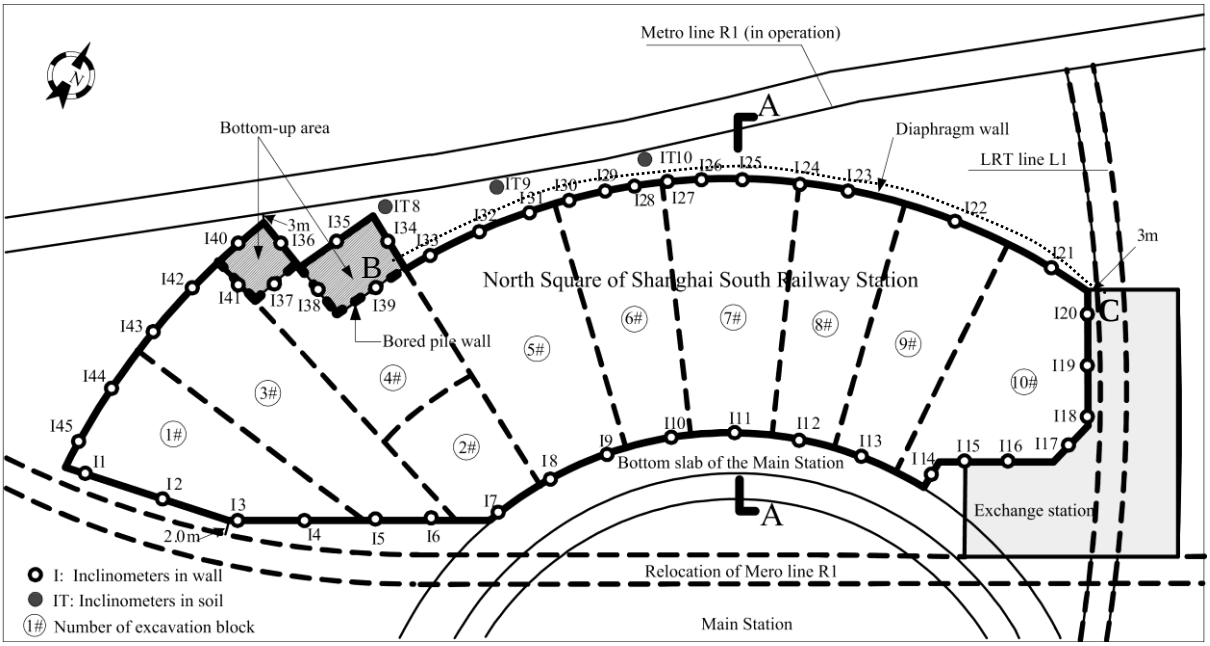

Fig.7.2 The excavation, adjacent facilities and instrumentation (Xu 2007)

The North Square excavation is close to several current and new Metro lines and next to the excavation for an Exchange station. On the east side, the new LRT (Light Rail Transit) Line 1 is approximately 3m from the diaphragm wall. The excavation for the new LRT Line 1 varies from 8.6m to 10.5m in depth, and was completed before the start of North Square excavation. To the Southeast, the North Square is next to the Exchange Station for the new Metro Lines R1 and LRT Line L1. The excavation for the Exchange Station is around 9.9m deep, and was completed before the start of the North Square excavation. The excavation for the new LRT Line 1 and the Exchange Station shares the diaphragm wall with the North Square on one side, and uses the SMW (Soil Mixing Wall) method on the other sides. To the South, the North Square excavation is next to the Main Station and close to the relocated Metro Line R1. The 0.7m thick floor slab of the Main Station is connected to the diaphragm wall of the North Square. The excavation for the Main Station was finished before the start of North Square excavation. To the Southwest, the North Square excavation is close to the relocated Metro Line 1, with a minimum distance of 2m to the diaphragm wall. The excavation for the relocated Metro Line R1 varies from 10.4m to

13.3m deep, and was finished before the start of North Square excavation. To the North, the currently operational Metro Line R1 is close to the North Square excavation, with a minimum distance of 3m to the diaphragm wall.

To avoid any damage to the adjacent infrastructure, a very high standard of construction is required, and the construction process was carefully monitored.

7.2.2 Geotechnical conditions and soil properties

According to the site investigation report, the construction site is underlain by thick layers of soft quaternary alluvial and marine deposits. The ground level is at an elevation of -2.2m, and the ground water table is between 0.5m to 1.0m below the ground surface. The geological profile and soil properties are shown in Fig.7.3.

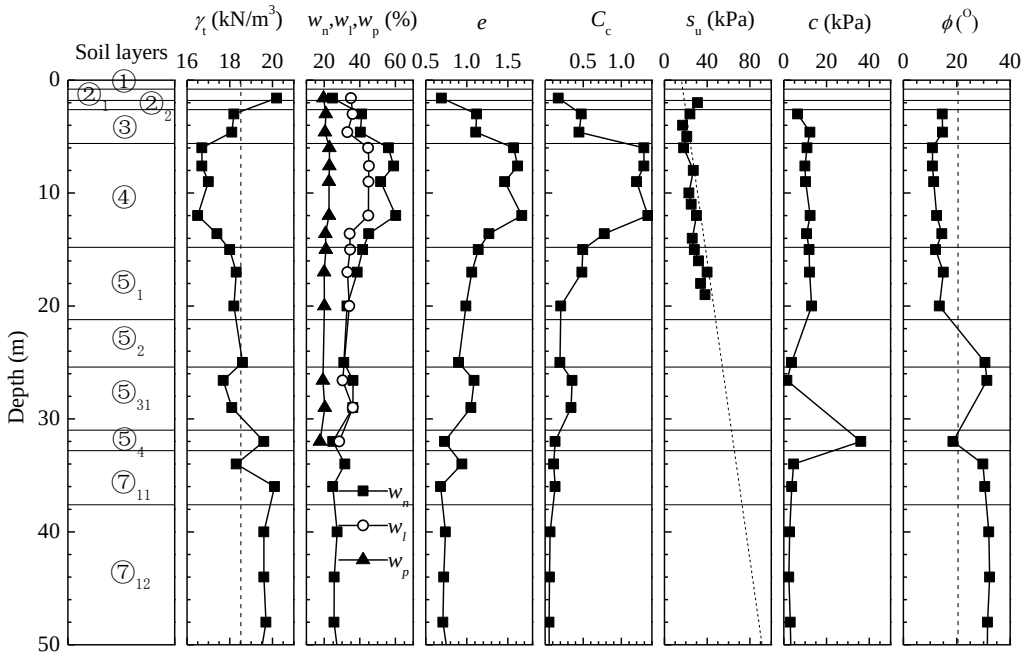

Note: γ_t = unit weight, w_n = water content, w_p = plastic limit, w_l = liquid limit, e = void ratio, C_c = compressive index, s_u = field vane shear strength, c = cohesive strength, ϕ = internal friction angle

Fig.7.3 Geotechnical profile and soil properties (Xu 2007)

The subsoil consists of a 1.2m thick fill layer which is mainly medium dense sand. Beneath the fill layer, there is a 2 m thick silty clay layer. Two layers of very soft silty clay with total thickness of 16.8m are underneath the silty clay layer. The subsequent soil layers are a silty sand layer, a silty clay layer and a silty sand layer. In general, the soils in this site are soft soils with low shear strength and low modulus of deformation.

In a similar situation with the Xingye Bank case history, the site investigation does not provide any information on the small-strain stiffness nonlinearity of the soil to calibrate the multiple-yield surface model, and the undrained shear strength profile is not deep enough for the numerical modelling. Therefore, the soil properties collected from publications, as shown in Chapter 3, are referred in this case study. A constant unit weight $\gamma = 18.5\text{kN/m}^3$ is used to set up the vertical geostatic stress in the ground, and a constant friction angle $\varphi = 20°$ is selected to derive the coefficient of lateral earth pressure. A smaller undrained shear strength, $s_u = 0.75(20 + 2z)\text{kPa}$, is adopted to match the data from the site investigation. A constant index of rigidity, $I_r = 1000$, is used.

7.2.3 The Retaining system

The retaining system of the North Square excavation was designed as part of the permanent structure, considering a number of factors, e.g. the cost, security of construction, and influence to adjacent infrastructure. The main structure, as shown in Fig.7.4, consists of the diaphragm wall, two levels of horizontal support system composed of beams and floor slabs, and vertical reinforced concrete piles and steel lattice columns. The bottom slab (1m thick) was cast in situ after the completion of the excavation. Soil cement columns and compaction grouting was used to improve the soil properties and restrain the lateral displacement the diaphragm wall.

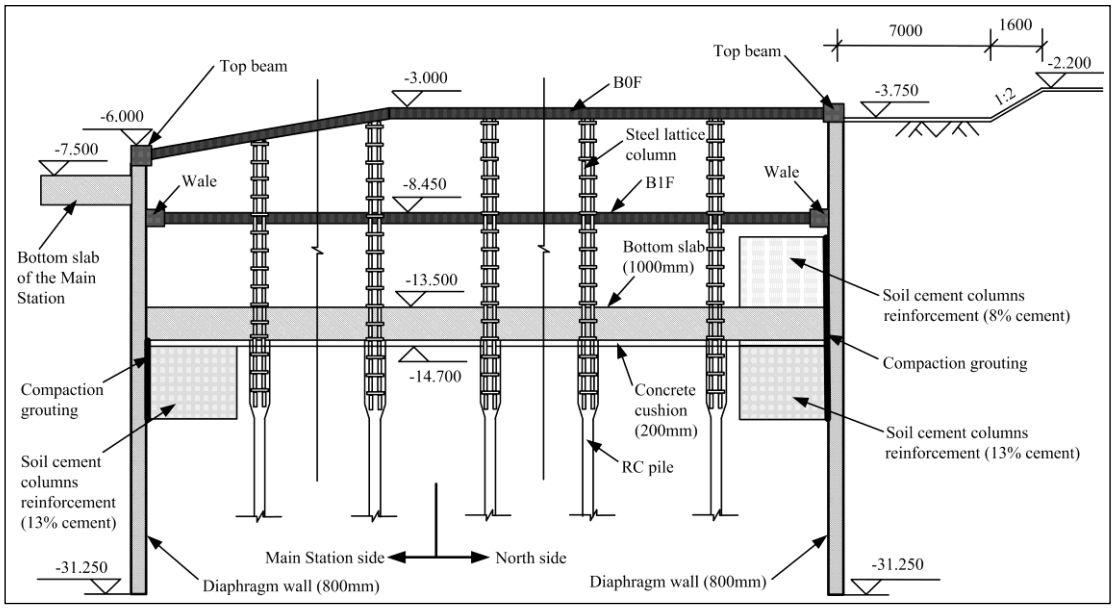

Fig.7.4 A-A cross section view of the North Square excavation (Xu 2007)

The Exchange Station shares the diaphragm wall with the North Square on the west side and uses SMW (Soil Mixing Wall) on the other sides. The retaining structure, as shown in Fig.7.5, has three levels of temporary steel struts at the elevation of -2.83m, -6.43m and -9.83m respectively. The excavation is 9.1m deep, using a bottom-up construction method.

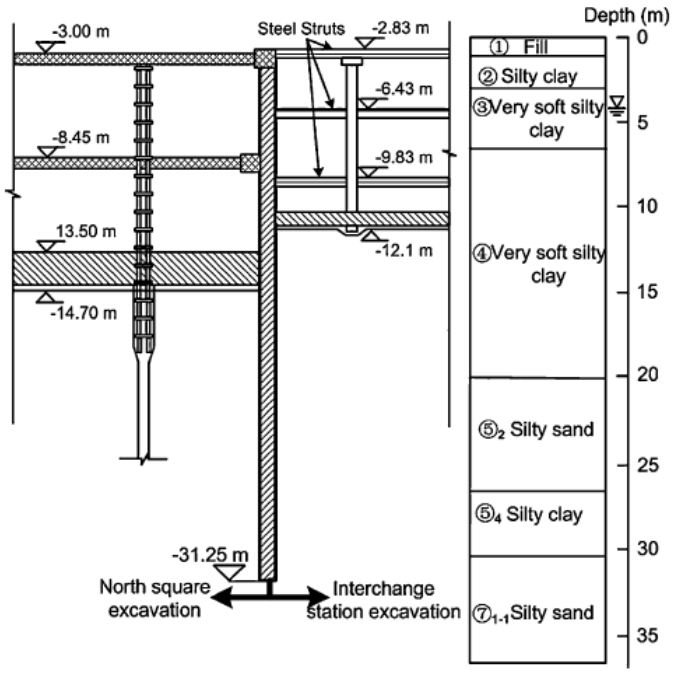

Fig.7.5 Section view of the Exchange Station excavation (Hou, Wang et al. 2009)

The diaphragm wall

The diaphragm wall is 0.8m thick, and its toe is at the elevation of -31.25m. Due to the slope in the roof floor slab, the diaphragm wall next to the Main Station is 3m shorter than the other part which is normally about 28m deep. The diaphragm wall was constructed as sections of wall panels, and the joints between panels are filled with flexible waterproofing materials.

Bored piles were used between the top-down and bottom-up excavation area on the North side for temporary partition. The bottom-up area was excavated after the relocation of the Metro Line R1, which is after the completion of the North Square excavation.

The horizontal support system

The horizontal support system, as shown in Fig.7.6, is composed mainly of concrete beams and floor slabs. The top floor slab was also used as the work space during the excavation. Large opening accesses were designed in the floor slabs to speed up the excavation process and

improve the lighting and ventilation conditions.

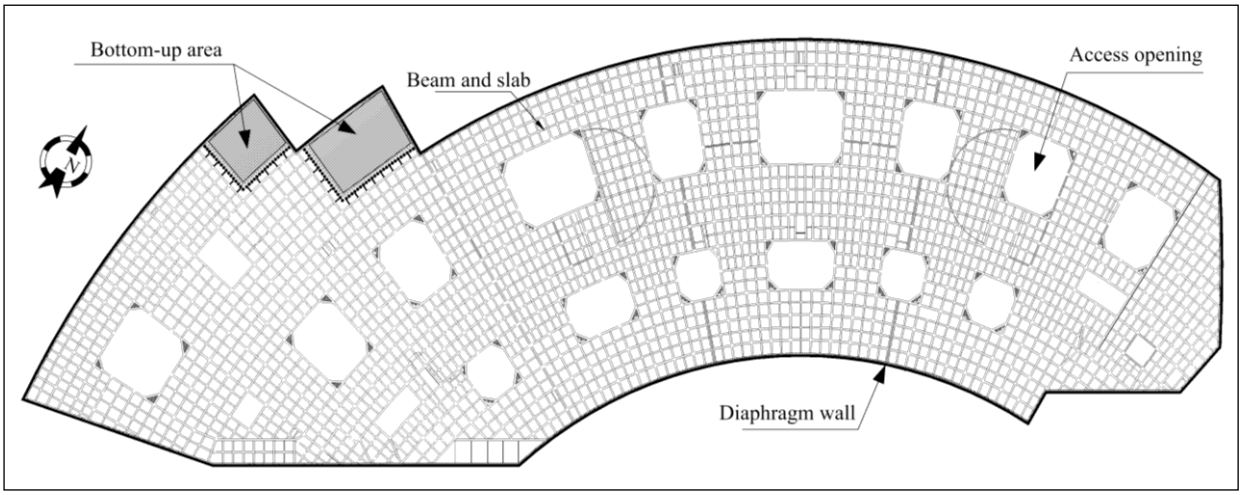

Fig.7.6 Plan view of the floor slab and beams (Xu 2007)

There are in total 44 rectangular large openings, 22 in each floor. The largest one is 700m^2 in area, and the others are between 400 ~ 500m^2. The floor slab is around 0.2m thick, and the section of the concrete beam is $500\text{mm} \times 900\text{mm}$.

The vertical support system

The vertical support system consists of bored piles (Φ700mm) and the steel lattice columns (450×450mm in section), as shown in Fig.7.7. The steel lattice columns are embedded into the piles which extend to around 45m below the ground. The piles are grouted at the toe to improve the bearing capacity and reduce the settlement.

Fig.7.7 Inside the excavation and details of retaining structure (Xu 2007)

7.2.4 Construction procedures

The excavation was constructed using a typical top-down method. The main construction sequence is summarized in Table 7.1.

Table 7.1 Construction sequence

Stage No.	Stage description
0	Install the diaphragm wall and piles;
1	Excavate to -3.750m inside and outside the excavation; excavate to -7.5m on the side close to the Main Station and to -5m on the side away from the Main Station with earth berms (10m wide); Install the roof floor slab(B0F) at -3m;
2	Excavate to -13.00m on the side close to the Main Station and to -10m on the side away from the Main Station with earth berms (10m wide); Install the floor slab (B1F) at -8.45m;
3	Excavate to -14.7m on the side close to the Main Station and to -13.00m on the side away from the Main Station with earth berms (10m wide); Cast the bottom slab on the side close to the Main Station;
4	Remove the remaining earth berms and excavate to-14.7m on the side away from the Main Station; Cast the remaining bottom slabs.

Considering the large scale of the excavation and the availability of labour and machinery, the excavation was divided into 10 zones and carried out in sequence from zone #1 to zone #10 in each layer, as shown in Fig.7.2. To restrain the lateral wall deflections, earth berms, as shown in Fig.7.8, were used on the North side of the excavation.

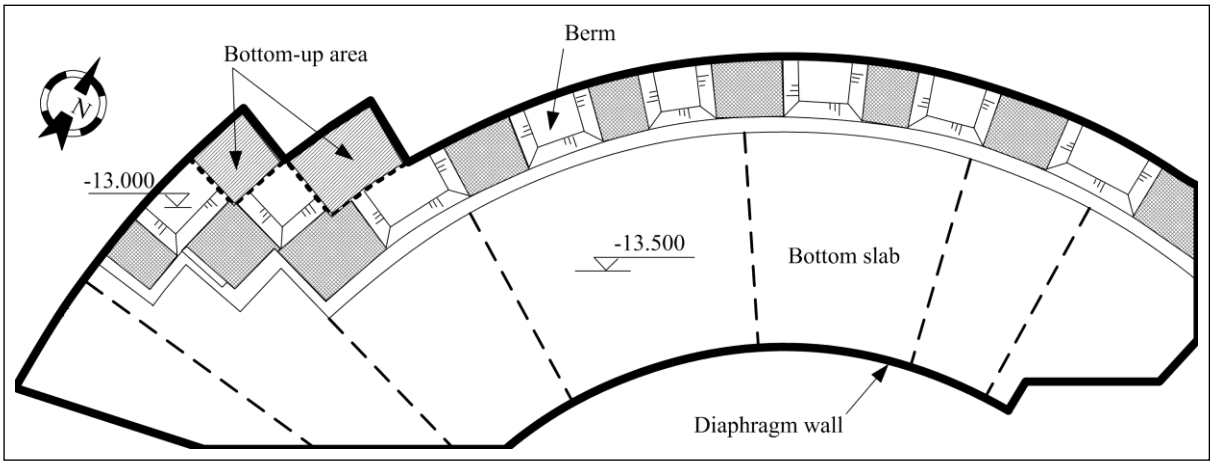

Fig.7.8 Earth berms at the north side of the excavation (Xu 2007)

7.2.5 Instrumentation

The excavation was carefully monitored during the construction to understand its performance and ensure its safety. The measured items, as shown in Fig.7.2, include the lateral deflection of the diaphragm wall, ground movement outside the excavation, and the vertical displacement of the diaphragm wall and piles. Details are described below.

1) Lateral deflection of diaphragm wall (from I1 to I45 at an interval of roughly 25m)using inclinometers.

2) Ground settlement along BC using level instruments, and soil lateral displacement at the positions from IT7 to IT10 using inclinometers to reflect the disturbance to the operating Metro Line R1;
3) Vertical displacement of the diaphragm wall at the positions from I1 to I45 using level instruments;
4) Vertical displacement of piles and columns using level instruments, as shown in Fig.7.9;

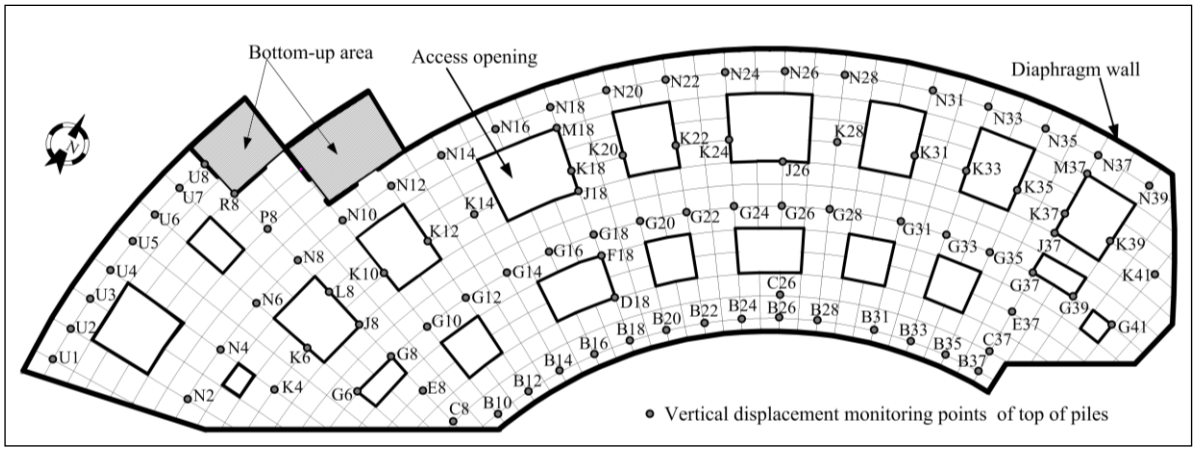

Fig.7.9 Monitoring points of piles (Xu 2007)

7.3 FEM model description and input parameters

7.3.1 FEM model description

Due to the irregular geometry and complex construction sequence, a 3D finite element model is created using a commercial finite element software ABAQUS, to capture the excavation behaviour more accurately. The numerical model considers the detailed retaining structure (e.g. the diaphragm wall, piles, columns, beams, and floor slabs), slope and opening accesses in the floor slabs, the cast-in-situ bottom slab, zoned construction sequence, earth berms, the excavation for the adjacent Exchange Station, and the bottom-up area excavation.

As shown in Fig.7.10, the model size is $1000\text{m} \times 500\text{m} \times 80\text{m}$, with boundaries sufficiently remote from the excavation. The four vertical sides have roller boundary conditions, while the bottom is fixed. The model has in total 188,593 elements and 214,360 nodes.

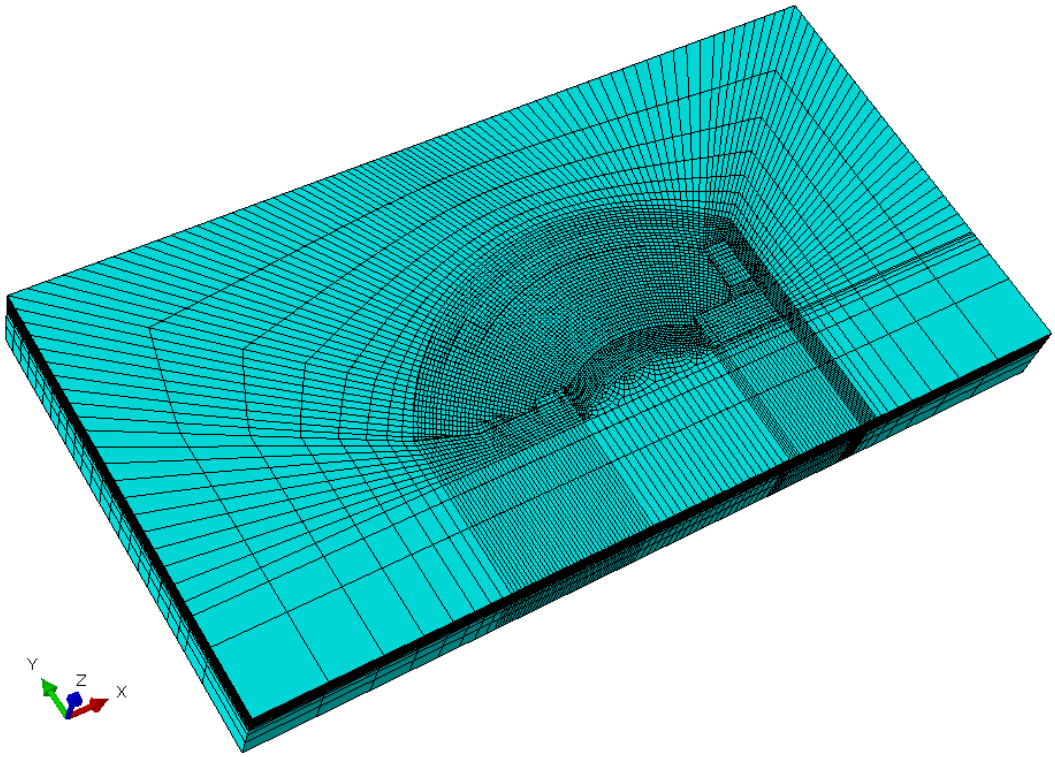

Fig.7.10 Geometry and mesh of the whole model

The soil is modelled using 8-noded hexahedral continuum elements with reduced integration (C3D8R), due to the large amount of elements in the model. Details of the mesh in the excavation region are shown in Fig.7.11.

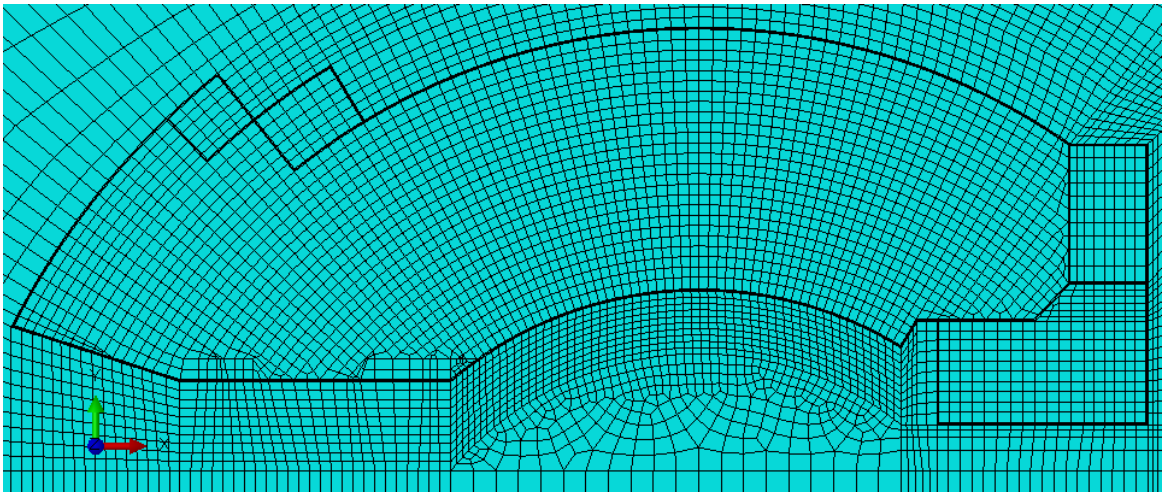

Fig.7.11 Details of mesh in the excavation area

The mesh of the retaining wall is shown in Fig.7.12. The SMW (Soil Mixing Wall) for the Exchange Station and the bored piles for the partition of the bottom-up area are included in the model. The diaphragm wall, SWM, and the bored piles, are modelled with 8-noded hexahedral continuum elements with reduced integration (C3D8R).

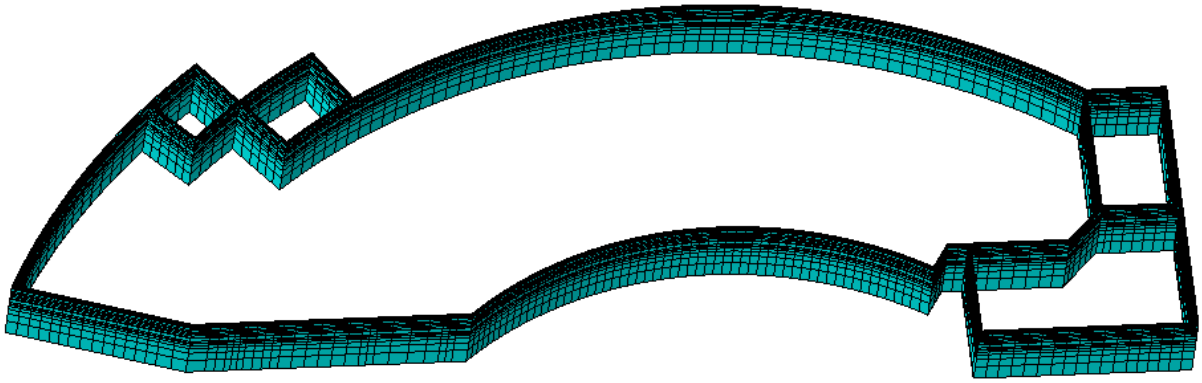

Fig.7.12 Geometry and mesh of the retaining wall

The geometry and mesh for the supporting system is shown in Fig.7.13. The opening accesses, the slope in the top floor slab, the piles and columns, are included in the model. The horizontal beams, vertical columns and piles are modelled with 3D 2-noded linear beam elements (B31). The concrete floor slabs are modelled with 4-noded quadrilateral shell elements with reduced integration (S4R).

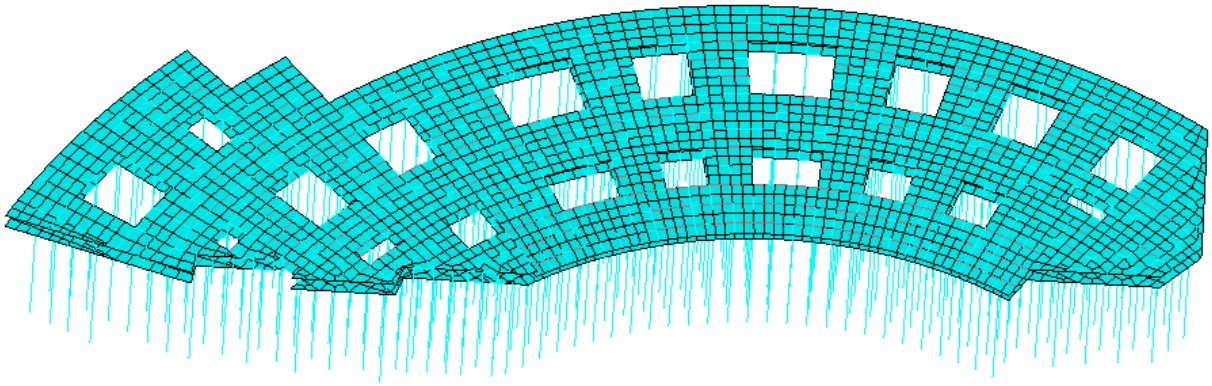

Fig.7.13 Geometry and mesh of the supporting system

The mesh of the floor slab and beams is shown in Fig.7.14 and Fig.7.15 respectively.

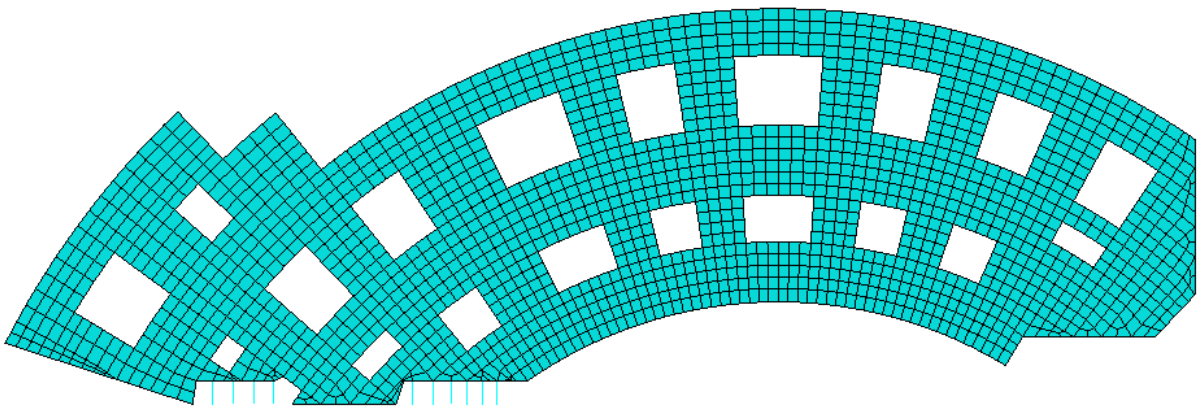

Fig.7.14 Geometry and mesh of the floor slabs

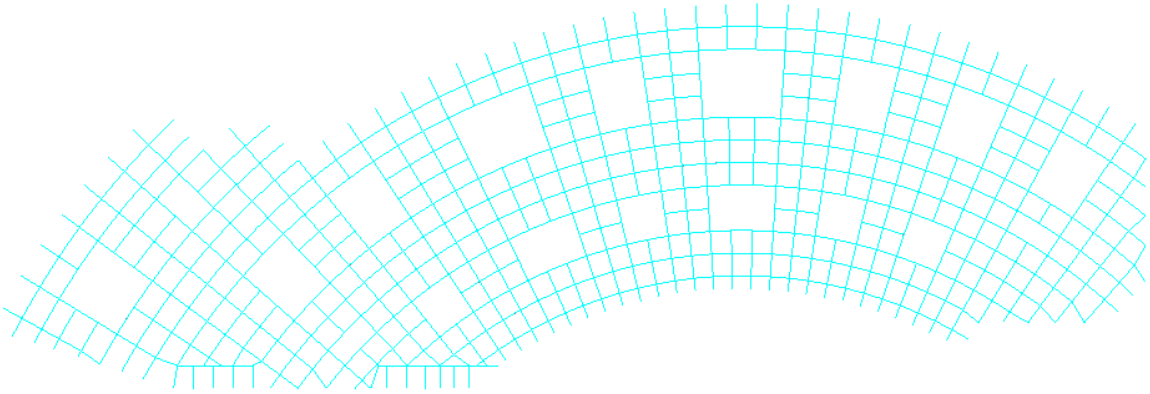

Fig.7.15 Geometry and mesh of the beams

The struts used in the bottom-up area and the Exchange Station are mainly composed of steel pipes which have the external diameter 609mm and wall thickness 16mm. Beam elements (B31) are used to model those struts and the mesh is shown in Fig.7.16 and Fig.7.17 respectively.

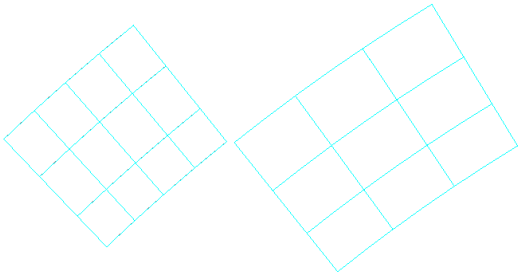

Fig.7.16 Struts in the bottom-up area

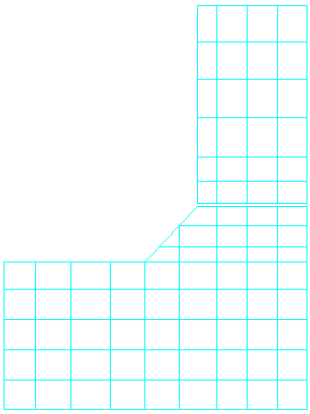

Fig.7.17 Struts in the Exchange Station

Tie constraints are used to connect the diaphragm wall, the floor slabs, the beams and vertical piles. The piles are embedded into the soil. The friction behaviour at the interface between the soil and the diaphragm wall, and between the soil and piles, are not accounted in the model.

7.3.2 Input material properties

The soil model and input parameters

The soil is represented by the multiple-yield surface model (Houlsby 1999) to consider the

small-strain stiffness nonlinearity. The input parameters for the small-strain stiffness are derived from the $G_t \sim \gamma$ curve for Shanghai clay using the method detailed in Chapter 3. The undrained shear strength s_u of the soil is slightly adjusted to agree with the data from the site investigation in Fig.7.3. The index of rigidity $I_r = 1000$ is the same as the value used in the Xingye Bank building case study. The input parameters for the soil are shown in Table 7.2.

Table 7.2 Input parameters for the soil

Soil properties	Values
Normalised small-strain stiffness $G_t/\mathrm{G}_0 \sim \gamma$	$\frac{G_t}{G_0} = \frac{1}{(1+\frac{\gamma}{0.1\%})^2}$
Undrained shear strength s_u	$s_u = 0.75(20 + 2z)$ kPa
Stiffness at very small strain G_0	$G_0/s_u = I_r = 1000$
Bulk stiffness K	$K \approx 50G$
Unit weight γ	$\gamma = 18.5\mathrm{kN/m^3}$
Coefficient of lateral earth pressure K_0	$K_0 = 1 - \sin\varphi\,, \varphi = 20°, K_0^t = 0.843$

The diaphragm wall and Soil Mixing wall

The diaphragm wall and the Soil Mixing Wall are modelled as an anisotropic elastic material to consider the discontinuities in the wall. The stiffness parameters of SMW (Soil Mixing Wall) are adopted based on experience and back analyses. The anisotropic property for the diaphragm wall $\beta = 0.1$ is selected based on the previous study in Chapter 5, while a smaller value $\beta = 0.001$ is selected for the SMW due to the looser connection between the piles. The input parameters are listed in Table 7.3.

Table 7.3 Input parameters for the retaining wall

Components	Material properties
The diaphragm wall	$E = 30\mathrm{GPa}, \nu = 0.2, \beta = 0.1$
The Soil Mixing wall	$E = 3\mathrm{GPa}, \nu = 0.2,\ \beta = 0.001$

The beams, floor slabs, and steel struts

The concrete beams and floor slabs are modelled as a linear elastic material with thermal effects. The steel struts in the bottom-up area and the exchange station area are represented by a linear elastic material. The input parameters are listed in Table 7.4.

Table 7.4 Input parameters for the horizontal support system

Components	Material properties
The beams and floor slabs	$E = 30\mathrm{GPa}, \nu = 0.2, \alpha = 10^{-5}/℃\,, \Delta T = -20℃$
The Steel struts	$E = 210\mathrm{GPa}, \nu = 0.3$

The piles and columns

The piles are columns modelled as a linear elastic material with concrete properties, with the parameters shown in Table 7.5. As indicated in the parametric studies in Chapter 4, the stiffness of vertical piles has little effect on the excavation behaviour.

Table 7.5 Input parameters for the piles and columns

Components	Stiffness properties
The piles and columns	$E = 30\text{GPa}, \nu = 0.2$

7.4 Strategy of Analyses

A strategy of analyses has been made, as shown in Fig.7.18, to organise this case study and present the results in a systematic way.

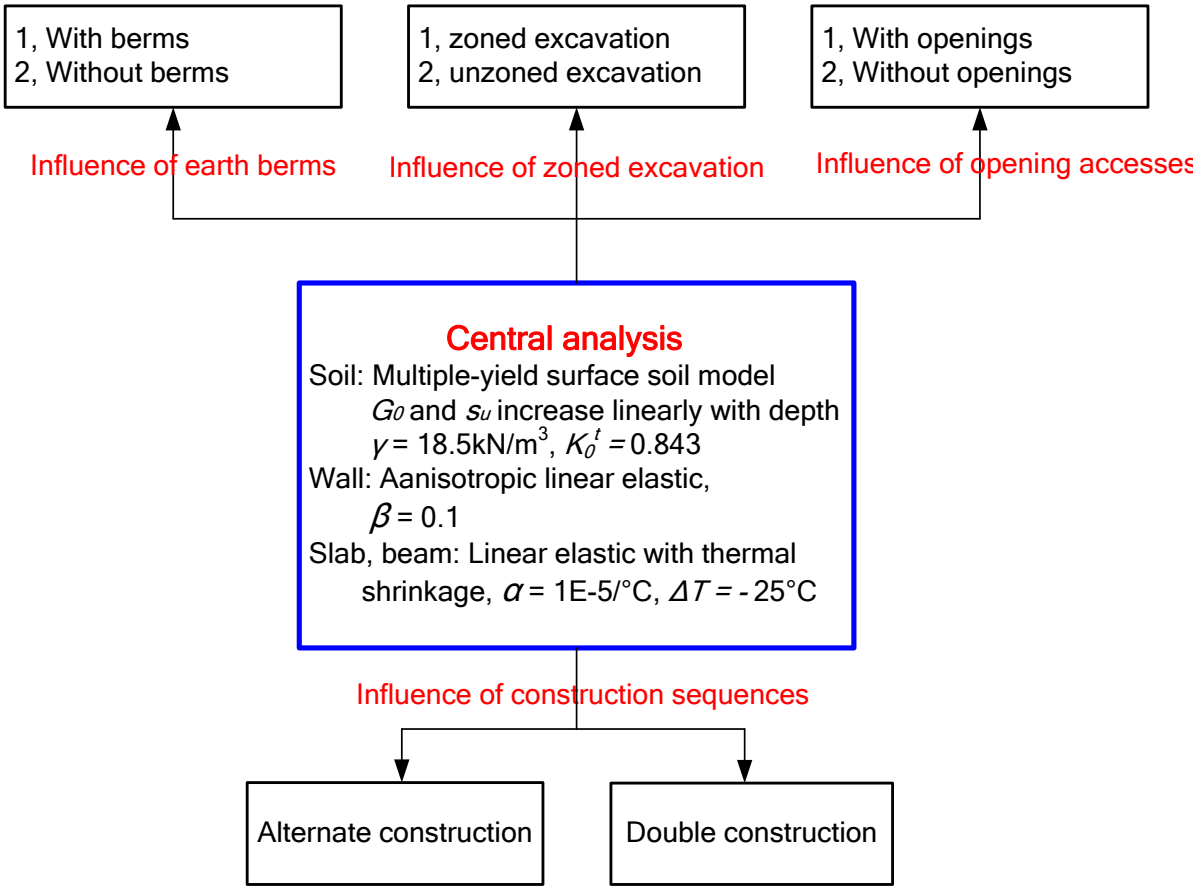

Fig.7.18 Strategy of the analyses

The central analysis is conducted first to evaluate appropriate input parameters, and calibrate with the field data. A series of parametric studies are then carried out to investigate the influence of several important aspects in deep excavations, e.g.

1) The influence of the unzoned excavation;

2) The influence of the construction sequence;

3) The influence of the earth berms;

4) The influence of the opening accesses.

The central analysis

The central analysis considers the detailed structural behaviour, and follows closely the actual construction sequence. Most of the input parameters (e.g. parameters for the soil and structural concrete components) are selected based on the understanding of the material properties and previous experiences, while some input parameters (e.g. the temperature reduction ΔT for the concrete beams and floor slabs, and the anisotropic stiffness ratio β for the retaining walls) are adjusted after initial calculations and calibrations with the field measurement.

The influence of unzoned construction scheme

The central analysis follows the zoned construction sequence, but takes a long time to run because there are a large number of analysis steps. On the contrary, if the whole layer of soil is removed at the same time followed by the installation of the horizontal support system (termed as unzoned excavation), it would greatly simplify the analysis and reduce the running time. For practical application, the unzoned construction scheme is also possible and will shorten the construction period, although it requires more input of labour and machinery. However, whether this proposed construction scheme would cause more ground movement and wall deflection is investigated through comparison with the central analysis and field measurement.

The influence of construction sequences

For a particular project, there might be several possible construction sequences, and each one will probably result in different wall deflections and ground movements. Richards and Powrie (1994) investigated the effect of different construction methods for a deep excavation through finite element analysis, e.g. open-cut, backfill, and top-down, and found significant differences in the excavation behaviour. As the soil is a nonlinear material, the variation of construction sequence might result in a different soil response. Two typical construction schemes are assumed in this chapter to explore their influence on the excavation behaviour.

The alternate excavation, as illustrated in Fig.7.19, follows the construction sequence from zone 1 to zone 10 in each level of excavation.

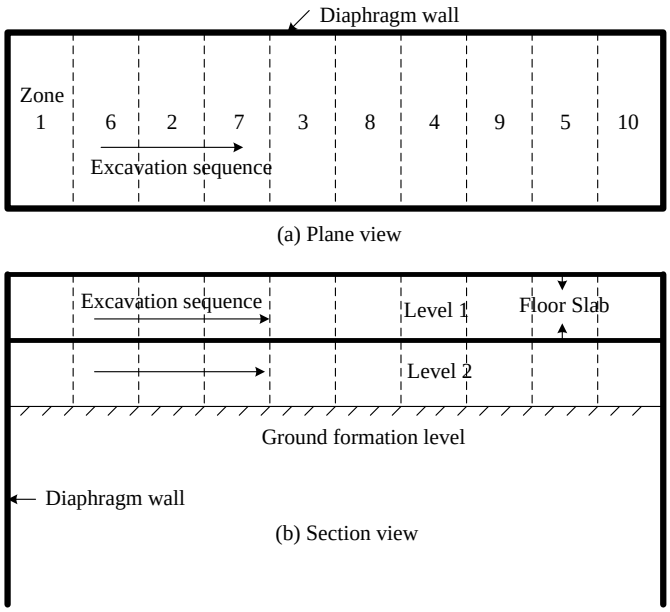

Fig.7.19 Alternate excavation

The double excavation, as shown in Fig.7.20, however, starts from the construction of zone 1 in both levels, and then moves to the next zone till the end.

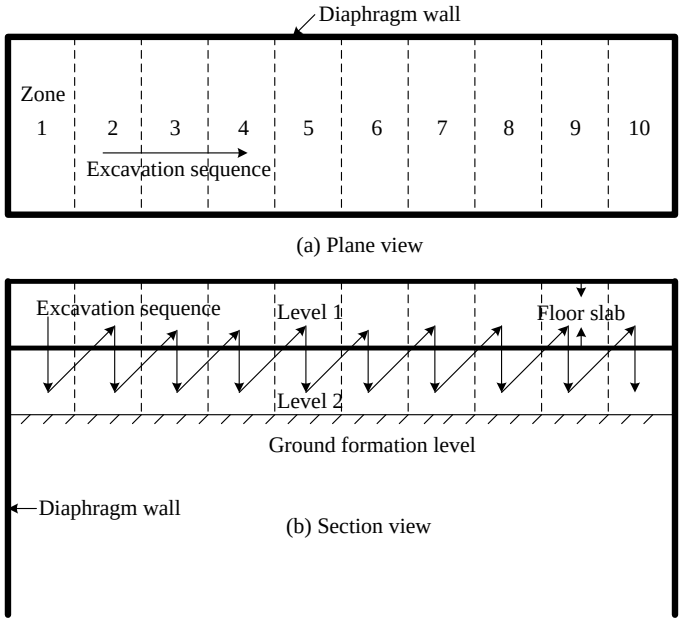

Fig.7.20 Double excavation

The influence of earth berms

Earth berms were used at the North side against the diaphragm wall during the excavation, as shown in Fig.7.8, to restrain the lateral movement of the diaphragm wall and hence the ground movement outside the excavation. The effectiveness of earth berms in the excavation has been

studied by several researchers both experimentally and numerically (Clough 1977, Georgiadis and Anagnostopoulos 1998, Gourvenec and Powrie 2000, Powrie and Daly 2002), and the results indicated that earth berms provide lateral support and increase the embedment depth of the retaining wall. However, the excavation with earth berms also complicates the construction process, and might postpone the construction period and increase the cost of the project. To investigate the influence of the earth berms, one analysis without earth berms was carried out to compare with the central analysis and field measurement.

The influence of opening accesses

The opening accesses in the floor slabs are not always considered explicitly in the numerical analysis of top-down deep excavations, probably due to the complexity in the modelling process, and some simplified methods were used instead, for instance, reducing the stiffness of the floor slabs (Simpson 1992, St. John, Potts et al. 1993). However, the reduced stiffness of the whole slab cannot represent the regional weakness in the slab due the openings. The openings were modelled explicitly in the central analysis. To investigate the influence of the openings, one analysis was conducted without any openings in the floor slabs, and the results are compared with the central analysis and field data.

7.5 Interpretation of results

Due to the large amount of data from both numerical analyses and field measurement, only selected results from the final stage of the excavation are presented, including wall deflections at four critical positions (I-6, I-12, I-25, I-44), ground settlement outside the excavation along BC, soil lateral deformation at IT-10, and vertical displacement of the top floor slab.

7.5.1 Central analysis

Wall deflections

The wall deflection at four critical positions is shown in Fig.7.21. As discussed in Chapter 5, the wall deflections from the field measurement can only reflect the pattern of the wall deformation, because the wall movement was assumed zero at the toe and only inclinometer reading was taken.

As the total wall deflections are not know, the results from the numerical analyses are adjusted to calibrate with the field data, in which the wall deflections at the toe are deducted from the total wall deflections. In general, the agreement between the numerical results and the field data is satisfactory. It is noted, however, that the computed wall deflection at I-12 is much smaller than the field measurement. When compared with the wall deflection at I-25, the smaller wall deflection at I-12 is reasonable because the diaphragm wall is shorter and the excavation depth is smaller on the I-12 side. The relatively large wall deflection at I-12 from field measurement might be caused by some unexpected reasons such as the construction quality, and the accuracy of the field measurement.

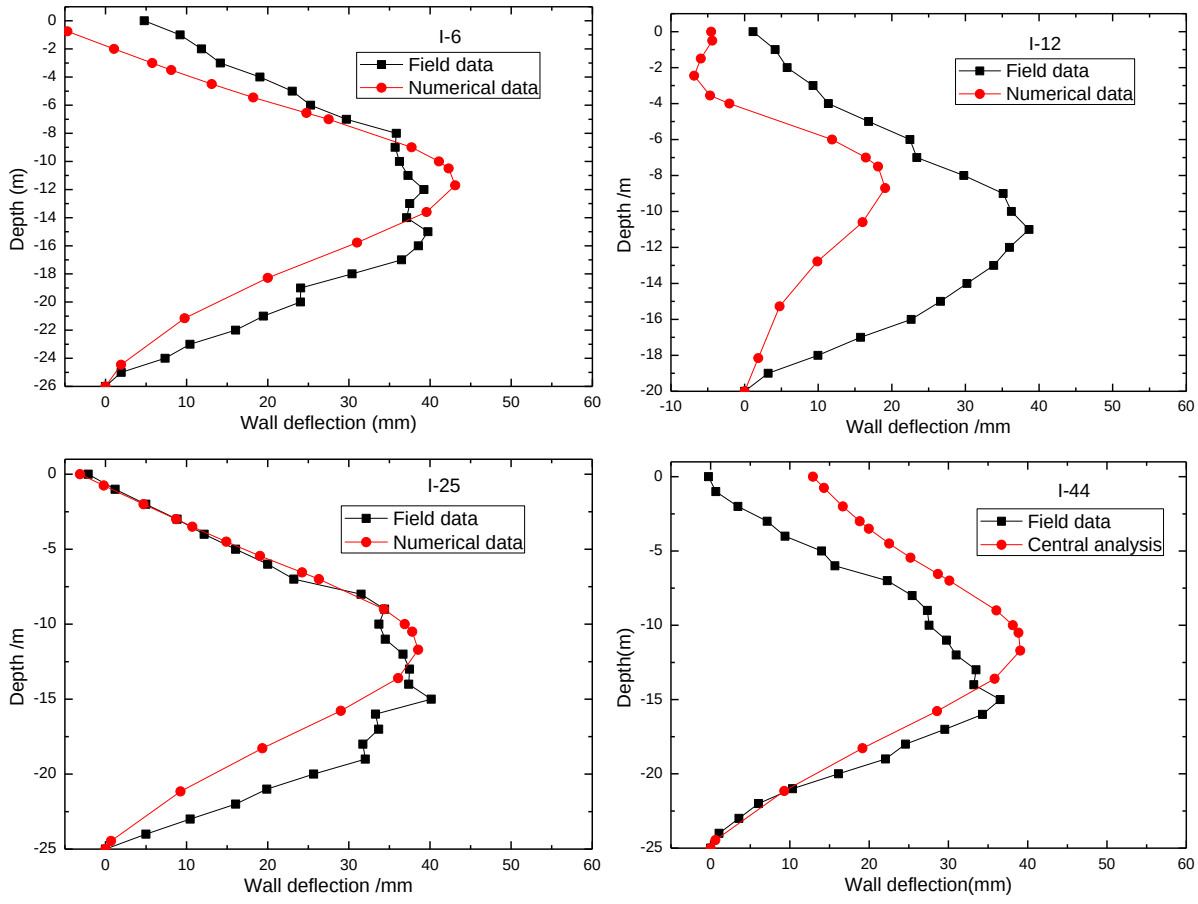

Fig.7.21 Wall deflections at four different points

Ground settlement

The computed ground settlement outside the excavation along BC on the north side, as shown in Fig.7.22, agrees well with the field measurement, although it is slightly smaller close to B than the field data. This discrepancy might be caused by the relatively large anisotropic stiffness ratio

($\beta = 0.1$) used for the diaphragm wall. When a smaller β is adopted, the ground settlements around points B and C are expected to be larger, and closer to the field data.

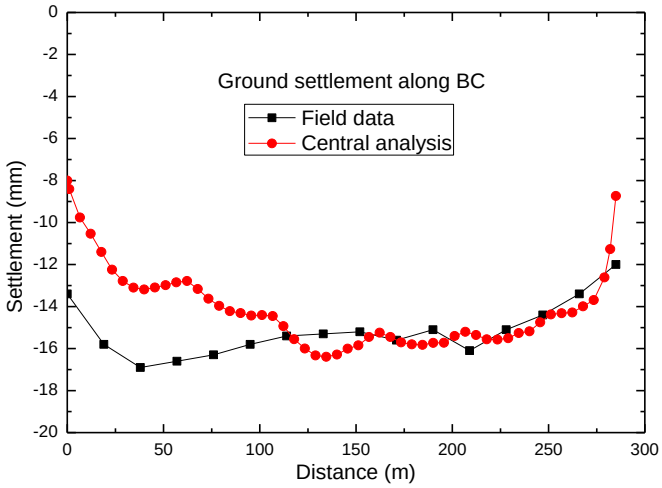

Fig.7.22 Ground settlement around the excavation along BC

Soil lateral movement

The computed soil lateral displacement at IT-10, as shown in Fig.7.23, is larger than the field measurement down to a depth 16m below ground level, and slightly smaller below the depth of 16m from the ground level. The computed maximum soil deflection is about 5mm larger, and occurs at a depth around 6m higher, than the field data. In general, the agreement is acceptable.

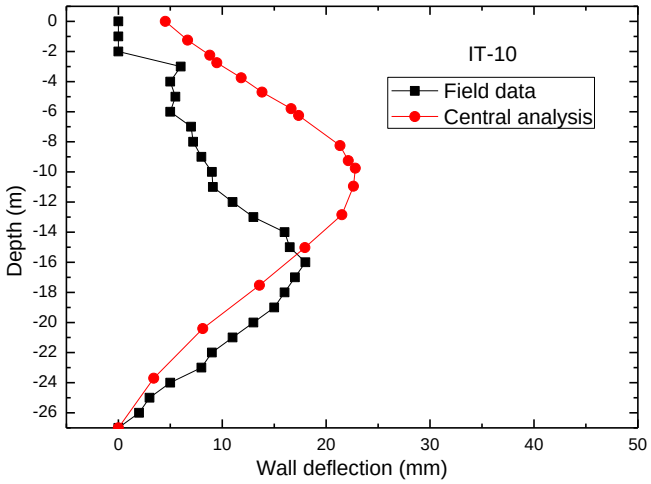

Fig.7.23 Soil lateral displacement at IT-10

Vertical displacement of piles and floor slab

The vertical displacement at the top floor slab is shown in Fig.7.24. The computed vertical displacement is upward, which is in contrast with the settlement from field measurements. The maximum settlement of the roof slab in the field measurement is 18mm, whereas the maximum heave of roof floor slab from the numerical analysis is around 22mm. Probably this is because

the contact between the soil and piles is not considered in the model, which means that slip is not allowed at the soil/pile interface and piles move upwards with the soil due to the stress relief. The settlement of piles in the field might be caused by other reasons during the construction, which are neglected in the numerical analysis. For example, the piles might penetrate into the weak layer of soil at the toe of the piles. It is also noted in the numerical analysis that there are two small areas of settlement. They are caused by the self-weight of the floor slab, because in those areas the floor slab is not supported by piles due to the simplicity to model the slope in the roof floor slab. Therefore, the two small areas of settlement can be ignored.

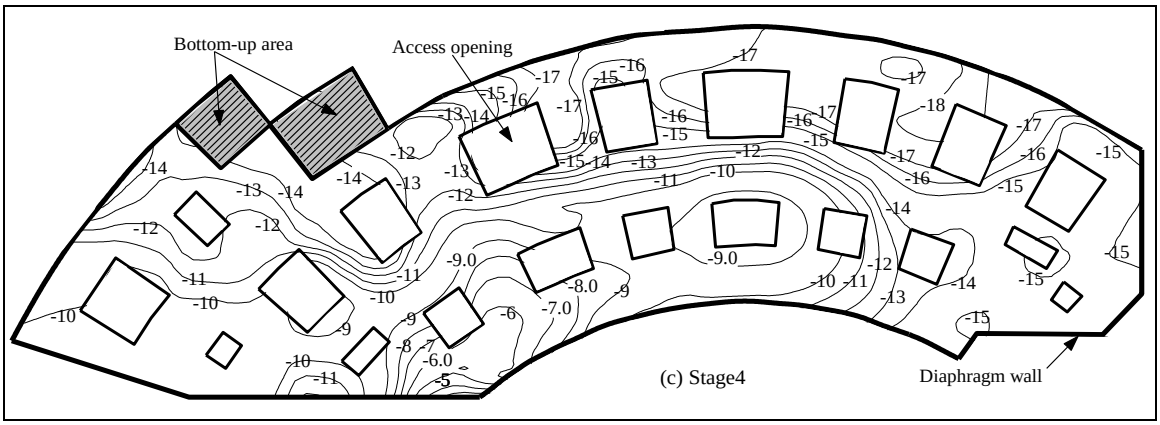

(a) Field measurement (Xu 2007) (unit: mm)

(b) Numerical results from central analysis

Fig.7.24 Vertical displacement at the roof floor slab (unit:m)

Contour display

The displacement contours of the soil and the retaining structures at the final stage of the construction are displayed in the following figures. It is clearly seen from Fig.7.25 that the ground settles (negative displacement) outside the excavation and heaves (positive displacement) inside the excavation, and relatively larger ground settlement occurs behind the centre of the wall than behind the corner, because of the corner effect. Fig.7.26 shows that the wall deforms more

close to the centre of the wall, and less close to the corner, and that the wall next to the Main Station deforms less than the side far from the Main Station. The vertical displacement of the supporting system in Fig.7.27 and roof floor slab in Fig.7.28 shows that the upward heave dominates the displacement, and the heave is larger in zone 1 and zone 2, and on the side away from the Main Station.

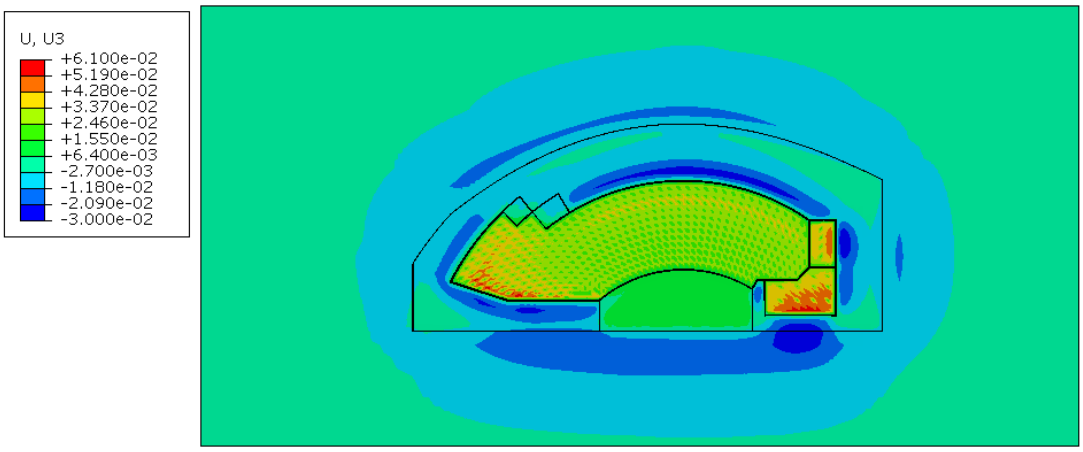

Fig.7.25 Vertical displacement of the soil (unit:m)

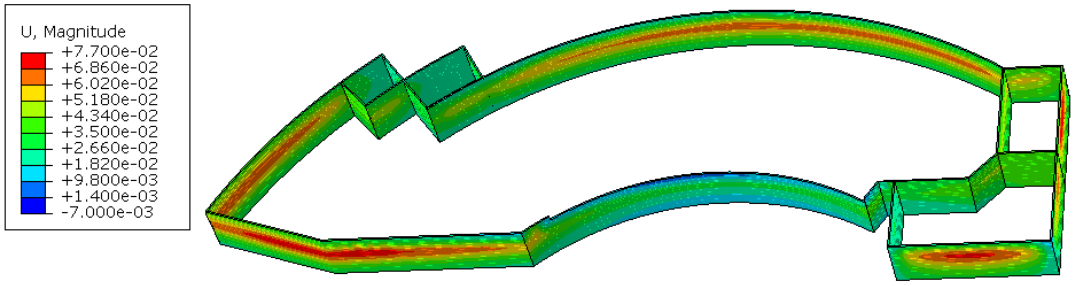

Fig.7.26 Displacement magnitude of the diaphragm wall (unit:m)

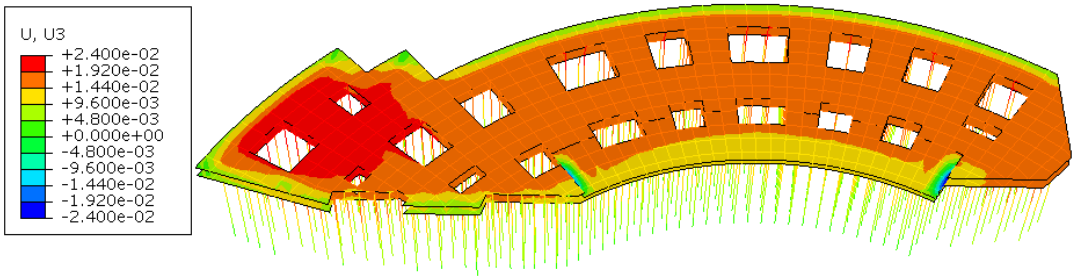

Fig.7.27 Vertical displacement of the support system (unit:m)

Fig.7.28 Vertical displacements of the top floor slab (unit:m)

7.5.2 Influence of the unzoned excavation

The results from the unzoned excavation are compared with the central analysis and field measurement in the figures below, followed by comments and discussions.

Wall deflection

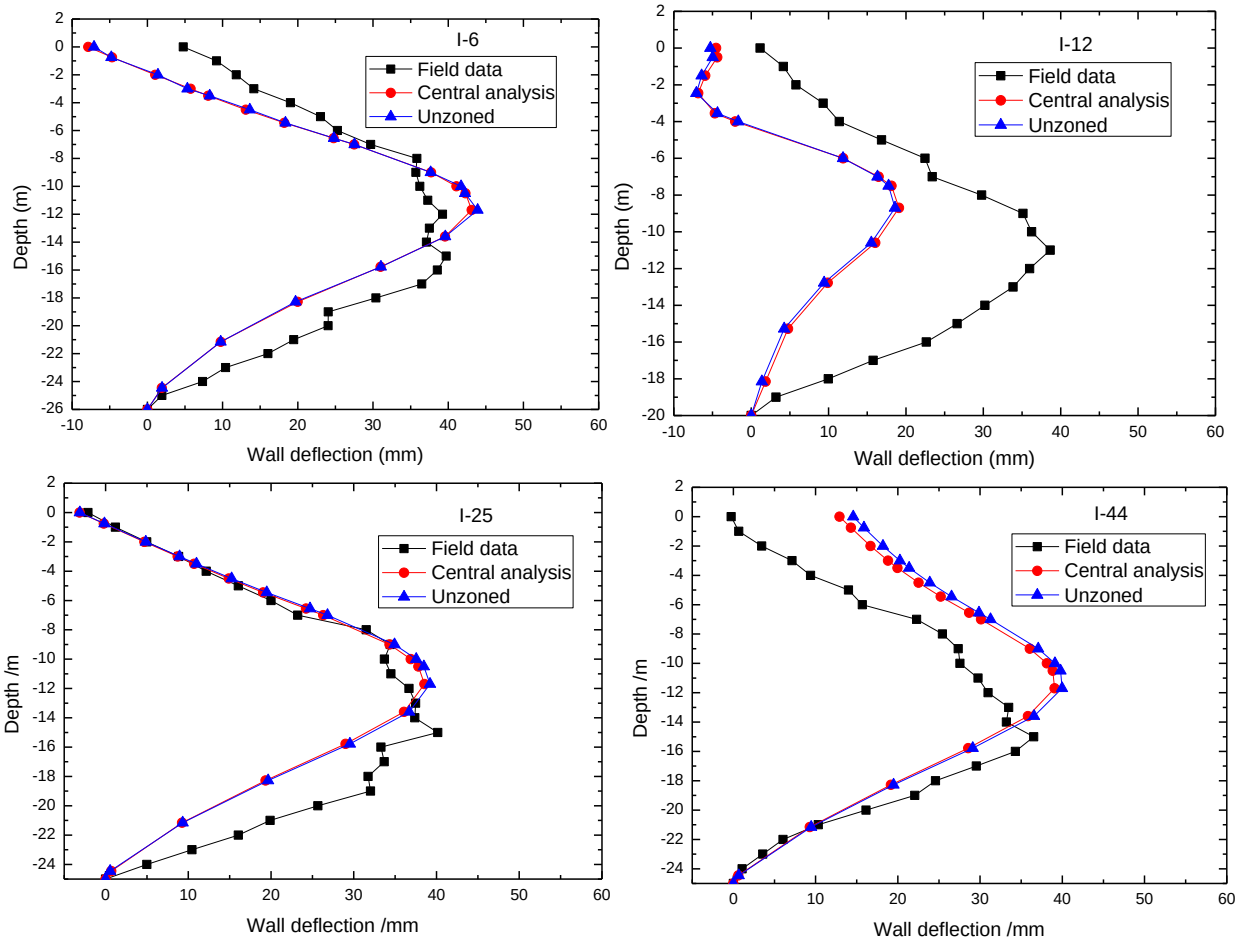

Fig.7.29 Wall deflections

Ground settlement

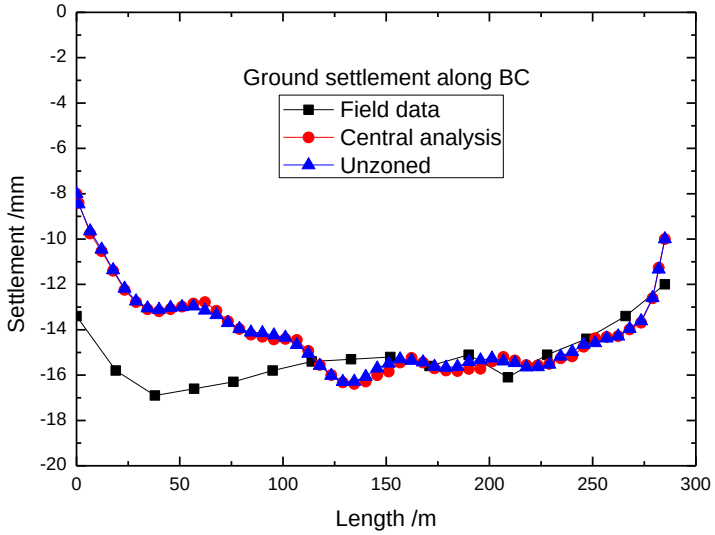

Fig.7.30 Ground settlement along BC

Soil lateral movement

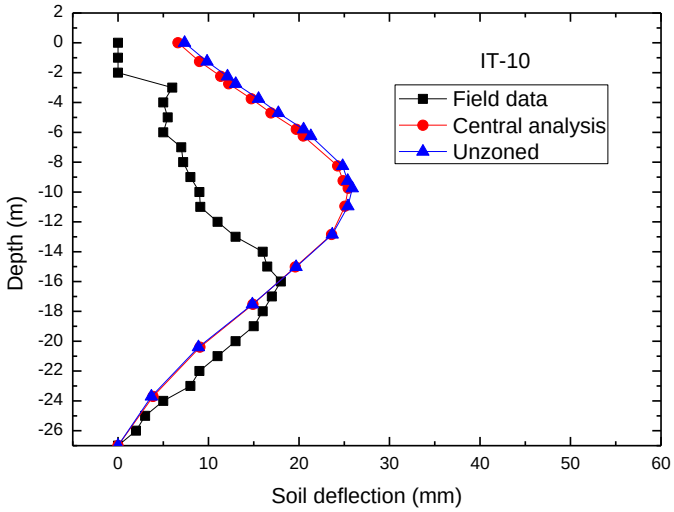

Fig.7.31 Soil lateral movement

Comments and discussions

As shown from Fig.7.29 to Fig.7.31, the results are almost identical between the zoned and unzoned excavation in terms of the wall deflections at the four selected positions, the ground settlement outside the excavation along BC, and the soil lateral displacement at IT-10. However, the unzoned excavation has many fewer steps of analysis, and takes much less time to run, thus is computationally cheap and time efficient. This indicates that for practical applications, the zoned construction sequence can be ignored in the initial assessment of the computed results, and to evaluate the appropriate input parameters.

7.5.3 Influence of construction sequences

The results from the two proposed construction sequences are shown in the following figures from Fig.7.32 to Fig.7.34.

Wall deflection

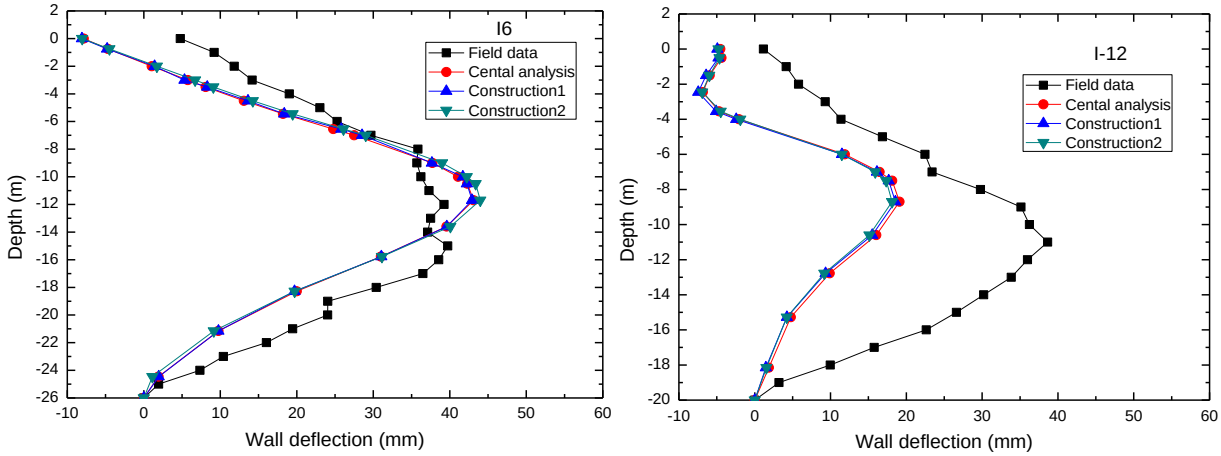

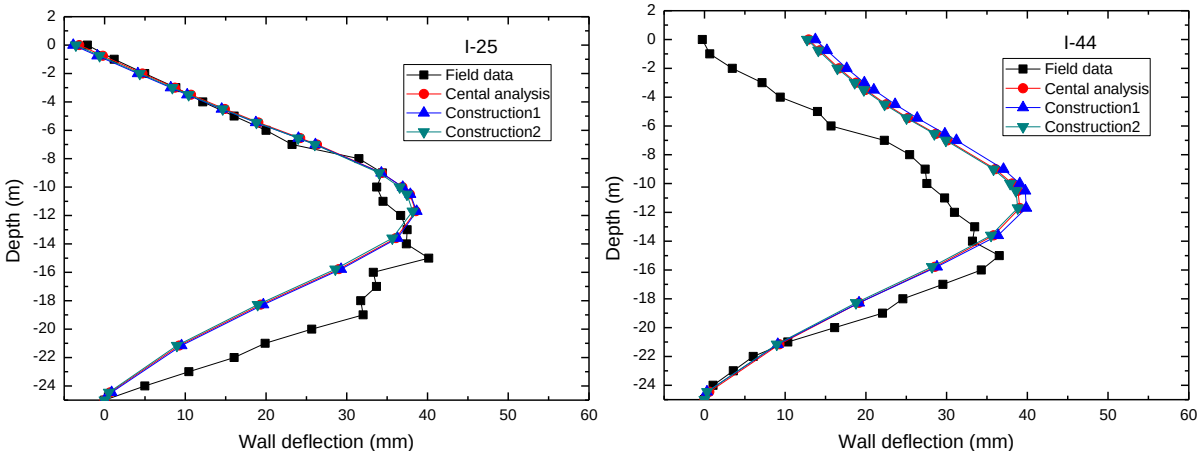

Fig.7.32 Wall deflection

Ground settlement

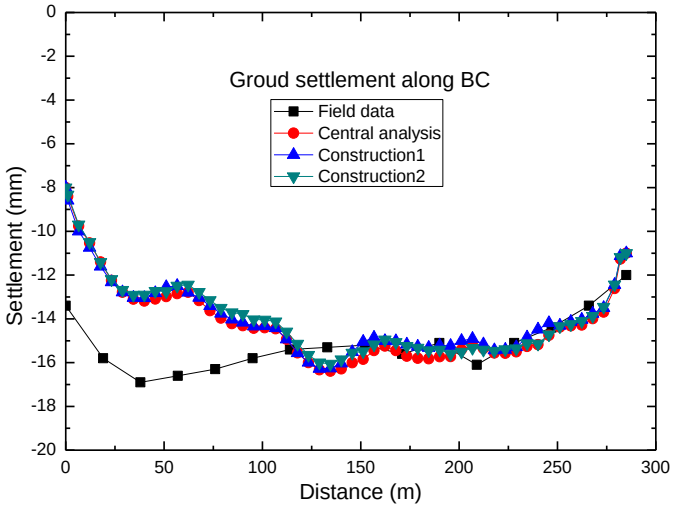

Fig.7.33 Ground settlement along BC

Soil lateral movement

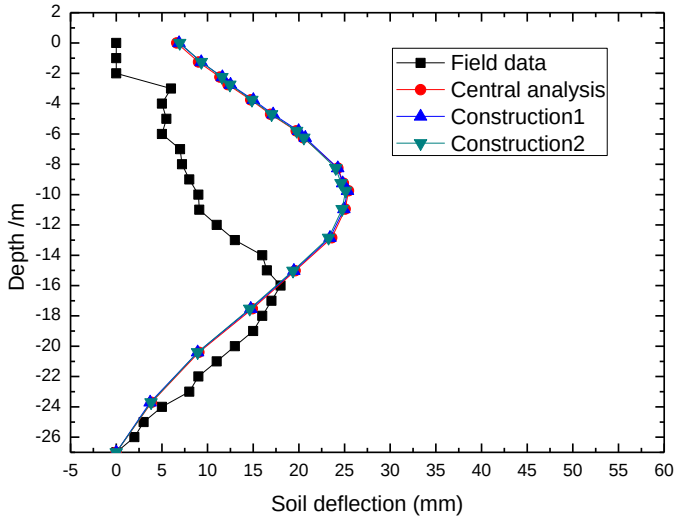

Fig.7.34 Soil lateral deflection

Comments and discussions

The results indicate that there is no significant difference between the two proposed construction sequences in terms of the wall deflections at four selected positions, the ground settlement

outside along BC outside the excavation, and the soil lateral deformation at IT-10. The results, contrary to the expectation, indicate that there is little effect of construction sequences on the ground and wall deformation at the final stage of the excavation. However, please note that there are presumably differences in the transient deformations at different stages of the excavation. This suggests that construction sequences may be not important to the deformation characterises of deep excavations, and efforts can be put into other aspects such as cost of the construction, and construction period.

7.5.4 Influence of the earth berms

Wall deflection

Through the comparison of the wall deflection at four positions as shown in Fig.7.35, it is suggested that the earth berms can significantly reduce the wall deflection up to 20% depending on the position of the wall. The wall deflection at I-12 is not affected because there are no earth berms on this side.

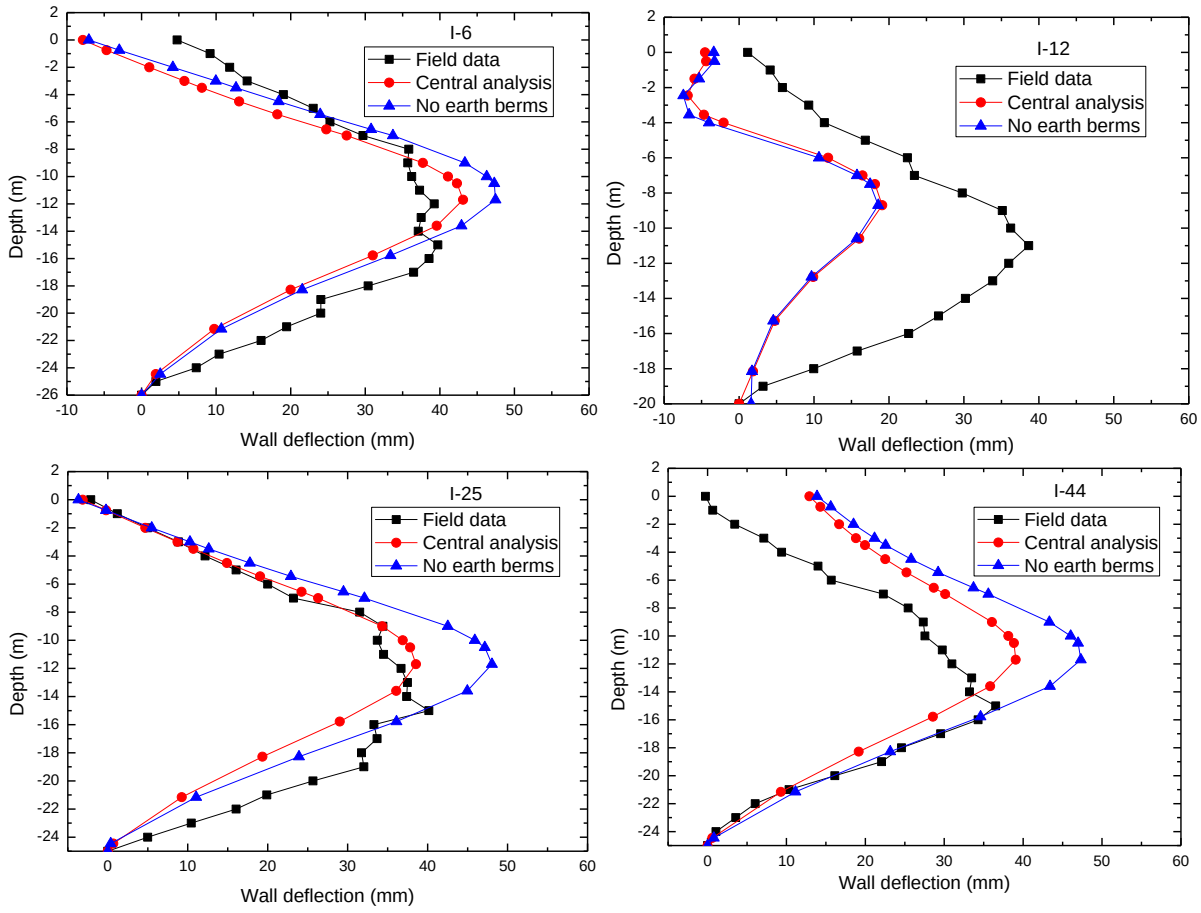

Fig.7.35 Wall deflections

Ground settlement

As shown in Fig.7.36, the ground settlement along BC is much smaller than the central analysis in which the earth berms are used. This result is consistent with the wall deflection shown in Fig.7.35, because the earth berms restrain the wall deflection and induces less ground movement.

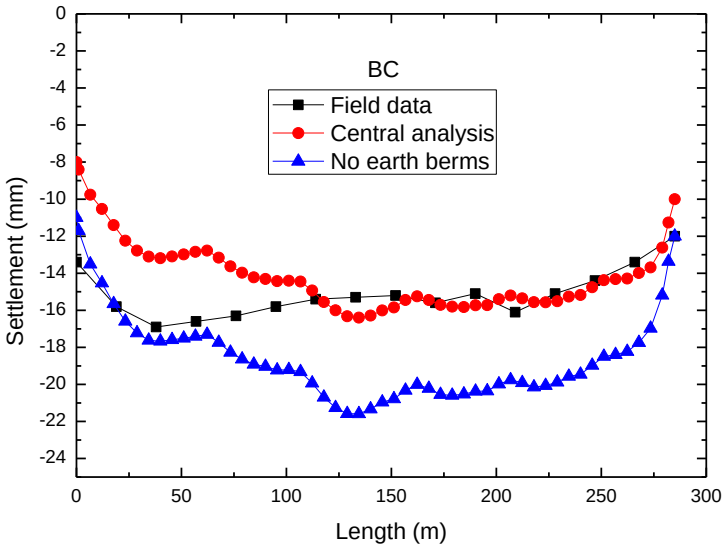

Fig.7.36 Ground settlements along BC

Soil lateral movement

Figure 7.7 shows that the soil lateral deflection at IT-10 is also significantly reduced when the earth berms are used in the excavation.

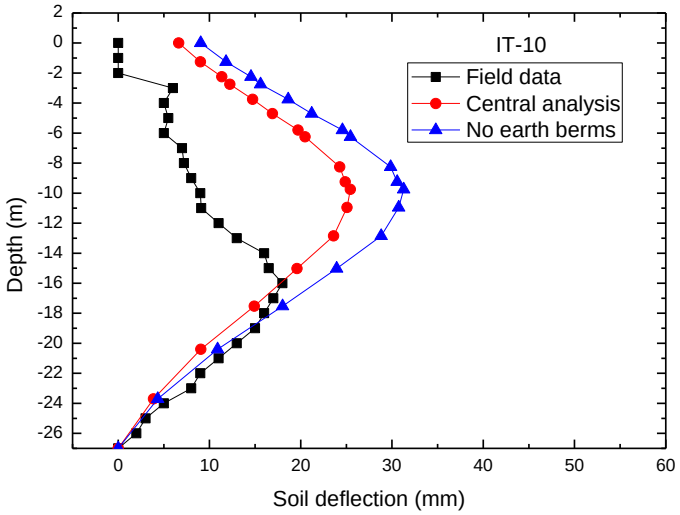

Fig.7.37 Soil lateral deflection

Comments and discussions

It has been shown that earth berms are very effective in reducing the wall deflections and ground movements, suggesting that they can be used when the displacement is a concern.

7.5.5 Influence of opening access

Wall deflection

The deflection of the diaphragm wall at four positions in Fig.7.38, confirms that the openings in the floor slabs reduce the overall stiffness of the retaining system and enlarge the wall deflection. The wall deflection at I-12 and I-44 is not significantly affected, probably because the openings do not reduce the regional stiffness of the retaining system close to those two positions.

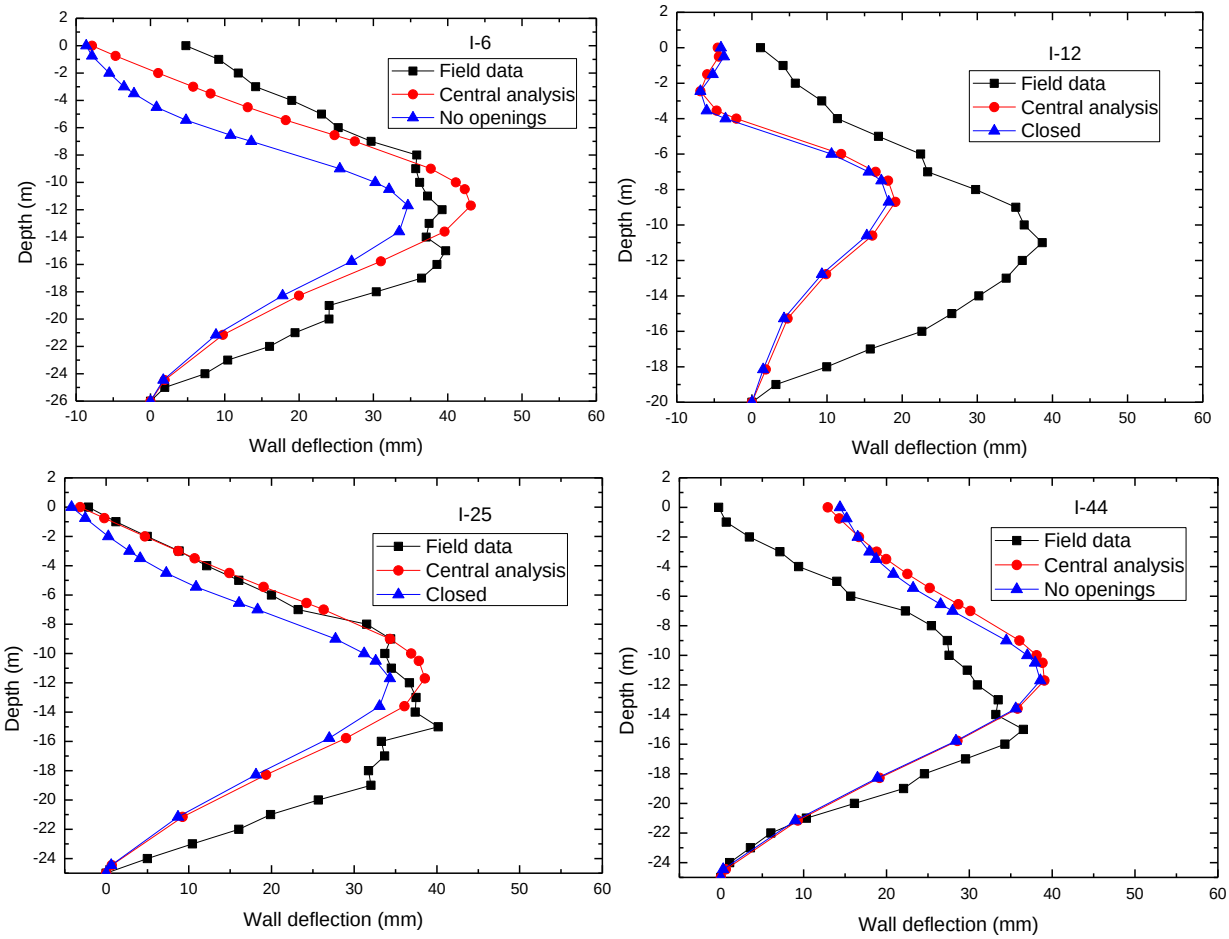

Fig.7.38 Wall deflections

Ground settlement

As shown in Fig.7.39, the computed ground settlement along BC outside is smaller when there are no openings in the floor slabs. It is also noticed that the ground settlement is larger in the region close to the openings, which means that the openings modify both overall and regional ground settlement outside the excavation.

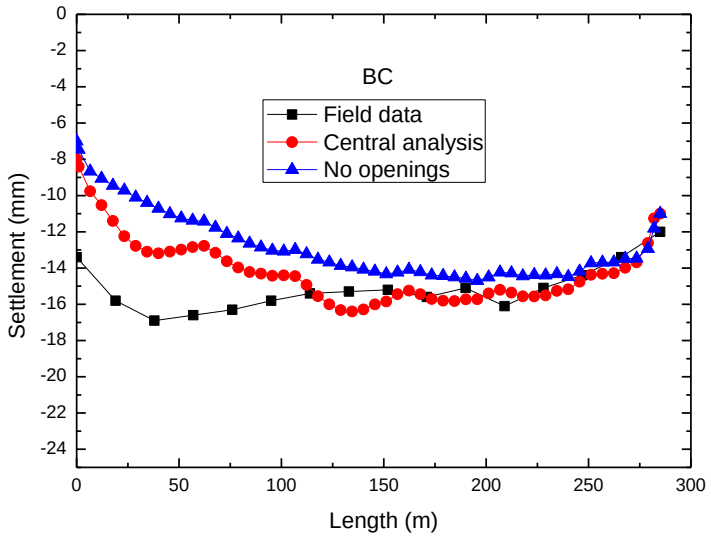

Fig.7.39 Ground settlements along BC

Soil lateral movement

Not surprisingly, Fig.7.40 shows that the soil lateral deflection at IT-10 is larger from the central analysis in which the openings are modelled explicitly.

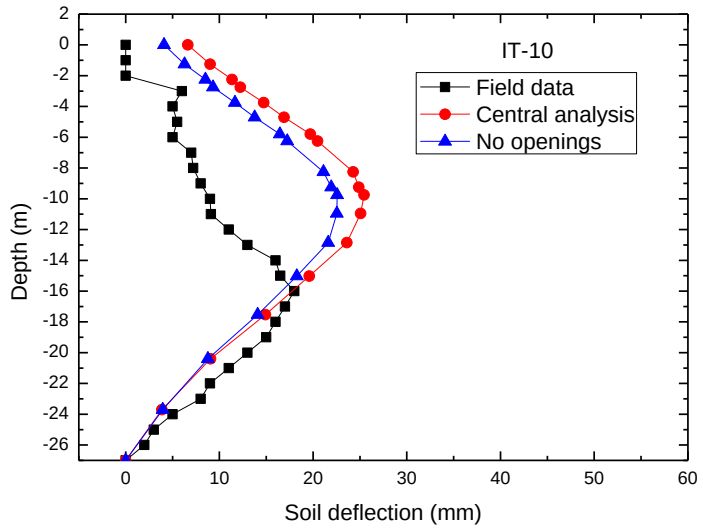

Fig.7.40 Soil lateral deflection

Comments and discussions

The results indicate that the openings in the floor slabs reduce the stiffness of the support system and result in larger wall deformations and ground movements. It is suggested that the openings should be included in the modelling process to obtain more accurate results. Although reducing the stiffness of the supporting system is a simplified way of considering the openings, the reduction factor is an uncertain parameter and largely depends on the size and distribution of the openings. In addition, this method cannot account for the regional weakness in the floor slabs caused by the openings.

7.6 Conclusions

This chapter shows again that advanced finite element analysis can capture the performance of this complex deep excavation very well. This is attributed to the consideration of a number of important aspects in the analysis such as (i) the detailed structural behaviour, e.g. the geometry of the retaining system, construction joints in the diaphragm wall, openings in the floor slabs, and thermal shrinkage of concrete beams and floor slabs, (ii) the actual construction sequence, e.g. top-down construction method, zoned and layered excavation sequence, and earth berms, and (iii) reliable material models and input parameters, e.g. small-strain stiffness nonlinearity, variable stiffness and strength parameters, and thermal effects. A series of parametric studies have been carried out to investigate the influence of several important aspects in the modelling procedure of deep excavations, e.g. the unzoned excavation, the variation of construction sequences, earth berms in the excavation, and opening accesses in the floor slabs. Some conclusions can be generated for practical use:

1) The assumed unzoned excavation produces almost identical results at the final stage of excavation to the central analysis which follows the zoned construction sequence, but it greatly simplifies the analysis and significantly reduces the time for calculations. This indicates that the simplified analysis can be used for initial calculations to calibrate the computed results with field data, and to optimise some undetermined input parameters.
2) The proposed two construction sequences result in almost the same wall deflections and ground movements at the final stage of excavation as the central analysis which follows the actual construction sequence, which is contrary to expectations, suggesting that there is little effect of construction sequence on the final deformations. However, please note that there are presumably differences in the transient deformations. For practical applications, engineers may need to pay more attentions to other factors such as the convenience for the construction, the cost of the project, and the construction period, rather than the construction sequence.

3) The use of earth berms in the deep excavation can effectively reduce the wall deflection and ground movement, compared to the excavation without earth berms. Especially when the excavation is situated close to important urban infrastructure and the excavation-induced ground movement is the major concern, excavation with earth berms is an effective way to mitigate the detrimental impact on the adjacent infrastructure induced by the ground movement. However, other factors such as the cost, and the construction period, should also be taken into account. In the numerical analysis, the earth berms need to be considered in detail in the modelling procedure; otherwise, the computed results are not reliable.

4) The opening accesses in the floor slabs are required in the design of top-down excavations to transport the excavated soils and improve the lighting and ventilation condition, but they also reduce the overall stiffness of the retaining system and cause larger wall deflection and ground movement. Therefore, the size of the openings needs to be considered carefully in the design process, on the balance between the convenience of construction and the potential increase in wall deformation and ground movement. In the numerical analysis, the openings need to be modelled explicitly in the modelling process to obtain more reliable results.

5) It is noted that the vertical heave of the roof floor slab from the numerical analysis is in contrast with the settlement from the field measurement. This is because the soil/pile contact is not considered in the numerical analysis, and the piles move upward with the soil due to the stress relief. If the slip is allowed at the interface between the soil and piles, the vertical heave of the floor slab is expected to be smaller, and settlement may happen. In general, as discussed in chapter 4, neglecting the soil/pile contact in the analysis would underestimate the wall deflection and ground movement, but the influence is relatively small. In this case study, there are thousands of piles in the excavation, considering the soil/pile contact would greatly increase the complexity of the analysis.

Chapter 8 Conclusions and recommendations

8.1 Conclusions

This thesis is concerned with evaluation of the capability of advanced finite element analysis in reproducing the observed performance of deep excavations in the field through detailed case history studies. Advanced finite element analysis is able to satisfy all the theoretical requirements, include a realistic soil constitutive model, incorporate proper boundary conditions, consider complex construction sequences, and provide information on all design requirements. Well-documented case histories reflect the real behaviour of deep excavations and provide valuable data to calibrate the numerical analysis. The 3D effect in deep excavations is obvious and significant, so 2D analysis may oversimplify the problem and thus lose the accuracy. However, most 3D analyses in literature are simplified square excavations, and are concerned with corner effects. Fully 3D analyses which consider the geometry of the excavation, detailed retaining structure, and actual construction sequence, are rarely seen in publications, and comparison with case history data is even rarer. In addition, advanced soil models are not commonly used in these analyses. To overcome these shortcomings, fully 3D finite element models are developed in this thesis, and an advanced soil model is selected to represent the soil. Two typical case histories are collected from Shanghai for case studies.

The previous chapters have investigated the performance of deep excavations and the influence of various key aspects through parametric studies on a simplified excavation and detailed analyses of two more complex case histories. These studies provide insight into this complex soil-structure interaction problem, and have practical implications on the design and analysis of deep excavations. Each chapter has given detailed discussions and conclusions separately. These conclusions are synthesised in this chapter to give a more comprehensive summary.

1) Advanced finite element analysis is an effective way to investigate the performance of deep excavations, in which detailed geotechnical and structural aspects such as (i) the

geometry of the excavation, (ii) structural components of the retaining system, (iii) ground conditions, (iv) sophisticated soil behaviour, and (iv) actual construction sequence, can be accounted for adequately. The capability of advanced finite element analysis in replicating the observed performance of deep excavations in the field has been evaluated in a comprehensive way through calibration with field measurements from two well-documented case histories in Shanghai, as shown in Chapter 5, Chapter 6, and Chapter 7, and the results obtained are promising. The standard procedure of advanced finite element analysis of deep excavations is described in Chapter 3, which includes modelling (i) the soil and structural components (both geometry and material properties), (ii) the soil-structure interface behaviour, (iii) boundary conditions, and (iv) the construction sequence. Some important issues in regard to the modelling process of deep excavations are discussed in Chapter 4, such as (i) selection of element types for the soil and structures, e.g. linear or quadratic elements, full or reduced integration, solid or shell elements to model the retaining wall, and solid or beam elements to model the pile, (ii) the operational stiffness of concrete structural components due to imperfections in the concrete such as cracks, (iii) thermal effects of horizontal support system, i.e. concrete beams and floor slabs, (iv) construction joints in the retaining wall, (v) the soil-structure interface behaviour, (vi) variation of stiffness and strength properties of the soil, and (vii) reliability of the simplified and improved analysis.

2) Research and practice have shown that accurate prediction of the performance of deep excavations, especially the ground movement, requires a realistic soil model that is able to consider the small-strain stiffness nonlinearity of the soil, which is confirmed again in this thesis. In addition, the soil model adopted needs to be calibrated with soil properties corresponding to geotechnical conditions in the construction site. Important features in the retaining structure, e.g. construction joints in the retaining wall, cracks in the concrete structural components, thermal effects of horizontal beams and floor slabs, have

significant influence on the excavation behaviour, and they can also be considered in the constitutive model for the structure. Moreover, a realistic contact model at the soil-structure interface is required to take into account the influence of the interface behaviour.

3) Detailed parametric studies, based on a simplified model which includes basic features of deep excavations, are necessary to understand the influence of various important aspects in deep excavations, and should be conducted before more sophisticated case studies. There are several advantages of this process, (i) it is easier to build up the model and less time-consuming to run the calculation, (ii) more details can be looked into, (iii) certain aspects which are difficult to account for in complex case studies, e.g. soil/wall contact and soil/pile contact, can be investigated more easily, (iv) numerical problems can be identified and solved more conveniently, and (v) skills and experiences learnt in this process are useful preparation for the more complex case history studies.
4) The parametric studies in Chapter 4 suggest that (i) although linear elements with reasonably fine meshes in the analysis produce similar patterns in the computed deformations compared with corresponding quadratic elements, linear elements suffer from shear locking and will produce too stiff response and over-predict the strength in some geotechnical problems, so higher order elements are recommended for more accurate analysis, (ii) solid elements are preferred to model the retaining wall, because shell element wall results in larger wall deflection and ground movement, and (iii) beam elements are more suitable to model piles when the soil/pile interface behaviour is not considered. The results also indicate that the computed wall deflections and ground movements are sensitive to (i) the operational stiffness of concrete structural components (i.e. the retaining wall, the horizontal beams and floor slabs) affected by imperfections such as cracks, (ii) the soil-structure interface behaviour, especially the shear resistance at the interface, (iii) thermal effects of concrete beams and floor slabs during curing process and due to the ambient temperature change, (iv) discontinuities in the retaining wall, and

(v) stiffness and strength properties of the soil. Neglecting any of these effects may affect the accuracy of the analysis, but considering all of them in one analysis may not be practical to use. Engineers need to decide which aspects are more important in a specific problem, and address these issues in the analysis with moderate level of complexity.

5) Case history studies are much more sophisticated than simplified parametric analysis, so appropriate simplifications and assumptions are necessary in the modelling procedure to reduce the complexity of the problem and avoid any numerical instability. For instance, the installation process of the diaphragm wall and bored piles is not modelled as Wished-In-Place (WIP), so the installation effect is not considered. When presenting the results, the ground and building movements induced in this process are deducted from the total movements in the field data, to consider only the effect of excavation. In addition, the soil-structure interface behaviour is also neglected in the case studies. To compensate this inaccuracy, the numerical results are calibrated with the field data through adjusting the undetermined parameter, ΔT, the temperature change for the shrinkage of concrete beams and floor slabs. There may be some limitations of this method, but it will not affect the general conclusions drawn from the parametric studies.

6) The first case study in Chapter 5, the basement excavation for the Shanghai Xingye Bank building, shows an example of fully 3D analysis of deep excavations using top-down construction method. Various aspects in the final displacement are examined, e.g. wall deflections at the wall centre and corner, the wall vertical movement, and ground settlements both perpendicular and parallel to the excavation. The results confirm that (i) the shell element wall results in larger (20% in this case study) wall deflections and ground movements compared to the solid element wall, (ii) thermal effects of concrete beams and floor slabs have a significant influence on the excavation behaviour, and (iii) the anisotropic wall approach is an effective way to consider the construction joints in the diaphragm wall, and the anisotropic ratio 0.1 is a good value for the diaphragm wall in

this case study. Results also found that the computed results are affected by (i) the initial horizontal stress state in the ground, and (ii) the capability of considering the small-strain stiffness nonlinearity in the soil model.

7) The extended case study in Chapter 6, including adjacent buildings, ground improvement and buried pipelines in the model, is an example to investigate the deformation of adjacent infrastructure induced by deep excavations. The main characterises of the deformation of buildings and pipelines are captured by the numerical analysis, and the parametric studies have shown that (i) the building weight has a large influence on the magnitude of the building settlement, (ii) the building stiffness has a relatively small influence and mainly affects the pattern of the settlement, iii) the stiffness of the raft foundation seems to have minor influence on the building settlement, but the piles underneath may have certain influence. This suggests that for an accurate prediction of the building settlement, (i) the building weight should be well estimated, and (ii) more information is needed about the foundation of the building. The results also indicate that (i) the ground improvement between the diaphragm wall and the adjacent buildings has little influence on the building settlement, probably because the ground improvement is relatively flexible compared with the soil, (ii) the buried pipeline generally follows the ground movement, and has a similar settlement pattern with but a larger magnitude than the ground surface settlement above the pipelines, probably due to the swelling of the soil, and (iii) the settlement of buried pipelines is not sensitive to the stiffness, wall thickness, and diameter of the pipeline. This indicates that the ground improvement and buried pipelines can be neglected during the modelling process. In practical applications, the effectiveness of the ground improvement should be revaluated, and increased cost also needs to be considered. The settlement of buried pipelines is suitable to be represented by the ground surface settlement over the pipeline.

8) A more complex case history, the North Square of Shanghai South Railway Station, is

analysed in Chapter 7, and the focus is on the effects of construction sequence, earth berms, and opening accesses. The results indicate that (i) a simplified analysis without considering the excavation sequence can be used for initial calculations to check the results and calibrate some undetermined input parameters, because there is no significant difference with the detailed analysis and it takes much less time to run, (ii) there is little effect of construction sequences (proposed in this case study) on the displacement at the final stage of the excavation, and more consideration may be put on other factors such as the convenience for the construction, the cost of the project, and construction time, rather than construction sequences, (iii) the use of earth berms in deep excavations can effectively reduce the wall deflection and ground movement, but other factors should also be considered, e.g. obstruction to the excavation, and construction time, and (iv) the openings in the floor slabs reduce the overall stiffness of the retaining system and result in larger wall displacement and ground movement, so the size of openings should be considered carefully in the design, and the openings should be modelled explicitly in the modelling process to obtain more accurate results.

8.2 Limitations in the analyses and recommendations for future work

Although a number of issues have been addressed in this thesis and various useful conclusions are drawn, there are still some limitations in the analyses and unsolved problems worth further investigation. These limitations are presented here, together with some recommendations for future research.

1) Linear elements are used extensively in this thesis, for example, in parametric studies in Chapter 4 for consistency purposes and to avoid numerical instabilities caused by quadratic elements in contact analysis in ABAQUS, and in complex case studies from Chapter 5 to Chapter 7 so that complicated geometries could be modelled with the limited computer resources available. However, as discussed earlier in Chapter 4, linear elements have deficiencies and are particularly susceptible to shear locking when

modelling almost incompressible material, like soil in undrained conditions. They will produce too stiff response which results in smaller displacements, and over-predict the strength in some geotechnical problems. This is one limitation of the analyses in this thesis and one possible reason for the discrepancy between the numerical results and field measurements. Therefore, linear elements should be avoided in the future analyses, and higher order elements will be used.

2) The wall installation process is modelled as Wished-In-Place in the thesis, but actually the installation effect is evident and important as shown in both field measurements and previous numerical analyses. Further work needs to incorporate both the installation process and subsequent excavation, by using the procedure described in Chapter 3. However, modelling the installation process of individual diaphragm wall panels is tedious, and will greatly increase the complexity of the analysis and running time for the calculation. A simplified method is under development by the author to incorporate the installation process in one step, which considers only the final effect of wall installation but ignores the intermediate effect of individual panels.

3) All the calculations conducted in this thesis are total stress analyses under undrained conditions, so the process of the dewatering and consolidation has not been considered, due to the limitation of the total stress soil model used in the analysis. To overcome this limitation, an advanced effective stress soil model is required in the analysis, e.g. the 3-SKH model (Stallebrass and Taylor 1997), and the MIT-E3 model (Whittle 1993), coupled with the pore water pressure. This process is under way as the current research with Prof Andrew Whittle in MIT, using the MIT-E3 and MIT-S1 soil model. Another limitation related to the soil model and soil parameters is the adoption of soil parameters derived from green filed conditions to represent the soil underneath buildings in the case study of basement excavation for Shanghai Xingye Bank building. As the total stress soil model cannot account for the change of stiffness and strength of the soil induced by

overlying buildings, the agreement with field measurements is fortuitous. This is a deficiency of the case studies in this thesis, and should be addressed in the future analysis.

4) The effects of more sophisticated soil behaviour, e.g. anisotropy, creep, and destructuration, cannot be considered in the soil model used in this thesis. The effect of anisotropy can be investigated very soon using the MIT-E3 model. A rate-dependent effective stress soil model is under development at MIT, and the effect of creep can be considered once this new soil model is completed. In a similar way, the effect of other soil behaviour can be taken into account by using a more advanced soil model.
5) The focused items in this thesis are mainly deformation characteristics such as the ground movement, the wall deformation, and settlements of adjacent buildings and buried pipelines. In the future research, it is useful to investigate the variation of other items during the excavation, e.g. strut loads, the axial force and bending moment of the diaphragm wall, and earth and pore water pressures. Such research is now undergoing in Singapore in collaboration with the Land Transport Authority, and extensive field instrumentation has been deployed in the new subway station projects to monitor these items. Numerical analyses will be calibrated and updated during the construction.
6) The total wall deflections in these collected case histories are unknown, because wall toe movement was assumed zero in the inclinometer reading and no corrections were made. This mistake has caused some difficulties to calibrate the numerical analysis. This limitation needs to be noted in the future case studies, and selected cases need to record the total wall displacement in the field measurement.
7) The soil-structure interface behaviour, i.e. soil/wall interface, and soil/pile interface, is not considered in the case studies due to the complexity in the mesh generation and numerical problems during the analysis. However, the parametric studies in Chapter 4 showed that the interface behaviour has a large influence on the excavation behaviour. In addition, it was found in Chapter 7 that neglecting the soil/pile contact would result in

upward movement of the piles and floor slabs, in contrast to the settlement observed in the field. Therefore, it is worth placing more efforts on this problem and including the soil-structure interface behaviour in the future case studies. Unfortunately, the soil/pile contact cannot be included when the pile is modelled with beam elements in ABAQUS, because the contact algorithm is based on the surface. For practical use, it is useful to develop an edge to edge contact algorithm in ABAQUS for the pile/soil contact.

8) The geometry of the adjacent buildings is simplified in the case study in Chapter 6, due to the limited known information. For example, the external and internal structures are assumed; openings are not included in the walls and slabs; the foundations are also assumed. These simplifications may affect the accuracy of computed building response and result in large discrepancy with the filed measurement. More detailed modelling is suggested in the future analysis if such information is known. In addition, the buildings are represented by a linear elastic material. It is worth trying the nonlinear structure material model to consider cracks in the reinforced concrete and masonry buildings, e.g. the concrete damaged plasticity model in ABAQUS. Similar issues are relevant to the modelling of buried pipelines. More geometric details and realistic material models have to be considered.

Despite limitations of the analyses and the further work needed in the future, this thesis has contributed to advanced finite element analysis of deep excavations and understanding the performance of this complex soil-structure interaction problem. Cautions should also be taken for applications, because conclusions are drawn on the basis of these specific parametric analyses and case studies.

References

Al-Tabbaa, A. and D. M. Wood (1987). "Some measurements of the permeability of kaolin." Geotechnique **37**(4): 499-503.

Arai, Y., O. Kusakabe, O. Murata and S. Konishi (2008). "A numerical study on ground displacement and stress during and after the installation of deep circular diaphragm walls and soil excavation." Computers and Geotechnics **35**(5): 791-807.

Augarde, C. E. (1997). Numerical modelling of tunnelling process for assessment of damage to buildings. DPhil thesis, University of Oxford.

Augarde, C. E. and H. J. Burd (2001). "Three-dimensional finite element analysis of lined tunnels." International Journal for Numerical & Analytical Methods in Geomechanics **25**: 243-262.

Augarde, C. E., H. J. Burd and G. T. Houlsby (2005). "The influence of building weight on tunnelling-induced ground and building deformation." Soils and Foundations **45**(4): 166-167.

Benz, T., P. A. Vermeer and R. Schwab (2009). "A small-strain overlay model." International Journal for Numerical and Analytical Methods in Geomechanics **33**(1): 25-44.

Bjerrum, L., C. J. Clausen and J. M. Duncan (1972). Earth pressures on flexible structures. 5th European conference on Soil Mechanics and Foundation Engineering. Madrid, Spain. **Vol 2**.

Bjerrum, L. and O. Eide (1956). "Stability of strutted excavations in clay." Geotechnique **6**(1): 32 - 47.

Blackburn, J. T. and R. J. Finno (2007). "Three-dimensional responses observed in an internally braced excavation in soft clay." Journal of Geotechnical and Geoenvironmental Engineering **133**(11): 1364-1373.

Bloodworth, A. G. (2002). Three-Dimentional analysis of tunnelling effects on structures to develop design methods. DPhil thesis, University of Oxford.

Bolton, M. D. and W. Powrie (1987). "The collapse of diaphragm walls retaining clay." Geotechnique **37**: 335-353.

Bolton, M. D. and W. Powrie (1988). "Behaviour of diaphragm walls in clay prior to collapse." Geotechnique **38**: 167-189.

Bolton, M. D. and D. I. Stewart (1994). "The effect on propped diaphragm walls of rising groundwater in stiff clay." Geotechnique **44**(1): 111-127.

Boone, S. J. (1996). "Ground-movement-related building damage." Journal of Geotechnical and Geoenvironmental Engineering **122**(11): 886-896.

Boone, S. J. and A. M. Crawford (2000). "Braced excavations: Temperature, elastic modulus, and strut loads." Journal of Geotechnical and Geoenvironmental Engineering **126**(10): 870-881.

Boscardin, M. D. and E. J. Cording (1989). "Building response to excavation-induced settlement." Journal of Geotechnical Engineering **115**(1): 1-21.

Bose, S. K. and N. N. Som (1998). "Parametric study of a braced cut by finite element method." Computers and Geotechnics **22**(2): 91-107.

Boulon, M. (1989). "Basic features of soil structure interface behaviour." Computers and Geotechnics **7**(1–2): 115-131.

Boulon, M. and R. Nova (1990). "Modelling of soil-structure interface behaviour a comparison between elastoplastic and rate type laws." Computers and Geotechnics **9**(1–2): 21-46.

References

Burd, H. J., G. T. Houlsby, C. E. Augarde and G. Liu (2000). "Modelling tunnelling-induced settlement of masonry buildings." Proceedings of the Institution of Civil Engineers: Geotechnical Engineering **143**(1): 17-29.

Burland, J. B. and R. J. R. Hancock (1977). "Underground car park at the house of commons, london: Geotechnical aspects." Structural Engineer **55**(2): 81-100.

Burland, J. B. and C. P. Wroth (1974). Settlement of buildings and associated damage. Proceedings of a Conference on Settlement of Structures. Cambridge**:** 611-654.

Burlon, S., H. Mroueh and I. Shahrour (2013). "Influence of diaphragm wall installation on the numerical analysis of deep excavation." International Journal for Numerical and Analytical Methods in Geomechanics **37**(11): 1670-1684.

Butterfield, R. and K. Z. Andrawes (1972). "On the angles of friction betweens sand and plane surfaces." Journal of Terramechanics **8**(4): 15-23.

Cai, H., J. Zhou and X. Li (2000). "Plastoelastic response of horizontally layered sites under multi-directional earthquake shaking." Tongji Daxue Xuebao/Journal of Tongji University **28**(2): 177-182.

Caquot, A. I. and J. Kerisel (1948). Tables for the calculation of passive pressure, activepressure, and bearing capacity of foundations. Paris Gauthier - villars, Imprimeur - Editeur, Libraire du Bureau des Longitudes, de L'ecole Polytechnique.

Charles, W. W. (1998). "Observed performance of multipropped excavation in stiff clay." Journal of Geotechnical and Geoenvironmental Engineering **124**(9): 889-905.

Chen, Q. S., G. Y. Gao and J. Yang (2011). "Dynamic response of deep soft soil deposits under multidirectional earthquake loading." Engineering Geology **121**(1-2): 55-65.

Clarke, B. G. and C. P. Wroth (1984). "Analysis of Dunton Green retaining wall based on results of pressuremeter tests." Geotechnique **34**: 549-561.

Clough, G. W. (1977). "Stabilizing berm design for temporary walls in clay." ASCE J Geotech Eng Div **103**(2): 75-90.

Clough, G. W. and L. A. Hansen (1981). "Clay anisotropy and braced wall behavior." Journal of the Geotechnical Engineering Division **107**(7): 893-913.

Clough, G. W. and T. D. O'Rourke (1990). Construction induced movements of insitu walls. ASCE Conference on Design and Performance of Earth Retaining Structures. Cornell University, Ithaca, New York**:** 439-470.

Clough, G. W., E. M. Smith and B. P. Sweeney (1989). Movement control of excavation support systems by iterative design. ASCE conference on current principles and practices on foundation and engineering. New York, ASCE. **Vol.2:** 869-884.

Coulomb, C. A. (1776). "Essai sur une application des regles des maximis et minimis a quelques problemes de statique relatifs a l'architecture." Memoires de l'Academie Royale pres Divers Savants **7**.

Darendeli , M. B. (2001). Development of a new family of normalized modulus reduction and material damping curves. PhD thesis, The University of Texas at Austin.

Dassargues, A., P. Biver and A. Monjoie (1991). "Geotechnical properties of the Quaternary sediments in Shanghai." Engineering Geology **31**(1): 71-90.

Day, R. A. and D. M. Potts (1994). "Zero thickness interface elements - numerical stability and application." International Journal for Numerical & Analytical Methods in Geomechanics **18**(10): 689-708.

References

Day, R. A. and D. M. Potts (1998). "The effect of interface properties on retaining wall behaviour." International Journal for Numerical and Analytical Methods in Geomechanics **22**(12): 1021-1033.

De Moor, E. K. (1994). "An analysis of bored pile/diaphragm wall installation effects." Geotechnique **44**(2): 341-347.

Dong, Y. P. (2011). Numerical Modelling of Ground Movement and Structure Deformation Induced by Excavation. PRS first year transfer report. Oxford, Department of Engineering Science, University of Oxford.

Dong, Y. P., H. J. Burd and G. T. Houlsby (2012). 3D FEM modelling of a deep excavation case history considering small-strain stiffness of soil and thermal contraction of concrete. BGA Young Geotechnical Engineers's Symposium 2012. University of Leeds**:** 12-13.

Dong, Y. P., H. J. Burd, G. T. Houlsby and Y. M. Hou (2013). Advanced Numerical Modelling of a Complex Deep Excavation Case History in Shanghai. 5th International Young Geotechnical Engineers' Conference. Paris. **2:** 253-256.

Dong, Y. P., H. J. Burd, G. T. Houlsby and Z. H. Xu (2013). 3D FEM Modelling of a Deep Excavation Case History Considering Small-strain Stiffness of Soil and Thermal Shrinkage of Concrete. 7th International Conference on Case Histories in Geotechnical Engineering. Chicago**:** # 3.28.b.

Farmer, I. W. and P. B. Attewell (1973). "Ground movements caused by a betonite-supported excavation in London Clay." Geotechnique **23**: 576-581.

Finno, R. and J. Roboski (2005). "Three-Dimensional Responses of a Tied-Back Excavation through Clay." Journal of Geotechnical and Geoenvironmental Engineering **131**(3): 273-282.

Finno, R., F. Voss, E. Rossow and J. Blackburn (2005). "Evaluating Damage Potential in Buildings Affected by Excavations." Journal of Geotechnical and Geoenvironmental Engineering **131**(10): 1199-1210.

Finno, R. J., D. K. Atmatzidis and S. B. Perkins (1989). "Observed performance of a deep excavation in clay." Journal of geotechnical engineering **115**(8): 1045-1064.

Finno, R. J., J. T. Blackburn and J. F. Roboski (2007). "Three-dimensional effects for supported excavations in clay." Journal of Geotechnical and Geoenvironmental Engineering **133**(1): 30-36.

Finno, R. J. and L. S. Bryson (2002). "Response of building adjacent to stiff excavation support system in soft clay." Journal of Performance of Constructed Facilities **16**(1): 10-20.

Finno, R. J., I. S. Harahap and P. J. Sabatini (1991). "Analysis of braced excavations with coupled finite element formulations." Computers and Geotechnics **12**(2): 91-114.

Finno, R. J., S. A. Lawrence, N. F. Allawh and I. S. Harahap (1991). "Analysis of performance of pile groups adjacent to deep excavation." Journal of geotechnical engineering **117**(6): 934-955.

Finno, R. J. and S. M. Nerby (1989). "Saturated clay response during braced cut construction." Journal of geotechnical engineering **115**(8): 1065-1084.

Franzius, J. N., D. M. Potts and J. B. Burland (2005). "The influence of soil anisotropy and Ko on ground surface movements resulting from tunnel excavation." Geotechnique **55**(3): 189-199.

Gao, F. and X. Sun (2005). "Characteristic analysis of Shear wave velocity of foundation ground in Shanghai region." Shanghai Geology **94**(02): 27-29.

Geddes, J. (1991). "Discussion of "Building Response to Excavation‐Induced Settlement" by Marco D. Boscardin and Edward J. Cording (January, 1989, Vol. 115, No. 1)." Journal of Geotechnical Engineering **117**(8): 1276-1278.

Georgiadis, M. and C. Anagnostopoulos (1998). "Effect of berms on sheet-pile wall behaviour." Geotechnique **48**(4): 569-574.

Goh, A. T. C., K. S. Wong, C. I. Teh and D. Wen (2003). "Pile response adjacent to braced excavation." Journal of Geotechnical and Geoenvironmental Engineering **129**(4): 383-386.

Gourvenec, S., W. Powrie and E. K. D. Moor (2002) "Three-dimensional effects in the construction of a long retaining wall." Proceedings of the ICE - Geotechnical Engineering **155**, 163-173.

Gourvenec, S. M. and W. Powrie (1999). "Three-dimensional finite-element analysis of diaphragm wall installation." Geotechnique **49**(6): 801-823.

Gourvenec, S. M. and W. Powrie (2000). "Three-dimensional finite element analyses of embedded retaining walls supported by discontinuous earth berms." Canadian Geotechnical Journal **37**(5): 1062-1077.

Grammatikopoulou, A. (2004). Development, implementation and application of kinematic hardening models for overconsolidated clays. PhD thesis, Imperial College, London.

Gunn, M. J. and C. R. I. Clayton (1992). "Installation effects and their importance in the design of earth-retaining structures." Geotechnique **42**(1): 137-141.

Hardin, B. O. and V. P. Drnevich (1972). "Shear modulus and damping in soils: Measurement and parameter effects." ASCE J Soil Mech Found Div **98**(SM6): 603-624.

Hashash, Y. M. A. and A. J. Whittle (1996). "Ground movement prediction for deep excavations in soft clay." Journal of Geotechnical and Geoenvironmental Engineering **122**(6): 474-486.

Hashash, Y. M. A. and A. J. Whittle (2002). "Mechanisms of load transfer and arching for braced excavations in clay." Journal of Geotechnical and Geoenvironmental Engineering **128**(3): 187-197.

Hou, Y. M., J. H. Wang and L. L. Zhang (2009). "Finite-element modeling of a complex deep excavation in Shanghai." Acta Geotechnica **4**(1): 7-16.

Houlsby, G. T. (1999). A model for the variable stiffness of undrained clay. Proceedings of the International Symposium on Pre-Failure Deformations of Soil. Torino. **Vol. 1:** 443-450.

Hsieh, P. G. and C. Y. Ou (1998). "Shape of ground surface settlement profiles caused by excavation." Canadian Geotechnical Journal **35**(6): 1004-1017.

Hsieh, P. G., C. Y. Ou and Y. L. Lin (2013). "Three-dimensional numerical analysis of deep excavations with cross walls." Acta Geotechnica **8**(1): 33-48.

Huang, Y., S. F. Brown and G. R. McDowell (2001). "Dynamic coupled analysis for rutting in flexible pavement foundations under cyclic loading." Yantu Gongcheng Xuebao/Chinese Journal of Geotechnical Engineering **23**(6): 757.

Hubbard, H. W., D. M. Potts, D. Miller and J. B. Burland (1984). "Design of the retaining walls for the M25 cut and cover tunnel at Bell Common." Geotechnique **34**: 495-512.

Jardine, R. J., D. M. Potts, A. B. Fourie and J. B. Burland (1986). "Studies of the influence of non-linear stress-strain characteristics in soil-structure interaction." Geotechnique **36**(3): 377 - 396.

Jardine, R. J., M. J. Symes and J. B. Burland (1984). "Measurement of soil stiffness in the triaxial apparatus." Geotechnique **34**(3): 323-340.

Jeong Woo, S., K. Oon Young, C. Choong Ki and K. Myoung Mo (2001). "Evaluation of ground and building settlement near braced excavation sites by model testing." Canadian Geotechnical Journal **38**(5): 1127-1133.

Kung, G., C. Juang, E. Hsiao and Y. Hashash (2007). "Simplified Model for Wall Deflection and Ground-Surface Settlement Caused by Braced Excavation in Clays." Journal of Geotechnical and Geoenvironmental Engineering **133**(6): 731-747.

Lambe, T. W. (1967). "Stress path method." Journal of Soil Mechanics & Foundations Division **95**(6): 309-331.

Lee, F., S. Hong, Q. Gu and P. Zhao (2011). "Application of Large Three-Dimensional Finite-Element Analyses to Practical Problems." International Journal of Geomechanics **11**(6): 529-539.

Lee, F., K. Yong, K. Quan and K. Chee (1998). "Effect of Corners in Strutted Excavations: Field Monitoring and Case Histories." Journal of Geotechnical and Geoenvironmental Engineering **124**(4): 339-349.

Lemos, L. J. L. and P. R. Vaughan (2000). "Clay-interface shear resistance." Geotechnique **50**(1): 55-64.

Leung, C., Y. Chow and R. Shen (2000). "Behavior of Pile Subject to Excavation-Induced Soil Movement." Journal of Geotechnical and Geoenvironmental Engineering **126**(11): 947-954.

Leung, C., J. Lim, R. Shen and Y. Chow (2003). "Behavior of Pile Groups Subject to Excavation-Induced Soil Movement." Journal of Geotechnical and Geoenvironmental Engineering **129**(1): 58-65.

Leung, E. and C. Ng (2007). "Wall and Ground Movements Associated with Deep Excavations Supported by Cast In Situ Wall in Mixed Ground Conditions." Journal of Geotechnical and Geoenvironmental Engineering **133**(2): 129-143.

Li, Q., C. W. W. Ng and G.-b. Liu (2012). "Low secondary compressibility and shear strength of Shanghai Clay." Journal of Central South University **19**(8): 2323-2332.

Li, Q., C. W. W. Ng and G. B. Liu (2012). "Determination of small-strain stiffness of Shanghai clay on prismatic soil specimen." Canadian Geotechnical Journal **49**(8): 986-993.

Lim, A., C. Y. Ou and P. G. Hsieh (2010). "Evaluation of clay constitutive models for analysis of deep excavation under undrained conditions." Journal of GeoEngineering **5**(1): 9-20.

Lings, M. L., C. W. W. Ng and D. F. T. Nash (1994). "The lateral pressure of wet concrete in diaphragm wall panels cast under bentonite." Proceedings - ICE: Geotechnical Engineering **107**(3): 163-172.

Liu, G. (1997). Numerical modelling of damage to masonry buildings due to tunneling. DPhil Thesis, University of Oxford.

Liu, G. B., R. J. Jiang, C. W. W. Ng and Y. Hong (2011). "Deformation characteristics of a 38 M deep excavation in soft clay." Canadian Geotechnical Journal **48**(12): 1817-1828.

Liu, G. B., C. W. W. Ng and Z. W. Wang (2005). "Observed performance of a deep multistrutted excavation in Shanghai soft clays." Journal of Geotechnical and Geoenvironmental Engineering **131**(8): 1004-1013.

Long, M. (2001). "Database for retaining wall and ground movements due to deep excavations." Journal of Geotechnical and Geoenvironmental Engineering **127**(3): 203-224.

Lou, M., Y. Li and N. Li (2007). "Analyses of the seismic responses of soil layers with deep deposits." Frontiers of Architecture and Civil Engineering in China **1**(2): 188-193.

Lu, X., P. Li, B. Chen and Y. Chen (2005). "Computer simulation of the dynamic layered soil-pile-structure interaction system." Canadian Geotechnical Journal **42**(3): 742-751.

Mair, R. J. (1993). "Unwin memorial lecture 1992: developments in geotechnical engineering research: application to tunnels and deep excavations." Proceedings - ICE: Civil Engineering

97(1): 27-41.

Mana, A. I. and G. W. Clough (1981). "Prediction of movements for braced cuts in clay." Journal of the Geotechnical Engineering Division **107**(6): 759-777.

Ng, C. (1999). "Stress Paths in Relation to Deep Excavations." Journal of Geotechnical and Geoenvironmental Engineering **125**(5): 357-363.

Ng, C. W., M. L. Lings, B. Simpson and D. F. T. Nash (1995). "An approximate analysis of the three-dimensional effects of diaphragm wall installation." Geotechnique **45**: 497-507.

Ng, C. W. W., Y. Hong, G. B. Liu and T. Liu (2012). "Ground deformations and soil-structure interaction of a multi-propped excavation in Shanghai soft clays." Geotechnique **62**(10): 907-921.

Ng, C. W. W., E. H. Y. Leung and C. K. Lau (2004). "Inherent anisotropic stiffness of weathered geomaterial and its influence on ground deformations around deep excavations." Canadian Geotechnical Journal **41**(1): 12-24.

Ng, C. W. W., M. L. Lings, B. Simpson and D. F. T. Nash (1995). "An approximate analysis of the three-dimensional effects of diaphragm wall installation." Geotechnique **45**(3): 497-507.

Ng, C. W. W., D. B. Rigby, G. H. Lei and S. W. L. Ng (1999). "Observed performance of a short diaphragm wall panel." Geotechnique **49**: 681-694.

Ng, C. W. W. and R. W. M. Yan (1999). "Three-dimensional modelling of a diaphragm wall construction sequence." Geotechnique **49**(6): 825-834.

O'Rourke, T. D. (1981). "Ground movements caused by braced excavations." Journal of the Geotechnical Engineering Division **107**(9): 1159-1178.

O'Rourke, T. D. (1993). Base stability and ground movement prediction for excavations in soft clay. Retaining structures, Thomas Telford, London**:** 131 - 139.

Ou, C.-Y., P.-G. Hsieh and D.-C. Chiou (1993). "Characteristics of ground surface settlement during excavation." Canadian Geotechnical Journal **30**(5): 758-767.

Ou, C. Y. (2006). Deep Excavation: Theory and Practice. London, Taylor & Francis.

Ou, C. Y., D. C. Chiou and T. S. Wu (1996). "Three-dimensional finite element analysis of deep excavations." Journal of Geotechnical and Geoenvironmental Engineering **122**(5): 337-345.

Ou, C. Y., P. G. Hsieh and Y. L. Lin (2010). "Performance of excavations with cross walls." Journal of Geotechnical and Geoenvironmental Engineering **137**(1): 94-104.

Ou, C. Y., J. T. Liao and W. L. Cheng (2000). "Building response and ground movements induced by a deep excavation." Geotechnique **50**(3): 209-220.

Ou, C. Y., J. T. Liao and H. D. Lin (1998). "Performance of diaphragm wall constructed using top-down method." Journal of Geotechnical and Geoenvironmental Engineering **124**(9): 798-808.

Ou, C. Y., B. Y. Shiau and I. W. Wang (2000). "Three-dimensional deformation behavior of the Taipei National Enterprise Center (TNEC) excavation case history." Canadian Geotechnical Journal **37**(2): 438-448.

Ou, C. Y., F. C. Teng and I. W. Wang (2008). "Analysis and design of partial ground improvement in deep excavations." Computers and Geotechnics **35**(4): 576-584.

Peck, R. B. (1969). Deep excavation & tunneling in soft ground. State-of-the-art report. 7th International Conference of Soil Mechanics and Foundation Engineering. Mexico City, International Society of Soil Mechanics and Geotenical Engineering**:** 225 - 281.

Pickhaver, J. A. (2006). Numerical Modelling of Building Response to Tunnelling. DPhil Thesis, University of Oxford.

Pickhaver, J. A., H. J. Burd and G. T. Houlsby (2010). "An equivalent beam method to model masonry buildings in 3D finite element analysis." Computers and Structures **88**(19-20): 1049-1063.

Potts, D. and R. A. Day (1990). "Use of sheet pile retaining walls for deep excavations in stiff clay." ICE Proceedings **88**(6): 889 - 927.

Potts, D. and L. Zdravkovic (2001). Finite element analyisis in geotechnical engineering: Application, Vol.2. London, Thomas Telford.

Potts, D. and L. Zdravkovic (2001). Finite Element Analysis in Geotechnical Engineering: Vol. 2 - Application. London, Thomas Telford Limited.

Potts, D. M. and A. B. Fourie (1984). "Behaviour of a propped retaining wall: Results of a numerical experiment." Geotechnique **34**(3): 383-404.

Potts, D. M. and A. B. Fourie (1985). "The effect of wall stiffness on the behaviour of a propped retaining wall." Geotechnique **35**: 347-352.

Potts, D. M. and L. Zdravkovic (1999). Finite Element Analysis in Geotechnical Engineering: Theory, Vol.1. London, Thomas Telford.

Potyondy, J. G. (1961). "Skin Friction between Various Soils and Construction Materials." Geotechnique **11**: 339-353.

Poulos, H. G. and L. T. Chen (1997). "Pile response due to excavation-induced lateral soil movement." Journal of Geotechnical Engineering **123**(2): 94-99.

Powrie, W. and R. J. Chandler (1998). "The influence of a stabilizing platform on the performance of an embedded retaining wall: A finite element study." Geotechnique **48**(3): 403-409.

Powrie, W. and M. P. Daly (2002). "Centrifuge model tests on embedded retaining walls supported by earth berms." Geotechnique **52**(2): 89-106.

Powrie, W. and C. Kantartzi (1996). "Ground response during diaphragm wall installation in clay: centrifuge model tests." Geotechnique **46**: 725-739.

Powrie, W. and E. S. F. Li (1991). "Finite element analyses of an in situ wall propped at formation level." Geotechnique **41**: 499-514.

Powrie, W., H. Pantelidou and S. E. Stallebrass (1998). "Soil stiffness in stress paths relevant to diaphragm walls in clay." Geotechnique **48**(4): 483-494.

Puller, M. (2003). Deep Excavations: a practical manual. London, Thomas Telford.

Rankine, W. (1857). "On the stability of loose earth." Philosophical Transactions of the Royal Society of London **147**: 9 - 27.

Richards, D. J., J. Clark and W. Powrie (2006). "Installation effects of a bored pile wall in overconsolidated clay." Geotechnique **56**(6): 411-425.

Richards, D. J. and W. Powrie (1994). "Finite element analysis of construction sequences for propped retaining walls." Proceedings - ICE: Geotechnical Engineering **107**(4): 207-216.

Richards, D. J. and W. Powrie (1998). "Centrifuge model tests on doubly propped embedded retaining walls in overconsolidated kaolin clay." Geotechnique **48**(6): 833-846.

Santos, J. A. d. and A. G. Correia (2001). Reference threshold shear strain of soil. Its application to obtain an unique strain-dependent shear modulus curve for soil. Proceedings of the Fifteenth International Conference on Soil Mechanics and Geotechnical Engineering. Istanbul, Turkey **1-3:** 267-270

Schäfer, R. and T. Triantafyllidis (2004). "Modelling of earth and water pressure development

during diaphragm wall construction in soft clay." International Journal for Numerical and Analytical Methods in Geomechanics **28**(13): 1305-1326.

Schäfer, R. and T. Triantafyllidis (2006). "The influence of the construction process on the deformation behaviour of diaphragm walls in soft clayey ground." International Journal for Numerical and Analytical Methods in Geomechanics **30**(7): 563-576.

Schanz, T., P. A. Vermeer and P. G. Bonnier (1999). "The hardening soil model: Formulation and verification." Beyond 2000 in computational geotechnics. Ten Years of PLAXIS International. Proceedings of the international symposium, Amsterdam, March 1999.: 281-296.

SGIDI (1997). Geotechnical site investigation report of Shanghai Xingye Bank Building. Shanghai, Shanghai Geotechnical Investigations & Design Institute Co. Ltd.

Simpson, B. (1992). "Retaining structures: displacement and design." Geotechnique **42**(4): 541-576.

Simpson, B., N. J. O'Riordan and D. D. Croft (1979). "Computer model for the analysis of ground movements in london clay." Geotechnique **29**(2): 149-175.

Skempton, A. W. and D. H. McDonald (1956). "The allowable settlements of buildings." ICE Proceedings: Engineering Divisions **5**: 727-768.

Skempton, A. W. and W. H. Ward (1952). "Investigations Concerning a Deep Cofferdam in the Thames Estuary Clay at Shellhaven." Geotechnique **3**(3): 119 - 139.

St. John, H. D., D. M. Potts, R. J. Jardine and K. G. Higgins (1993). "Prediction and performance of ground response due to construction of a deep basement at 60 Victoria Embankment." Predictive soil mechanics. Proc. of the Wroth memorial symposium, Oxford, 1992: 581-608.

Stallebrass, S. E. (1990). The effect of recent stress history on the deformation of overconsolidated soils. PhD thesis, City University, London.

Stallebrass, S. E. and R. N. Taylor (1997). "The development and evaluation of a constitutive model for the prediction of ground movements in overconsolidated clay." Geotechnique **47**(2): 235-253.

Stokoe, K. H., M. B. Darendeli, R. D. Andrus and L. T. Brown (1999). "Dynamic soil properties: Laboratory, field and correlation studies." Earthquake geotechnical engineering. Proceedings of the 2nd international conference on earthquake geotechnical engineering, Lisbon, June 1999. (3 vols.). 811-845.

Stroud, M., M. T. Hutchinson, H. D. St John and N. G. A. Yarwood (1994). "Loads on struts in excavations." Proceedings - ICE: Geotechincal Engineering **107**(4): 241-246.

Symons, I. and D. R. Carder (1992). "Field measurements on embedded retaining walls." Geotechnique **42**: 117-126.

Symons, I. F. and P. Tedd (1989). "Behaviour of a propped embedded retaining wall at Bell Common Tunnel in the longer term." Geotechnique **39**: 701-710.

Takemura, J., M. Kondoh, T. Esaki, M. Kouda and O. Kusakabe (1999). "Centrifuge model tests on double propped wall excavation in soft clay." Soils and Foundations **39**(3): 75-87.

Tan, Y. and B. Wei (2011). "Observed Behaviors of a Long and Deep Excavation Constructed by Cut-and-Cover Technique in Shanghai Soft Clay." Journal of Geotechnical and Geoenvironmental Engineering **138**(1): 69-88.

Tedd, P., B. M. Chard, J. A. Charles and I. F. Symons (1984). "Behaviour of a propped embedded retaining wall in stiff clay at Bell Common Tunnel." Geotechnique **34**: 513-532.

Terzaghi, K. (1943). Theoretical Soil Mechanics. New York, John Wiley & Son.

Terzaghi, K. and R. B. Peck (1967). Soil Mechanics in Engineering Practice. New York, John Wiley & Sons.

Vermeer, P. A. and R. B. J. Brinkgreve (1998). PLAXIS: Finite element code for soil and rock analysis. Balkema, Rotterdam.

Wang, J., Z. Xu and W. Wang (2010). "Wall and Ground Movements due to Deep Excavations in Shanghai Soft Soils." Journal of Geotechnical and Geoenvironmental Engineering **136**(7): 985-994.

Wang, W. D. and J. H. Wang (2007). Design, analysis and case histories of deep excavations supported by permanent structures. Beijing, China Architecture & Building Press.

Wang, Z. W. (2004). Research on Deformation and Earth Pressure of Deep Metro Excavation in Soft Clay Based on Time and Small Strain. Ph.D Thesis, Tong Ji University.

Whittle, A. J. (1987). A constitutive model for overconsolidated clays with application to cyclic loading of friction piles. PhD thesis, Massachusetts Institute of Technology.

Whittle, A. J. (1993). "Evaluation of a constitutive model for overconsolidated clays." Geotechnique **43**(2): 289-313.

Whittle, A. J., D. J. Degroot, C. C. Ladd and S. Tian-Ho (1994). "Model prediction of anisotropic behavior of Boston blue clay." Journal of Geotechnical Engineering - ASCE **120**(2): 199-224.

Whittle, A. J., Y. M. A. Hashash and R. V. Whitman (1993). "Analysis of deep excavation in Boston." Journal of Geotechnical Engineering - ASCE **119**(1): 69-90.

Wisser, C. (2002). Numerical modelling of tunnel installation and compensation grouting. DPhil Thesis, University of Oxford.

Wisser, C., C. E. Augarde and H. J. Burd (2005). "Numerical modelling of compensation grouting above shallow tunnels." International Journal for Numerical and Analytical Methods in Geomechanics **29**(5): 443-471.

Wong, I. H. and T. Y. Poh (2000). "Effects of jet grouting on adjacent ground and structures." Journal of Geotechnical and Geoenvironmental Engineering **126**(3): 247-256.

Wong, I. H., T. Y. Poh and H. L. Chuah (1996). "Analysis of case histories from construction of the Central Expressway in Singapore." Canadian Geotechnical Journal **33**(5): 732-746.

Wong, I. H., T. Y. Poh and H. L. Chuah (1997). "Performance of excavations for depressed expressway in Singapore." Journal of Geotechnical Engineering **123**(7): 617-625.

Wong, K. and B. Broms (1989). "Lateral Wall Deflections of Braced Excavations in Clay." Journal of Geotechnical Engineering **115**(6): 853-870.

Wood, L. A. and A. J. Perrin (1984) "Observations of a strutted diaphragm wall in London clay: a preliminary assessment." Geotechnique **34**, 563-579.

Wood, L. A. and A. J. Perrin (1984). "Observations of a strutted diaphragm wall in london clay: A preliminary assessment." Geotechnique **34**(4): 563-579.

Wu, T. H. and S. Berman (1953). "Earth Pressure Measurements in open cut: Contract D-8, Chicago Subway." Geotechnique **3**(3): 248 - 258.

Xu, Y.-S., S.-L. Shen and Y.-J. Du (2009). "Geological and hydrogeological environment in Shanghai with geohazards to construction and maintenance of infrastructures." Engineering Geology **109**(3–4): 241-254.

Xu, Z. H. (2007). Deformation Behaviour of Deep Excavations supported by Permanent Structure in Shanghai Soft Deposit. PhD, Shanghai Jiao Tong University, China.

References

Young, D. K. and E. W. L. Ho (1994). "The observational approach to design of a sheet-piled retaining wall." Geotechnique **44**(4): 637-654.

Zdravkovic, L., D. M. Potts and H. D. St. John (2005). "Modelling of a 3D excavation in finite element analysis." Geotechnique **55**(7): 497-513.

Zhang, P. S. and J. Y. Shi (2008). "Effect of stress path circumgyration on shear modulus under small strain and initial stress state." Yantu Gongcheng Xuebao/Chinese Journal of Geotechnical Engineering **30**(3): 379-383.

Appendix A - Field data of basement excavation for Shanghai Xingye Bank building

The field data regarding to wall deformations, ground movements, and settlements of adjacent buildings and buried pipelines, are collected from Xu (2007) and shown in this appendix.

A.1 Lateral displacement of the diaphragm wall

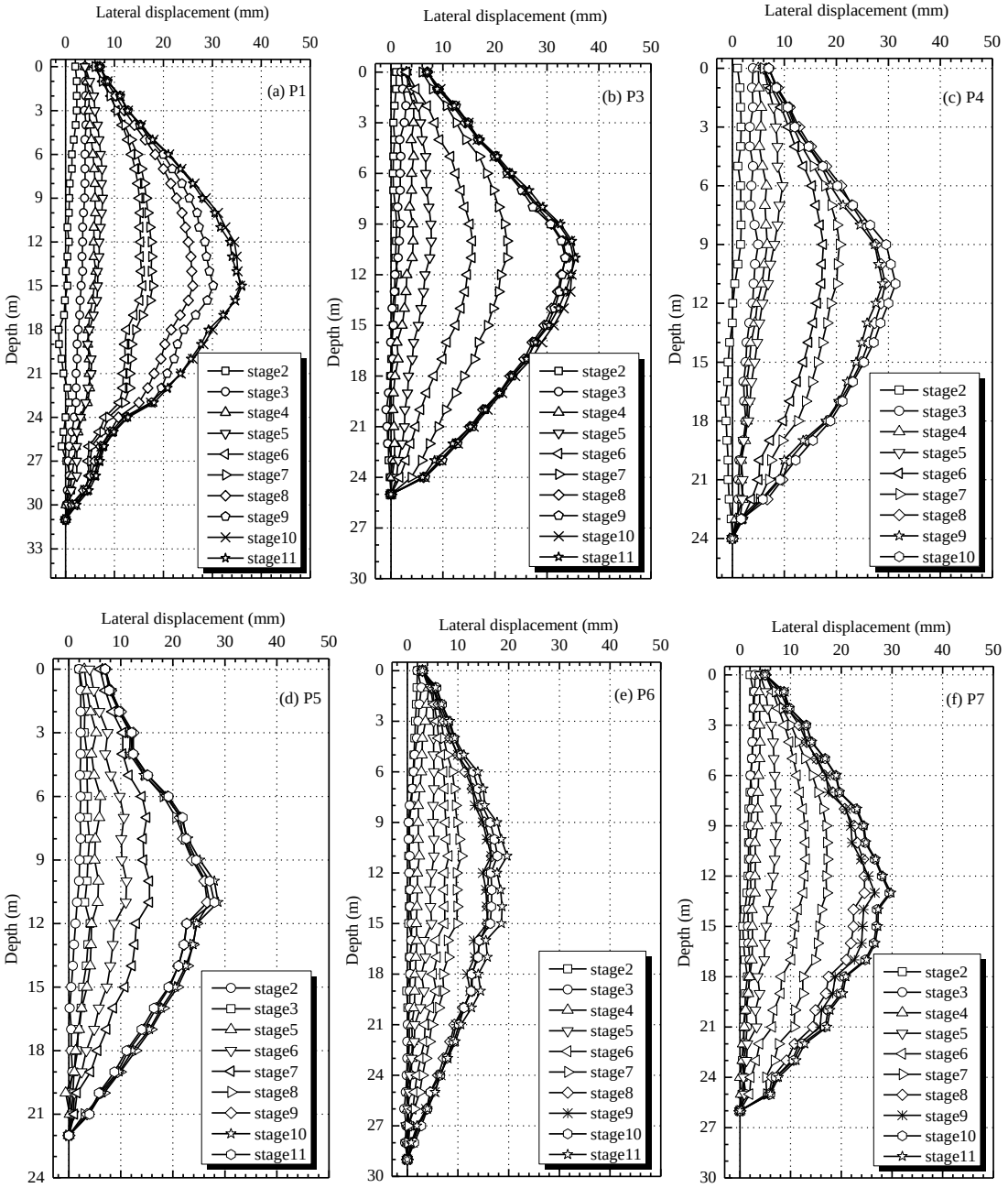

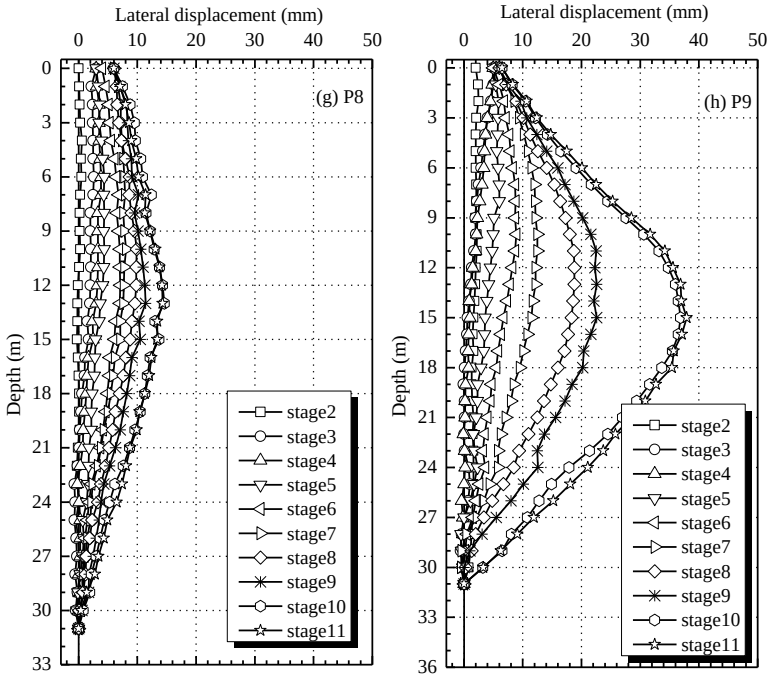

Fig.A.1Lateral displacement of the diaphragm wall at different stages

A.2 Vertical movement of the diaphragm wall

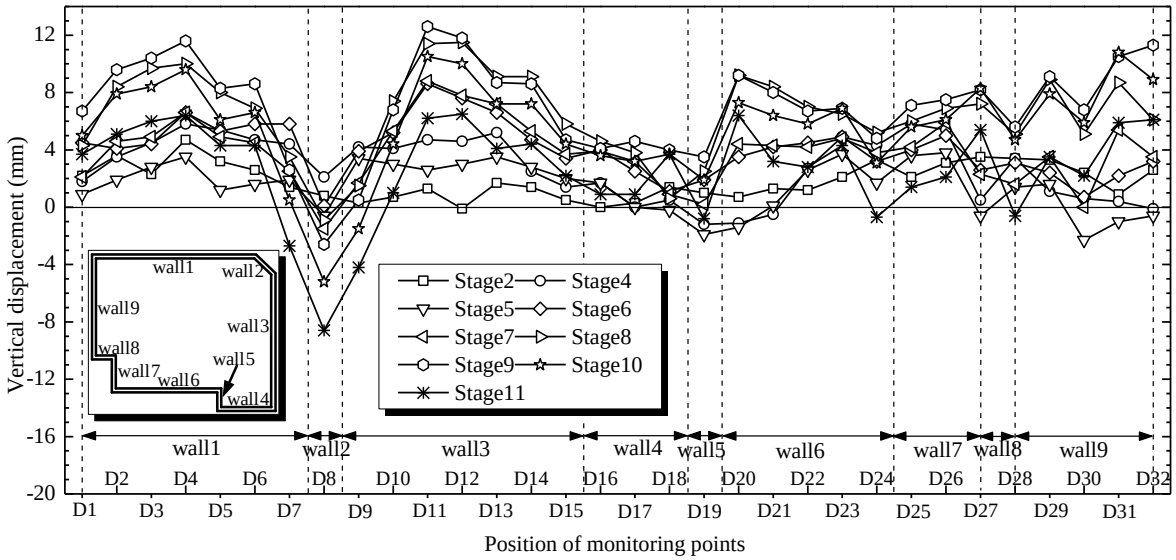

Fig.A.2 Vertical movement of the diaphragm wall at different stages

A.3 Lateral displacement of the ground

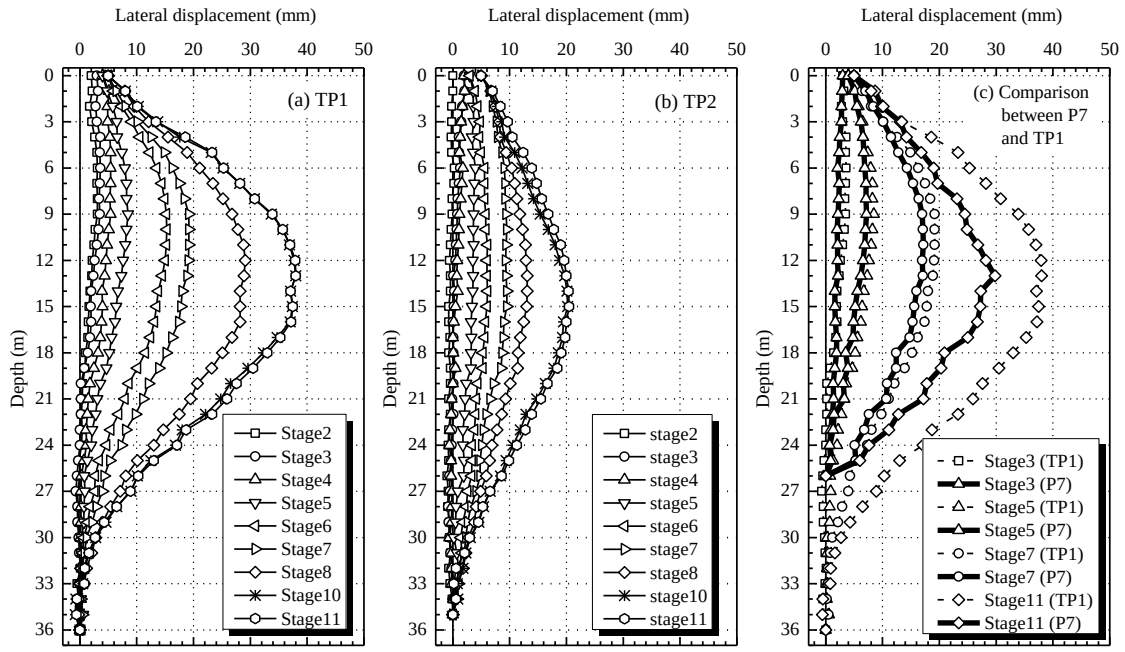

Fig. A.3 Lateral displacement of the ground at different stages and comparison between soil and wall lateral displacement

A.4 Ground settlement and adjacent wall deflection

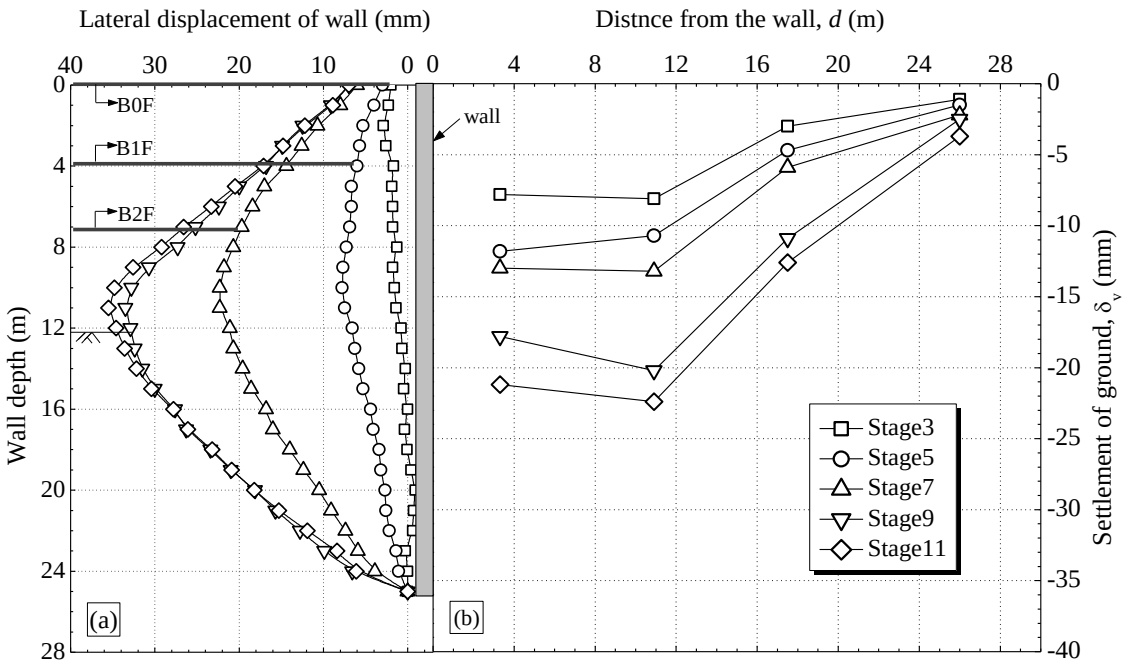

Fig.A.4 Ground settlement on Section AA9~AA12 and adjacent wall deflection (at P3) at different stages

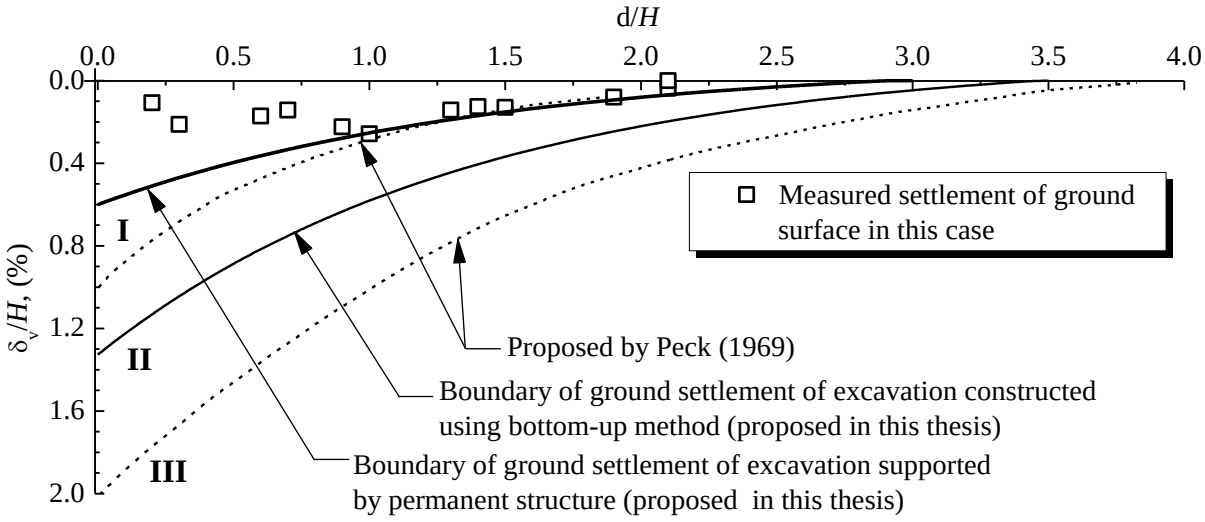

Fig.A.5 Distribution of ground settlement on the direction perpendicular to the diaphragm wall

A.5 Pipeline settlement

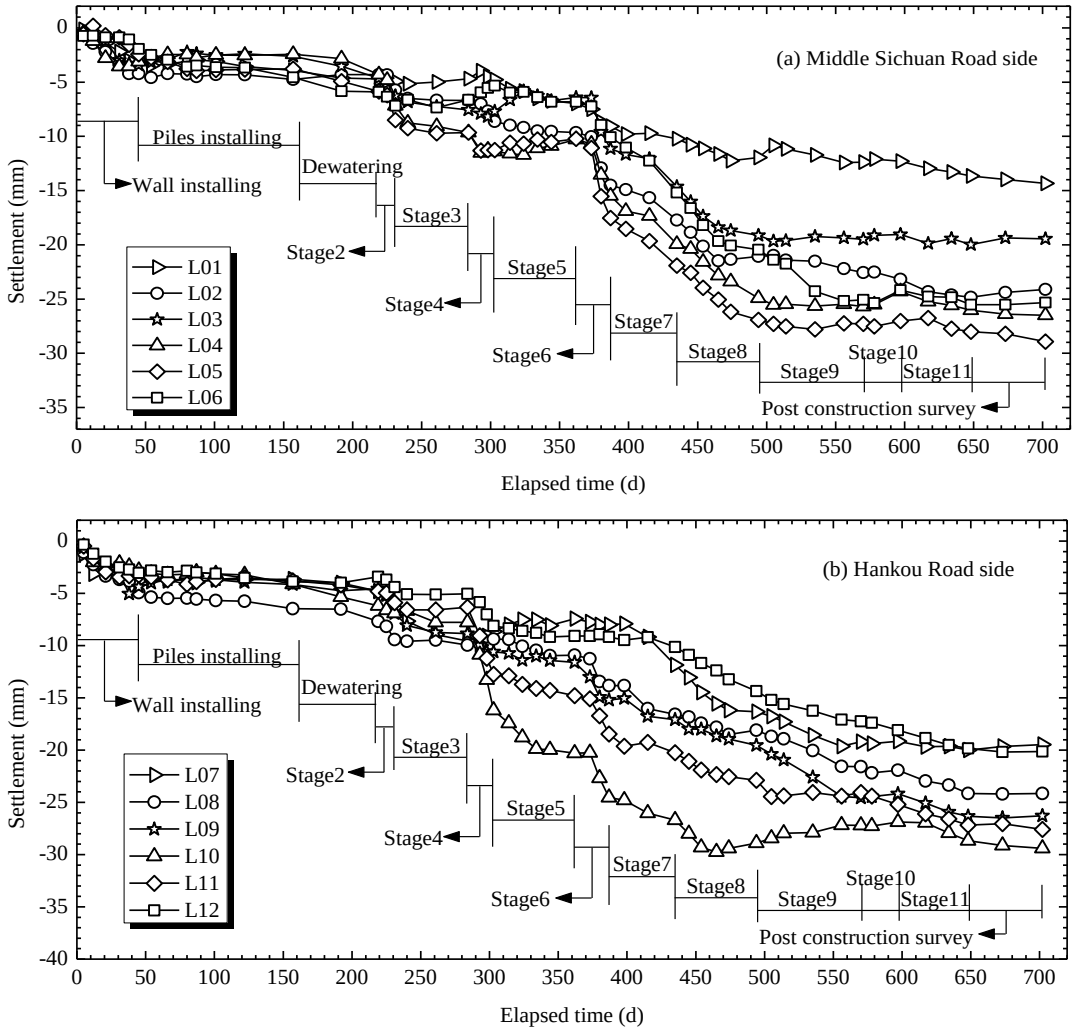

Fig.A.6 Electrical power pipeline settlement with time (a) L01 ~ L06, (b) L07 ~ L12

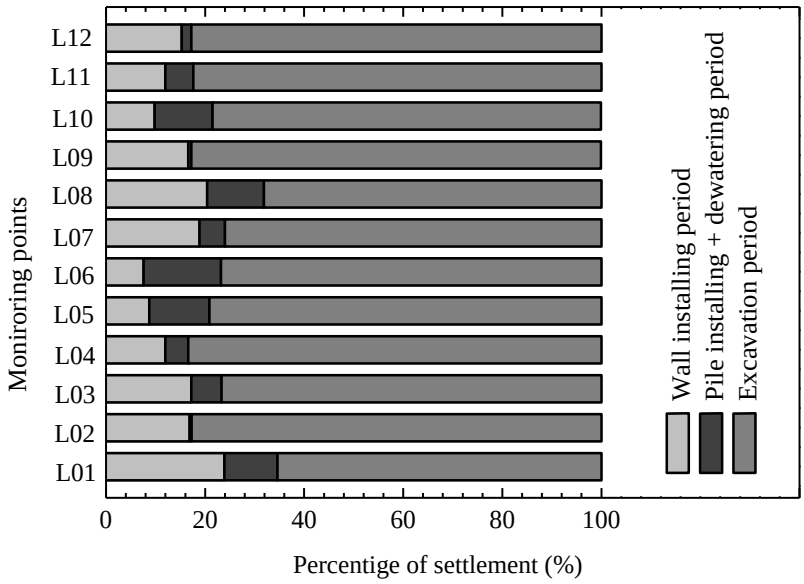

Fig.A.7 Percentage of electrical power pipeline settlement caused in different construction stages

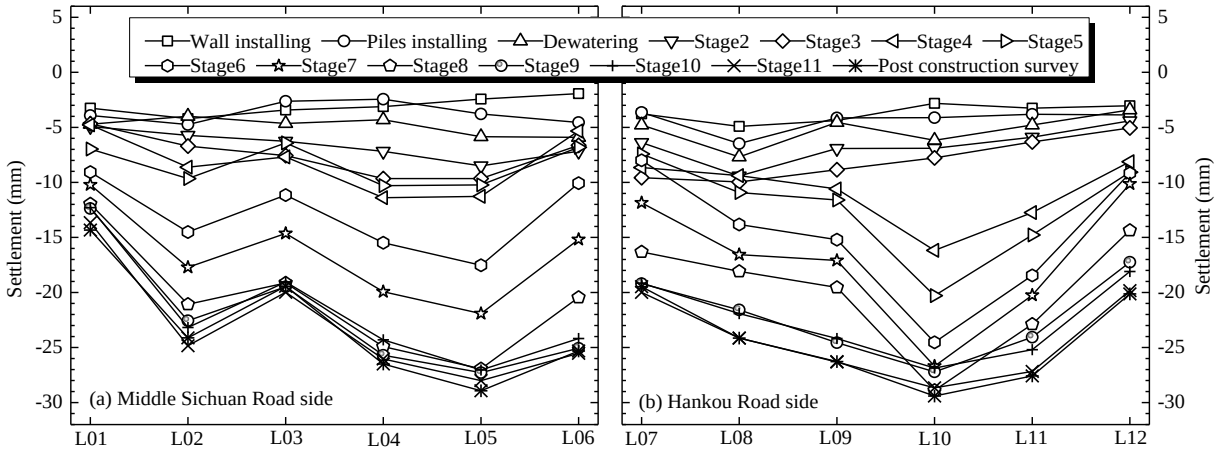

Fig.A.8 Settlement of electrical power pipeline on the direction parallel to the wall at different stages

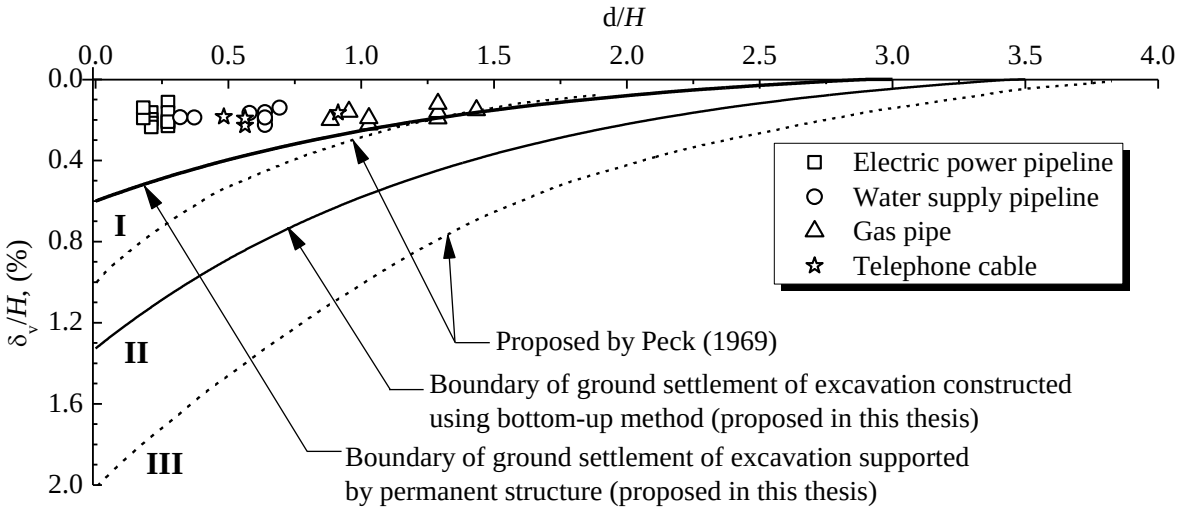

Fig.A.9 Distribution of pipeline settlement on the direction perpendicular to the wall

A.6 Building deformation

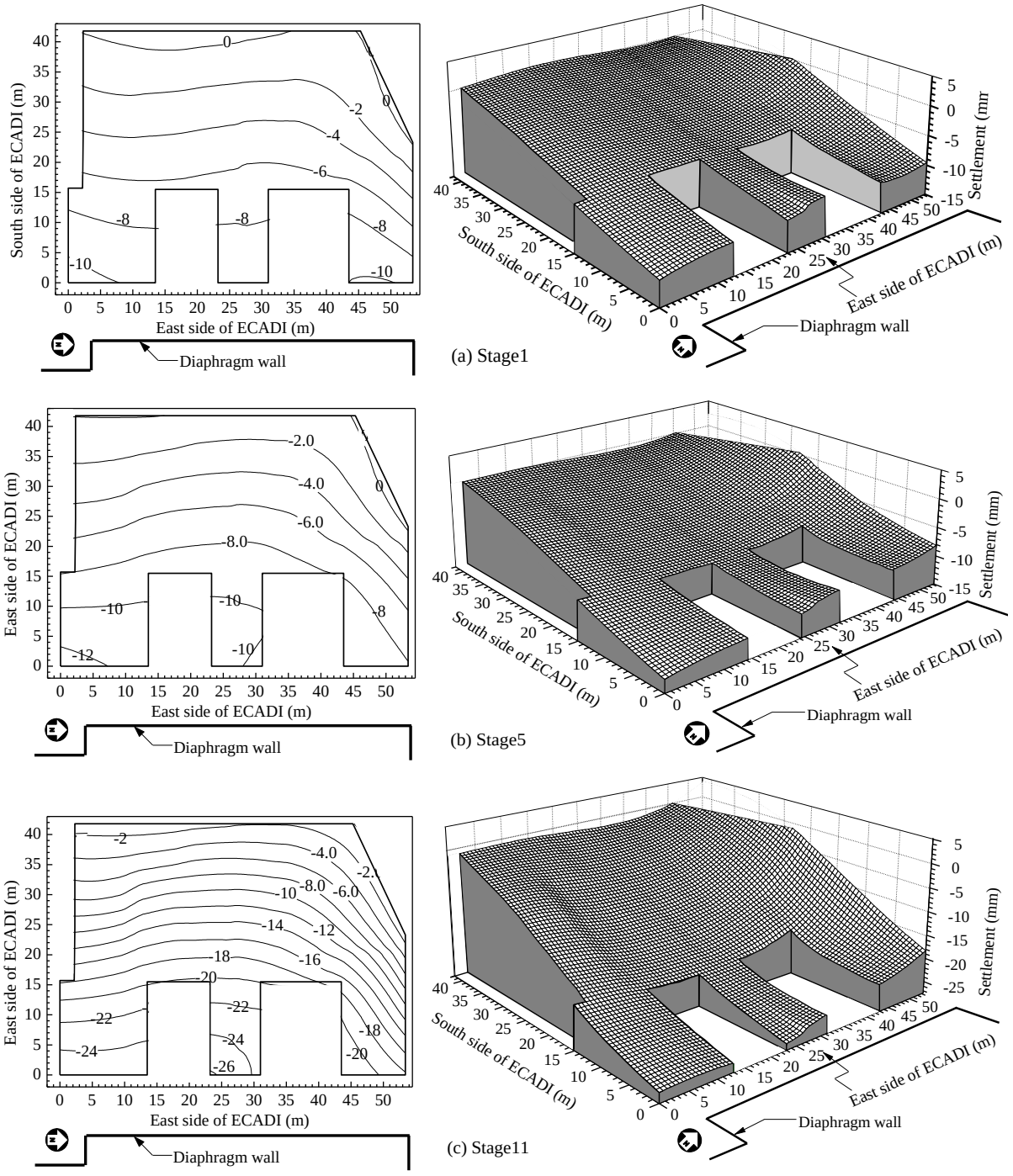

Fig.A.10 2D settlement contours and 3D settlement distribution of the ECADI building at different stages

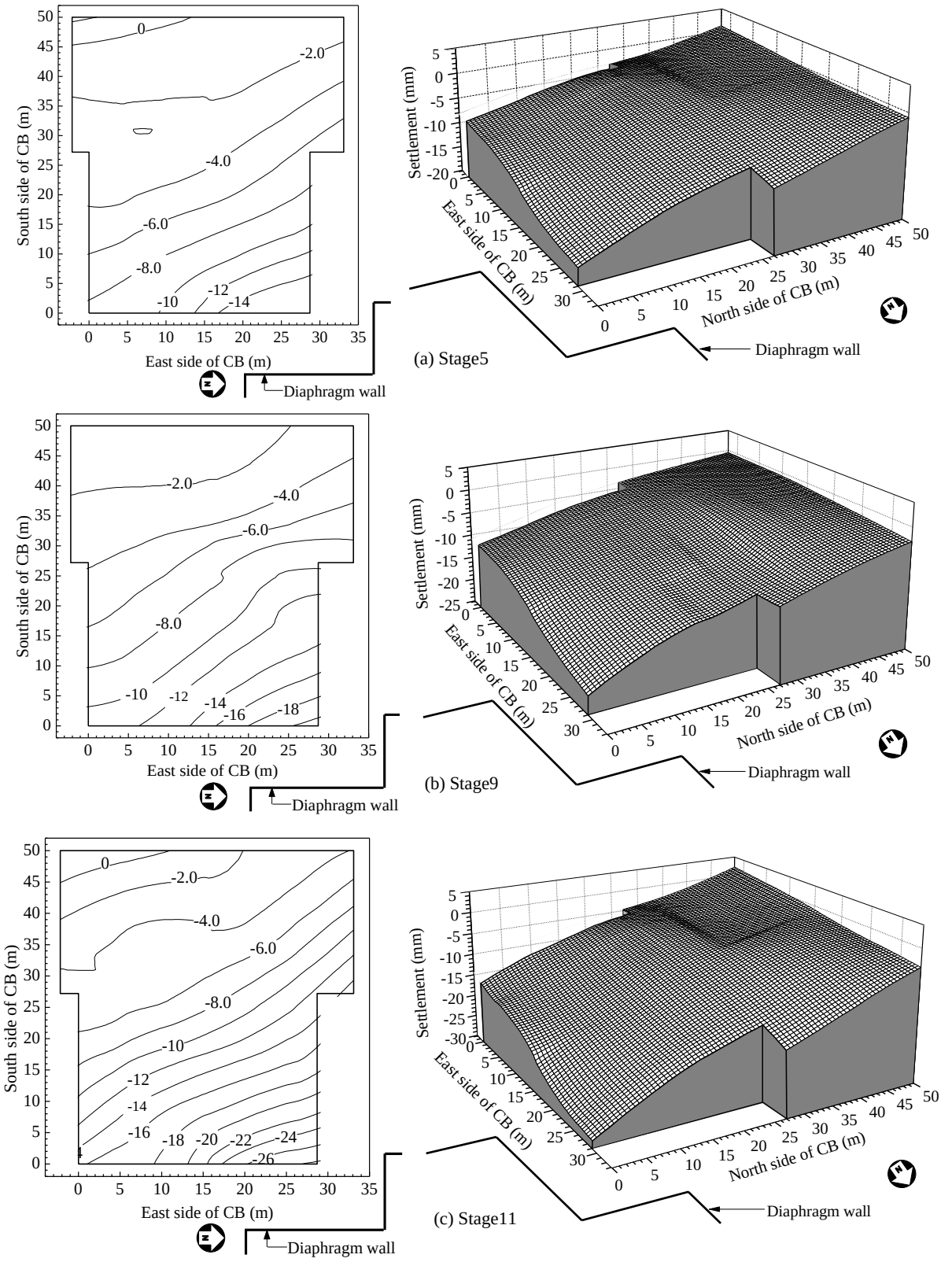

Fig.A.11 2D settlement contours and 3D settlement distribution of the CB building at different stages

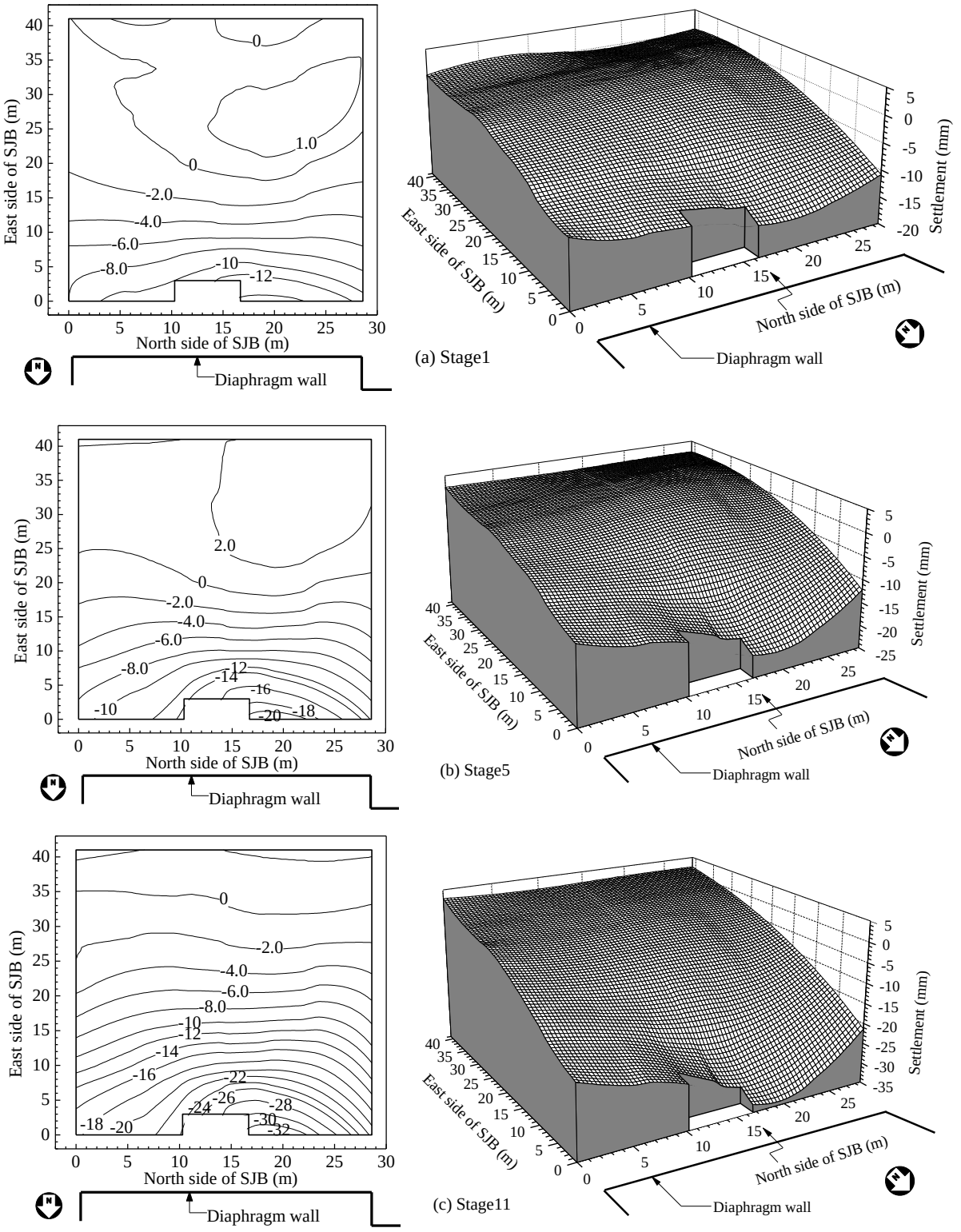

Fig.A.12 2D settlement contours and 3D settlement distribution of the SJB building at different stages

Appendix B - Field data of excavation for North Square of Shanghai South Railway Station

The field data regarding to wall deformations, ground movements, and vertical movements of top of piles, are collected from Xu (2007) and shown in this appendix.

B.1 Lateral displacement of the diaphragm wall

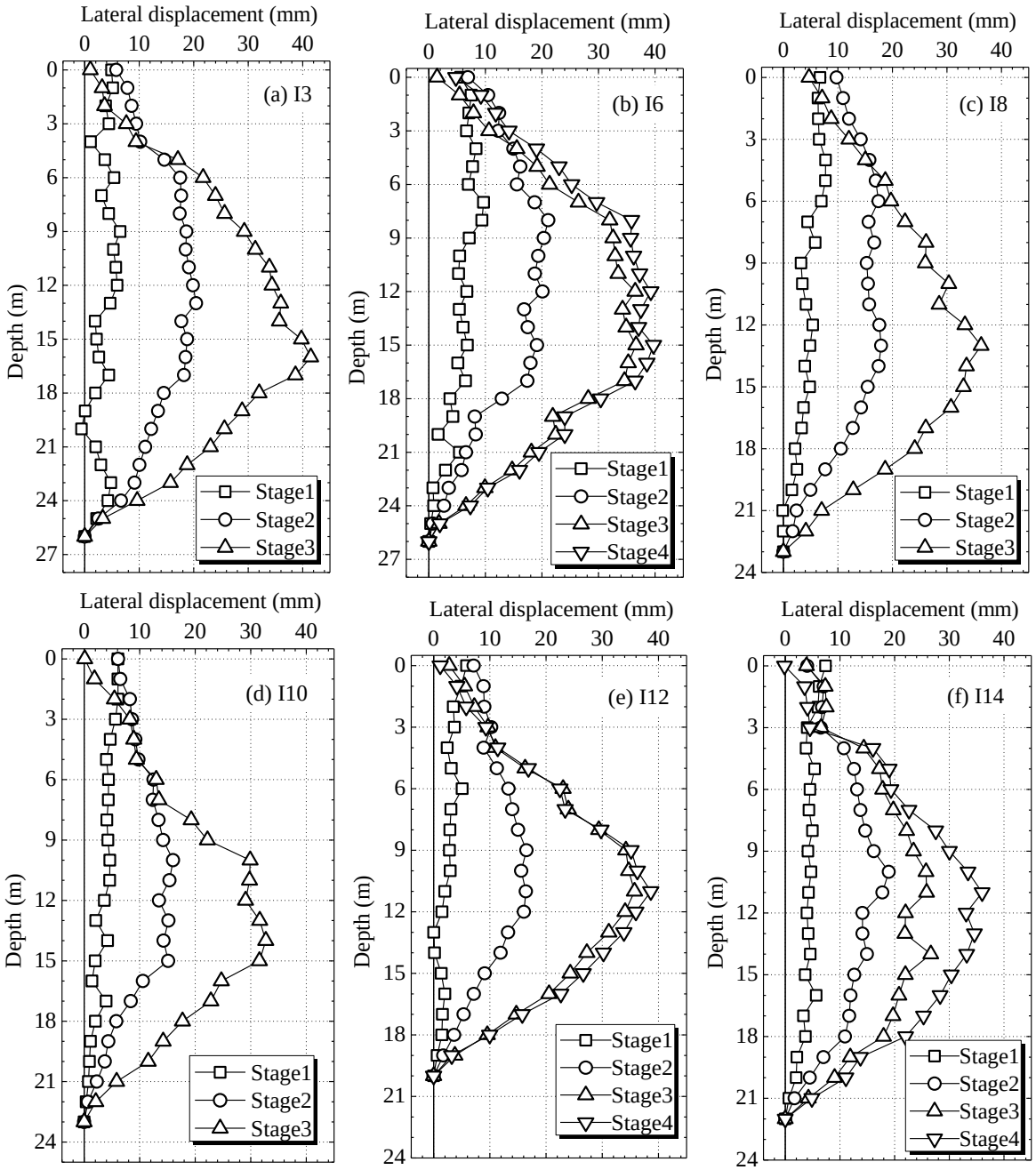

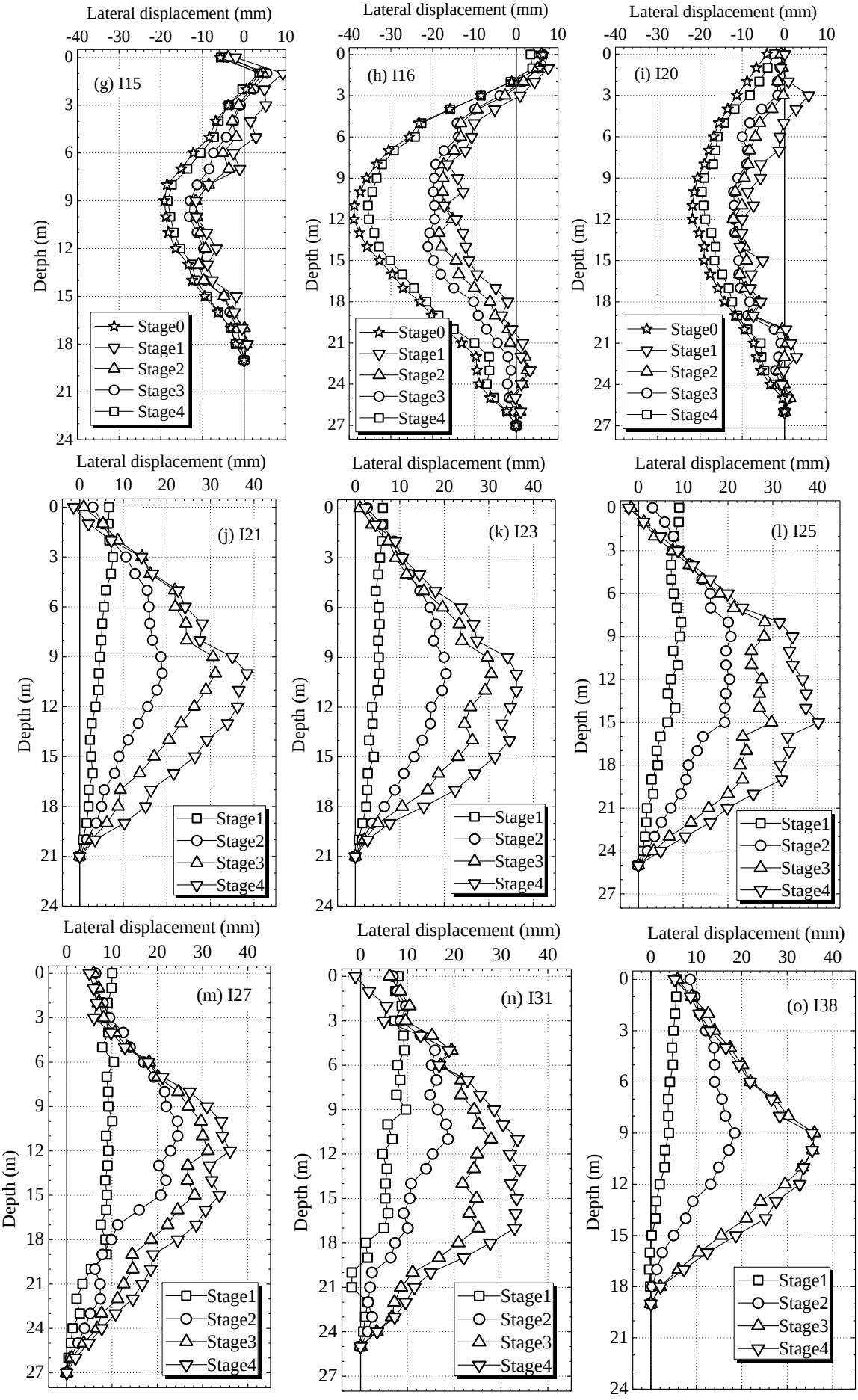
(g) I15
(h) I16
(i) I20
(j) I21
(k) I23
(l) I25
(m) I27
(n) I31
(o) I38
Lateral displacement (mm)
Depth (m)
Stage0
Stage1
Stage2
Stage3
Stage4

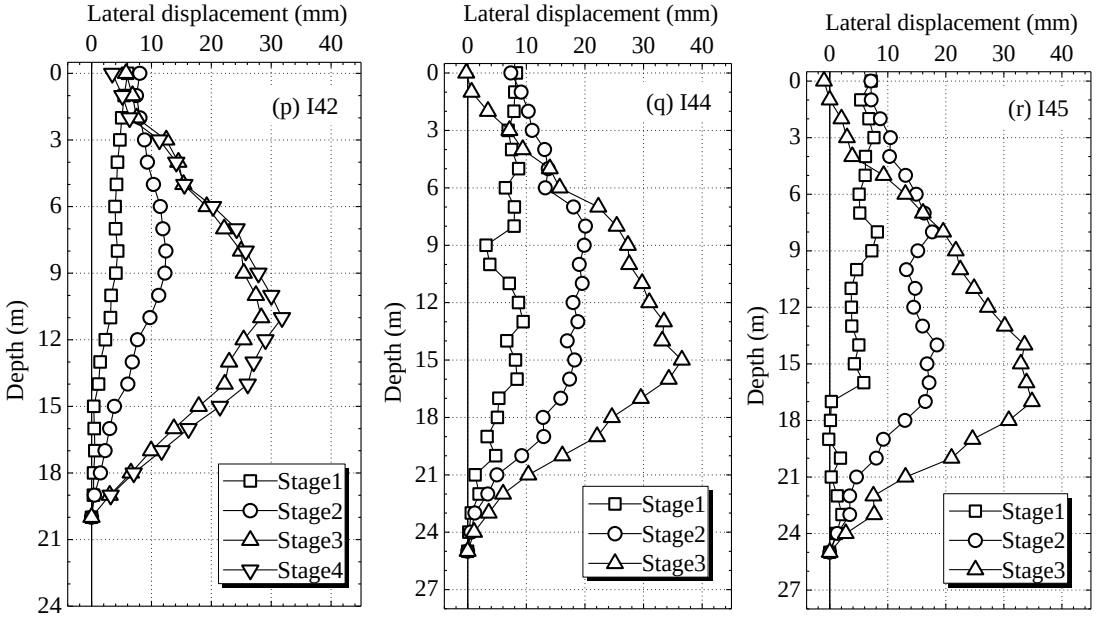

Fig.B.1 Lateral displacement of the diaphragm wall at different stages

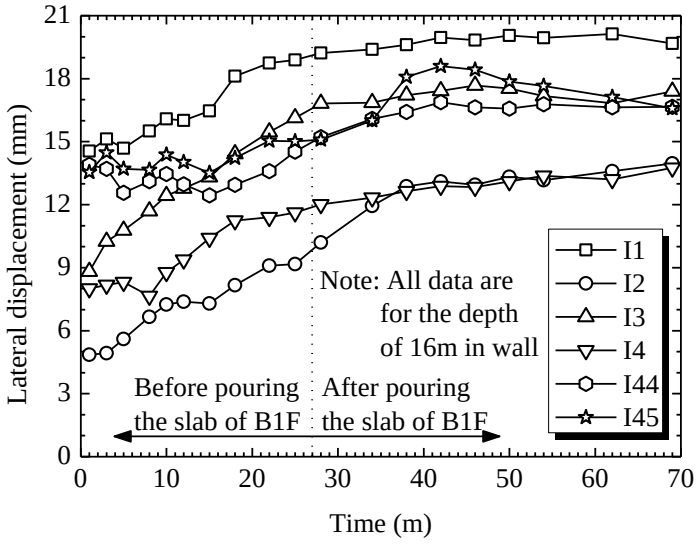

Fig.B.2 Lateral displacement of the wall at the depth of 16m versus time

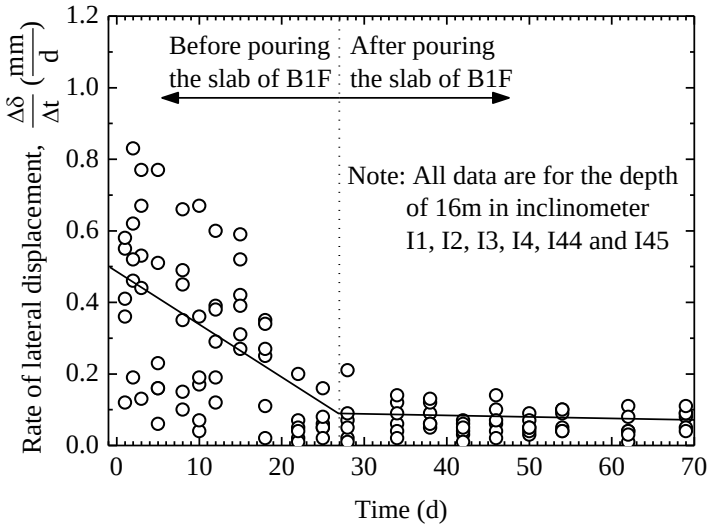

Fig.B.3 Relationship between the rate of lateral of wall at the depth of 16m and time

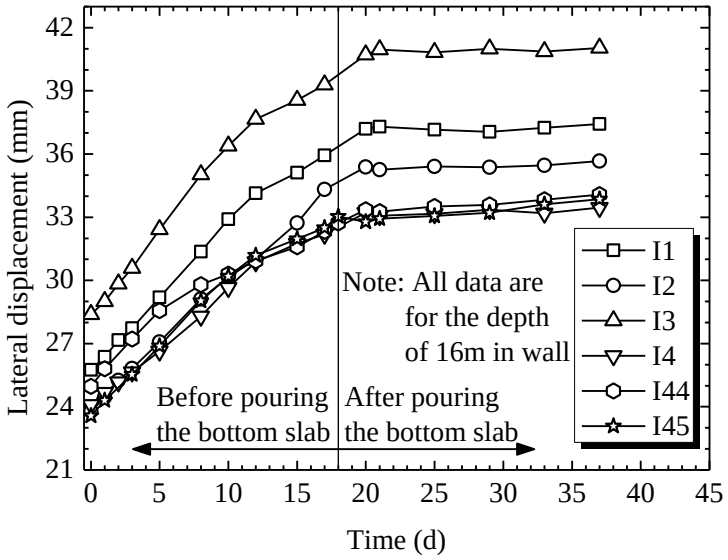

Fig.B.4 Lateral displacement of wall at the depth 16m versus time

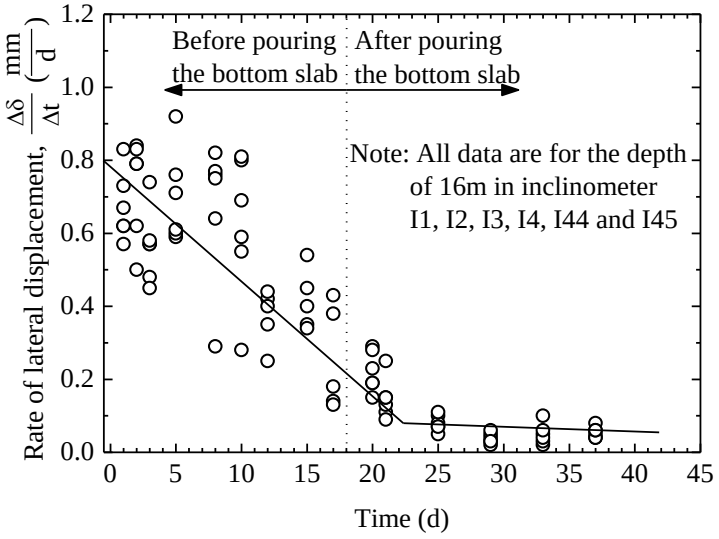

Fig.B.5 Relationship between the rate of lateral of the wall at the depth of 16m and time

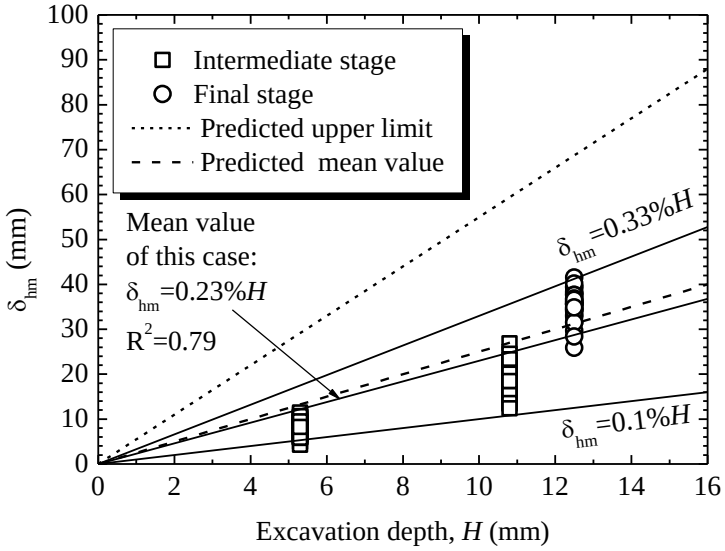

Fig.B.6 Relationship between maximum lateral displacement of diaphragm wall and excavation depth

B.2 Vertical displacement of diaphragm wall

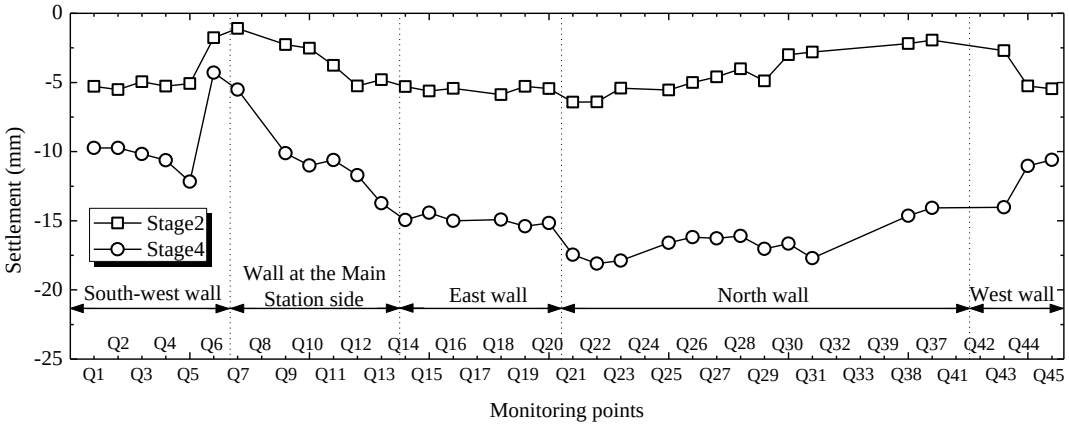

Fig.B.7 Vertical displacement of the diaphragm wall at different stages

B.3 Vertical displacement of piles and horizontal support system

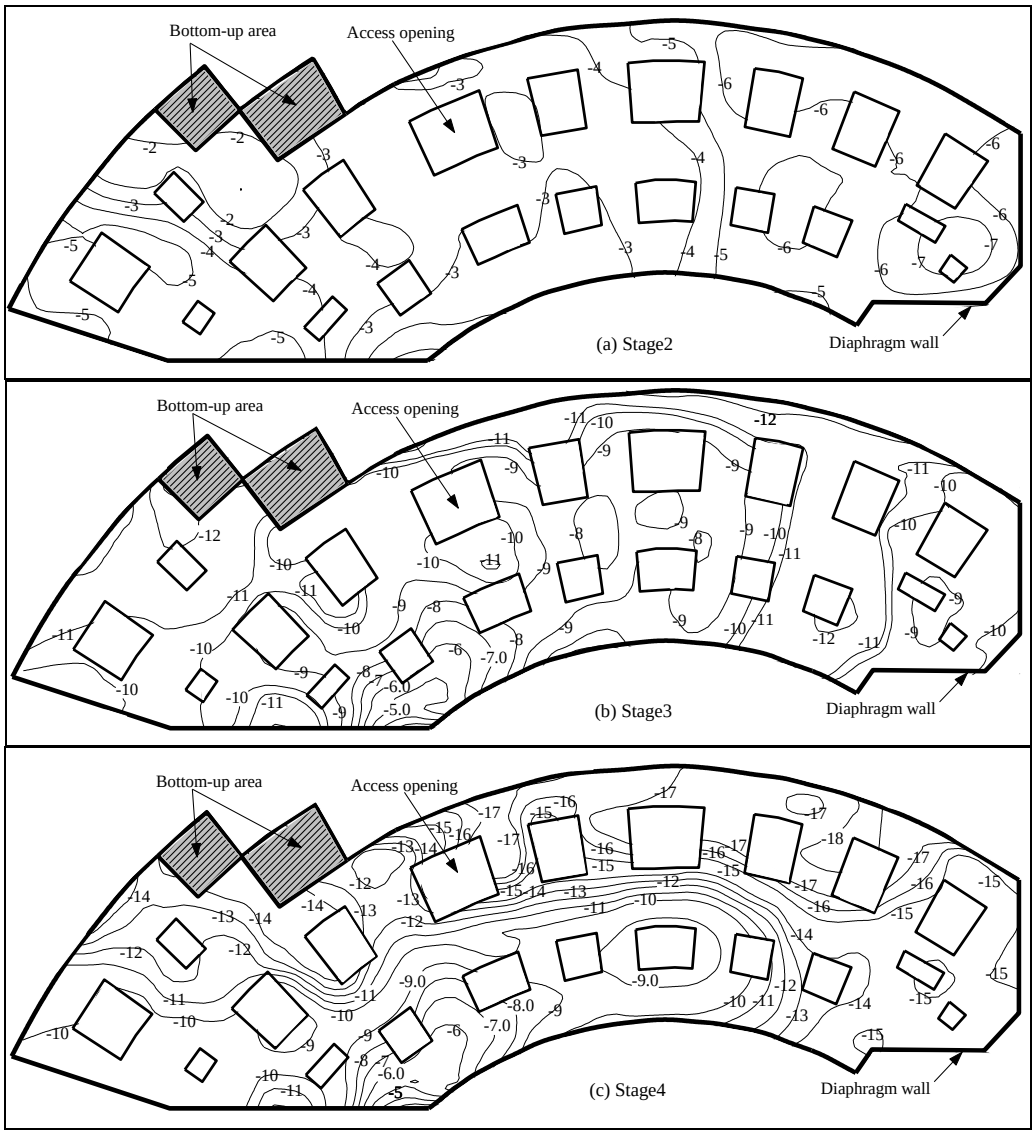

Fig.B.8 Contour plots of settlement of first level slab at different stages (unit: mm)